DAMAGE DETECTION IN SUSPENSION BRIDGES USING VIBRATION CHARACTERISTICS

Wasanthi Ramyalatha Wickramasinghe

MEng. (Structural), BSc Eng. (Hons)

A thesis submitted in fulfilment of the requirements for the degree of

Doctor of Philosophy

School of Civil Engineering and Built Environment

Science and Engineering Faculty

Queensland University of Technology

September 2015

Dedicated to my Parents, Brother and Husband with Love

Abstract

Transport infrastructure systems, particularly bridges, in many cities are rapidly aging and structural deterioration can set in. Environmental influences, changes in load characteristics and random actions accelerate the structural deterioration and can cause damage leading to expensive retrofitting or bridge failure. Among different bridge types, suspension bridges are increasingly used in today's infrastructure system to span large distances and are rich in architectural features and aesthetical aspects. However, their main cables and hangers can suffer from severe corrosion and fatigue damage. There is thus a need for a simple and reliable procedure to detect and locate such damage so that appropriate retrofitting can be carried out to prevent bridge failure. Structural Health Monitoring (SHM) has emerged as a technique that can address this need.

Current SHM systems are integrated with a variety of damage detection methods, which are global and local in nature. Limitations in local methods necessitate the non-destructive and global techniques for damage diagnosis. This has led to continuous development in vibration based damage detection (VBDD) methods in SHM systems. The basic principle of vibration-based SHM is damage in a structure changes its structural properties which in turn results in changes in its vibration characteristics. A change in the vibration characteristics can hence be used to detect damage in a structure.

Due to the difficulties of extracting many vibration modes in large civil structures like suspension bridges, applicability of existing vibration based damage detection methods has been limited. Moreover, these bridges vibrate with lateral, vertical, torsional and coupled modes and their vibration patterns are complex making it very difficult to identify the damage sensitive modes. This research therefore focused on a vibration based damage detection method which incorporates only a few lower order modes to detect and locate damage in the main cables and hangers of suspension bridges. Towards this end, it proposed mode shape component specific damage indices (DIs) based on modal flexibility and demonstrated their effectiveness under a range of damage scenarios.

The proposed method was verified by numerical investigations using finite element (FE) models of four types of structures to cover simple to complicated structures. Self-performed experiments and vibration data in the literature were used to validate these FE models. This research also studied (i) variation of damage severity, (ii) single, multiple and complex damage scenarios, (iii) influence of noise in the modal data, (iv) influence of cable parameters and (v) impact of higher vibration mode in the proposed damage detection method. A flowchart representing the application of the proposed damage detection methodology to the inverse problem is also developed and presented.

Improved results for damage detection in suspension bridges were obtained by the proposed technique compared to those from the traditional modal flexibility method. The research outcomes enable the timely retrofitting of cables and hangers to ensure the safe operation of suspension bridges in the infrastructure and optimal allocation of public resources for retrofitting and maintenance.

KEYWORDS:

Suspension bridges, Main cables, Hangers, Damage detection, Modal flexibility, Component specific damage indices, Noise, Bending stiffness, Sag-extensibility

Table of Contents

List of Figures

List of Tables

List of Abbreviations

2D	Two Dimensional
3D	Three Dimensional
ANN	artificial neural network
ATM	Adaptive Template Method
BCSC	Bi-Concave Side Cables
COMAC	Coordinate Modal Assurance Criterion
DATS	Data Acquisition and Transmission System
DIs	Damage Indices
DLAC	Damage Localization Assurance Criterion
DMS	Data Management System
DOF	Degrees of Freedom
DPCS	Data Processing and Control Systems
ECOMAC	Enhanced Coordinate Modal Assurance Criteria
eDAQ	Electronic Data Acquisition System
EFDD	Enhanced Frequency Domain Decomposition
EMA	Experimental Modal Analysis
FDD	Frequency Domain Decomposition
FE	Finite Element
FFT	Fast Fourier Transformation
FRF	Frequency Response Function
FSS	Frequency Shift Surface
GDLI	Generalized Damage Localization Index
ITD	Ibrahim Time domain
LSCE	Least Squares Complex Exponential
LVDTs	Linear Voltage Displacement Transducers

MAC	Modal Assurance Criterion
MDI	Modified Damage Index
MDLAC	Multiple Damage Localization Criterion
MF	Modal Flexibility
MPC	Multipoint Constraints
MRITD	multiple Reference Ibrahim Time Domain
MSEC	Modal Strain Energy Correlation method
MSEDI	Modal Strain Energy based Damage Index
NI	National Instruments
OMA	Output Only Modal Analysis/ Operational Modal Analysis
PNN	Probabilistic Neural Network
PP	Peak Picking
PRCE	Polyreference Complex Exponential
RD	Random Decrement
RFC	Relative Flexibility Change
SAC	Signature Assurance Criteria
SCBFI	Strain Change Based on Flexibility Index
SCCM	Spectral Centre Correction Method
SES	Structural Evaluation System
SHM	Structural Health Monitoring
SS	Sensory System
SSI-COV	Covariance-Driven Stochastic Subspace Identification
SSI-DATA	The Data Driven Stochastic Subspace Identification
TEO	Teager Energy Operator
TSC	Top Supporting Cables
RPC	Reverse Profiled (Bottom) Cables
UPC	Un-weighted Principal Component

VBDD	Vibration Based Damage Detection
WASHMS	Wind and Structural Health Monitoring System
WCC	Wave Form Chain Code
WT	Wavelet Transform

Publications

Journal Papers:

- Wickramasinghe, W. R., Thambiratnam, D. P., & Chan, T. H. (2015) Use of Modal Flexibility Method to Detect Damage in Suspended Cables and the Effects of Cable Parameters. Electronic Journal of Structural Engineering (EJSE) (Published).
- Wickramasinghe, W. R., Thambiratnam, David P., Chan, Tommy H.T. & Theanh, N. (2015) Vibration Characteristics and Damage Detection in a Suspension Bridge, Journal of Sound and Vibration (Under Review).

Conference Papers:

- Wickramasinghe, W. R., Thambiratnam, D. P., & Chan, T. H. (2014a). Damage detection in cable structures using vibration characteristics. Paper presented at the Proceedings of the 4th International Conference on Structural Engineering and Construction Management 2013.
- Wickramasinghe, W. R., Thambiratnam, D. P., & Chan, T. H. (2014b). Modal flexibility method for structural damage detection in suspension bridges. Paper presented at the 6th International Conference on Structural Health Monitoring of Intelligent Infrastructure, SHMII-6 2013.

Statement of Original Authorship

The work contained in this thesis has not been previously submitted to meet requirements for an award at this or any other higher education institution. To the best of my knowledge and belief, the thesis contains no material previously published or written by another person except where due reference is made.

Signature:

Date: 7th September 2015

Acknowledgements

I would like to express my sincere gratitude to my principal supervisor, Professor David Thambiratnam, for giving me this great opportunity along with his invaluable guidance, as well as continuous encouragement and support to conduct my research work successfully. Further, his wide knowledge in structural dynamics, detailed and constructive comments have been great value to me. The special thank also extended to my associate supervisor, Professor Tommy Chan, for his kind support, advice, helpful comments and suggestions on my work. In addition, his extensive technical knowledge, experience and dedication contributed to the success of this project.

The completion of my experimental work is a combine effort of number of people. First, I would like to thank all the staff members of the Banyo Pilot Plant Precinct and Engineering Precinct of QUT. In particular, I greatly acknowledge Jean Christophe Bonavia, Lincoln Hudson and Barry Hume for their extensive assistance related to the preliminary work of the experimental bridge. Also my acknowledgement should be extended to Kelsey Osborne and Marcel Boberg for their continued support and collaboration throughout the experimental work. It is a great pleasure to thank Dr. Theanh (Andy) Nguyen for his remarkable help in all technical matters concerning modal testing and also Craig Cowled, who gave me the knowledge of the basics of experimental testing.

I must thank all academic and non-academic staff members including School of Civil Engineering, the Built Environment Research Portfolio Office, HPC unit and librarians. I sincerely thank QUT Research Student Centre and QUT Science and Engineering Faculty HDR Student Support Team for their direct and indirect support during my PhD candidature. Also I gratefully acknowledge the financial support provided by QUT which allowed me to carry out my research work.

My acknowledgements go to all members in the Structural Health Monitoring Research Group at QUT to their help, sharing knowledge and feedbacks on my work. My thanks also spread to all my colleagues for their continuous encouragement and support.

Further, I would like to express my sincere gratitude to my parents and brother who have always been behind me and supporting to my success. Last but not least, I would like to extend my gratitude and respect to my loving husband Chandana Rupasinghe for his endless patience, constant words of encouragement and for all the sacrifices he made while I pursued my PhD.

Wasanthi Wickramasinghe

Queensland University of Technology, Australia

September 2015

Chapter 1: Introduction

1.1 BACKGROUND

Bridges in modern society are necessary parts of the infrastructure, providing means of connecting communities and reducing travel time. They are designed to have long life spans. During the course of their life-cycle, they are subjected to structural deterioration due to environmental influences, changes in load characteristics and random actions (Shih et al., 2011a). These factors can cause structural damage and therefore have detrimental influences on the serviceability and ultimate capacity of the structure; subsequently resulting in expensive retrofitting or bridge failure. This reveals the importance of structural health monitoring (SHM) of bridges to monitor the performance of bridges and detect, locate and quantify damage when it occurs. This will enable the estimation of the remaining service life and appropriate retrofitting. Thus it is a challenging task for the current SHM systems, particularly for complex civil structures like suspension bridges.

Suspension bridges are increasingly used in today's infrastructure systems due to their cost effective structural form, longer spans, lightness (less material requirement and flexibility) and aesthetics. However with age, their main cables and hangers can suffer from severe corrosion and fatigue. Environmental influences such as weather changes and temperature fluctuations, cause imperfections in the cable protection system allowing moist air and water to enter into the interior of the cable and exposing it to moisture for long periods of time. This can, result in reductions of cable diameter up to 30% (Sloane et al., 2012) due to severe corrosion. Figure 1.1 illustrates severe corrosion identified in a main cable during detailed inspection. Further, cables are also susceptible to long term fatigue damage after many years in service.

Similarly, hangers of suspension bridges are also more prone to corrosion than the other structural elements due to their small cross section areas (Qiu et al., 2014). Such corrosion causes reduction in resistance capacities of hangers towards to sudden breakage of hangers. Even though hangers are small components of a suspension bridge, sudden breakage of these can produce a very strong vibration and

large changes of internal forces of the bridge (Qiu et al., 2014) resulting in collapse of the whole bridge. Main cables and hangers are therefore, critical elements for the overall structural performance and safety of suspension bridges. Damage detection in these elements is therefore a priority in terms of optimal allocation of public resources for retrofitting and maintenance of such structures.

Figure 1.1 Detailed visual inspection of a suspension bridge main cable with corrosion (Higgins, 2004)

A variety of damage detection techniques have been used to assess deterioration and damage of structures during the last few decades, encompassing both local and global methods. Local methods such as acoustic or ultrasonic emission, magnetic particle inspection, eddy currents and radiography require prior localization and accessibility of damaged zones to evaluate the state of the structure. However, the main cables and hangers are practically inaccessible for visual inspection and do not show any evidence of damage on their exterior during conventional visual inspections. In addition, main cables are employed with corrosion protection system which shields the load carrying wires from sight during visual inspections. Application of local methods to detect damage in suspension bridge main cables and hangers is time consuming, expensive, and consequently inefficient.

Limitations of the local methods can be overcome by focusing on global methods of damage detection which comprise a variety of techniques based on the vibration characteristics of a structure. Damage or deterioration in a structure causes

changes in its properties (mass, damping and stiffness) which in turn cause changes in its vibration characteristics (natural frequencies, modal damping and mode shapes). Change in vibration characteristics of a structure can therefore be used as the basis for vibration based damage detection (VBDD) techniques. These VBDD techniques have been recently received a considerable amount of attention for damage detection due to their relative simplicity and the moderate cost of dynamic measurements (Materazzi & Ubertini, 2011). They have been applied successfully to beam and plate elements (Shih et al., 2009), trusses (Mehrjoo et al., 2008; Shih et al., 2011a; Wang et al., 2012) and simple structures in reinforced concrete (Wahalathantri et al., 2015).

Successful application of VBDD methods to detect damage in deck (main girder) (Yeung & Smith, 2005), towers, and bearings in suspension bridges have been achieved in previous research (Chan et al., 2011; B. S. Wang et al., 2000; J. Y. Wang et al., 2000). Recently, Talebinejad et al. (2014) made an attempt to detect damage in hangers, main cables, tower legs, bulk heads and deck of a suspension bridge using four VBDD techniques. That study focused on very few damage cases with very high severity on main cables and hangers and will not fully address multiple damage cases and small damage intensities successfully. Consequently, application of these methods in main cable and hangers require further development. This research therefore will propose a VBDD approach to detect and locate damage in main cable and hangers of a suspension bridge using derivatives of basic vibration parameters.

Among different VBDD techniques, methods based on modal flexibility, which depends on both the natural frequencies and mode shapes, have shown the potential for successful damage detection. Theoretically, structural deterioration reduces stiffness and increases flexibility. Increase in structural flexibility can therefore serve as a good indicator of the degree of structural deterioration. Alternatively, modal flexibility of a structure converges rapidly with increasing frequency and can be therefore computed using few lower natural frequencies and mode shapes (Pandey & Biswas, 1994). Modal flexibility can therefore be a promising approach for damage detection in large civil structures such as suspension bridges with limited number of lower order modes.

This study therefore, derives and applies modal flexibility based damage indices (DIs) to detect and locate damage in suspension bridges. Numerical investigations using Finite Element (FE) models are employed to study the potential of the proposed DIs in detecting and locating damage. The FE models used in this study are validated using vibration data from the literature and self-performed experiments. Competency of the DIs were examined for both single and multiple damage scenarios using simulated damage in the FE models by varying the stiffness at the particular locations of interest together with varied damage severity. Results indicate that the proposed modal flexibility based DIs can successfully detect and locate damage in the main cables and hangers of suspension bridges. The research outcomes will enable bridge engineers and managers to detect damage in suspension bridges at an early stage and hence minimise expensive retrofitting and prevent catastrophic bridge failures.

1.2 RESEARCH PROBLEM

The need for prior localization of damaged zones and practical inaccessibility make the local damage detection techniques inefficient in detecting damage in main cables and hangers of suspension bridges. Consequently, VBDD methods are promising in detecting damage in such structures. However a very limited number of VBDD applications have been identified for suspension bridges and these applications focus on the damage detection of deck, bearings and towers based on the natural frequency as a damage index candidate. Difference in natural frequency of a damaged and intact structure is very small in complex structures like suspension bridges; therefore it is difficult to investigate damage in these elements by merely considering the natural frequency. Even though very few investigations had been attempted in damage detection of cables and hangers recently, they addressed only the single and very high severity damage cases. Therefore, an appropriate VBDD based method needs to be proposed to detect and locate damage in suspension bridge main cables and hangers.

Suspension bridges are very complex structures and associated with higher number of degrees of freedoms. In such structures, only a limited number of lower order modes can be measured practically (Ni et al., 2002) which are far less than the modes that can be derived from analytical models. Therefore it is essential to emphasis on a damage detection method which uses lower order modes.

In general, cable structures vibrate in lateral, vertical, torsional and coupled modes (Huang et al., 2005). Subsequently, it is very difficult to identify modes that are sensitive to damage in a suspension bridge. It is therefore necessary to propose appropriate DIs that are able to detect damage in the presence of complex and coupled vibration modes.

1.3 AIMS AND OBJECTIVES

The main aim of this research is to develop and apply special modal flexibility based procedures to detect and locate damage in suspension bridges using changes in their vibration properties. This study focused mainly on the damage in the main cables and hangers of the suspension bridges. To achieve this aim, the specific research objectives are listed as follows;

1. Investigate the capability of existing modal flexibility based DIs to detect and locate damage in a suspended cable and the main cable and hangers of a suspension bridge.
2. Develop and apply a component specific modal flexibility based DI to overcome the shortcomings in 1 above and to detect and locate damage accurately in a suspended cable that exhibits vertical and lateral vibration modes.
3. Investigate the influence of (i) noise in the modal data and (ii) cable parameters on the performance of the special DI developed in 2 above.
4. Develop and apply component specific modal flexibility based DIs to detect and locate damage accurately in the main cable and hangers of two dimensional (2D) and three dimensional (3D) suspension bridges which exhibit complex and coupled vibration.
5. Investigate the competency of the above DIs in the presence of noise in the modal data and when higher order modes are used in the damage detection procedure.

1.4 RESEARCH SCOPE

- The complete SHM system consists of five components and involves a research area which include; (1) Sensory System (SS), (2) Data Acquisition and Transmission System (DATS), (3) Data Processing and

Control Systems (DPCS), (4) Data Management System (DMS) and (5) Structural Evaluation System (SES). The last component of the SHM system mainly addresses the damage diagnosis and damage prognosis processes. Damage diagnosis (assessment) process still remains unsolved for complex civil structures such as suspension bridges. This research is limited to the two aspects of damage assessment namely; detecting and locating damage in suspension bridges.

- It focuses mainly in detecting and locating damage in suspension bridge main cables and hangers. Damage detection has not been successfully achieved in those elements for single and multiple damage scenarios with moderate level of damage severity.
- FE models are employed to study the potential of the proposed DIs due to complications in obtaining mass normalized mode shapes in real testing.
- Corrosion and fatigue have localized effects on hangers and cables which do not require complicated damage models to simulate damage. Therefore this research uses change of Young's Modulus (E) in simulating damage at a particular location of an element considered.

1.5 SIGNIFICANCE OF RESEARCH

Suspension bridges meet the steadily growing demand for lighter and longer bridges in today's infrastructure systems. However with age, their main cables and hangers could suffer from corrosion and fatigue. Thus, there is a need for a simple and reliable procedure to detect and locate such damage, so that appropriate retrofitting can be conducted to prevent bridge failure. The method proposed in this study evaluates damage in the main load bearing elements which are the main cables and hangers with respect to location and severity. The research findings will provide new information on the use of modal flexibility based DIs to detect and locate damage in the main cables and hangers of suspension bridges in order to enable necessary retrofitting to prevent failure. Mode shape component specific DIs are derived and applied to achieve this. Also, this research is significant as it contributes towards the safe and efficient operation of suspension bridge structures. It will benefit the community by saving significant amounts of money used in the maintenance of infrastructure systems and will provide assurance of human safety.

Moreover, the research outcomes will contribute towards the knowledge and development of SHM systems.

1.6 THESIS OUTLINE

The outline of this thesis is as follows;

Chapter 1: Introduction

Chapter 1 presents the background to the research topic and the research problem in the area of damage detection in suspension bridges. It also defines the aims and objectives of the research and states the research scope. Finally, it highlights the significance of research and outlines the thesis content.

Chapter 2: Literature Review

Chapter 2, first, provides a comprehensive literature review on bridges and their failures. Next, it provides the details of SHM including damage detection and application of VBDD techniques in suspension bridges. Finally, it concludes with a summary of literature review with the identified knowledge gaps.

Chapter 3: Theory of Damage Detection and Finite Element Modelling of Suspension Bridges for SHM

Chapter 3 describes basic structural dynamics, Modal Flexibility method and derivation of component specific DIs. Since this study extensively uses FE models to obtain vibration parameters for the damage detection studies, different FE modelling techniques used to develop suspension bridges, modal analysis and model updating associated with SHM are also discussed.

Chapter 4: Damage Detection in Cables and Hangers of a Suspension Bridge

Chapter 4 illustrates the application of the proposed method through numerical examples of a suspended cable and a two dimensional model of a main span in a suspension bridge. In the first section, damage detection of cables for single and multiple damage scenarios in both noise free and noisy conditions is treated. Influence of cable parameters on damage detection is also presented. In the second section, damage detection of hangers for single and multiple damage scenarios in both noise free and noisy conditions are presented.

Chapter 5: Experimental Testing of the Laboratory Cable Bridge Structure

Chapter 5 describes the two experiments namely; static test and dynamic tests conducted in this study to validate the FE models. These validated FE models will be used in chapter 6 for damage detection studies in the three cable systems which serve different structural purposes.

Chapter 6: Damage Detection in the Laboratory Cable Bridge Structure

Chapter 6 first describes the development and validation of the FE model of the Laboratory Cable Bridge Structure used in obtaining vibration parameters to illustrate the application of proposed method of damage detection. This chapter also demonstrates damage detection in the three different cables of the Laboratory Cable Bridge Structure which serves different structural purposes.

Chapter 7: Damage Detection in a 3D Suspension Bridge

Chapter 7 first describes the FE modelling and validation of the Ölfusá Suspension Bridge using field measured vibration properties. Second, it illustrates the application of proposed method of damage detection in both noise free and noisy modal data. Thirdly, influence of higher order modes and complex damage scenarios in DIs is discussed. Finally, guidelines for the application of DIs in real structure are presented.

Chapter 8: Conclusions

Chapter 8 presents the research findings and its contributions to knowledge. Finally, recommendations for further research are provided.

Chapter 2: Literature Review

2.1 INTRODUCTION

This chapter reviews the background for the research motivation, overview of SHM, damage detection methodologies and their application in suspension bridges. The chapter begins with research motivation pertaining to the increasing need to strengthen, repair or replace suspension bridges due to various types of damage. Secondly, it highlights the importance of SHM and its different components in the context of suspension bridges. Thirdly, this chapter analyses the shortcomings and limitations of current damage detection methods that have been developed over the past three decades to characterise structural damage by examining changes in measured dynamic response. Next, applications of these techniques particularly in suspension bridges are discussed. Finally, identified areas of research and development need to be addressed are presented.

2.2 RESEARCH MOTIVATION

Nowadays, one of the major concerns among the Engineering community is the ageing and structural deterioration of large number of transportation infrastructure systems, particularly, bridges. Many factors influence on structural deterioration of bridges and hence cause damage to its components. Increases in traffic, causes change the load patterns on bridges than was originally intended. This resulted in exceeding the load carrying capacity of structural components leading to damage or catastrophic failure of the whole structure. Further different environmental conditions such as flood, hurricanes, winter storms, tornadoes and earthquakes accelerate the structural deterioration in bridges. According to an IEEE technical report (Schneidewind et al., 2010) for year 2010, overloading, deterioration and lateral excitation caused by vehicles have significant effects on major bridge failures.

Among different bridge types, suspension bridges are increasingly used in today's infrastructure system due to its ability in bridging larger spans and are rich in architectural features and aesthetical aspects. They are very flexible structures and always have four main types of vibration modes: lateral, torsional, vertical and longitudinal modes (Huang, 2006). The recent vibration tests on suspension bridges

clearly identified these vibration modes (Conte et al., 2008; Pakzad & Fenves, 2009; Siringoringo & Fujino, 2008).

The life expectancy of suspension bridges are directly correlated to the condition of their cable system (Deeble Sloane et al., 2012) and main problems of cables in suspension bridges are corrosion and wire breaks (Wit & Hovhanessian, 2013). The corrosion is an electrochemical reaction of which the corroding metal is oxidized in the presence of aqueous environment and electrolyte and environmental factors as mentioned before accelerate this chemical reaction. In cables, corrosion begins with entering the moist air and water in to the interior of them through imperfections of the coating system. Once they enter in to the cable, evaporation of them is impossible and as a result wires of the cables directly exposed to the moist environment for long period of time (Sloane et al., 2012). Further Hopwood and Havens (1984) reported that the exposure of high strength steel wires for long period of time causes a corrosion reaction more aggressive than direct immersion of steel into a corrosive solution. There are many examples were reported over the world about corrosion problems in suspension bridge main cables. Some of them are described next.

Due to negligence in maintaining suspension bridges for many years, majority of them within the United States are structurally deficient (Sloane et al., 2012). The investigation report stated that many of the suspension bridges in greater New York area are approaching or exceeded 100 years of service life. In depth inspection of main cables in these bridge revealed, presence of many broken wires, brittle fracture of wires and extensive corrosion (Betti & Yanev, 1999; Sloane et al., 2012). Rehabilitation of the corroded wires was conducted on the Brooklyn Bridge and the Williamsburg Bridge (Betti & Yanev, 1998; Mayrbaurl, 2000; Suzumura & Nakamura, 2004) in New York City reported corrosion has been a major issue in suspension bridges. It has been identified that the wire samples tested from the Williamsburg Bridge reached the corrosion pits up to 30% loss of diameter (Sloane et al., 2012).

Some cable corrosion issues were identified in the newest suspension bridges in Japan. Furuya et al. (2000) reported that the water within the main cables of several newest suspension bridges in Japan. The presence of water creates highly humid environment inside the high strength steel wire causing corrosion to occur

after 10 years of bridge completion (Suzumura & Nakamura, 2004). A survey conducted on existing suspension bridges before construction of Akashi Kaikyo bridge in Japan reported that rust was found on steel wires, which are located in two to three layers below the outer surface of the main cables (Yanaka & Kitagawa, 2002). In 2002, strengthening of main cable was carried out in the Waldo-Hancock suspension bridge due to corrosion and subsequent loss of load carrying capacity (Andersen D, 2004). Cost for the total project was US $22.4 million. Figure 2.1 illustrates the corrosion and wire breaks in Waldo-Hancock suspension bridge south cable.

Figure 2.1 Cable corrosion and wire breaks in Waldo-Hancock Suspension Bridge (Andersen D, 2004)

Nowadays, increasing trends of budget allocation for maintenance of infrastructure are recorded around the world. Corrosion of suspension bridge cables reported in the literature leads not only to expensive retrofitting but also cable failures and loss of lives. In 1944, upstream cable of the Ölfusá Suspension Bridge failed due to deterioration and a truck towing another truck across the bridge fell to the river (Pálsson, 2012). The current bridge over river Ölfusá was built in the same place and in 1945.

Another very important structural member of a suspension bridge is hangers. Diameters of hangers are very small and are more prone to severe corrosion (Qiu et al., 2014). This corrosion damage reduces their structural capacity and which result in sudden failure. The sudden failure of hangers causes strong vibration and huge changes to the internal forces of the structure. This can have detrimental influences on the serviceability and ultimate capacity of the structure; more often resulting in

bridge failure. Such situations were reported in China in 2000. Severe corrosion in eight hangers of the Yibin Southgate Bridge and deck supported by them was fallen to the river (Qiu et al., 2014). Construction of Kutai Kartanegara Bridge (Mahakam II suspension bridge) in Indonesia was completed in 2002. Recently, this bridge was collapsed in 30 seconds due to failure of one hanger and loss of lives of 11 people with loss of 30 people were reported in this disaster (Qiu et al., 2014).

Apart from corrosion, main cables and hangers are also susceptible to long term fatigue damage after many years in service (Petrini & Bontempi, 2011). Further, main cables and hangers are practically inaccessible for visual inspection and do not produces any evidence of damage on the exterior in conventional visual inspections. In addition, main cables are employed with corrosion protection system which shields the load carrying wires from sight during visual inspections. Combination of all these factors reveals requirement of SHM for continuous monitoring and safety evaluation of bridges for their safer performance in an infrastructure system.

(a) (b)

Figure 2.2 Kutai Kartanegara Bridge (a) before collapse (b) after collapse (Qiu et al., 2014)

2.3 STRUCTURAL HEALTH MONITORING (SHM)

A variety of definitions can be given to SHM because it covers different fields. SHM is referred to the process of implementing a damage identification strategy for aerospace, civil and mechanical engineering infrastructure (Farrar & Worden, 2007). However, Catbas et al. (2008) defined SHM as tracking the responses of a structure along with inputs, if possible, over a sufficiently long duration to determine anomalies, to detect deterioration and to identify damage for decision making. In 2011 Chan et al. (2011) presented very comprehensive definition for SHM. They stated that SHM is not only confined to damage detection but also composed of two

components; structural performance monitoring (SPM) and structural safety evaluation (SSE). SPM refers to the "monitoring (observation) of structural performance in structure and its components under its designed performance limits at serviceability limit state by on structure instrumentation system" while SSE refers to "the evaluation of possible damage in structure or its components and/or the assessment of its health status by analytical tool, which are developed and calibrated in the course of SHM, basing on its designated performance limits at ultimate limit states". Significant life safety and economic benefits motivated this theme in research and development during the last few decades and is evident by the SHM systems installed in many long span bridges around the world as listed below.

- The Skarnsundet Bridge in Norway was instrumented with 37 sensors and fully automatic data acquisition system to monitor wind, acceleration, inclination, strain, temperature and dynamic displacements during construction and in service (Myrvoll et al., 1996).
- The New HaengJu Bridge in Korea was instrumented with 65 sensors and a signal processor (Chang & Kim, 1996).
- The Wind and Structural Health Monitoring System (WASHMS) is a SHM system installed on six cable supported bridges in Hong Kong. It is the most heavily instrumented bridge project in the world (Chan et al., 2011).
- The Storck's Bridge in Switzerland instrumented with a fibre optical surveillance system with 14 optical sensors and 26 electrical sensors (Chan et al., 2011).
- The New Carquinez Bridge in California consists of wind and earthquake monitoring system with 76 accelerometers (Hong et al., 2010).

2.3.1 Components of SHM System

Different components involved in SHM system are defined by many researchers (Chan et al., 2011; Li et al., 2004; Worden & Dulieu-Barton, 2004; Xu & Xia, 2011). According to the categorization of Xu and Xia (2011), the SHM system consists of five main components (Figure 2.3) as listed below. First two components are installed in the bridge and remaining three components are in the control office.

- Sensory System (SS)
- Data Acquisition and Transmission System (DATS)
- Data Processing and Control Systems (DPCS)
- Data Management System (DMS)
- Structural Evaluation System (SES)

SS consist of different types of sensors distributed along the bridge to capture different signals. Three types of parameters were monitored by those sensors; (i) loading sources (Wind, seismic and traffic); (ii) Structural response (Displacement, inclination, acceleration and strain); (iii) Environmental effects (temperature, humidity, rain and corrosion). There is a rapid development of sensor technologies in a SHM system during last few decades.

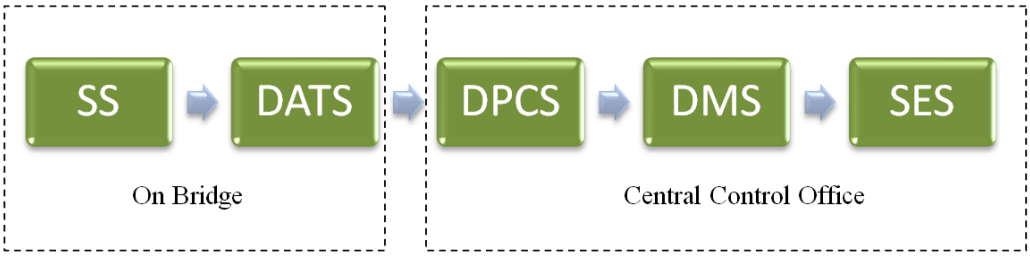

Figure 2.3 Architecture of SHM system (Xu & Xia, 2011)

The DATS collects the data from the sensors and transmit signals to the central database server. Data acquisition is the intermediate process which collects signals from sensors and converts them and transmits in to a central data base server. The next process DPCS have five functions; (i) Control and display of the operation of the data acquisition system; (ii) Pre-processing of the raw signals received from DATS; (iii) Archiving data into database or storage; (iv) Post processing of the data and (v) Viewing the data. Collected and processed data in a SHM system should be stored and managed in an appropriate manner to enable efficient data retrieval for later assessment is conducted by DMS of a SHM system. Different applications of processed and stored data includes on line and off line SES. Online structural condition evaluation system compares the measured field data against the design values, pre-determine patterns and analyses results. Off line incorporates verities of model based and data driven algorithms and model updating.

As described above, the SHM process itself is a broader research area. The last step of it mainly addresses the damage diagnosis and damage prognosis processes. Damage diagnosis process still remains unsolved for the complex civil structures like suspension bridges. This research therefore focuses on the damage detection process for suspension bridges.

2.4 DAMAGE DETECTION

The fundamental concept of damage detection needs to compare two different states of a structure; one which assumes to represent the initial or undamaged state and the second which is referred to as the damaged state. Li et al. (2007) defined structural damage as a weakening of a structure that negatively affects its performance and is a deviation in the structure's original geometric or material properties that may cause undesirable stresses, displacements, or vibrations. Damage on a structure can be classified as linear or nonlinear (Doebling et al., 1996). When the initially linear elastic structure remains linearly elastic after damage, it is identified as linear damage situation. If an initially linear elastic structure behaves in a nonlinear manner after damage, it is defined as nonlinear damage.

In general damage detection methods can be categorized as local or global techniques (Doebling et al., 1998; Zapico & González, 2006). Local methods evaluate the state of the structure by direct visual inspection or using non destructive evaluation techniques such as acoustic emission, ultrasonic, magnetic particle inspection, radiography and eddy current. These methods all need prior localization of the damaged zones (Shih, 2009). They are time consuming and expensive (Chang et al., 2003). However they only utilise data acquired from the damaged structure and baseline data or theoretical models of undamaged structure are not necessary to be used (Yan et al., 2007). For this reason local damage detection is very effective for small and regular structures. It is very difficult to detect damage using local damage detection methods in large and complicated structures in a closed environment (Chan et al., 2003; Yan et al., 2007). These limitations can be overcome by focusing on the global methods which offer a variety of techniques based on vibration characteristics.

The main objectives of global methods of damage detection are (i) to identify damage at the earliest stage, (ii) to locate damage precisely, (iii) to quantify the severity of damage and (iv) to predict the remaining lifetime of the structure. These

objectives were classified by Rytter (1993) as four different levels of damage evaluation. Worden and Dulieu-Barton (2004) and Farrar and Worden (2012) introduced and intermediate level to the above classification and defined five levels of damage evaluation. The new level was introduced to define the type of damage. The new classification is listed as follows;

Level 1 – Determination of the existence of damage

Level 2 – Determination of the location of the damage

Level 3 – Determination of the type of the damage

Level 4 – Determination of the extent of the damage

Level 5 – Prediction of the remaining service life of the structure

In this classification, Level 1 to Level 4 referred as damage diagnostic state and Level 5 is the damage prognostic state. A robust damage detection method will be able to address damage diagnostic state successfully. The scope of this research has been confined to the damage diagnostic state using vibration response and will address up to the Level 2 of damage evaluation in suspension bridges.

2.5 CLASSIFICATION OF VBDD METHODS

The fundamental theory for vibration based damage detection is that the changes in the structural properties of a structure (mass, damping and stiffness) due to damage will cause detectable changes in modal properties (natural frequencies, modal damping and mode shapes) (Alvandi & Cremona, 2006; Fan & Qiao, 2011; Shih et al., 2011b). The dynamic characteristics of a structure are functions of its stiffness and mass therefore variations in modal frequencies and mode shapes can be an effective indication of structural deterioration. The damage state of a structure can hence be evaluated from changes in its dynamic characteristics.

There are many classifications to the VBDD methods. According to the method of evaluating measured modal parameters, VBDD techniques can be classified as model based and non-model based methods (Huang et al., 2012; Salehi et al., 2011). The model based methods identify damage by using analytical model. Usually these analytical models are FE models updated according to the measured responses of the undamaged and damaged states of the structure. However FE models are developed based on the simplified assumptions and those often associate with modelling

inaccuracies. In order to detect the damage from the analytical model an excellent quality initial FE model is necessary and this became more realistic with the development of model updating methods. Recent research has been achieved this very successfully for large civil structures like bridges, buildings and towers (Ren & Peng, 2005; H. Wang et al., 2010; Weng et al., 2011; Weng et al., 2012). Even though the model based approach is more expensive and time consuming, are more suitable for complex structures (Abdel Wahab & De Roeck, 1999). For example, damage detection methods such as artificial neural network (ANN) based approaches used in large civil structures are more often based on analytical models.

The Non model based damage detection methods are straightforward and inexpensive and do not require any analytical model. They also referred to as Damage Index (DI) methods (Salehi et al., 2011) or the response based methods (Abdel Wahab & De Roeck, 1999). This method used the changes in modal parameters between the intact and damage states of the structure to develop DI for the use of damage detection process. Eliminating modelling errors is the main merits of this method. Possibility of implementing as automated process (Abdel Wahab & De Roeck, 1999) is an advantage of non-model based method in SHM system.

Hejll (2004) reviewed VBDD according to their analytical process. One category is the forward identification methods and the other is the inverse identification methods. In the forward identification study theoretical vibration parameter of a structure is obtained by numerical analysis at its undamaged state. Then, damage was introduced randomly and vibration parameters were acquired. Finally, analytically examined results were used to build necessary algorithms using simulated and measured changes to address damage detection problems. In the inverse identification unknown damage properties are identified using developed algorithms. Forward identification study is therefore used to solve the inverse problem.

In this research vibration based DI approach was used to develop a method to detect damage in suspension bridge main cables and hangers. It requires frequencies and mass normalized mode shapes to compute DIs. This fact leads the use of updated FE models for extracting vibration response in this research.

DIs can be formulated using different primary vibration properties as well as secondary vibration properties. A list of basic VBDD methods are in Table 2.1 and

use of them in different damage detection applications are described in next section. Further, their advantages and limitations are reviewed in Table 2.2.

Table 2.1 Most commonly used VBDD methods

Category	VBDD Method
Primary Vibration Properties	Natural frequency based methods
	Damping based methods
	Direct mode shape based methods
Secondary Vibration Properties	Curvature mode shape based methods
	Flexibility based methods
	Modal strain energy based methods

2.5.1 Natural Frequency Based methods

Presence of damage or deterioration in a structure causes changes in natural frequencies. Therefore natural frequency change is a basic feature for damage detection. The main reason for vast popularity of natural frequency in damage detection is, its easy determination with a relatively high level of accuracy (Palacz & Krawczuk, 2002). Cawley and Adams (1979) pioneered the use of changes in natural frequencies to detect damage. However an extensive review on using natural frequency for structural damage detection was conducted by Salawu (1997)

Contursi et al. (1998) and Messina et al. (1998) developed Damage Localization Assurance Criterion (DLAC) and Multiple Damage Localization Criterion (MDLAC) to detect single and multiple damage respectively. However Salawu (1997) concluded that the natural frequency changes alone may not be sufficient for a unique detection of the location of the structural damage. This is because similar cracks in two different locations cause the same amount of frequency change. Further, Doebling et al. (1998) stated the feasibility of locating damage using the frequency changes is limited because due to requirement of very precise measurement. Moreover, significant damage may cause very small changes in natural frequencies particularly for larger structures and these may not be detected

due to measurement errors. Another drawback is that natural frequencies are easily affected by environmental changes such as temperature or humidity fluctuations

In order to identify the location and size of damage in a beam type structure, Kim and Stubbs (2003) developed frequency based damage detection method. The method functioned well for single damage scenarios however multiple damage scenarios were not successfully addressed. An extension of this work was conducted on model plate girder to predict the severity of damage using natural frequencies (Kim et al., 2007). In that study, authors also attempted to filter the effect from environmental temperature fluctuations. Both damage localization and severity estimation results were accurate when pre damage and post damage frequencies obtained at same temperature. However that accuracy decreased when temperature gap increased.

A new approach based on auxiliary mass spatial probing using the spectral centre correction method (SCCM), to provide a simple solution for damage detection using the time history of beam-like structures was attempted by Zhong et al. (2008). The efficiency and practicability of the proposed method was evaluated using a numerical simulation. It was difficult to locate a crack directly from these natural frequency curves, therefor derivatives of natural frequency curves were proposed. It was identified that the method enables clear and unambiguous identification and location of cracks in a beam-like structure.

A novel approach based on the curvature of frequency shift surface (FSS) was used to detect damage in plate structures by Zhang et al. (2013). The method was verified both numerically and experimentally. This method used the curve fitting technique based on local regression to simulate the FSS curvature for the intact state; therefore it requires only the data from the damaged state. Results illustrated, the curvature of FSS is sensitive to local damage and it can be used to detect local damage successfully.

Previous literature illustrates the presence of environmental effects, measurement noise and random errors affects the precise estimation of small differences in frequency variations. However, recent literature demonstrates it can be achieved by applying multivariate statistical tools to long time histories with data continuously collected from SHM systems. Further it describes variation of natural

frequencies are lower than 0.4% can be detected successfully (Magalhães et al., 2012).

2.5.2 Damping Based Methods

Damping has also being used as an indicator of damage. When damage occurs in a structure damping ratios are increased, however use of that towards damage detection has not achieved much successful in the literature. Salawu and Williams (1995) conducted forced vibration test on a multi span reinforced concrete highway bridge before and after the structural repairs. Results were found that there was no identifiable pattern in changing modal damping ratio. Successful application of damping ratio as a damage indicator has been proved by Razak and Choi (2001) and Curadelli et al. (2008).

2.5.3 Direct Mode Shape Based Methods

A mode shape is a deflection pattern of a structure corresponds to particular natural frequency. If a structure is damaged, changes in mode shapes will occur in the vicinity of damage. There are two popular methods available to compare two sets of mode shapes namely; the Modal Assurance Criterion (MAC) and the Coordinate Modal Assurance Criterion (COMAC). The Mac has been originated in early 1980s is defined as;

$$MAC(i,j) = \frac{\left(\{\phi_i^A\}^T\{\phi_j^B\}\right)^2}{\left(\{\phi_i^A\}^T\{\phi_i^A\}\right)\left(\{\phi_j^B\}^T\{\phi_j^B\}\right)} \qquad 2.1$$

In the above equation, $\emptyset_i^A$ is the i^{th} mode shape of the structure before damage, while $\emptyset_j^B$ is the j^{th} mode shape of the structure after damage. MAC is a scale factor from 0 to 1 and a measure of similarity of two mode shapes. MAC is equal to 1 implies a perfect match and 0 means mode shape dissimilarity. Allemang (2003) described the variety of uses of MAC in different applications. Some uses such as validation of experimental modal models, correlation with analytical modal models (mode pairing), optimal sensor placement and structural fault/damage detection are promising in SHM. West (1986) and Wolff and Richardson (1989) conducted preliminary investigation of mode shapes in damage detection using MAC.

The coordinate modal assurance criterion (COMAC) was proposed by Lieven and Ewins (1988) is;

$$COMAC(i) = \frac{\left(\sum_{i=1}^{n}\{\emptyset_i^A\}_r^T\{\emptyset_i^B\}_r\right)^2}{\left(\sum_{i=1}^{n}\{\emptyset_i^A\}_r^T\{\emptyset_i^A\}_r\right)\left(\sum_{i=1}^{n}\{\emptyset_i^B\}_r^T\{\emptyset_i^B\}_r\right)} \quad 2.2$$

In the Equation 2.2, $\{\emptyset_i^A\}_r$ is the i^{th} component of the r^{th} undamaged mode shape; $\{\emptyset_i^B\}_r$ is the i^{th} component of the r^{th} damaged mode shape; n is the highest mode number of interest. It is possible to identify structural damage location where the COMAC is close to zero.

Salawu and Williams (1995) conducted the full scale forced vibration test before and after structural repair on a multi span reinforced concrete highway bridge and investigated damage detection capability of MAC and COMAC it was observed that the MAC indicated changes and suggested the modes that were most influenced by the repairs. Further, the COMAC values were found to give good indications of the presence and location of the repairs.

Choi et al. (2005) presented a method based on the changes in the distribution of the compliance of the structure as an index. The changes in the compliance distribution were obtained using the mode shapes before and after damage. The proposed index was verified by numerical examples (simply supported beam and a continuous two span beam) and experimental data (free-free beam structure). The results showed that the compliance index could identify damage location and severity estimation. Both the numerical and experimental studies revealed that the compliance index could identify single and multiple damage locations. Further, authors suggested that the performance of locating and quantifying damage may be improved when composite DIs used simultaneously.

Kim et al. (2006) formulated a vibration based damage evaluation method to detect, locate and quantify damage using the lower frequency ranged mode shapes. The method proposed by them provided a single representative DI using more than one mode. It intended to resolve the mode selection problem, the singularity problem, the axial force problem, and the absolute severity estimation problem. Furthermore, the proposed method did not require any special knowledge about mass density, applied axial force or foundation stiffness. In order to obtain good damage accuracy results, a dense measurement of grid and the accurate extraction of the mode shapes were essential.

Previous literature illustrates the mode shapes are more uncertain and can be influenced by the environmental noise and hard to capture mode shapes using limited no of sensors. However newly introduced different mode shape construction methods (Bai et al., 2014; Yang et al., 2014) enable them to be used in damage detection process accurately.

2.5.4 Curvature Mode Shape Based Methods

The Mode shape curvature was identified as an effective method in locating damage of a structure. This is based on the assumption that damage only affects the stiffness of the structure. The Curvature of mode shapes is derived using central difference approximation as follows;

$$\emptyset'' = \frac{\emptyset_{(j+1)i} - 2v\emptyset_{ji} + \emptyset_{(j-1)i}}{l^2} \quad 2.3$$

Where $\emptyset$ is the mode shape component, i being the mode number, j the node number at two adjacent elements and l is the distance between the nodes. The location of the damage is then detected by the largest computed absolute difference between the curvature mode shape of the damaged and undamaged states of the structure as follows:

$$\{\Delta\emptyset''\} = |\{\emptyset_d''\} - \{\emptyset_u''\}| \quad 2.4$$

Pandey et al. (1991) successfully applied absolute change in mode shape curvature to localize damage in cantilever and simply supported beam models. Abdel Wahab and De Roeck (1999) examined the mode shape curvature method to actual measured data on a prestressed concrete bridge.

Hamey et al. (2004) used mode shape curvature based method to identify damage in carbon/epoxy composite beam experimentally and conclude that these methods can be effectively applied in health monitoring of composite simple beam structures with single damage scenarios.

Investigations by Alvandi and Cremona (2006) stated that, this method has low probabilities of correct estimation of damage location with high noise levels and this has been critical with complex and simultaneous damage cases.

The mode shape curvature method was applied to detect honeycomb damage in reinforced concrete beam model by Dawari and Vesmawala (2013). The numerical results demonstrate the mode shape curvatures changes are observed to be highly localized to the region of damage.

Cao et al. (2014) proposed the improved form of mode shape curvature, using Wavelet Transform (WT) and a Teager Energy Operator (TEO) to detect cracks in beams. The new method was named as the TEO-WT curvature mode shape which has higher immunity to noise and sensitivity to multiple damage scenarios. The new method was tested analytically in cantilever beams, experimentally in steel beams. The test results proved the proposed method was sensitive to multiple damage scenarios and robust against noise.

2.5.5 Flexibility Based Methods

Dynamically measured flexibility matrix to estimate the changes in a structure is another method of vibration based damage detection. Modal flexibility is a modal derivative, made of natural frequencies and mass normalized mode shapes. Modal flexibility, F_x at a location x of a structure can be written as;

$$F_x = \sum_{i=1}^{m} \frac{1}{\omega_i^2} \phi_{xi} \phi_{xi}^T \qquad 2.5$$

Where i ($i=1, 2, 3 \ldots m$) is the mode number considered. m and ω_i are the total number of modes considered and the natural frequency of the structure at mode i, respectively. Theoretically, structural deterioration reduces stiffness and increases flexibility. Increase in structural flexibility can therefore serve as a good indicator of the degree of structural deterioration.

Different combinations of equations/indices were developed by various researchers using flexibility values of damage and intact structure to identify damage during last few decades. Pandey and Biswas (1994) presented the flexibility matrix for detecting the presence and location of structural damage and concluded that this

method can be applied successfully to real life structures. It has been used by a number of researchers for damage localization in beam and plate like structures (Farrar & Jauregui, 1998; Pandey & Biswas, 1995; Shih et al., 2009; Toksoy & Aktan, 1994).

Patjawit and Kanok-Nukulchai (2005) proposed a method to monitor the global weakening of a bridge structure. A Global Flexibility Index (GFI) was proposed based on the spectral norm of the flexibility matrix. The modal flexibility matrix was evaluated from the dynamic responses at these reference points under forced vibration. A laboratory study was conducted using a simple steel beam and a reinforced concrete beam to validate the proposed method. The results indicated that change in the GFI value was sufficiently sensitive to identify the global weakening of the structure, caused by deteriorations.

Choi et al. (2008) developed a new damage indicator combining DI method and changes in flexibility to locate and evaluate damage in timber structures. Method was capable in identifying four damage locations simultaneously. However severity estimation was less effective as number of damage locations increased.

Relative flexibility change (RFC) between intact and damaged state of the cable stayed bridge was studied by Ni et al. (2008). The RFC index performs well for locating damage in single-damage cases in the absence of ambient effects however some difficulties were encountered in detecting and locating damage at cross girders. This study highlighted the importance of acquiring the modal data of the intact and damaged structure under the same or similar ambient conditions. Moragaspitiya et al. (2013) successfully developed a modal flexibility based index to predict axial shortening of vertical load bearing elements of reinforced concert buildings.

Montazer and Seyedpoor (2014) developed a new DI named as strain change based on flexibility index (SCBFI) which used for locating multiple damage cases of truss systems. The damage detection capability of the SCBFI was verified using two numerical test examples. Results showed the SCBFI index used only three modes to locate multiple damage in truss systems even with noisy data.

Recently, Sung et al. (2014) developed a method based on modal flexibility to detect damage in cantilever beam type structures. It was successfully applied to

identify damage in a 10-storey building by both numerically and experimentally for single and multiple damage cases.

2.5.6 Modal Strain Energy Based Methods

Modal strain energy based damage detection methods were developed based on the relative difference in modal strain energy before and after damage. A mode shape stores large amount of energy in a particular load path. In a damage situation, modal strain energy in that load path alters due to sensitivity of the frequency and shape of that mode. Therefore changes in modal strain energy also be considered as a logical indicator of locating damage of structures (Carden & Fanning, 2004).

Development of damage detection algorithms based on modal strain energy was pioneered by Stubbs et al. (1992) and applied to localize the damage in steel bridge (Stubbs et al., 1995). This application was only for one dimensional structural system which is exhibiting flexural behaviour. Cornwell et al. (1999) extended this method to two dimensional plate like structure and verified it by testing for experimental data.

Stubbs and Kim (1996) presented modal strain energy based DI to identify damage in an elastic beam-type structure. This method required the determination of more complete mode shapes hence an interpolation using cubic polynomials was used to determine mode shape values between sensor locations. Statistical methods were then used to examine changes in the DI and to associate these changes with possible damage locations. Both damage location and severity were identified precisely from the proposed approach.

Shi et al. (1998) used the modal strain energy change to detect, locate and quantify damage (Shi et al., 2002) successfully. Investigations have been conducted on numerical example and an experiment on a single-bay two-story portal steel frame structure. Results indicate that the proposed approach is noise sensitive, however it can locate single and multiple damage cases. The results demonstrated that the algorithm was effective and robust for quantifying damage with a maximum of 14% error under a 5% measurement noise.

Kim and Stubbs (2002) expanded their method using an improved algorithm with an objective of improving the accuracy of locating and quantifying damage by eliminating limits in the existing algorithms. A two span continuous beam was used

to verify the accuracy of the new algorithm numerically. The results presented that the new algorithm improved the accuracy of locating and quantifying damage compared to the existing damage detection algorithms. However, the method was not validated with experimental results.

The DI proposed by previous researchers have been modified by Jianchun et al. (2005) and its application on timber structures were tested. The results of numerical investigations revealed that the modified algorithm was capable of overcoming the problems associated with reliable detection of multiple damages in terms of damage location and severity. The study also investigated that the cubic spline method was suitable technique for reconstructing mode shapes with finer coordinates.

Li et al. (2006) introduced a modal strain energy decomposition method to detect damage in a 3D frame structures. This method was based on decomposing the modal strain energy of each structural member in to two components. Two damage indicators namely; axial damage indicator and transverse damage indicator were calculated for each member to locate the damage. The method required only few mode shapes of damaged and baseline structures to detect damage. The numerical results of the 3D five storey frame structure revealed that the axial damage indicator was able to locate damage occurring in horizontal elements, and the transverse damage indicator was able to locate damage occurring in vertical elements. However, damage quantification was not addressed.

Modified damage index (MDI) method based on modal strain energy, was developed by Choi et al. (2007) to detect damage in a timber beam. Performance of the MDI was investigated experimentally and mode shape reconstruction technique was utilized to enhance the capability of damage detection algorithms. The MDI method was found to perform better than their original form for locating single and multiple damage scenarios. However this method was not effective for the very small damage cases.

Shih et al. (2009) proposed a multi-criteria approach to detect damage in beam and plate structures. The approach was based on three non-destructive damage detection methods to avoid the discrepancies occur in using above methods individually. The multi-criteria approach used frequency to detect the presence of damage while modal strain energy and modal flexibility used to locate the damage. The novel approach was successful in detecting damage in beam and plate structures.

However, the study concluded that the more investigations need to be done for multiple damage scenarios since they are more complex than single damage scenarios.

L. Wang et al. (2010) presented an improved modal strain energy correlation method (MSEC) where the prediction of modal strain energy change vector was differently obtained by running the eigensolutions on-line in optimisation iterations. In this method genetic algorithm was used to operate the iterative searching process. The results demonstrate that the improved MSEC method sufficed to meet the demand in detecting the damage of truss bridge structures, even under the noisy measurement data.

Wahalthantri et al. (2012) proposed a new DI called the Generalized Damage Localization Index (GDLI) based on the probabilities of condition detection results of the Modal Strain Energy based Damage Index (MSEDI) to detect damage in reinforced concrete structures. Further, that work proposed a sequential curve fitting technique to minimize the impact of noise on calculation of mode shape curvatures for subsequent calculation of MSEDI. The proposed method was numerically verified by a simply supported beam. The results depicted improved damaged detection capabilities in reinforced concrete beams, however higher noise levels and lower damage severity indicates increased false alarms.

Wahalathantri et al. (2015) proposed a novel base line updating method to solve the problems associated with constant baseline method for calculating the MSEDI to locate flexural cracks in reinforced concrete structures. Numerical simulation was used to verify the new method which indicates the potential to detect both crack formation and propagation of the reinforced concrete structures.

Table 2.2 Summery of VBDD methods

Method	Advantages	Disadvantages
Natural Frequencies	• Simplest parameter to identify in modal analysis • Complicated sensors not required to capture the natural frequencies • Less statistical variation from random error sources • Easy to identify in ambient vibration test • Frequency variations less than 0.4% can be identified successfully in long time monitoring systems • Addresses the Level 1 damage detection problems	• Not sensitive to small damage • Detection of damage at Level 2 and Level 3 is challenging • Cannot distinguish damage at symmetrical locations in a symmetric structure
Damping Factors	• Fundamental parameter to identify in modal analysis • Addresses the Level 1 damage detection problems	• Determination of damping ratio in real structures is unreliable • Very few method have been developed and difficult to use in practical applications
Mode Shapes	• Convenient to identify parameter in modal analysis • Combination of MAC and COMAC work more effectively in damage detection • Addresses the Level 2 damage detection problems	• Requires more sensors to measure mode shapes • Affected by measurement noise • Not sensitive enough to detect damage in their early stages • Hard to accurately detect higher modes

Method	Advantages	Disadvantages
Modal flexibility	• Addresses the Level 2 damage detection problems • Few modes required to estimate the flexibility matrix • Sensitive to damage using incomplete modal measurements • More sensitive to local damage	• Insensitive to damage such as concrete cracks • Required well distributed sensors • Require mass normalized mode shapes
Modal Strain Energy	• Addresses the Level 3 damage problems • Only require limited modal characteristics	• Incomplete measurement and noise affects the performance • Accuracy depends on the mode shape data • Require higher order modes for accurate damage detection
Modal Shape Curvature	• Localizes the damage accurately • More sensitive to local damage • Higher order modes are sensitive to damage	• Comprehensive measurement grid is required for effective estimation • Need complete mode shape data for reliable estimation

2.6 APPLICATION OF VBDD METHODS IN SUSPENSION BRIDGES

This section presents the different applications of VBDD methods in detecting and locating damage in suspension bridges. The research work conducted by other researchers previously enable to identify a best performing VBDD method to use in this study and to identify the extent of the damage detection of cables and hangers are treated. Also to consider which vibration mode need to me considered in this study.

Quan and Weiguo (1998) used three wave form detection indices based on the frequency response function (FRF) namely; wave form chain code (WCC), the adaptive template method (ATM) and signature assurance criteria (SAC) and three mode shape based methods namely; coordinate modal assurance criteria (COMAC), the flexibility and the curvature of mode shapes to detect damage in deck of the Tsing Ma suspension bridge. The results revealed that the WCC and ATM are more sensitive to damage, however they were incapable in locating damage in the deck. Among three different mode shape based DIs, the flexibility and the curvature of mode shapes were sensitive to the damage and are able to locate damage in the deck successfully. The study focused only on damage detection in deck of Tsing Ma Suspension Bridge due to higher design safety factors in main cables and towers. However, due to structural deterioration literature indicates there were failures in main cables and hangers of suspension bridges which need to be addressed in damage detection.

B. S. Wang et al. (2000) did a comparative study of different DIs for long span bridges. A validated 3 D FE model of Tsing Ma Bridge was used for the simulation studies. Damage to the structural elements was modelled by assuming a reduction in the member stiffness but no change in mass. Six damage scenarios were introduced. Two on vertical and side bearing (Ma Wan tower disconnection), three on deck and one on hangers were simulated. Six mode shape based damage detection methods were selected for the study. Coordinate Modal Assurance Criteria (COMAC) and Enhanced Coordinate Modal Assurance Criteria (ECOMAC) identify damage in the deck only. Change in Flexibility and Stiffness methods identify damage in the deck and vertical bearing. Strain energy based DI and Mode Shape Curvature Methods successfully located all the damage scenarios but some errors had been observed in detecting damage in the hanger and side bearing. Therefore, the research concluded that the Strain energy based DI Method and Mode Shape Curvature Method are more suitable for detection of damage in suspension bridges. However, cable damage and damage quantification were not addressed in that study.

J. Y. Wang et al. (2000) conducted sensitivity analysis of three different modal parameters including frequency, mode shapes and modal flexibilities in damage detection using Tsing Ma long span suspension bridge. 3D FE model was developed and validated by using the measured modal data obtained at different erection stages

of the bridge. Ten damage scenarios occurring at bearings, hangers and deck members were simulated in the validated FE model. The study proved that the flexibility method was more sensitive to damage than natural frequency and mode shape. Sensitivity of natural frequency is relatively low for damage and using frequency information alone was not enough to locate the damage. However cable damage was not addressed in this study.

Ni et al. (2001) proposed method based on probabilistic neural network (PNN) based on frequency to detect damage in deck of Tsing Ma Suspension bridge. The traditional PNN and adaptive PNN were applied to detect damage in several locations of the deck. The investigations show that the classification accuracy is better in adaptive PNN and it was perfect in when measured data were heavily polluted. That is even when the natural frequency measurement noise level is larger than the damage caused frequency change; the deck damage was successfully located by adaptive PNN. Subsequently, deck damage was treated only in this study and it is necessary to focus damage detection in other components of a suspension bridge.

Yeung and Smith (2005) developed a method using vibration signatures together with neural network pattern recognition to identify damage in a suspension bridge under moving traffic. A successful damage detection criterion was obtained. Only damage in the main girder and parapet girder were addressed.

A numerical study to investigate the interaction between damage location, size and the mode of vibration in a simple suspended cable was conducted by Bouaanani (2006). Twelve types of cable with variety of bending stiffness and sag extensibility were considered in the study. The impact of the damage in the percentage change in frequency and mode shapes of twelve cable types with various bending stiffness and sag extensibility were studied with single damage at varied locations along the cable. Study was able to identify some definite trends for lateral vibration modes. Damage was simulated at each numerical model by 50% reduction in cross sectional area and 75% reduction in moment of inertia. The study was limited only to the suspended cable with high damage severity and single damage scenarios.

Lepidi et al. (2009) identified that the damage in the suspended cables could be determined through information selected in the dynamical response. This damage was described as a reduction of cable cross section as shown in Figure 2.4 below. A frequency based procedure was used to identify the damage parameters. The

possibility of effectively identifying the damage intensity and extent was confirmed. The effectiveness of the damage detection procedure was tested on real cables through an experimental test. Study was limited only to the cables, without entire structure.

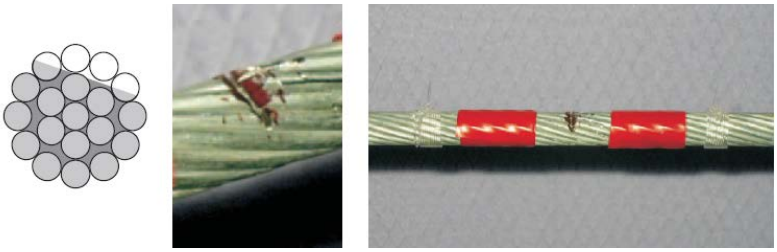

Figure 2.4 Artificially induced damage in a cable (Lepidi et al., 2009)

Materazzi and Ubertini (2011) studied the vertical vibration of a suspension bridge with damaged main cables by the continuum formulation. A parametric study was conducted to investigate the sensitivity of natural frequencies and mode shapes to the damage in the cable. From that study they concluded that the use of frequency variations for damage detection appears to be, in the case of suspension bridges, comparatively more promising than that of mode shape variations. However, application of continuum formulation is limited to two dimensional models of suspension bridges.

Chan et al. (2011) has developed a novelty index based auto associative neural network based on the frequency data obtained from validated FE modal analysis of Tsing Ma Bridge. They created five neural networks to cater for the different vibration modes. Fifteen damage scenarios were introduced to the FE model including damage at bearings, tower, deck, hanger and side span cable. Where the maximum frequency change ratio between damage and undamaged state was less than 0.3% damage was not captured. If it was in between 0.3% and 1.0% damage was just detectable. Damage was detected accurately when maximum frequency change ratio exceeds 1.0%. Therefore damage at hangers, some locations in the deck and vertical bearings was not detected successfully. This study also did not address the main cable damage and use frequency data alone to develop the system for damage detection.

A numerical study of applying four VBDD methods to detect damage in the New Carquienz Bridge was examined by Talebinejad et al. (2014). VBDD methods used in this study are the flexibility method, the stiffness method, uniform load

surface and uniform load surface curvature method. The damage scenarios considered in the hangers with damage intensity of 50%, 75%, 90% and 100% are successfully identified using all four methods even in the multiple damage scenarios. The main cable damage at mid span with 90% damage intensity was only detected by uniform load surface curvature method; however none of the methods were able to identify damage in tower leg. The damage with 90% severity at bulkhead was detected by the flexibility and stiffness methods. It was observed that all the methods were successfully identified the deck damage with 90% damage severity. Multiple damage scenarios were only considered in hanger damage and all the damage scenarios considered are very high in severity. Low to moderate damage severities at cables and hangers should be treated extensively to identify damage at early stages.

A continuum model describing the finite vertical and torsional vibrations of single span suspension bridges with damage in a main cable has been studied by Ubertini (2014). It was observed that variation of frequencies in symmetric modes due to damage is comparatively more significant. The study investigated the most damage sensitive frequency among vertical vibration modes is frequency of the second symmetric mode and that of torsional vibration modes is the frequency of first symmetrical mode. It was concluded that the relative severe damage can be detected by frequency changes in suspension bridges otherwise it needs to collect long term data from SHM system to eliminate the environment conditions. The study reviewed only the efficiency of different modes of both vertical and torsional vibration in damage detection of cables using a continuum model. Further investigations need to be done incorporating different vibration modes of the suspension bridges.

Ni et al. (2015) conducted a feasibility study on detecting and locating structural damage of long span cable-supported bridges using multi-novelty indices. An improved novelty index was formulated in terms of auto-associative neural networks (ANNs) for damage alarming. They created five neural networks to cater for the different vibration modes. Fifteen damage scenarios were introduced to the FE model including damage at bearings, tower, deck, anchorage bearing, hangers, railway beams and side span cable. In this study the ANN-based novelty detectors were successfully alarm the damage if the damage caused maximum modal frequency change ratio is greater than 1.0%. When the maximum modal frequency

change ratio is between 0.3% and 1.0%, damage alarming capability was weak. No any damage was detected if the maximum modal frequency change ratio is less than 0.3%. In this study, damage region was identified by multi-novelty indices in terms of modal flexibility values derived using the measured modal frequencies and incomplete mode shape components. In order to study the competency of multi-novelty indices, damage in the deck region was examined and it was successfully identify the damage region by these indices. However damage locating in cables and hanger are remaining unsolved.

2.7 REMARKS OF THE LITERATURE REVIEW

From the above literature review, the following remarks can be made and addressing them is the motivation for this research.

- It is identified that main cables and hangers of suspension bridges are more prone to severe corrosion. Further, they are practically inaccessible for visual inspection and do not produces any evidence of damage on the exterior during conventional visual inspections. In addition, main cables are employed with corrosion protection system which shields the load carrying wires from sight during visual inspections. Apart from corrosion, these elements are susceptible to long term fatigue damage after many years in service. Since, improvements in design methodologies and construction technologies itself have not been able to increase the reliability and safety of suspension bridges. These facts reveal the requirement of SHM for the safer performance of suspension bridges in an infrastructure system.
- The majority of long span suspension bridges are instrumented with the SHM system and the technology of SS, DATS, DPCS and DM has developed very rapidly. However final step (SES) in the SHM system needs further development, especially the area of research in damage detection for large civil structures like suspension bridges.
- Damage detection methods can be categorized as local or global methods. Local methods require prior localization of the damaged zones, are time consuming and expensive. Therefore, application of local methods on damage detection is inefficient for the large civil structures. Since uses of

global method is more appropriate in this regard. These methods also fall to different categories. Among these categories, vibration based approaches associates with DI based on VBDD methods are more promising.

- DIs can be formulated using different primary vibration properties as well as secondary vibration properties. Based on the literature review on most commonly used VBDD methods it was identified that they have been applied successfully to beam and plate elements, trusses and simple structures in reinforced concrete steel and timber. Not much focus on damage detection of large civil structures can be identified in the literature.
- Limited research has been conducted in the damage detection process of suspension bridges using vibration response. Successful application of VBDD methods to detect damage in deck (main girder), towers, bearings, and bulk heads was identified in the literature. However, damage detection of main cable and hangers was not fully examined for single and multiple damage scenarios under moderate damage severity conditions.
- Two recent studies were focused on influence of vertical and torsional vibration modes for damage detection of suspension bridge main cables using continuum approach. Further, recent tests on suspension bridges also verify that early modes of vibration consist of different modes namely; vertical, lateral, torsional and coupled modes. These reveal that it is worth developing a VBDD based damage detection method considering different vibration modes of suspension bridges. None of the studies have successfully developed a method for damage detection when damage occurs in the main cable and hangers considering their particular dominant modes of vibration.

Based on the literature review findings, a compressive research is proposed to bridge the gaps in the knowledge. In the process, modal flexibility and mass (modal) participation in different modes is chosen as basis to derive effective DIs to address damage detection problem in main cables and hangers of suspensions bridges. Single and multiple damage scenarios, influence of 5% noise in the modal data, influence of cable parameters and impact of higher vibration mode in damage detection are the

other parameters need to be examined. Therefore, four objectives of the research are defined based on the key features of the literature review.

Chapter 3: Theory of Damage Detection and Finite Element Modelling of Suspension Bridges for SHM

3.1 INTRODUCTION

Among different vibration based damage detection (VBDD) techniques, modal flexibility has been one which has shown the potential for successful damage detection. This study therefore uses the modal flexibility method. It develops and applies two component specific DIs, which incorporate the lateral and vertical components of the mode shapes, to detect and locate damage in suspension bridges. This chapter first, presents the background and theory on modal the flexibility method and derivation of mode shape component specific DIs. Next, it describes two different FE modelling techniques focused on SHM of suspension bridges namely; spine beam models and hybrid models. Afterwards, it explains the theoretical basis of the modal analysis technique used in this study to obtain vibration parameters of the damaged and undamaged states of a suspension bridge. The different element types used to simulate suspension bridge FE models in this study are next presented. Finally, the importance of the model updating process and the different model updating methods are described.

3.2 PRINCIPLES OF VIBRATION

Vibration of a structure with *N* degrees of freedom (DOF) is governed by the equation of motion;

$$[M]\{\ddot{u}\} + [C]\{\dot{u}\} + [K]\{u\} = \{P\} \quad 3.1$$

In the Equation 3.1, $[M]$ is the mass matrix, $[C]$ is the damping matrix, and $[K]$ is the stiffness matrix and $\{P\}$ is force vector. Also,$\{u\}$, $\{\dot{u}\}$ and $\{\ddot{u}\}$ are the displacement, velocity and acceleration vectors respectively. All these matrices and vectors have an order of *N* in size, corresponding to the number of DOF of the structure.

For the free vibration with absence of damping the Equation 3.1 reduces to;

$$[M]\{\ddot{u}\} + +[K]\{u\} = \{0\} \quad 3.2$$

The equation 3.2 can be used to determine the vibration properties namely; natural frequencies and mode shapes of a structure. According to the literature review on vibration based damage detection methods, it has been identified that modal flexibility which depends on both the natural frequencies and mode shapes has promising feature such that rapid convergence with increasing natural frequency. Therefore it is appropriate for damage detection of large civil structures like suspension bridges, however application of this method in these bridges which has different vibration modes is challenging. In this study, validated FE models were utilized to extract vibration properties to compute the modal flexibility based DIs. The next section of this chapter presents the derivation of the modal flexibility matrix and associated DIs used in this study for damage detection in the main cables and hangers of suspension bridges.

3.3 MODAL FLEXIBILITY METHOD

The modal flexibility (MF) method is a widely accepted technique in damage detection which associates vibration characteristics of a structure that include natural frequencies and mass normalized mode shapes. MF of a structure converges rapidly with increasing frequency and can be therefore computed using a few lower natural frequencies and mass normalized mode shape vectors (Pandey & Biswas, 1994). It does not require any analytical model of a structure to evaluate the flexibility and can be used with only the experimental data collected from the structure (data from experimental modal analysis can be used directly in computing modal flexibility). However, online monitoring systems instrumented in large scale structures can only measure ambient vibration response which means mass normalized mode shape data are not available. In order to improve the application of the MF method in large scale structures, many researchers (Doebling & Farrar, 1996; Gao & Spencer, 2002; Parloo et al., 2005; Yan & Golinval, 2005) developed various methods to calculate the modal flexibility with ambient vibration measurements with and without use of FEM. The MF method is widely used in SHM application due to its accuracy, convenient computation and ease of application (Moragaspitiya et al., 2013). Derivation of flexibility matrix is as follows (Shih, 2009);

The solution of equation 3.2 is

$$\{u\} = \{\phi\} sin\omega t \tag{3.3}$$

Substituting Equation 3.3 into Equation 3.2, it becomes

$$[K][\phi] - [\omega^2][M][\phi] = 0 \tag{3.4}$$

Multiplying Equation 3.4 by $[\emptyset]^T$ yields:

$$[\phi]^T[K][\phi] - [\omega^2][\phi]^T[M][\phi] = 0 \tag{3.5}$$

For normalized eigenvectors, the orthogonality condition is given by

$$[\phi]^T[M][\phi] = [I] \tag{3.6}$$

Substituting Equation 3.6 in to Equation 3.5 yields:

$$[\phi]^T[K][\phi] - [\omega^2][I] = 0 \tag{3.7}$$

$$[\phi]^{-1}[K]^{-1}[\phi]^{-T} = \left[\frac{1}{\omega^2}\right][I] \tag{3.8}$$

$$[K]^{-1} = [\phi]\left[\frac{1}{\omega^2}\right][\phi]^T \tag{3.9}$$

Modal flexibility can be written as;

$$[F] = [\phi]\left[\frac{1}{\omega^2}\right][\phi]^T \tag{3.10}$$

Modal flexibility, F_x at a location x of a structure can be written as

$$F_x = \sum_{i=1}^{m} \frac{1}{\omega_i^2} \phi_{xi} \phi_{xi}^T \tag{3.11}$$

In the above equation, i ($i=1, 2, 3 \ldots m$) is the mode number considered. In complex structures measured modes are less than the analytical modes available, with only a limited number of lower order modes being measured practically (Ni et al., 2002). In the above equation, m and ω_i are the total number of modes considered and the natural frequency of the structure at mode i, respectively.

When a structure is subjected to damage or deterioration, its stiffness is reduced and the flexibility is increased. This alters its vibration characteristics. The

resulting modal flexibilities of the structure are represented in Equations 3.12 and 3.13 respectively at the damaged and undamaged states of the structure.

$$F_{xD} = \left[\sum_{i=1}^{m} \frac{1}{\omega_i^2} \phi_{xi} \phi_{xi}^T\right]_D \quad 3.12$$

$$F_{xH} = \left[\sum_{i=1}^{m} \frac{1}{\omega_i^2} \phi_{xi} \phi_{xi}^T\right]_H \quad 3.13$$

Here, subscripts D and H denote the damaged and undamaged (healthy) states of the structure respectively. Equation 3.14 below captures the change in modal flexibility of the structure due to damage.

$$F_{xD} - F_{xH} = \left[\sum_{i=1}^{m} \frac{1}{\omega_i^2} \phi_{xi} \phi_{xi}^T\right]_D - \left[\sum_{i=1}^{m} \frac{1}{\omega_i^2} \phi_{xi} \phi_{xi}^T\right]_H \quad 3.14$$

In this study, F_{xD} - F_{xH} is normalized by the F_{xH} and hence the damage index for locating damage in a structure is written as in Equation 3.15.

$$DI = \frac{\left[\sum_{i=1}^{m} \frac{1}{\omega_i^2} \phi_{xi} \phi_{xi}^T\right]_D - \left[\sum_{i=1}^{m} \frac{1}{\omega_i^2} \phi_{xi} \phi_{xi}^T\right]_H}{\left[\sum_{i=1}^{m} \frac{1}{\omega_i^2} \phi_{xi} \phi_{xi}^T\right]_H} \quad 3.15$$

Since suspension bridges have different vibration modes, it is very difficult to identify damage sensitive modes in a suspension bridge and in particular to measure the rotational coordinates of torsional and coupled modes practically. Most damage detection methods therefore, incorporate mode shapes that include translational coordinates. This research therefore, proposes two DIs, which are derived by

decomposing the modal flexibility of a structure into two parts. One index is based on the structure's vertical components of the mode shapes and the other is based on its lateral components of mode shapes. Equation 3.15 is hence rewritten as Equations 3.16 and 3.17 to accommodate the component specific modal flexibilities, where the subscripts *V* and *L* denote the vertical and lateral components of mode shapes, respectively.

$$DI_V = \frac{\left[\sum_{i=1}^{m} \frac{1}{\omega_i^2} \phi_{xi} \phi_{xi}^T\right]_{DV} - \left[\sum_{i=1}^{m} \frac{1}{\omega_i^2} \phi_{xi} \phi_{xi}^T\right]_{HV}}{\left[\sum_{i=1}^{m} \frac{1}{\omega_i^2} \phi_{xi} \phi_{xi}^T\right]_{HV}} \quad 3.16$$

$$DI_L = \frac{\left[\sum_{i=1}^{m} \frac{1}{\omega_i^2} \phi_{xi} \phi_{xi}^T\right]_{DL} - \left[\sum_{i=1}^{m} \frac{1}{\omega_i^2} \phi_{xi} \phi_{xi}^T\right]_{HL}}{\left[\sum_{i=1}^{m} \frac{1}{\omega_i^2} \phi_{xi} \phi_{xi}^T\right]_{HL}} \quad 3.17$$

Since damage alters the stiffness of the structure and increases its flexibility, theoretically, peaks should appear in the DI curves defined in Equation 3.16 and Equation 3.17 corresponding to the damage location. However, the mass moving in each direction for each mode (mass participation factor) varies for different vibration modes in a suspension bridge. A high value of mass participation factor in a direction indicates that the mode will be excited in that direction. The direction of which more mass (modal) contribution of a mode predict damage accurately. Hence it is worthy to study the competency of the DIs based on the vertical and lateral components of mode shapes for detecting and locating damage in suspension bridges.

This study compares the performance of the proposed component specific DIs with that of the (component specific) modal flexibility (MF) difference which is the originally developed method for damage detection by Pandey and Biswas (Pandey & Biswas, 1995; 1994). In this study, MF difference is also calculated using both vertical and lateral components of mode shapes as shown in Equations 3.18 and 3.19 respectively. These equations were obtained by rewriting the Equation 3.14 for the two specific components of the mode shapes considered herein.

$$MFD_V = \left[\sum_{i=1}^{m} \frac{1}{\omega_i^2} \phi_{xi} \phi_{xi}^T\right]_{DV} - \left[\sum_{i=1}^{m} \frac{1}{\omega_i^2} \phi_{xi} \phi_{xi}^T\right]_{HV} \quad 3.18$$

$$MFD_L = \left[\sum_{i=1}^{m} \frac{1}{\omega_i^2} \phi_{xi} \phi_{xi}^T\right]_{DL} - \left[\sum_{i=1}^{m} \frac{1}{\omega_i^2} \phi_{xi} \phi_{xi}^T\right]_{HL} \quad 3.19$$

This study, evaluates the potential of the DIs defined in Equation 3.16 and Equation 3.17 for detecting and locating damage using four case studies and compared the results with those obtained from the MF differences defined in Equations 3.18 and 3.19. These case studies include long span large diameter suspended cable, main span of a two dimensional suspension bridge, complex cable bridge model and 3D real suspension bridge.

3.4 FE MODELLING OF SUSPENSION BRIDGES

Obtaining vibration response using real structures and experimental models of a bridge to develop VBDD techniques is an expensive and time consuming procedure. Simulation of different damage scenarios in a real bridge or an experimental model is also quite a difficult process. Since the FE method has been widely accepted as an analysis tool in SHM, the above mentioned constraints can be overcome by using validated FE models to simulate a real structure.

Due to the complex configuration of suspension bridges, numerical models (FE models) usually differ from as built structures. Therefore they need to be fine-tuned to match with the real structure. However, a FE model of the bridge should be first developed based on the as built drawings. There are two categories of FE modelling techniques for suspension bridges; the spine beam type modelling and hybrid type modelling (Xu & Xia, 2011).

3.4.1 Spine Beam Model

In a spine beam model, line elements including beam elements, truss elements and rigid links are used to model the components of a suspension bridge. Usually spring elements and rigid links are necessary to connect different parts of the FE

model. More often pylons and suspenders are modelled with beam elements and truss elements respectively. It is important that the FE code should have the capability to simulate the geometric nonlinearity due to cable tension in modelling main cables.

In FE modelling, the deck of a suspension bridge is more challenging and the equivalent section property approach is more often used in modelling it. In this approach, basically the deck is modelled as beam (spine beam) suspended by suspenders through rigid links and all the section properties of the deck are assigned to that spine beam. The equivalent cross section area of the deck is calculated by adding all cross sectional areas of the deck and assigned to the spine beam. If the deck section is composite, these areas should be converted to a single material according to the modular ratio. Similarly, inertia about the vertical and transverse axes are calculated and assigned to the spine beam. Further, mass moments of inertia of the all deck members are included according to their distances from the centroid of the deck section. Figure 3.1 illustrates a detailed view of a spine beam model (Ubertini, 2008).

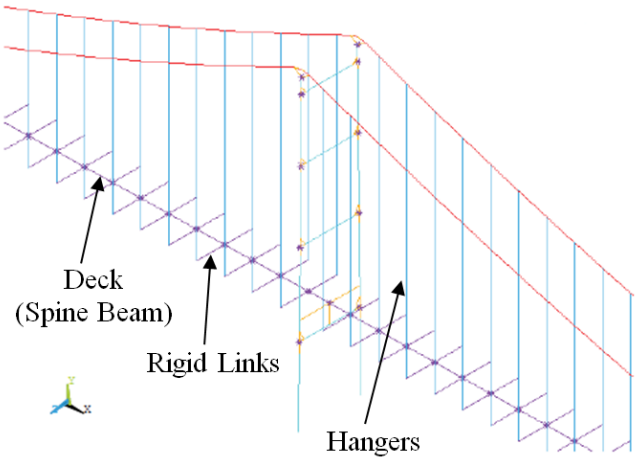

Figure 3.1 Spine beam model (Ubertini, 2008)

This simplified model type is very effective to capture the dynamic characteristics and global structural behaviour without complex computational effort. This model can therefore be used in preliminary designs and aerodynamic analysis.

3.4.2 Hybrid Model

Hybrid type modelling is very effective to capture the local responses of critical members and obtain more accurate results (Xu & Xia, 2011). These models

include the finer details of the bridge components by highlighting local behaviours. The entire bridge can be modelled by combination of line elements, shell elements and solid elements where appropriate. However special attention should be taken at the interface between different element types. Usually multipoint constraints (MPC) are used to avoid displacement incompatibility among nodes.

In this type of models, the deck plate is modelled with shell elements while the cross members in the deck are model with beam elements. Similar to the spine beam model, pylons and suspenders are modelled with beam elements and truss elements respectively. This type of modelling is very expensive and time consuming however more efficient for SHM applications. The Figure 3.2 illustrates the hybrid model of a deck segment of the Tsing ma Suspension Bridge. This model consists of combination of various element types including beam, truss and plate elements.

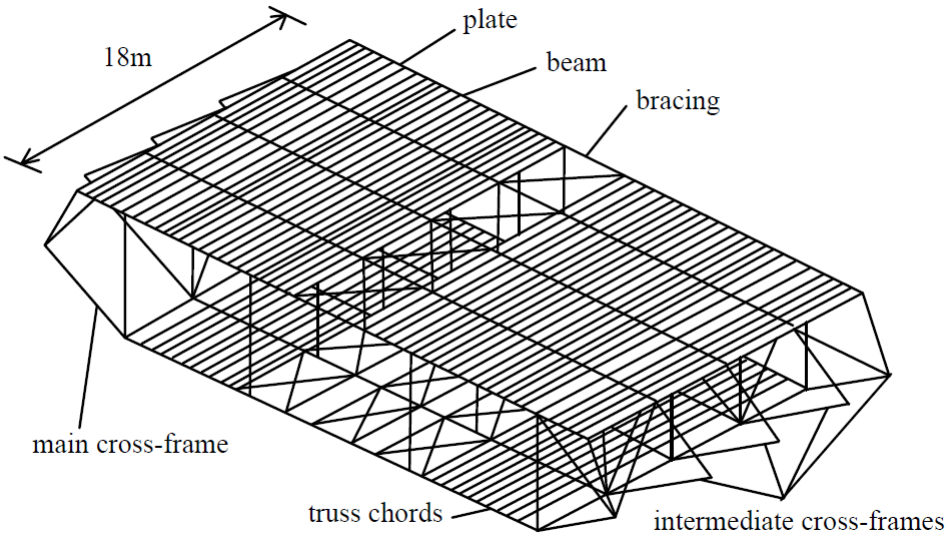

Figure 3.2 Hybrid Model - Deck segment of Tsing Ma Suspension Bridge (Xu & Xia, 2011)

In this research, hybrid type FE models were developed to obtain the vibration properties of suspension bridges to study the competency of mode shape component specific DIs (and MF differences) to detect and locate damage. All the FE models used in this study were developed in the ANSYS Workbench.

3.4.3 Pre Stressed Modal Analysis

Suspension bridges are flexible structures and hence gravity rigidity caused by dead load has a significant influence in their dynamic properties, therefore geometric nonlinearity must be considered in the analysis (H. Wang et al., 2010). Generally, an

effect named as stiffening effect is caused due to dead load and hence this effect needs to be considered for structures with small bending stiffness compared to axial stiffness, such as cables, thin beams, and shells. In a FE analysis, this influence can be taken into account through considering stress stiffening (also called geometric stiffening) which is the stiffening of a structure due to its stress state. The effect of stress stiffening is accounted by generating an additional stiffness matrix, which is named as the stress stiffness matrix. This matrix is computed based on the stress state of the equilibrium configuration of the structure and minimum of two iterations are required.

In modal analysis of a suspension bridge, influence of stress stiffening can be taken into account through conducting the static analysis under the dead load and cable tensions before conducting dynamic analysis. In the static analysis, the internal forces caused by the dead loads acting on the bridge are obtained and the stress stiffening matrix is incorporated to formulate the updated tangent stiffness matrix. Moreover, in this analysis, matrix $[K]$ in Equation 3.4 is modified by the inclusion of the stress stiffness matrix calculated by the static analysis. The modified Equation 3.4 can be written as follows (ANSYS Inc.(Canonsburg)).

$$\big[[K]+[S]\big][\phi]-[\omega^2][M][\phi]=0 \qquad 3.20$$

Where $[S]$ is the Stress Stiffening matrix. Then the modal analysis is performed for the deformed equilibrium configuration obtained by considering the effect of the dead loads acting on the bridge to extract natural frequencies and vibration modes. In the ANSYS Workbench this analysis procedure is called as pre stressed modal analysis and is conducted according to the following two steps;

- The static analysis is first conducted to obtain the initial equilibrium configuration under dead load and cable pre-tensions by turning the large deflections ‘on’ to cater geometric nonlinearities.
- The modal analysis (free vibration) is then performed starting from the deformed equilibrium position.

In this study, pre stressed modal analysis was conducted in every analysis for both damaged and undamaged states and corresponding vibration parameters were extracted to calculate component specific DIs.

3.5 FE MODELLING IN THIS STUDY

In this study, three types of elements in ANSYS Workbench (ANSYS Inc.(Canonsburg)) were used in FE modelling, namely; LINK 180, BEAM 188 and SHELL 181 where appropriate. Characteristics of these elements are described below.

LINK 180 element type is an 3D spar that can be useful to model links, springs, sagging cables and trusses in a variety of engineering applications. This element can be defined by two nodes, cross section area, added mass per unit length and material properties. LINK 180 offers tension only or compression only options and the user can specify the desired behaviour using real constants. The dominant structural action of suspension bridge main cable is tension, consequently LINK 180 element type will be used to simulate the main cables by allowing for tension only option. Additional coding is required to assign this element type in Mechanical module of ANSYS Workbench.

BEAM 188 is based on Timoshenko beam theory and has six or seven DOF at each node. This includes translations in three directions, rotations about three directions and seventh degree of freedom (warping magnitude). This element is well suited for linear, langrage rotation and large strain nonlinear applications. Therefore, BEAM 188 is more appropriate to simulate other structural elements such as deck and hangers which can carry both flexural and axial effects. Also this element can be used to simulate the large diameter cables where flexural rigidity needs to be considered.

SHELL 181 element type is used to analyse thin to moderately thick shell structures. It is a four node element with six DOF at each node. This includes translations in three directions and rotations about three directions. This element is well suited for linear, large rotation and large strain nonlinear applications. In this study SHELL 181 element type was used to model the deck and end supports of suspension bridge models.

3.6 MODEL UPDATING

Accurate FE models are required in many civil engineering applications such as conceptual designs, detailed designs, SHM, damage detection and structural evaluation (Liu et al., 2014; H. Wang et al., 2010). Dynamic responses of an FE

model can differ from the measured responses due to uncertainties in geometry, material properties and boundary conditions. Model updating is therefore required to correct the modelling errors of a FE model using measured responses to refine baseline FE model to predict static and dynamic behaviour accurately. In this process, mass, stiffness and damping parameters are basically modified in order to minimize the differences between FE model and measured responses. The most common target responses in model updating are the natural frequencies (due to the accuracy with which they can be measured) and mode shapes.

Model updating process has four stages: developing initial FE model, modal testing, manual tuning of the initial FE model and automatic updating (Pálsson, 2012). In the first step, initial FE model is constructed using information from structural drawings from designers and as built drawings from contactor. Next step is modal testing which involves obtaining the response of the structure either from forced or ambient vibration tests. The third step of model updating is the manual tuning process in which changes are made manually to the geometry and material parameters of the structure using trial and error method. In this process, engineering judgement is an important factor to improve the correlation between the model and the measured responses. In many situations, it is essential to conduct manual updating initially, to overcome convergence difficulties in automatic updating. Moreover, the geometry of the structure has to be well defined before starting the automatic updating phase. In the automatic updating phase, a set of parameters are selected to fine tune and the FE model is updated using iterative procedures towards some target response.

Automatic model updating methods are basically classified into two categories: direct methods and iterative methods. The direct methods are based on altering the mass and stiffness matrices directly to minimize the difference between analytical and measured responses. This procedure is not related to the physical parameters of the structure. The iterative methods are based on changing the parameters used as input to the model, and thus indirectly altering the mass and stiffness matrices of the FE model. Even though the iterative methods are time consuming, they are more widely used because the results can be expressed as physical parameters. Further, many FE programs do not support direct changes in the system matrices which makes it difficult to use the direct methods with existing FE models. The iterative

methods are sensitivity based; therefore a sensitivity matrix is defined to monitor the changes of the target response related to a certain parameter change. Due to large no of DOF in large scale structures iterative methods are time consuming. Therefore sub-structuring is associated with iterative model updating methods.

Initial FE models developed in this research showed reasonably good agreement of the natural frequencies with the measured frequencies. Therefore manual tuning was conducted by incorporating very minor changes to the initial FE models. The mode shapes obtained from the numerical simulation also compared reasonably well with those obtained in modal testing.

3.7 SUMMARY

This chapter presented the theory and background of the modal flexibility method and the derivation of the mode shape component specific DIs used in this research. Merits and demerits of two main SHM oriented FE model types namely spine beam models and hybrid models were discussed. Considering the accuracy as the main factor in this research, it is decided to develop hybrid type FE models to obtain the vibration properties of suspension bridges to study the competency of the proposed DIs and the MF changes. The importance of incorporating initial deformed equilibrium configuration of a suspension bridge to obtain stress stiffening matrix before conducting modal analysis was highlighted. The need for pre stressed modal analysis to obtain vibration properties of a suspension bridge in this study was hence established. Finally, the different element types used in FE modelling and model updating processes used to establish the validated FE models of this research were elaborated.

Chapter 4: Damage Detection in Cables and Hangers of a Suspension Bridge

4.1 INTRODUCTION

This chapter consists of two sections, of which the first section presents the damage detection in a long span large diameter suspended cable. Initially, a FE model of such a cable is developed and validated using field measured data are described. Afterwards, numerical simulation of four damage cases in the validated FE model at particular locations of interest is described. Next, investigation of the damage detection capability of component specific DIs (derived in chapter 3) is presented and the results are compared with that of modal flexibility difference (MF difference). The impact of random measurement noise in the modal data on the damage detection capability of the component specific DIs is next examined. Long span large diameter cables are characterized by the two critical cable parameters named bending stiffness and sag-extensibility. Finally, the influence of these parameters in the damage detection capability of the component specific DIs is evaluated by a parametric study with two single damage cases.

The second section of this chapter presents, the damage detection in hangers of a suspension bridge. To achieve this, a FE model of a 2D suspension bridge is developed and validated to obtain vibration characteristics. Similar to the previous section, few damage cases were simulated in the hangers of the 2D FE model and vibration parameters both at undamaged and damaged states were extracted. Next, investigation of the damage detection capability of vertical damage index (DI_V) is presented and compared with that of MF difference. Finally, performance of vertical damage index under noisy modal data is evaluated.

4.2 FE MODELLING OF A SUSPENDED CABLE

FE models of real structures validated with the measured vibration responses have been extensively used in damage detection studies. It reduces the cost and time associated with experimental testing and difficulties in studying different damage

scenarios in real structures. This section presents FE modelling of a long span large diameter suspended cable.

In this study, the main span cable of the Tsing Ma Suspension Bridge is simulated numerically in ANSYS Workbench. The geometric and mechanical properties of the cable were obtained from Xu et al. (Xu et al., 1997) and Bouaanani (Bouaanani, 2006). The main span length and the cable sag are 1397.8m and 112.5m respectively. Other parameters of the cable are modulus of elasticity E=200GPa, horizontal component of the tension force H_s=122.64MN, mass per unit length m=5832 kg/m and cross sectional area A=0.759m^2.

Since this is a large diameter sagged cable, flexural rigidity was taken into account by simulating it using BEAM 188 elements in ANSYS Workbench. Also this element type includes stress stiffness term which is supported for the large deflection effects in cables. It was considered as pinned at two ends which are placed at the same vertical elevation. Displacements at ends were therefore fixed in all three directions and rotations were released. The cable was divided into 100 elements of each 13.978m long in the analysis. In order to consider the geometric nonlinearity of cables, the analysis was conducted in two steps. First the nonlinear static analysis under self-weight was performed and the subsequent modal analysis was conducted using the last solution obtained at the end of the static step (pre stressed modal analysis was conducted).

4.3 VALIDATION OF THE FE MODEL OF A SUSPENDED CABLE

To validate the FE model, measured frequencies (f_{mea}) of the cable from a series of ambient vibration tests (Xu et al., 1997) with the numerical (f_{fem}) results were compared by equation.

$$f_{error} = \frac{(f_{mea} - f_{fem})}{f_{mea}} \times 100. \qquad 4.1$$

These frequencies were measured during construction when the cable has just been erected between two towers. Table 4.1 and Table 4.2 compares the results and shows that the percentage difference of the FE analysis results as less than 4.5%, confirming the accuracy of the FE model developed and validating it for use in damage detection studies.

Table 4.1 Comparison of out-of-plane frequencies of the main span cable of the Tsing Ma Suspension Bridge

Modes	Measurements (Bouaanani, 2006) Hz	FE Analysis Hz	f_{error} (%)
1(Lateral)	0.0530	0.0535	-0.95
2(Lateral)	0.1050	0.1067	-1.60
3(Lateral)	0.1560	0.1601	-2.60

Table 4.2 Comparison of in-plane frequencies of the main span cable of the Tsing Ma Suspension Bridge

Modes	Measurements (Bouaanani, 2006) Hz	FE Analysis Hz	f_{error} (%)
1(Vertical)	0.1020	0.1030	-0.98
2(Vertical)	0.1430	0.1490	-4.19
3(Vertical)	0.2070	0.2100	-1.44

4.4 DAMAGE DETECTION IN A SUSPENDED CABLE

The FE model validated in the previous section of this chapter is considered as the undamaged baseline model. Four damage cases were introduced in the cable model to synthesize the various damage scenarios. Three damage cases are single damage scenarios with 25% stiffness reduction at the mid span, quarter span and near the support of the cable. One damage case has a 10% stiffness reduction in two different locations of the cable to cater for a multiple damage scenario.

In the discussion of results, damage detection results of the component specific DIs are presented and compared with those from MF difference. The component specific DIs namely: vertical damage index and lateral damage index (defined in chapter 3) were calculated by using the vertical and lateral components of the first three vertical and lateral vibration modes respectively. Similarly, MF difference vertical and MF difference lateral were calculated using the vertical and lateral

components of the first three vertical and lateral vibration modes respectively. Following abbreviations are used in the presentation of the results.

DI_V Damage Index Vertical - calculated by using vertical components of mode shapes

DI_L Damage Index Lateral - calculated by using lateral components of mode shapes

MFD_V Modal Flexibility Difference Vertical - calculated by using vertical components of mode shapes

MFD_L Modal Flexibility Difference Lateral - calculated by using lateral components of mode shapes

4.4.1 Damage Scenarios

Damage in cables of a suspension bridge is mainly due to corrosion and fatigue, which alter the stiffness of the structure. Simulation of damage in FE models are basically done by changing the young's modulus or changing the cross section area or removing elements at damage location. This study simulates damage in the cable model by reducing Young's modulus of the damaged elements.

Figure 4.1 and Table 4.3 represent the exact locations of the damage cases considered in this study. In order to calculate the modal flexibility based DIs defined previously, the first three in-plane (vertical) and out-of-plane (lateral) natural frequencies and mode shapes were extracted from the FE analysis of both damaged and undamaged states of the cable. The maximum severity of damage considered in this study was 25% in single damage scenarios and 10% in multiple damage scenarios which cause the measurable changes in the natural frequency of the structure in reality. These values treated the moderate to low damage severities.

Figure 4.1 Cable structure with damaged elements

Table 4.3 Damage cases considered in cable model

Damage Case	Location	Severity of Damage
Single damage scenario		
DC 1	Element 50,51 (X=684.710m to X=713.09m)	25%
DC 2	Element 25 (X=332.41m to X=346.36m)	25%
DC 3	Element 1 (X=0.00m to X=13.797m)	25%
Multiple damage scenario		
DC 4	Element 25 and Element 89 (X=332.41m to X=346.36m) and (X=1245.9m to X=1259.7m)	10%

4.4.2 Damage Detection without Noise in Modal Data

Damage detection results for each damage case considered are illustrated below. Results include plots of damage indices (DI_V and DI_L) and plots of modal flexibility difference (MFD_V and MFD_L) for each damage case considered. Damage location is indicated with red dotted lines.

•Single Damage Scenarios

Three damage cases were examined to study the damage locating capability of DIs and MF difference calculated using vertical and lateral components of mode shapes.

1. Damage Case 1 (DC 1)

The first damage case studied is that in the middle of the cable with a 25% stiffness reduction of the elements 50 and 51. Numerical results of the DI_V and DI_L are shown in Figure 4.2 (a) and (b) respectively. Both graphs show the damage index

curves reach their maximum values at the nodes of the damaged location. In this case, both DI_V and DI_L detect the damage successfully at the middle of the cable, and confirm the actual location of the damage considered. Similar trends can be observed in the plots of MFD_V and MFD_L (Figure 4.2 (c) and (d)). In conclusion, both component specific DIs and MF difference are capable of detecting and locating damage for this case.

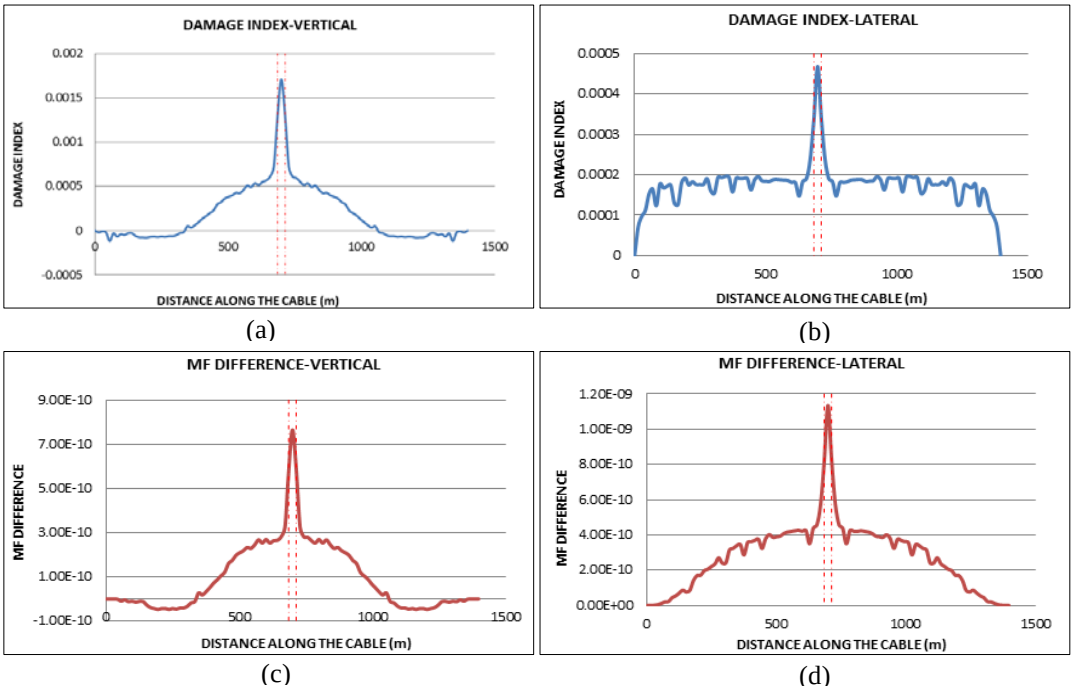

Figure 4.2 DC1 - Damage indices (a) DI_V (b) DI_L and MF difference (c) MFD_V (d) MFD_L

2. Damage Case 2 (DC 2)

Figure 4.3 (a) and (b) illustrate the DIs for the second damage case with a 25% stiffness reduction in element 25 of the cable. The curve related to the DI_V peaks not only at the damage location but also at the mid span of the cable. However, the DI_L peaks at the exact damage location being considered (element 25). Further, similar pattern of curves can be observed in MFD_V and MFD_L curves in Figure 4.3 (c) and (d) respectively. Based on the examination of the four graphs, it can be concluded that incorporating lateral components of vibration modes for detecting damage in a long span large diameter suspended cable is a successful approach using both damage index (DI_L) and MF difference (MFD_L). Therefore, competency of the DI_L in damage detection of suspended cable is further evaluated through Damage Case3 considered in this study.

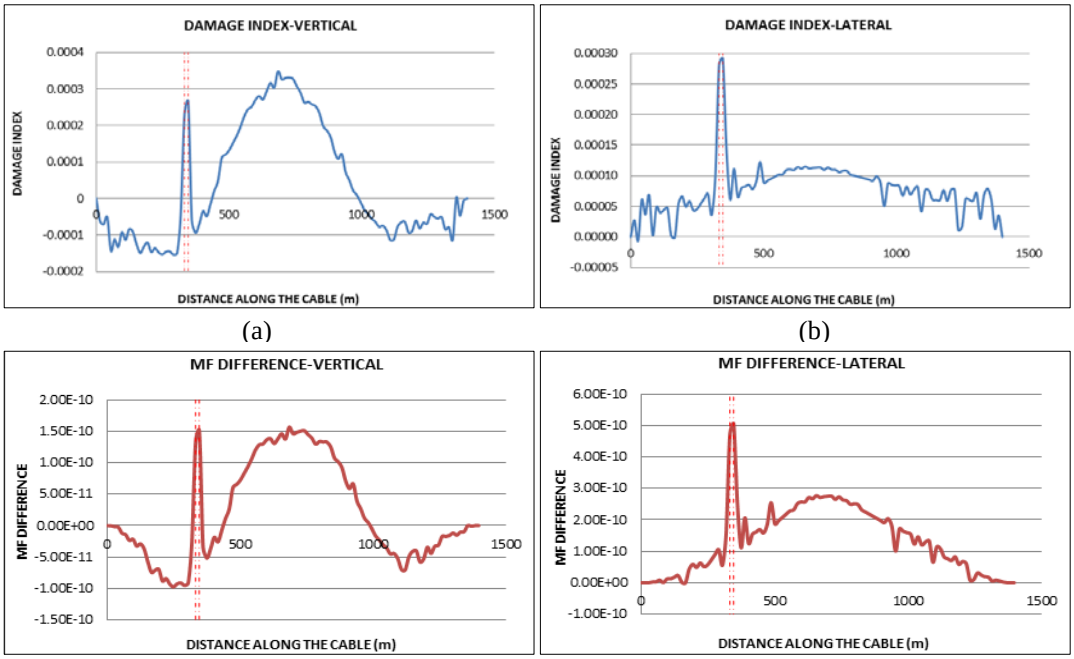

Figure 4.3 DC2 - Damage indices (a) DI_V (b) DI_L and MF difference (c) MFD_V (d) MFD_L

3. Damage Case 3 (DC 3)

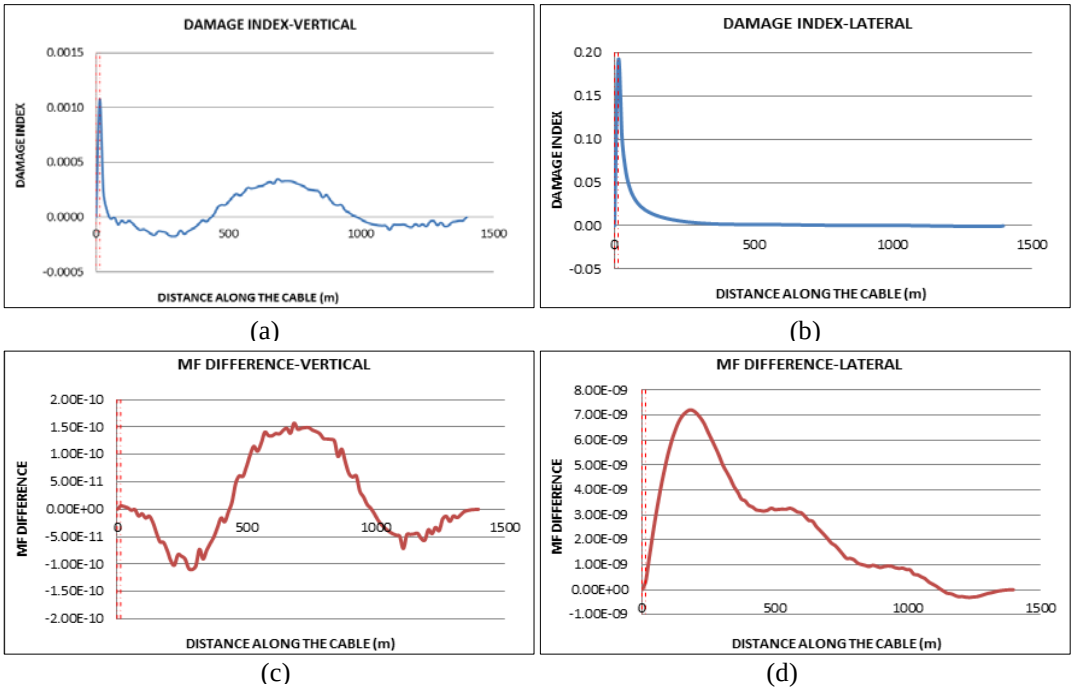

Figure 4.4 DC3 - Damage indices (a) DI_V (b) DI_L and MF difference (c) MFD_V (d) MFD_L

Two curves of the DIs for damage case 3 are shown in Figure 4.4 (a) and (b). Damage Case 3 is simulated in element 1 of the cable model with 25% stiffness reduction. The DI_V shows two peaks representing the damage location. However, a plot of the DI_L demonstrates only one peak, as in Figure 4.4 (b) for the exact damage location considered. This again verifies the DI_L calculated using lateral components

of mode shapes of a suspended cable have the ability to detect damage more accurately than $DI_{V,}$ MFD_V and MFD_L.

• Multiple Damage Scenarios

One damage case was examined to study the damage locating capability of component specific DIs with comparing MF difference calculated using vertical and lateral components of mode shapes.

4. Damage Case 4 (DC 4)

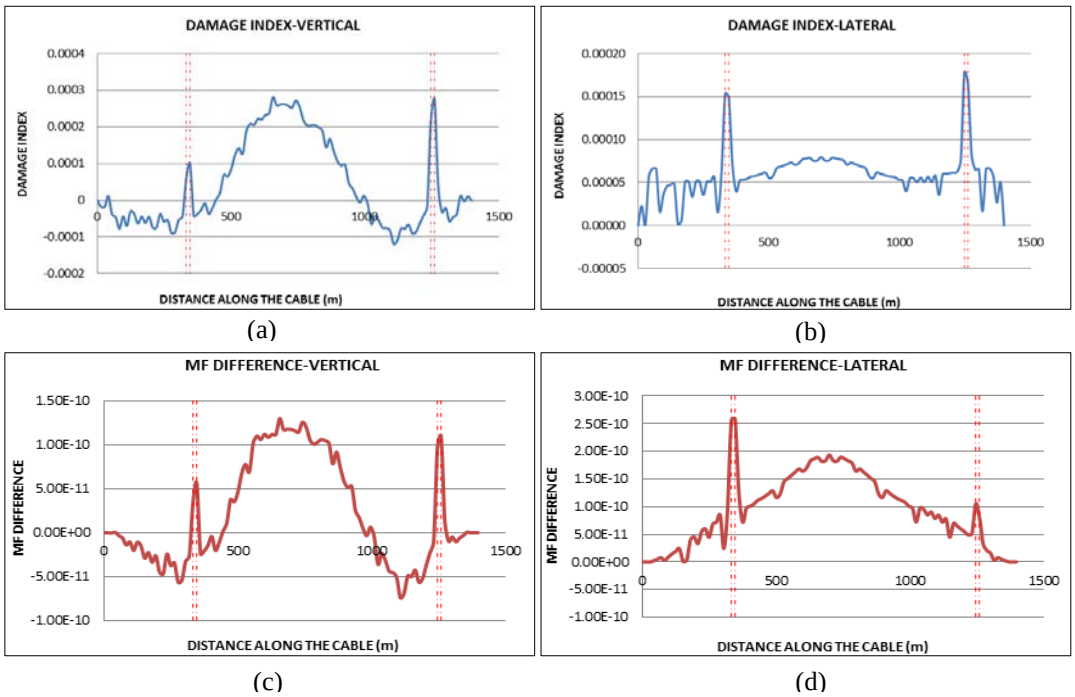

Figure 4.5 DC4 - Damage indices (a) DI_V (b) DI_L and MF difference (c) MFD_V (d) MFD_L

Damage case 4 is set up to study the damage locating capability of DIs in multiple damage cases. Element 25 and 89 are subjected to a 10% stiffness reduction in the cable model to simulate damage. The behaviour of the DI_V and DI_L are illustrated in Figure 4.5 (a) and (b), respectively. The DI_V shows three maximum points (peaks) in the graph, of which two represent the damage location and the other is a false alarm. The graph of the DI_L has two sharp peaks which correspond to the actual damage locations considered in the simulations. Same results can be observed in locating damage using MF differences. An analysis of the four graphs identified that the lateral components of mode shapes have better damage detection capability than vertical components of mode shapes in a long span large diameter suspended cable.

It is clearly evident that the DI_L calculated based on the lateral components of mode shapes is capable of detecting and locating damage under single and multiple damage scenarios. This is due to the more mass (modal mass) being distributed in lateral direction of the vibration modes of a suspended cable. The use of this damage index also enables to reduce the false alarms. The next section examines the competency of component specific DIs under the influence of measurement noise.

4.4.3 Influence of Measurement Noise in Damage Detection

In reality, measured vibration responses are associated with uncertainties such as measurement noise and computational errors in modal frequencies and mode shapes, respectively (Shi et al., 2000a). It is therefore necessary to examine the performance of the two DIs in the presence of noise in the modal data. In this study, vibration responses are generated using a validated FE model and there is no noise associated with numerical simulation. Also the measurement noise associated with frequency is very low; therefore 5% random noise is introduced to mode shapes which are generated from the FE model. The contaminated signal for mode shape can be represented as (Shi et al., 2000b).

$$\overline{\phi_{xi}} = \phi_{xi}\left(1 + \gamma_x^{\phi}\rho_x^{\phi}\left|\phi_{max,i}\right|\right) \qquad 4.2$$

Where $\overline{\phi_{xi}}$ and ϕ_{xi} are mode shape components of the i^{th} mode at location x with and without noise, respectively; γ_x^{ϕ} is a random number with a mean equal to zero and a variance equals to 1; ρ_x^{ϕ} refers to the random noise level considered and $\phi_{max,i}$ is the largest component in the i^{th} mode shape.

Figure 4.6 - Figure 4.9 illustrates the damage locating results of the two DIs with and without noise. In Damage Case 1 both DIs detect the exact damage location successfully. However, all other cases have similar features for the DI_V as observed earlier (noise free condition). The DI_L has very clear sharp peaks at the damage locations in both single and multiple damage cases considered in the cable. Therefore it can be concluded that the damage index based on lateral components of mode shapes performs well in locating damage even in the presence of 5% noise in the

mode shape data. This implies the DI_L is suitable in detecting damage in a long span large diameter suspended cable.

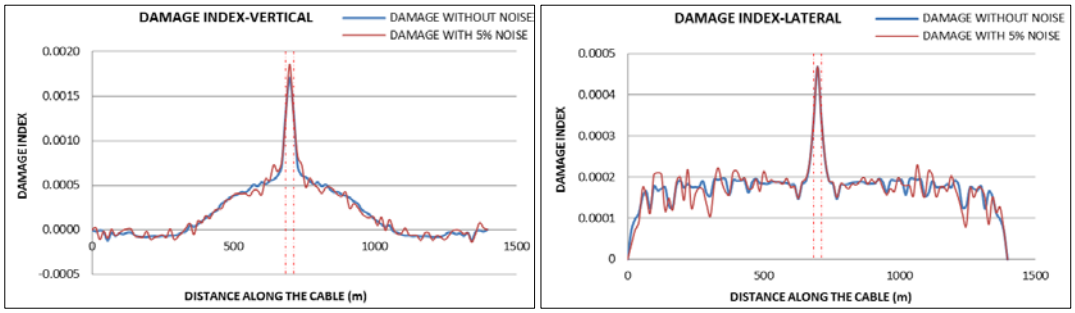

(a) (b)

Figure 4.6 DC - Damage indices (a) DI_V (b) DI_L

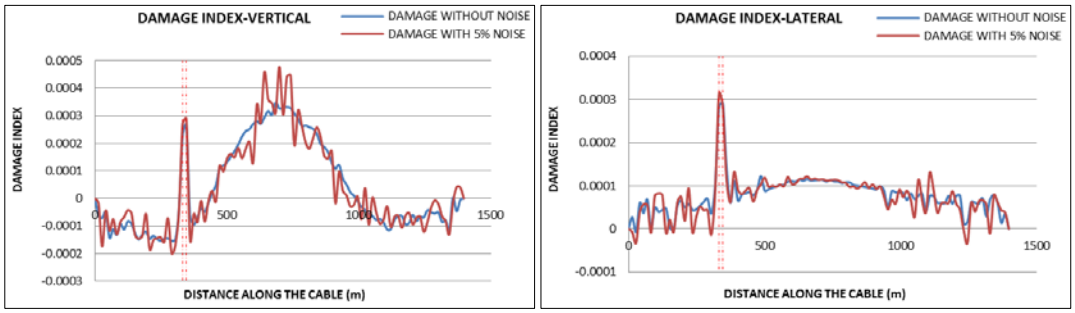

(c) (d)

Figure 4.7 DC2 - Damage indices (a) DI_V (b) DI_L

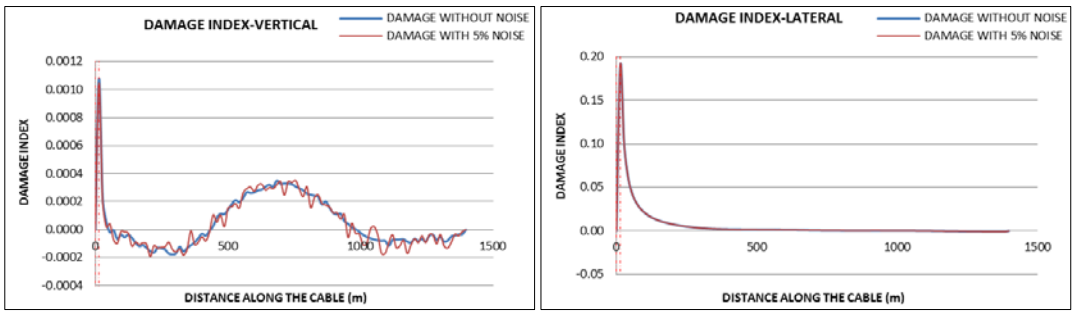

(e) (f)

Figure 4.8 DC3 - Damage indices (a) DI_V (b) DI_L

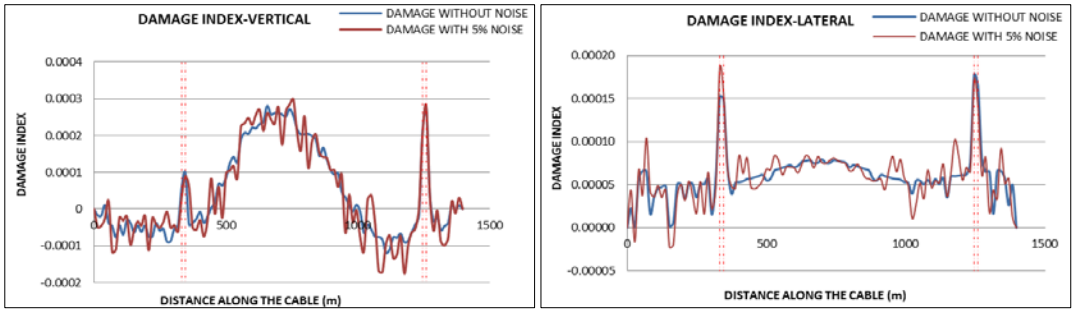

(g) (h)

Figure 4.9 DC4 - Damage indices (a) DI_V (b) DI_L

4.5 EFFECT OF CABLE PARAMETERS ON DAMAGE DETECTION

Various applications of large diameter suspended cables can be found in civil structures with considerably large sags and bending stiffness, all of which contribute to noticeable changes in the dynamic characteristics. It is therefore worthwhile to examine the effects of sag and bending stiffness in damage detection of large diameter sagged cables. These two factors are examined by defining two dimensionless parameters ξ and λ^2 characterizing the bending stiffness and sag extensibility respectively.

$$\xi = L\sqrt{\frac{H_s}{EI}} \tag{4.3}$$

$$\lambda^2 = \frac{EAL}{H_s L_e}\left(\frac{mgL}{H_s}\right)^2 \tag{4.4}$$

where L, E, A, H_s, I, m, g and L_e are the span, Young's modulus, cross section area, horizontal tension, second moment of area, mass per unit length, acceleration of gravity and length of the cable respectively. The bending stiffness parameter (ξ), differentiates the cable and beam actions: when ξ is very small, the beam action predominates, and when ξ is very large the cable action predominates. The sag-extensibility parameter λ^2, accounts for combined axial and geometric stiffness effects (Bouaanani, 2006).

4.5.1 Cable Model for Parametric Study

To study the influence of different cable parameters on the damage detection capability of both DI_V and DI_L, cable models with span (1300m) and cross section area (0.75m^2) along with different combinations of sag-extensibility and bending stiffness are considered. Modulus of elasticity of the cable considered is 200GPa. Cable models are numerically simulated in the ANSYS Workbench as pinned at two ends at the same vertical elevation and are divided into 97 elements. Pre-stressed modal analysis was conducted, as previously to consider the effect of geometric nonlinearity of cables.

Two damage cases are simulated in the FE model at the middle (Damage Case 1, x=643.22m to x =656.78 m) and quarter span (Damage Case 2, x=319.48m to x =332.87 m) of the cable as shown in Figure 4.10. For the purpose of comparison, all

the cables are subjected to the same intensity of damage by reducing the stiffness by 25%.

Figure 4.10 Cable structure with damaged scenarios for parametric study

4.5.2 Damage Detection and Sag-Extensibility

It is expected that the modal flexibility based damage indicators are influenced by the sag-extensibility of the cables. In this section therefore, effects of sag-extensibility on damage detection by using lateral and vertical components of mode shapes is studied by considering three different sag extensibilities for a suspended cable. These values are selected according to the wide range of sag to main span length ratios for suspension bridges. The literature identifies the ratio of sag to main span length for suspension bridges as ranging from 0.083 (Tacoma Narrows bridge) to 0.113 (Golden Gate bridge) (Enrique Luco & Turmo, 2010). Table 4.4 represents the cable parameters used in this parametric study.

Table 4.4 Properties of the investigated cables

Cable no.	I (m^4)	H (N)	Sag/Span	λ^2	ξ
1	0.0448	1.3450×10^8	0.070	335	159
2	0.0448	1.0455×10^8	0.090	695	140
3	0.0448	8.5000×10^7	0.110	1255	127

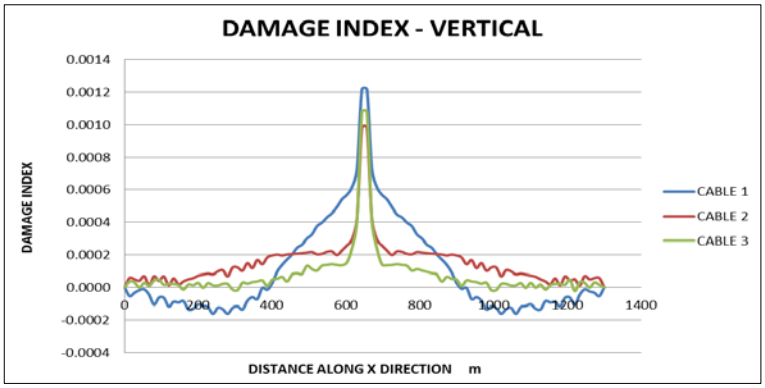

Figure 4.11 DC 1 - DI_V - Cable 1, 2 and 3

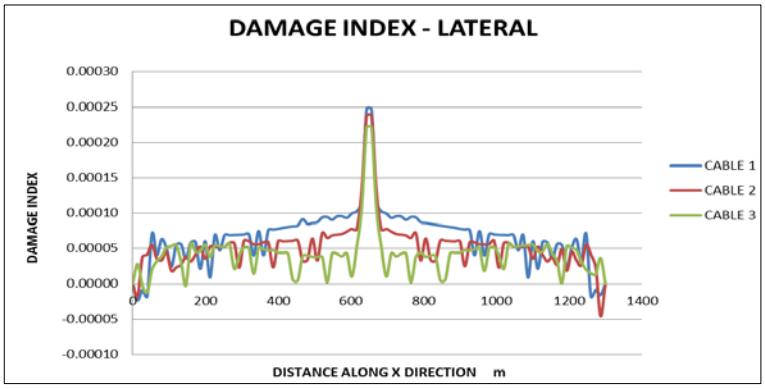

Figure 4.12 DC 1 - DI_L - Cable 1, 2 and 3

Figure 4.11 and Figure 4.12 illustrate the DI_V and DI_L in the three different cables (different sag-extensibility values) for the first damage case (damage at middle of cable). One common peak at the middle of the both graphs successfully locates the damage at the mid span of the cable. However, variations in the values of the peaks can be observed in both the DI_V and DI_L curves corresponding to three different sag-extensibility values. Also it is observed, cables with small sag to span ratio yield larger peaks in both cases.

Two graphs of the DIs related to the second damage case (damage at quarter span of cable) are shown in Figure 4.13 and Figure 4.14 below. The DI_V shows two peaks representing the damage location. However, plot of the DI_L demonstrates only one sharp peak, in Figure 4.14 which locates the actual damage correctly. For the damage case 2 it is evident that the cables with large sag to span ratios show the higher peaks in both DIs, which is contrary to what was observed with mid span damage. It is also observed that peaks appearing at the middle of the DI_V graph decrease with increase of sag-extensibility. In other terms, false alarms in the DI_V plots for cables with high sag-extensibility decrease. Results of this parametric study

pertains to the comparison of the damage detection capabilities of the DIs with different sag-extensibilities demonstrate that DI_L based on the lateral components of mode shapes has a very good potential for locating damage in a suspended cable.

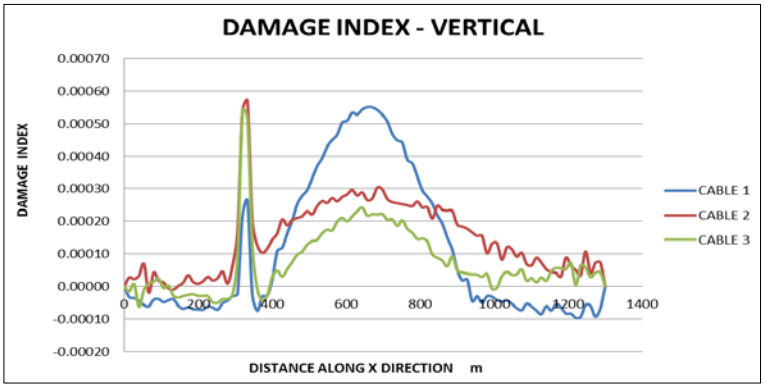

Figure 4.13 DC 2 - DI_V - Cable 1, 2 and 3

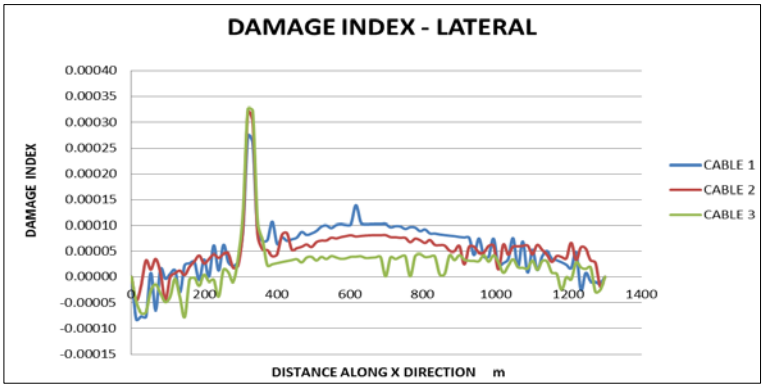

Figure 4.14 DC 2 - DI_L - Cable 1, 2 and 3

4.5.3 Damage Detection and Bending Stiffness

Flexural rigidity has commonly been ignored in most large diameter sagged cable analysis. However, cables with moderate to large diameters as used in suspension bridges are categorized by small to moderate bending stiffness parameter, which are critical especially when accurate modelling is needed for their structural identification. It is therefore, important to investigate the effect of bending stiffness of cables on the damage detection capability of the DI_V and DI_L. Different bending stiffness values ξ for a specific cable are illustrated in Table 4.5.

Table 4.5 Properties of the investigated cables

Cable no.	I (m^4)	H (N)	Sag/Span	λ^2	ξ
A	0.0448	1.3450×10^8	0.070	335	159
B	0.0336	1.3450×10^8	0.070	335	184
C	0.0224	1.3450×10^8	0.070	335	225

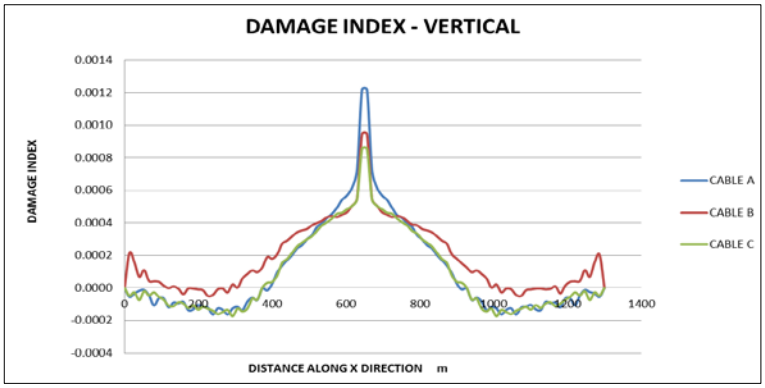

Figure 4.15 DC 1 - DI_V - Cable A, B and C

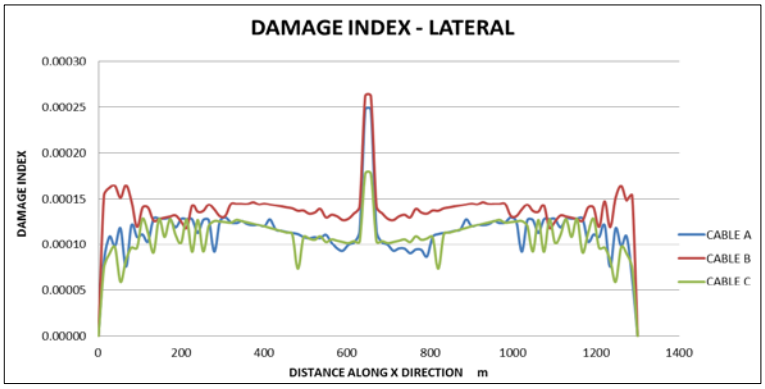

Figure 4.16 DC 2 - DI_L - Cable A, B and C

Figure 4.15 and Figure 4.16 demonstrate the DI_V and DI_L curves for the first damage scenario considered. Both indices are able to detect the damage correctly in this case and also highlight that the damage detection capability is reduced when bending stiffness parameter increases. That is, damage in the cables with higher flexural stiffness can be successfully located by these two component specific DIs. However, it is also noted that the damage indicator curves are sharp enough to identify the damage location in all three cases with different stiffness values.

Next, the damage locating capability of the DIs for the second damage scenario is illustrated in Figure 4.17 and Figure 4.18. Again, the DI_V shows false alarms in locating damage at quarter span. That false alarm can be eliminated by considering the DI_L, as discussed before. Therefore DI_V has an ability to capture the damage only at mid span correctly. However, DI_L based on lateral components of mode shapes is still valid for cables with a wide range of bending stiffness values.

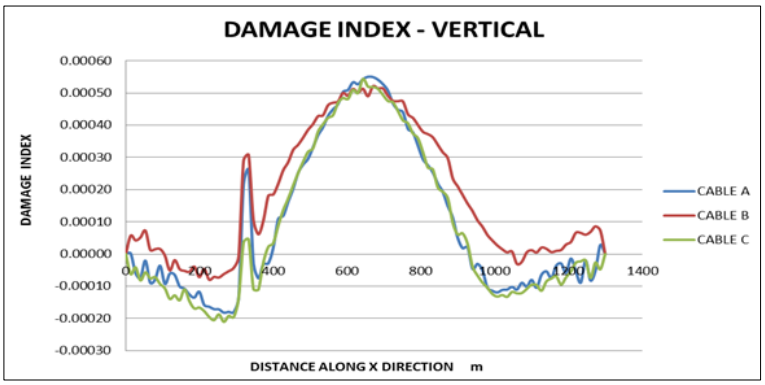

Figure 4.17 DC 1 - DI_V - Cable A, B and C

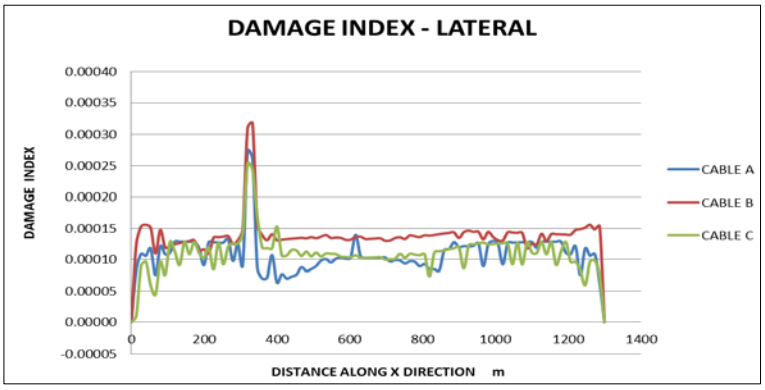

Figure 4.18 DC 2 - DI_L - Cable A, B and C

4.6 FE MODELLING OF MAIN SPAN OF 2D SUSPENSION BRIDGE

Main focus of this study is to examine the competency of component specific DIs in detecting damage of suspension bridge hangers. To achieve this, a validated FE model is required to extract the vibration characteristics of hangers at both damaged and intact states. Therefore, next section of this study presents the validation of the 2D FE model of the main span of the New Carquienz Bridge in California, USA.

The 2D FE model developed in this study was validated using the continuum formulation results of main span of the New Carquienz Bridge by Materazzi and

Ubertini (2011). Their study was limited to the vertical vibration of suspension bridge main span and hence, only frequencies and mode shapes related to vertical vibration modes were available to compare with the FE model. Consequently, 2D FE model also set up only to vibrate vertically and the vertical vibration modes were obtained. As result, competency of the DI_V only in detecting damage of suspension bridge hangers with compared to MFD_V was investigated.

In this study, ANSYS Workbench is used to simulate the main span of the New Carquienz Bridge as a 2D FE model. Main span of the bridge is 728 m long and with 57 equally spaced hangers at 12.55m. Cable sag at undamaged state is 77.2m. Other parameters of the bridge are, sag extensibility (non-dimensional Irvine parameter) λ^2=240 and non-dimensional parameter μ^2=3.5x10^{-3}. Sag/span ratio of the bridge is approximately equals to 0.1.

Material properties (such as Young's Modulus, density and Poisson's ratio) and section properties used in the analysis are similar to those used in the continuum formulation study of this suspension bridge by Materazzi and Ubertini (Materazzi & Ubertini, 2011) and are provided in Table 4.6 and Table 4.7 respectively.

Table 4.6 Material properties of the main span of the New Carquienz Bridge

Material	Density (kg/m^3)	Young's Modulus E (GPa)	Poisson Ratio ν
Main Cable	8249	196.5	0.3
Hanger	8249	137.9	0.3

Table 4.7 Section properties of the main span of the New Carquienz Bridge

Member	Cross Section Dimension (m^2)
Main Cable	0.165140
Hanger	0.006207

Main cables of the bridge were simulated using LINK 180 element type with tension only option. BEAM 188 element type was used to simulate deck and hangers.

The main cable was modelled as hinged at fixed anchors placed at the same vertical elevation. The displacements at these hinges were hence fixed in all three directions and rotations were released. The deck was modelled as a uniform, linearly elastic beam, simply supported at its ends. Consequently rotations were released in all three directions at each end of the deck while displacement was free in the longitudinal direction at one end. In order to consider geometric nonlinearity of cables, the analysis was conducted in two steps. First nonlinear static analysis under self-weight was performed and subsequently modal analysis was conducted using the last solution obtained at the end of the static step (pre stressed modal analysis was conducted). FE model of the bridge is illustrated in Figure 4.19.

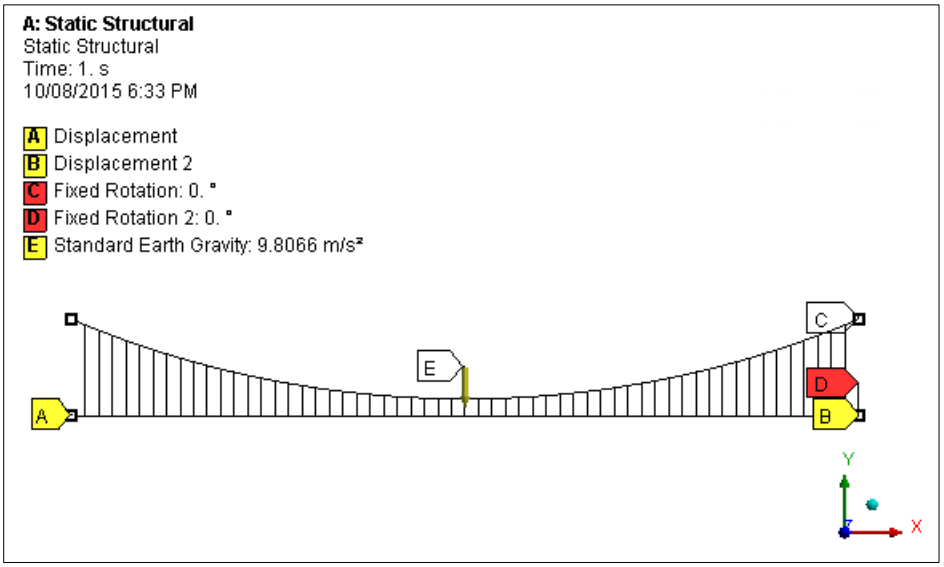

Figure 4.19 FE Model of the Main Span of the New Carquienz Bridge

4.7 VALIDATION OF THE FE MODEL OF THE 2D SUSPENSION BRIDGE MAIN SPAN

Mode shapes of first eight vertical vibration modes of the bridge were extracted from the analysis. Mode 1, 4, 6 and 8 are antisymmetric modes and mode 2, 3, 5 and 7 are symmetric modes. Frequencies of the first eight vertical modes of the bridge main span are illustrated in Table 4.8 In validating the FE model, natural frequencies obtained from the computer simulation were compared with those obtained from the results of continuum formulation study of suspension bridges by Materazzi and Ubertini (Materazzi & Ubertini, 2011). Comparison was conducted using Equation 4.5.

$$f_{error} = \frac{(f_{con} - f_{fem})}{f_{con}} \times 100 \qquad 4.5$$

Where (f_{con}) and (f_{fem}) are frequencies obtained by continuum formulation and FE model results respectively. The f_{error}, of FE analysis results are less than 6%, which confirms the accuracy of the FE model developed in this study. Therefore this validated 2D FE model will be used in damage detection studies.

Table 4.8 Summary of the FE analysis and Continuum formulation results

Mode Shape	Mode No.	FE Analysis Hz	Continuum formulation (Materazzi & Ubertini, 2011) Hz	f_{error} (%)
Antisymmetric	1	0.140	0.133	5.19
Symmetric	2	0.199	0.197	1.18
Symmetric	3	0.307	0.306	0.17
Antisymmetric	4	0.315	0.311	1.23
Symmetric	5	0.436	0.433	0.72
Antisymmetric	6	0.563	0.560	0.45
Symmetric	7	0.718	0.717	0.18
Antisymmetric	8	0.892	0.893	-0.10

4.8 DAMAGE DETECTION IN HANGERS

Damage detection of cables were extensively treated in the later chapters, hence this study was limited to that of hangers. The FE model validated in previous section of this chapter is considered as the undamaged baseline model. Four damage cases were introduced in the 2D FE model to simulate the various damage scenarios. Three damage cases are single damage scenarios with 10% stiffness reduction in the hanger 29, hanger 14 and hanger 1. One damage case is defined with 10% and 5% stiffness reductions in two different hangers namely; hanger 14 and hanger 44 respectively to cater for multiple damage scenarios.

Since this 2D simulation associates only with the vertical vibration modes, only damage index (DI_V) calculated using vertical components of mode shapes and MF

difference (MFD_V) calculated using vertical components of mode shapes were compared in the discussion of results. Following abbreviations are used in the presentation of the results.

DI_V Damage Index Vertical - calculated by using vertical components of mode shapes

MFD_V Modal Flexibility Difference Vertical - calculated by using vertical components of mode shapes

Both DI_V and MFD_V are initially calculated for each node in every hanger. Next, the average values of DI_V and MFD_V corresponding to each hanger are calculated and presented in bar graphs.

4.8.1 Damage Scenarios

Since, damage in FE models can be simulated by changing the Young's modulus or changing the cross section area or removing elements at damage location, this study simulated damage in the 2D FE model by reducing Young's modulus of the specified hangers. Figure 4.20 and Table 4.9 represent the exact locations of the damage cases considered in this study. The first four modes in the vertical direction are considered in this damage detection study only. Natural frequencies and mode shapes corresponding to these modes were extracted from the FE analysis of both damaged and undamaged states of the particular hanger considered.

Table 4.9 Damage cases considered in hangers

Damage Case	Location	Severity of Damage
Single damage scenario		
DC 1	Hanger 29	10%
DC 2	Hanger 14	10%
DC 3	Hanger 1	10%
Multiple damage scenario		
DC 4	Hanger 14 and Hanger 44	10% 5%

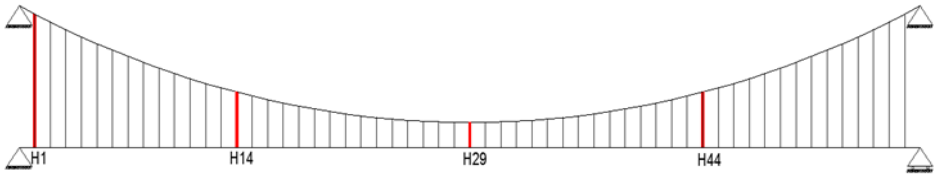

Figure 4.20 Locations of damage considered in hangers

4.8.2 Damage Detection without Noise in Modal Data

Damage detection results for each damage case considered are illustrated below. Results include bar graphs of DI_V and MFD_V for 57 hanger of the main span.

• Single Damage Scenarios

Three damage cases were examined to study the damage locating capability of DI_V and MFD_V.

1. Damage Case 1 (DC 1)

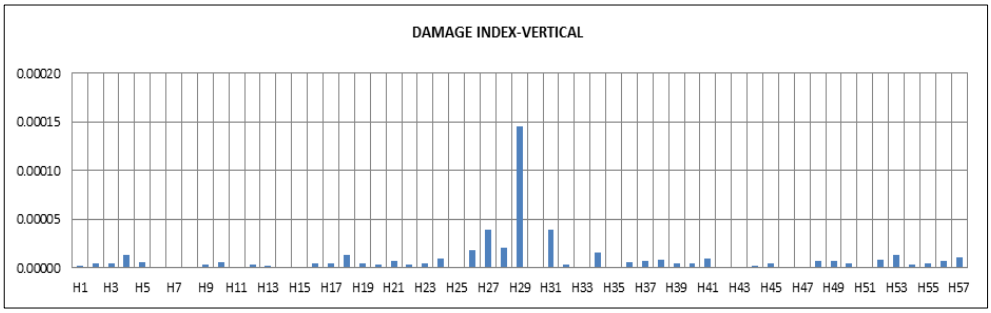

(a)

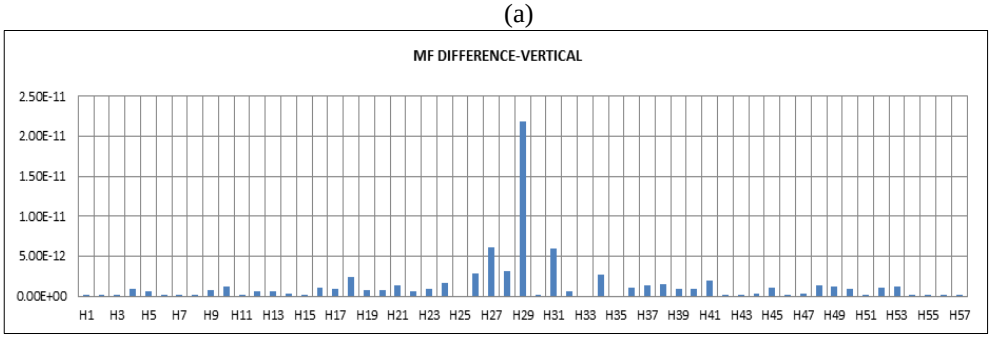

(b)

Figure 4.21 DC1 - Damage index (a) DI_V and MF difference (b) MFD_V

The first damage case studied is that with a 10% stiffness reduction of the hanger 29. Figure 4.21 (a) and (b) illustrates the bar graphs of DI_V and MFD_V respectively. Both graphs show higher values at the location of the damaged hanger. In this case, both DI_V and MFD_V are able to successfully identify the damaged hanger considered.

2. Damage Case 2 (DC 2)

Figure 4.22 (a) and (b) show the DI_V and MFD_V values for the second damage case with a 10% stiffness reduction in hanger 14. The bar graph clearly indicates the damaged hanger not only using the DI_V but also from the MFD_V. Based on the examination of the two graphs, it can be concluded that incorporating vertical components of mode shapes for detecting damage in hangers is a successful approach using both damage index and MF difference. The, competency of the DI_V and MFD_V in damage detection of hangers is further evaluated through Damage Case 3 considered in this study.

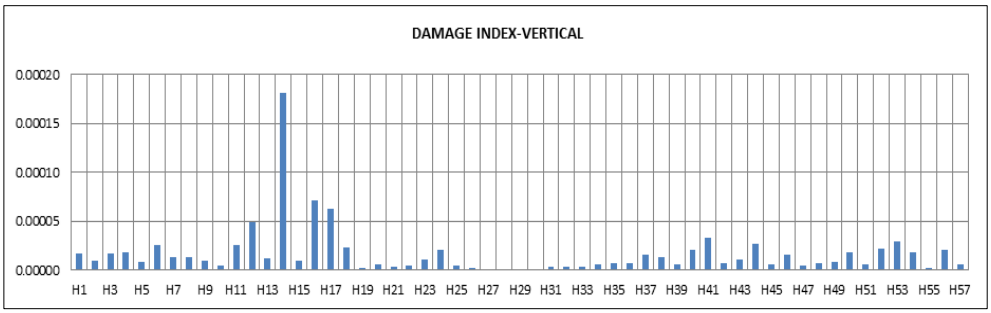

(a)

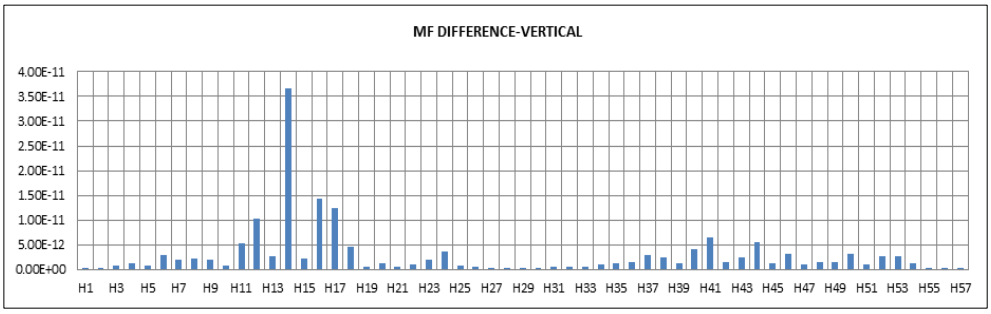

(b)

Figure 4.22 DC2 - Damage index (a) DI_V and MF difference (b) MFD_V

3. Damage Case 3 (DC 3)

Two bar graphs related to the DI_V and MFD_V for damage case 3 are shown in Figure 4.23 (a) and (b). Damage Case 3 is simulated in hanger 1 of the 2D FE model with 10% stiffness reduction. The DI_V indicates the damage location correctly. However, the plot of MFD_V demonstrates false damage locating results, as in Figure 4.23 (b). Therefore, this damage case verifies the damage index calculated using vertical component of the mode shapes have better ability to detect damage more accurately than MF difference calculated using these.

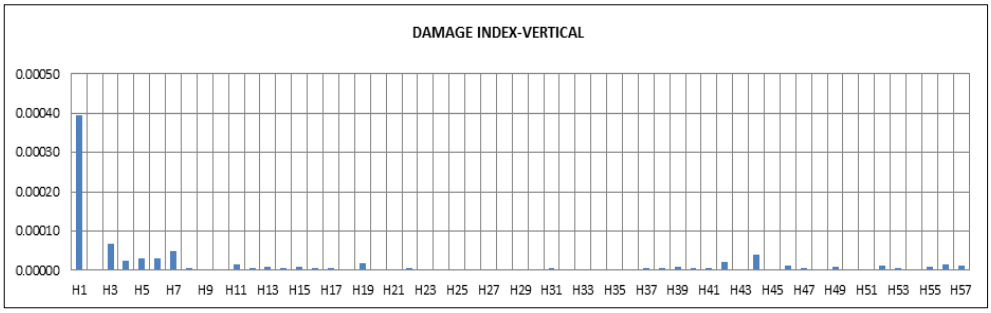

(a)

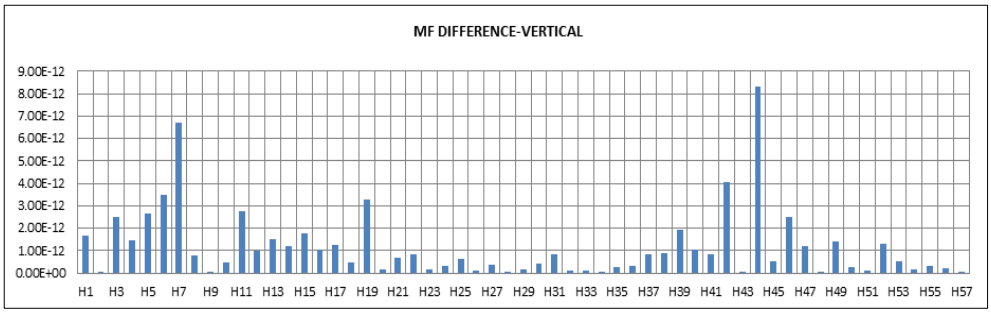

(b)

Figure 4.23 DC3 - Damage index (a) DI_V and MF difference (b) MFD_V

4. Damage Case 4 (DC 4)

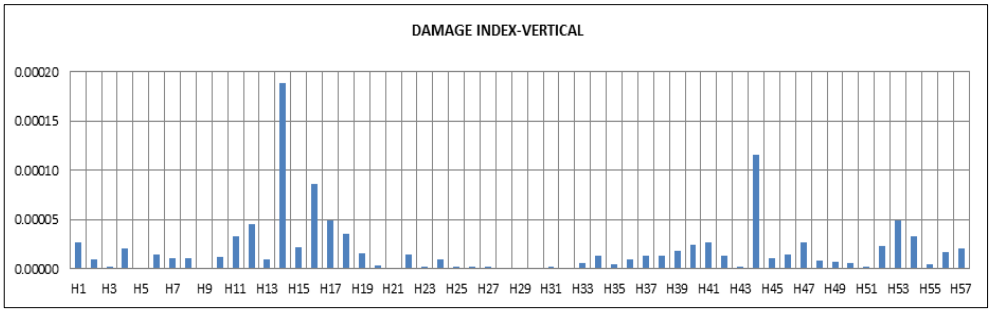

(a)

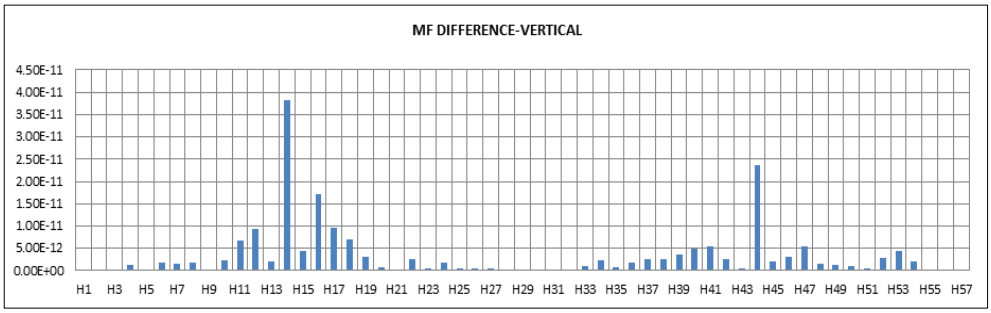

(b)

Figure 4.24 DC4 - Damage index (a) DI_V and MF difference (b) MFD_V

In damage case 4 hangers 14 and 44 are subjected to a 10% and 5% stiffness reduction in the 2D FE model to simulate damage. Two bar charts related to the DI_V and MFD_V calculated using vertical component of the mode shapes are illustrated in Figure 4.24 (a) and (b) respectively. Both graphs clearly indicate the locations of the damaged hangers successfully.

Based on the damage detection results of the hangers, it is clearly evident that the damage index (DI_V) calculated using vertical components of the mode shapes is capable of detecting and locating damage in hangers under single and multiple damage scenarios. The next section examines the competency of damage index (DI_V) under the influence of measurement noise.

4.8.3 Damage Detection with Noise in Modal Data

A method mentioned in the previous section of this chapter is used to calculate the noise in modal parameters generated from the FE model. Since, the measurement noise associated with frequency is very low; 5% random noise is introduced to mode shapes. In the next section, four damage cases defined before are examined under the noisy modal data.

Figure 4.25 - Figure 4.28 illustrates the damage locating results of the damage index (DI_V) calculated using vertical components of the mode shapes with and without noise in the modal data. Based on the analysis of the bar graphs, it can be clearly observed that the DI_V successfully locates the damage in every damage case considered. Therefore it can be concluded that the vertical damage index (DI_V) performs well in locating damage of hangers even in the presence of 5% noise in the mode shape data.

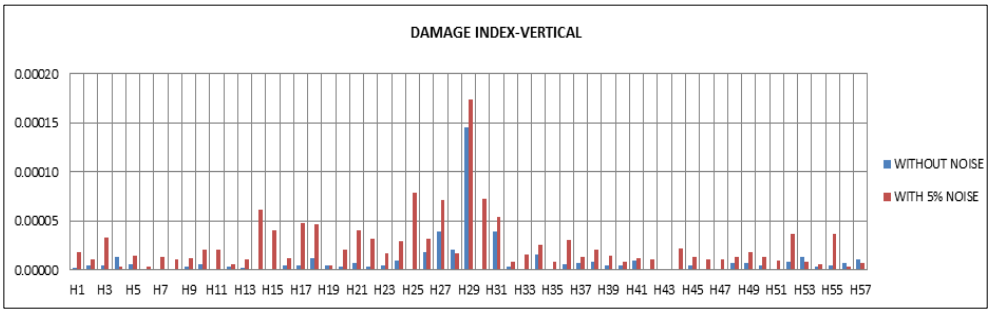

Figure 4.25 DC1 - DI_V

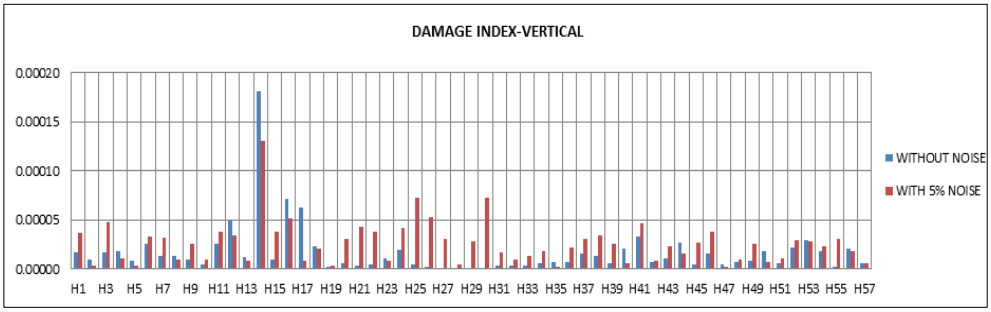

Figure 4.26 DC2 - DI_V

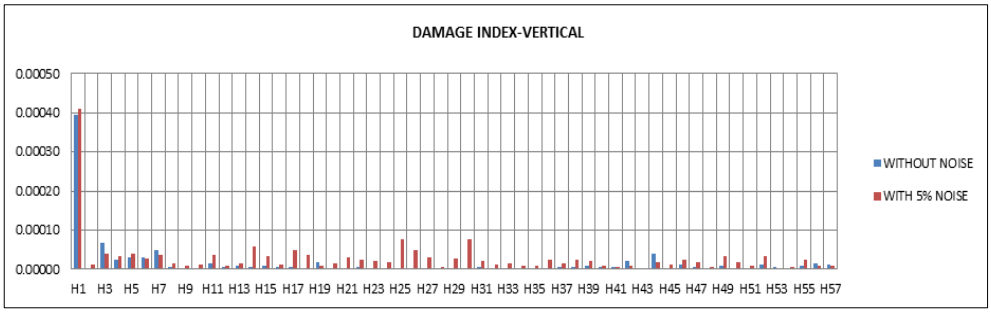

Figure 4.27 DC3 - DI_V

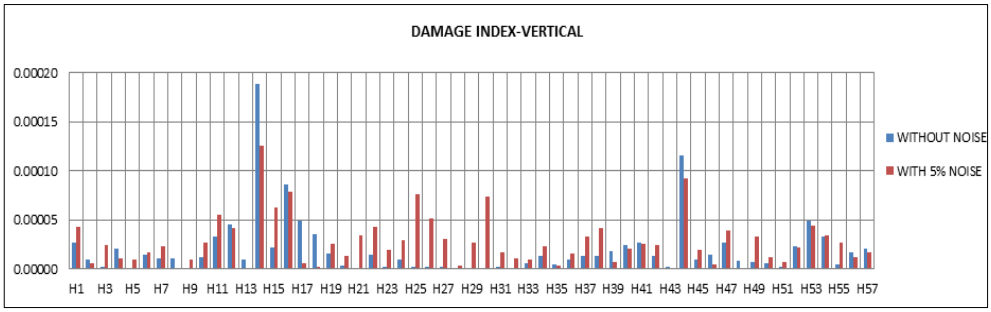

Figure 4.28 DC4 - DI_V

4.9 SUMMARY

Large diameter and long span suspended cables are used as main structural components in cable supported structures such as suspension and cable stayed bridges, overhead transmission lines, cable cars, cable supported roofs, and guyed towers. Damage in such cables needs to be detected at an early stage and there has been no attempt made recently to achieve this using vibration characteristics. First section of this study therefore, examined the capability of modal flexibility based DIs to detect damage in large diameter and long span suspended cables. There, the damage detection capability of the two DIs incorporating vertical and lateral components of mode shapes (DI_V and DI_L) was evaluated with and without noise in numerically generated modal data. Further, damage locating ability of DIs also compared with MF difference (MFD_V and MFD_L). Damage index calculated using lateral components of the mode shapes (DI_L) performs well in locating damage in the cable model with single and multiple damage scenarios even with 5% measurement noise in mode shapes.

Bending stiffness and sag-extensibility are two important parameters of a long span large diameter suspended cable. Hence, influence of these parameters on the damage detection capability of the two DIs was evaluated. It is observed that the

damage detection capability of the DIs reduce (indicated by reduced peaks) with the increase of sag-extensibility and bending stiffness parameters. However it is important to note that the damage index (DI_L) curves are sharp enough to identify the damage location in all the different cases studied. Subsequently, it can be concluded that the lateral modes are more sensitive to damage and lateral damage index (DI_L) derived from modal flexibility is competent in detecting and locating damage in large diameter and long span suspended cables, under all damage scenarios considered.

Apart from cables, hangers are also very important structural members in a suspension bridge. Defects in such elements also need to be detected at their earliest to enhance serviceability of the suspension bridges. The second section of this chapter examined the capability of vertical damage index (DI_V) in locating damage in hangers of a 2D suspension bridge model. Results also compared with MF difference (MFD_V) to show the competency of the vertical damage index. In each case considered, vertical damage index (DI_V) performs well in locating damage in hangers even the presence of 5% noise in the modal data. This study was limited to the two dimensional structure using vibration parameters in the vertical vibration modes. Further studies are conducted in next chapters to confirm the sensitivity of component specific DIs using vibration properties of all the modes (vertical, lateral and coupled modes) of a suspension bridge.

Chapter 5: Experimental Testing of the Laboratory Cable Bridge Structure

5.1 INTRODUCTION

This chapter presents two different tests conducted on the laboratory cable bridge structure to validate the FE model. Subsequently, this model will be used in the damage detection studies. Two tests namely; static test and dynamic test were conducted to obtain static and dynamic behaviours respectively. This chapter, firstly, provides details of the laboratory cable bridge structure and its calibration before testing (preliminary works involved in preparation for testing). Secondly, it describes the static test conducted to verify the bridge geometry (symmetricity), connections and boundary conditions of the FE model. Thirdly, it elaborates the fundamentals of dynamic testing of structures and details of the dynamic test conducted. Finally, it discusses the static and dynamic behaviour of the structure using vertical deflections and extracted modal parameters.

5.2 DESCRIPTION OF THE LABORATORY CABLE BRIDGE

The cable bridge used in this study was designed and constructed in the Structures Laboratory at Queensland University of Technology in 2006. It was used to study the dynamic performance of slender suspension footbridges under human-induced dynamic loading. The entire bridge system was mainly made of aluminium and stainless steel materials in an effort to reduce corrosion and overall mass. It consists of two components: namely, cable bridge model and support system (as shown in Figure 5.1). In this study, the cable bridge model is the main focus and its vibration parameters are the major concern in experimental testing. The support system provides anchorage to the cable bridge model. Due to the relocation of the bridge structure, all the load cells were in a damaged condition. They were replaced and preliminary tests were conducted on them prior to static and dynamic testing.

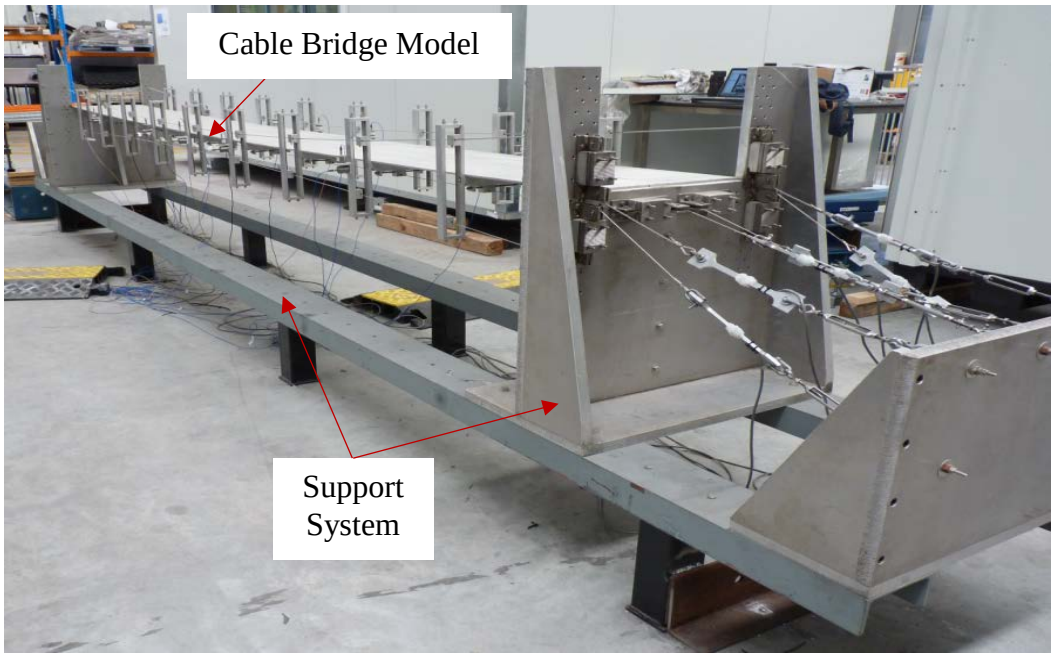

Figure 5.1 The cable bridge model and support system

5.2.1 The Cable Bridge Model

The cable bridge model consists of a cable system, transverse bridge frames and deck units. It was designed originally to have a span of 4.5 m, and ability to vary the span to 3.0 m or 1.5 m. The cable system comprises of three cable clusters: top supporting cables (TSC), pre-tensioned reverse profiled (bottom) cables (RPC) in the vertical plane and pre-tensioned bi-concave side cables (BCSC) in the horizontal plane. Stainless steel wire strands (7x19) of 3.2mm and 1.6mm nominal diameter are used for the top supporting cables and both reverse profiled (bottom) cables in the vertical plane and the bi-concave side cables in the horizontal plane respectively. The two parallel top supporting cables have catenary profiles which provide tension forces to support the whole structural gravity of the cable bridge model, applied loads and internal forces induced by the pre-tensioned bottom cables. Function of two parallel pre-tensioned reverse profiled (bottom) cables in the vertical plane is to introduce pre-tension forces and provide internal vertical forces to transverse bridge frames and the top supporting cables. The main structural function of the pair of pre-tensioned bi-concave side cables in the horizontal plane is to provide internal horizontal forces and horizontal stiffness to the cable bridge model. When the pre-tensioned bottom and/or side cables are slack, they can carry small tension forces only to support their own gravity and cannot resist any external loads or cannot contribute to stiffness and tension forces of the structure. However, small tension

forces in these cables can provide sufficient restraining forces to prevent the transverse frames from swaying in the lateral direction.

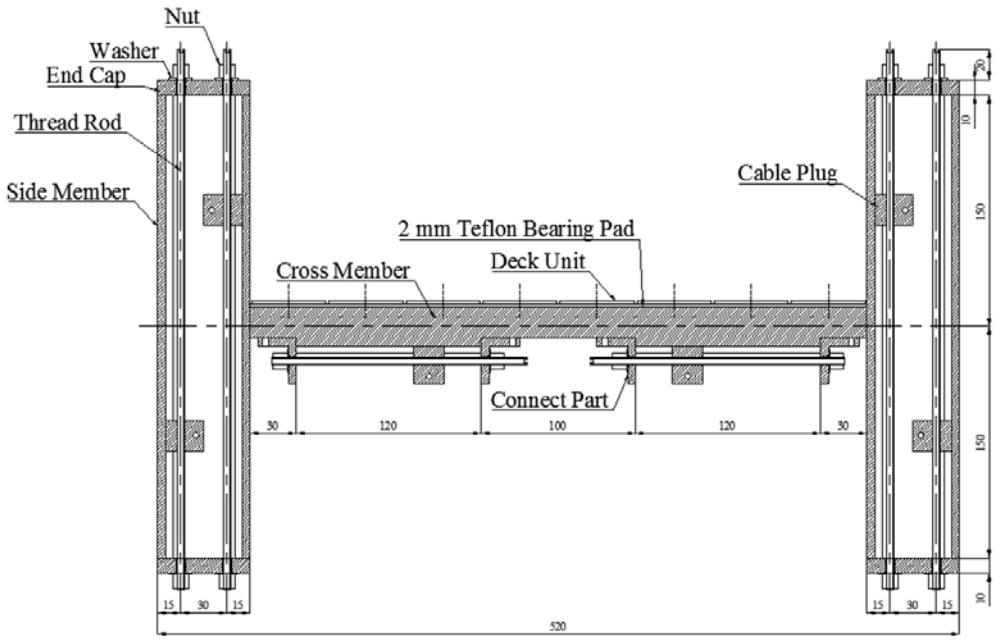

Figure 5.2 Details of transverse bridge frame

Nine transverse bridge frames (one bridge frame illustrated in Figure 5.2) at 450mm from each other are hung from the top cables, and further restrained by the pre-tensioned reverse profiled (bottom) cables in the vertical plane and the pre-tensioned bi-concave side cables in the horizontal plane. The main function of the transverse bridge frames is to support the deck and hold the cables in the desired profiles. These frames comprise of a cross member (to support the deck), side members, end caps, and cable plugs (to hold cables in the required profiles). Transverse bridge frames have in plane stiffness to protect against collapse under in plane forces and contribute very little in the way of longitudinal, lateral and rotational stiffness for the entire system.

In each bridge frame, six cable plugs are intended to hold the cables with required cable profiles. Top supporting cables and pre-tensioned reverse profiled (bottom) cables in the vertical plane are supported by the cable plugs arranged at the two sides of the bridge frame. These cable plugs can be adjusted along the sockets in the transverse frame's side members via tuning of the thread rods. Maximum moving distance of these cable plugs is 270 mm. Additional two cable plugs are arranged

under the cross member of the bridge frame to hold the bi-concave side cables in the horizontal plane. These two cable plugs have a maximum moving distance of up to 90 mm. In each span, eight deck segments (450mm x 48mm x 5mm) are supported on the cross member of the transverse bridge frames. The bridge deck units and main parts of the transverse bridge frames are made of Aluminium, except thread rods which are made of stainless steel.

5.2.2 The Support System

Anchorage to the cable bridge is provided by the support system. It encompasses headstocks, cable clamps, load cells, turnbuckles, end supports and basements. The two aluminium headstocks of the support system provide different supports to the cables for different cable configurations. The details of the support system are illustrated in Figure 5.3. The main functions of the cable clamps (a closer view in Figure 5.4) which were designed to be attached on the headstocks are: (1) to lock the cables and to reduce slip of cables; (2) to change the directions of the cables to align with the load cells.

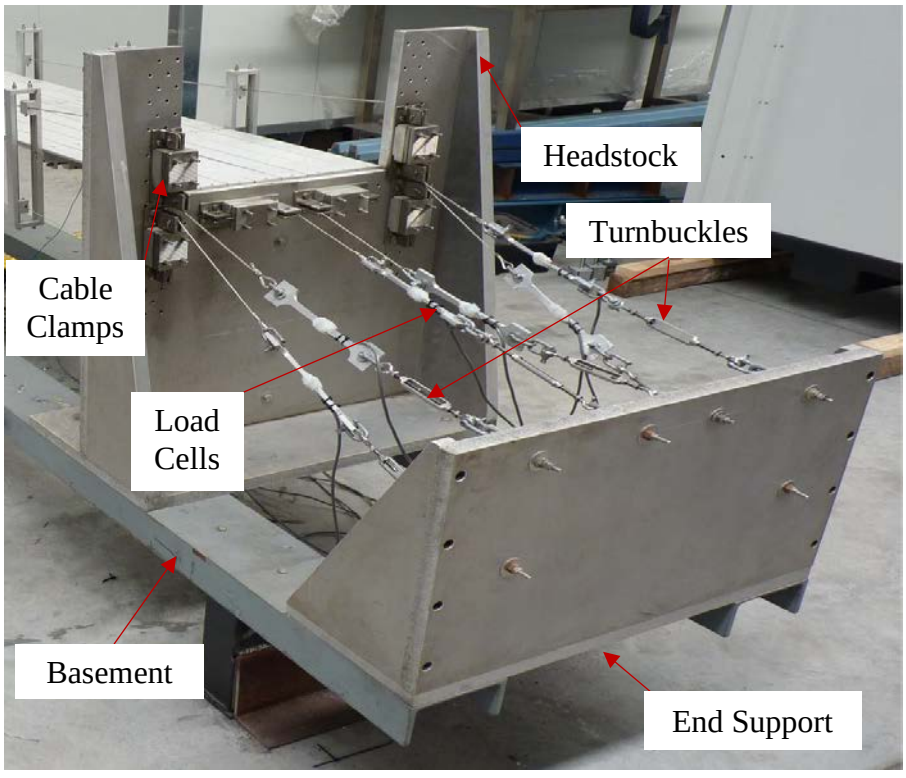

Figure 5.3 The support system

Figure 5.4 Details of the cable clamp

Twelve aluminium specimens (Figure 5.5) with two transducer specific strain gauges mounted on either side are used to measure the tension forces in the cables and are called as load cells. The turnbuckles attached to each load cell and the end supports via a D-shackle are used to provide different cable tension forces by varying the cable lengths. The function of the two aluminium end supports is to transfer the forces to the basement. The basement is comprised of two Parallel Flange Channel steel beams (150PFC) and is designed to keep the bridge model with the required span length by bolting the headstocks at different locations.

Figure 5.5 Load Cell

5.2.3 Connectivity of the Support System and Cable Bridge Model

The schematic diagram (Figure 5.6) illustrated below describes the connectivity mechanism of the support system and the cable bridge model. Six cables are drawn through the headstock and cable clamps (not locked) and connect to the load cells via D-shackles. Next, the other ends of the load cells are connected to the turnbuckles by

means of D-shackles. Then, turnbuckles are connected to the end support to ensure the stability of the bridge. Finally, tension forces of the cables are adjusted by tuning the turnbuckles and reading the load cells simultaneously. Once, the desired tension forces have been attained, the cables are locked by the cable clamps to minimize the slip of the cables.

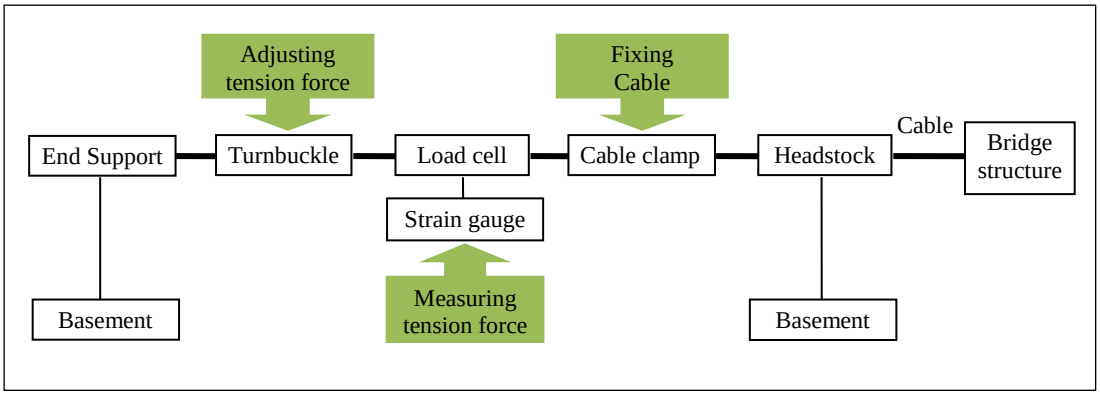

Figure 5.6 Connectivity mechanism of the support system (Huang, 2006)

5.3 RECONSTRUCTION/RENOVATION AND CALIBRATION OF THE CABLE BRIDGE

As mentioned before, this experimental bridge was last used in the year 2006 and is now located at the Banyo Pilot Plant Precinct of Queensland University of Technology. It was in a poor condition with a damaged tensioning system. The next two sections describe the process of renovation and calibration of the cable bridge model.

5.3.1 Preparation and Calibration of Load Cells

As the condition of the existing strain gauges attached to the load cells were unknown, the system was rebuilt by mounting new strain gauges on the Aluminium load cells and calibrating them to establish the relationship of tension force and voltage changes for each load cells. Each load cell consists of two transducer specific strain gauges (90^0 - two element strain gauges) of model FCB-2-23-120 connected with full bridge type III configuration. This configuration (Figure 5.7) has four active strain-gauge elements of which two are mounted in the direction of axial strain with one on one side of the strain specimen (top), and the other on the opposite side (bottom). The other two act together as a poisson gauge and are mounted transverse (perpendicular) to the principal axis of strain with one on one side of the strain specimen (top), the other on the opposite side (bottom). Bridge type III configuration

(Figure 5.8) was selected because it compensates for temperature and lead resistance and rejects bending strain.

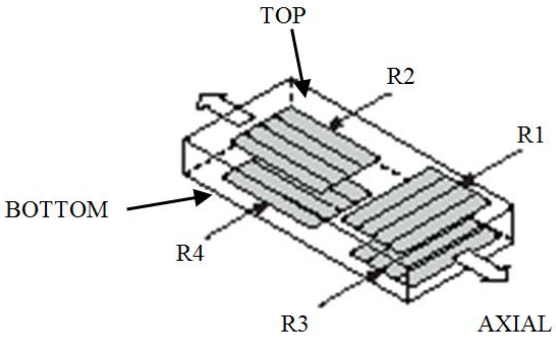

Figure 5.7 Strain gauge configuration

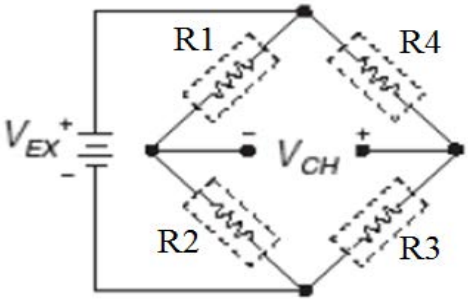

Figure 5.8 Bridge type III configuration

Figure 5.9 Load Cell attached to the Instron machine while calibrating

After mounting the strain gauges on the aluminium specimens, they were calibrated to establish the relationship of tension force to the voltage changes. In achieving this, firstly, each aluminium specimen was connected to the tensile testing machine (Instron) and subjected to a tensile load of minimum 0N to the maximum of 2500N with the load rate of 5 N/s (Figure 5.9). Simultaneously, strain gauge output which was connected to an Electronic Data Acquisition System (eDAQ) was measured at five-second intervals. The voltage values recorded from the strain gauge and the tensile force applied by the Instron machine are displayed on the laptop and the desktop screens respectively as shown in Figure 5.10.

Figure 5.10 Arrangement for load cell calibrating

The collected data was subsequently exported to Microsoft (MS) Excel to create a plot of load vs voltage. Once the data had been plotted, a linear trend line equation (in the form of y=mx+c) was fitted with the date to find the intercept and the slope of each graph corresponding to each load cell. Calibration curves for each load cell are illustrated in Appendix A. Thirdly; all the load data with the intercept and the slope of each graph were entered to the LabVIEW to convert the strain gauge voltage to a tensile force output in Newtons. As the trend line is an average of the collected data, the equation required fine tuning using a trial and error method until the voltage reading matched the applied Instron force. This process was necessary for each aluminium specimen since, as different material behaviour and minor dimensional variations of the aluminium specimens meant the same formula could not be applied in each case. Afterwards, each loading cell was numbered from 1-12 and assigned a port on the eDAQ. Finally, the 12 load cells were re-tested and re-

programmed a second time to ensure the accuracy of individual strain conversion formula prior to use within the bridge model.

5.3.2 Replacement of Suspension Cables

The condition of the suspension cables of the original bridge model was unknown and a cable failure was experienced during preliminary tensioning; therefore, it was decided to replace all cables in the bridge. Installation of the cables required a specific crimping process to ensure strength at the ends of the cable. To further reduce the chances of cable failure during testing, the cable clamps were reversed to avoid cable damage due to the serrated edge. To ensure accurate results in the comparative suspension bridge FEM, tensile testing to obtain important material properties such as the elastic modulus and breaking strength was undertaken.

5.4 EXPERIMENTAL TESTING PROCEDURE

Once preliminary works were completed, two experimental tests: static and dynamic tests were conducted. Two bridge model cases were considered to investigate the static and dynamic behaviour of the bridge. In case 1, the bridge model was designed to have a cable configuration with only top supporting cables and pre-tensioned reverse profiled bottom cables in vertical plane with desired tension forces of 1400N and 300N respectively. While, in case 2, the bridge model was designed to have all the pre-tensioned cables including top supporting cables, pre-tensioned reverse profiled (bottom) cables in the vertical plane and pre-tensioned bi-concave side cables in the horizontal plane with desired tension forces with 1400N, 400N and 300N respectively. However, due to the sensitivity of the loading cells, the results section will present an average of the tensile values during testing. A preliminary FE model was established to approximately identify the static and dynamic behaviour of the bridge before conducting experiments. In each case, cable plugs in the middle bridge frame were adjusted to have a cable sag of 105 mm (measured from end cap) for the supporting top cables and reverse profiled bottom cables in the vertical plane, and a cable sag of 110 mm (measured from inner side member) for the reverse profiled side cables in horizontal plane. The experiment process is shown in the diagram below (Figure 5.11).

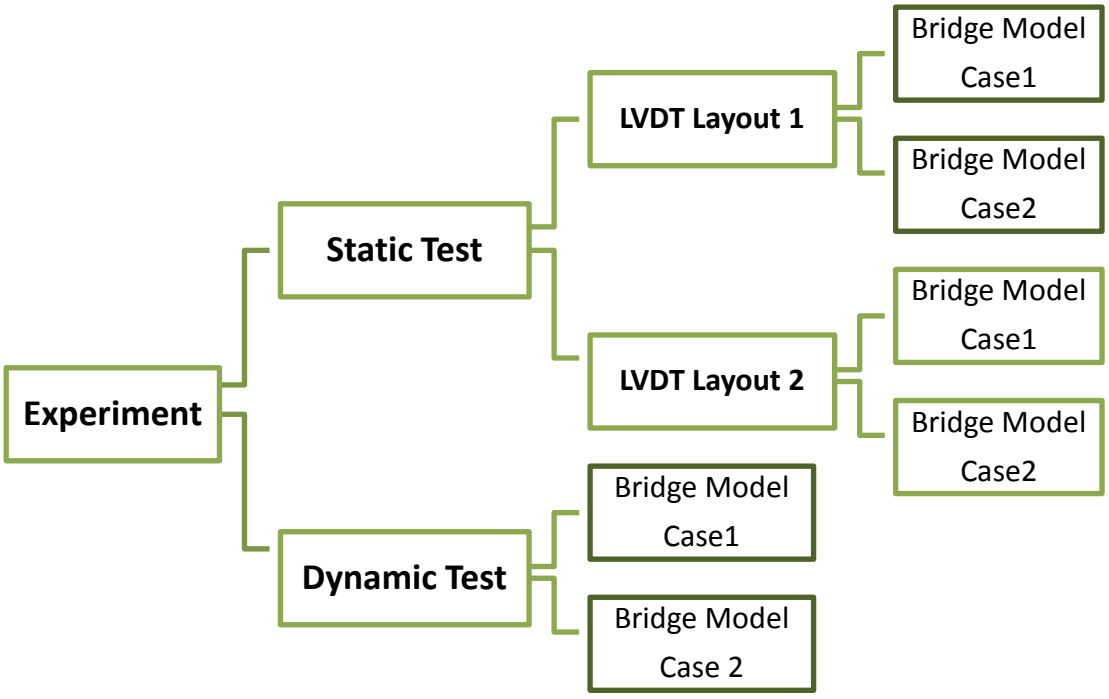

Figure 5.11 The experiment process

5.5 STATIC TEST

As a precursor to the dynamic test, the static test was conducted to obtain the static behaviour of the suspension bridge when subjected to static loading. Test results are used to verify the symmetricity (bridge geometry), connections and boundary conditions of FE Model. As mentioned before, the static test was conducted for two bridge model cases. The instrument setup, testing procedure and experimental results of the two tests are briefly discussed in next sections.

5.5.1 Instrument Setup

Two vertical deflection measurement layouts were considered in the static test for each bridge model case. Both layouts (Layout 1 and 2) were used to check the symmetrical behaviour of the bridge and verify the FE model. A series of weights (approximately 900g) were used to apply the static load on the deck of the cable bridge model. A maximum load of 6.888kg was selected in this study based on previous static load test results in order not to exceed the linear behaviour of the bridge material and availability of number of weights. The loading frame consists of an aluminium plate supported by two aluminium bars on the bridge deck to transfer the vertical load to the deck units, and therefore the deck units at the two middle

segments are subjected to uniform line loads. Figure 5.12 shows the loading frame and applied loading.

Figure 5.12 Static vertical loading system

Linear Voltage Displacement Transducers (LVDTs) each with 100mm capacity fixed underneath the bridge were used to measure the vertical deflections due to applied load. Those LVDTs are connected to the eDAQ and data was recorded and saved automatically in the computer during loading. In the Layout 1, LVDTs were placed at three different locations along the bridge length. While, in Layout 2 LVDTs were arranged to measure the vertical deflection at the three locations of the cross member of the middle bridge frame. Figure 5.13 and Figure 5.14 illustrate the two LVDT layouts separately.

(a) LVDTs installed underneath the bridge in Layout 1

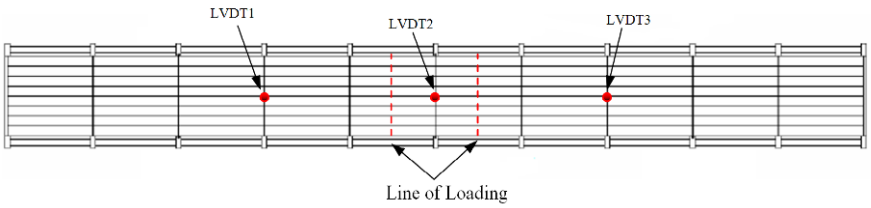

(b) Schematic diagram of LVDT locations in Layout 1

Figure 5.13 Deflection measurement Layout 1

5.5.2 Testing Procedure

Firstly, eDAQ was turned on and the system was carefully checked for errors. Then the cables were set up to the required tension level for the pre designed test bridge model case considered. Secondly, three LVDTs were installed underneath the bridge as mentioned in Layout 1 and loading frame was installed on the bridge deck and time was recorded manually. After one minute, the first weight was installed on the loading frame and time was recorded. Next, remaining weights were installed on top of each other at one minute intervals. One minute time gap was selected in between consecutive loadings to avoid false deflection reading due to bouncing of the bridge deck while loading. After one minute of loading the last weight, eDAQ was stopped and data was transferred to a MS Excel. A similar test procedure was conducted on the bridge model Case2 for Layout 1 and both bridge model cases for Layout 2 of LVDT arrangement. Static tests were repeated three times for each of the

bridge model cases discussed previously for comparison and to improve the accuracy of results.

(a) LVDTs installed underneath the bridge in Layout 2

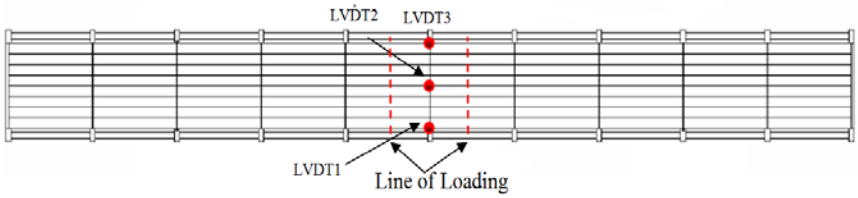

(b) Schematic diagram of LVDT locations in Layout 2

Figure 5.14 Deflection measurement Layout 2

5.5.3 Static Test Results

The tests described above, investigate symmetricity and static behaviour of the bridge under the planned static load. In LVDT layout 1, two bridge model cases were conducted and results are illustrated in Table 5.1 and Table 5.2 respectively. In bridge model case1 top supporting cables and pre-tensioned reverse profiled (bottom) cables in vertical plane were setup to average tension values of 1446N and 326N respectively. In bridge model case2, top supporting cables, pre-tensioned reverse profiled (bottom) cables in vertical plane and pre-tensioned bi-concave side cables in the horizontal plane were set up to average tension values of 1403N, 485N and 270N respectively.

In order to check the symmetricity of the bridge across the center line of the bridge deck, LVDTs were placed along the longitudinal direction of bridge deck in Layout 1. In both bridge model cases approximately equal vertical deflection values can be observed in the LVDT1 and LVDT3 (in Table 5.1and Table 5.2) which are located at each side of the center of the bridge. This implies cable bridge model is symmetric across the center line of the bridge deck.

Table 5.1 Layout 1 – case1

Loading Sequence	Load kg	Total Load kg	Total Load N	Vertical Deflections mm		
				LVDT1	LVDT2	LVDT3
Loading Frame	2.416	2.42	23.70	1.60	2.60	1.53
Load 1	0.895	3.31	32.48	2.08	3.57	1.99
Load 2	0.894	4.21	41.25	2.61	4.52	2.53
Load 3	0.900	5.11	50.08	3.27	5.54	3.15
Load 4	0.897	6.00	58.88	3.79	6.55	3.67
Load 5	0.886	6.89	67.57	4.36	7.50	4.28

Table 5.2 Layout 1 – case 2

Loading Sequence	Load kg	Total Load kg	Total Load N	Vertical Deflections mm		
				LVDT1	LVDT2	LVDT3
Loading Frame	2.416	2.42	23.70	1.21	2.18	1.17
Load 1	0.895	3.31	32.48	1.66	2.95	1.58
Load 2	0.894	4.21	41.25	2.29	2.92	2.21
Load 3	0.900	5.11	50.08	2.73	4.99	2.71
Load 4	0.897	6.00	58.88	3.45	6.05	3.35
Load 5	0.886	6.89	67.57	4.02	7.06	3.90

For the purpose of calibrating and updating FE models, LVDTs were arranged to measure the vertical deflection of the middle cross member of the bridge in layout 2. As in previous Layout, different cable tensions were setup in both bridge model cases. In bridge model case 1 top supporting cables and pre-tensioned reverse profiled (bottom) cables in vertical plane were setup to average tension values of 1469N and 332N respectively. In bridge model case 2, top supporting cables, pre-tensioned reverse profiled (bottom) cables in vertical plane and pre-tensioned bi-

concave side cables in the horizontal plane were set up to average tension values of 1301N, 322N and 265N respectively. Table 5.3 and Table 5.4 illustrate the results obtain in each bridge model case.

Table 5.3 Layout 2 – case 1

Loading Sequence	Load kg	Total Load kg	Total Load N	Vertical Deflections mm		
				LVDT1	LVDT2	LVDT3
Loading Frame	2.416	2.42	23.70	2.52	2.56	2.54
Load 1	0.894	3.31	32.47	3.55	3.56	3.53
Load 2	0.895	4.21	41.25	4.68	4.60	4.63
Load 3	0.886	5.09	49.95	5.73	5.72	5.71
Load 4	0.897	5.99	58.75	6.89	6.85	6.84
Load 5	0.900	6.89	67.57	7.93	7.91	8.00

Table 5.4 Layout 2 – case 2

Loading Sequence	Load kg	Total Load kg	Total Load N	Vertical Deflections mm		
				LVDT1	LVDT2	LVDT3
Loading Frame	2.416	2.42	23.70	2.90	2.85	2.90
Load 1	0.894	3.31	32.47	3.90	3.76	3.74
Load 2	0.895	4.21	41.25	4.98	4.76	4.71
Load 3	0.886	5.09	49.95	6.05	5.80	5.72
Load 4	0.897	5.99	58.75	7.07	6.77	6.65
Load 5	0.900	6.89	67.57	8.19	7.85	7.82

In both bridge model cases approximately equal vertical deflection values can be observed in the LVDT1 and LVDT3 which are located at each side of the cross member of middle bridge frame. This indicates cable bridge model is symmetric along the longitudinal direction of the bridge deck. In order to validate the FE model of the cable bridge, in the next chapter, the above experimentally obtained vertical deflection results in LVDT 2 will be compared with those obtained from the FE model.

5.6 DYNAMIC TEST

The use of experimental tests to obtain the dynamic response of civil structures is a well-established practice, which can be dated back to the mid Twentieth Century (Rainieri & Fabbrocino, 2014). Input-Output Modal Analysis (also known as Experimental Modal Analysis - EMA) is the traditional method of obtaining the dynamic parameters of a structure basically by measurements of the excitation and the vibration response. It has been applied in different fields, such as automotive engineering, aerospace engineering, industrial machinery and civil engineering. However, applications of this technique are challenging in large structures due to their lower frequency range and complexities in excitation. Therefore, Output Only Modal Analysis (OMA) (also known as Operational Modal Analysis) has recently gained the attention of the Engineering community. OMA is an experimental procedure to estimate the modal parameters of a structure from measurements of the vibration response only. This research used the OMA technique to obtain the vibration parameters of the laboratory cable bridge model.

Upon completion of the static test, dynamic testing was performed on the cable bridge model to (1) obtain natural frequencies of the bridge; (2) obtain mode shapes of the bridge; (3) obtain a validated FE model by comparing the experimental results and (4) use the validated FE model to simulate a range of damage cases to study damage detection. Dynamic test was also conducted for the two bridge model cases similar to the static test and modal parameters of the bridge were extracted. Before describing the experiments, the fundamentals of OMA technique and the data driven stochastic subspace identification (SSI-DATA) will be discussed briefly in the next two sections.

5.6.1 Fundamentals of OMA Technique

In conventional Input-Output Modal Analysis, both excitation and vibration responses are measured to extract the modal parameters. However large civil structures such as high rise buildings, dams, wind turbines and bridges are difficult to excite artificially and then measure the excitation. At the same time these structures are excited by random forces such as vehicle traffic, wind and waves and their magnitudes are difficult to measure simultaneously with artificial excitation. Therefore incorrect measurement of excitation can result in inaccurate modal parameter estimates. Additionally, in EMA large amount of data is required to obtain

a very accurate modal model and hence the testing time is longer. This will affect to the daily functionality of a structure. In case of a bridge there is often a need for bridge closure to traffic during testing which results in a disturbance of activities of the general public. Moreover, EMA needs large excitations to vibrate a structure at all the points and such forces can cause local damage to the structure. Considering the above facts, in large structures OMA techniques are more efficient in determining the vibration parameters. It uses vibration responses only and input excitation is assumed as zero mean Gaussian white noise.

OMA is based on three assumptions (Reynders, 2012); (1) Linearity (the response of the system to a given combination of inputs is equal to the same combination of the corresponding outputs), (2) Stationarity (the vibration properties of a structure do not change over the time) and (3) Observability (the sensor lay out has been properly designed to obtain the modes of interest and avoiding node points). Two main groups of OMA methods can be identified; as frequency domain methods and time domain methods.

A variety of methods in both frequency and time domains that can be identified in OMA are schematically illustrated in Figure 5.15 (Cunha et al., 2007). The fundamental frequency domain method is peak-picking (PP), which is based on the evaluation of normalized average power spectral densities and ambient response transfer functions related to the response at all the measurement points. Modal parameter estimation using frequency domain decomposition (FDD) method is an improvement to the PP method by performing single value decomposition of the matrix of response spectra. It was further improved by Brinker et al. (Brincker, Ventura, et al., 2001) to estimate the modal damping factor. The enhanced frequency domain decomposition (EFDD) method obtains the power spectral densities of a set of single degree of freedom systems and auto correlation functions by taking inverse Fourier transform of power spectral densities. In EFDD modal parameters are estimated from the inspection of the decay of auto correlation functions.

The time domain methods involve the choice of a model to idealise the experimental data. These methods can be directly applied to the response correlation functions or discrete response time series. The evaluation of those functions can be done by Fast Fourier Transformation (FFT) or random decrement (RD) method. The OMA techniques based on impulse response functions are Ibrahim Time domain

(ITD), the multiple Reference Ibrahim Time Domain (MRITD), the Least Squares Complex Exponential (LSCE), the Polyreference Complex Exponential (PRCE) and Covariance-Driven Stochastic Subspace Identification (SSI-COV). The Data Driven Stochastic Subspace Identification (SSI-DATA) involves direct application of response time series. The experiment conducted in this research used SSI-DATA method for the modal parameter estimation due to its advantage of automation in SSI-Data over the FDD family (Nguyen et al., 2014).

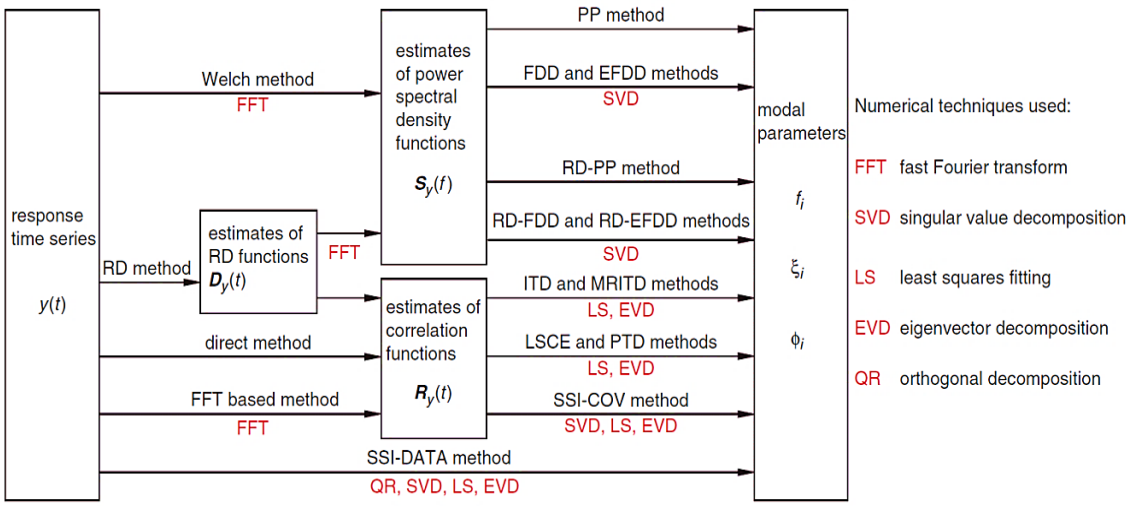

Figure 5.15 Schematic representation of OMA techniques (Cunha et al., 2007)

5.6.2 The Data Driven Stochastic Subspace Identification (SSI-DATA)

Data Driven Stochastic Subspace Identification (SSI-DATA) has been identified as the well-known robust time domain method in the OMA family. It can take into account furious modes from measurement noise, avoid spectrum leakage and cope well with dense and closely spaced modes (Brincker, Andersen, et al., 2001; Nguyen et al., 2014; Zhang et al., 2009). SSI-DATA method relies on directly fitting parametric state space models to the measured responses of a linear and time invariant physical system as described below (Nguyen et al., 2014).

$$x_{t+1} = Ax_t + w_t \; ; \; y_t = Cx_t + v_t \qquad 5.1$$

Here, x_t and y_t are the state vector and the response vector at time t, respectively. A is the system state matrix whereas, C is the observation matrix.

Amongst two stochastic processes, w_t is the process noise (i.e. the input) that drives the system dynamics whilst v_t is measurement noise of the system response. In later phase, subspace models are first established for different dimensions up to the user-defined maximum value. Estimates of matrices A and C (i.e. $\hat{A}$ and $\hat{C}$, respectively) are then obtained by the least square solution. By performing the eigenvalue decomposition of the system matrix estimate ($\hat{A}$), its discrete poles (μ_i) and eigenvectors (Ψ) can be found as follows (Brincker & Andersen, 2006):

$$\hat{A} = \Psi[\mu_i]\Psi^{-1} \tag{5.2}$$

The continuous time poles and subsequently modal frequencies and damping ratios are then obtained:

$$\lambda_i = \frac{\ln(\mu_i)}{\Delta t} \tag{5.3}$$

$$f_i = \frac{|\lambda_i|}{2\pi} \tag{5.4}$$

$$\xi_i = \frac{R_e(\lambda_i)}{|\lambda_i|} \tag{5.5}$$

where Δt is simply the sampling period. The mode shape matrix is finally derived from the observation matrix and eigenvectors:

$$\Phi = \hat{C}\Psi \tag{5.6}$$

Among different estimation algorithms for SSI-DATA (Structural Vibration Solutions A/S. 2011), Un-weighted Principal Component (UPC) has been most commonly used in OMA of civil structure. In this experiment, modal parameters were extracted by the SSI-DATA (UPC) in ARTeMIS modal analysis software. The instrument setup used in the experiment, testing procedure and dynamic test results will be discussed briefly in the next few sections.

5.6.3 Instrument Setup

Prior to dynamic testing, the data acquisition system was established; which encompassed 15 single-axial PCB® 393B05 integrated circuit piezoelectric accelerometers (Figure 5.16), positioned to measure vertical and lateral accelerations.

They are self-calibrated after a small period (less than 2 minute); which enable to automatically pickup correct accelerations without further calibrations. The sensitivity and frequency range of each accelerometer is 10V/g (±10%) and f 0.7 – 450Hz (±5%) respectively (PCB, 2014). They were attached to the bridge via aluminium equal angles glued to a number of bridge frames using CN adhesive (epoxy-based resin).

Figure 5.16 Accelerometers attached to a bridge frame

These accelerometers were attached to each of the five bridge frames. Two accelerometers measured the accelerations in the vertical direction and the third measured the accelerations in the lateral direction. Additionally, dummy accelerometers (Figure 5.17) were installed in the lateral direction at the five bridge frames to simulate identical point mass loading on both sides of the bridge frame. Layout of accelerometers is illustrated in Figure 5.18 (Dummy accelerometers are not included). The data acquisition system was operated by a National Instruments (NI) data acquisition system including NI cDAQ 9172 chassis, NI 9234 dynamic signal acquisition modules and LabVIEW signal Express software.

Figure 5.17 Dummy accelerometers

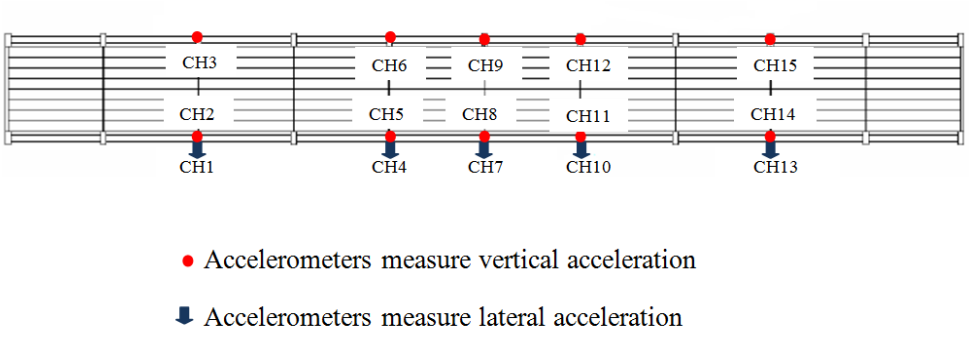

Figure 5.18 Accelerometer layout in the plan view of bridge deck

5.6.4 Testing Procedure

Before testing commenced, it was required to determine two important parameters. The first parameter is the length of time series to record the vibration data. It is necessary to ensure that the length of time series is adequate to cover complete or nearly complete behaviour of the structure under ambient vibration. The total length of time series should be in the range (Cantieni, 2005);

$$T_{min} = \frac{1000 \sim 2000}{f_{min}} \qquad 5.7$$

Where f_{min} is the expected lowest natural frequency measured in Hz. According to the preliminary FE modal analysis, f_{min} is 3.5Hz. Therefore T_{min} is 9.5 minutes (T_{min}=2000/3.5=571.4sec). Since the T_{min} was calculated from preliminary FE analysis, it is necessary to choose a minimum recording time length to be longer than 9.5 minutes. In this experiment, therefore recording time was selected as 10 minutes.

The second parameter to consider is the sampling rate of measurements. Commercial software package such as ATReMIS modal analysis software recommends sampling frequency can be f_s=3f_{max}, where f_{max} is the highest natural frequency of interest. However selected sampling rate was 2.56 kHz which is a relatively high value.

Since the cable bridge model was located in the laboratory and not subjected to any ambient loading, artificial excitation was adopted. In an effort to excite the structure, two researchers provided random tapping through a foam (to reduce the negative impact as the bridge model is very flexible) with respect to both time and

space (as random excitation is desired in OMA), at alternating frames. Figure 5.19, below illustrates the excitation method.

Figure 5.19 Different excitation of the bridge model

Before conducting any tests, the twelve load cells were checked carefully and the turnbuckles attached to the cables were adjusted to obtain required tension forces. Load cell readings were automatically recorded by eDAQ while conducting the experiment to check any tension losses occurring during testing. The test was conducted for two bridge model cases similar to the static test. All the acceleration data were captured in the time domain and were transferred to the ARTeMIS modal analysis software to obtain modal parameters.

All the dynamic tests were conducted at the undamaged state of the bridge which is considered as the baseline structure. This cable bridge structure was built in 2006; and there are no extra components of the bridge available to replace if these was damaged. Therefore, no any attempt was made to damage the bridge physically to obtain the vibration parameters at the damage condition. It was decided to simulate damage on FE model instead.

5.6.5 Dynamic Test Results

The natural frequencies and mode shapes were determined by SSI-DATA (UPC) in ARTeMIS modal analysis software. Two bridge model cases were considered in the dynamic test. In bridge model case1, top supporting cables and pre-tensioned reverse profiled (bottom) cables in vertical plane were setup to average tension values of 1446N and 326N respectively. In bridge model case2, top supporting cables, pre-tensioned reverse profiled (bottom) cables in vertical plane and pre-tensioned bi-concave side cables in the horizontal plane were set up to average tension values of 1403N, 485N and 270N respectively. In each bridge model case only the first five modes were obtained in the experiment for the damage

detection studies. Experimentally investigated natural frequencies for the bridge model case1 are listed in the table below (Table 5.5). The graphical representation of the mode shapes are illustrated in the Figure 5.20 to Figure 5.24. Two sets of dynamic test results were obtained from the two different bridge models, to enhance the validation of the FE models.

Table 5.5 Cable tension and natural frequencies - case 1

	Tension Force (N)
Top Supporting Cable	1446
Pre-tensioned Reverse Profile Bottom Cable (Vertical)	326
Pre-tensioned Bi-concave Side Cables (Horizontal)	-
Mode Shape	Natural Frequency (Hz)
1st Bending - Symmetric	3.714
2nd Bending - Anti-symmetric	5.875
1st Torsion	5.970
3rd Bending - Symmetric	8.369
2nd Torsion	10.407

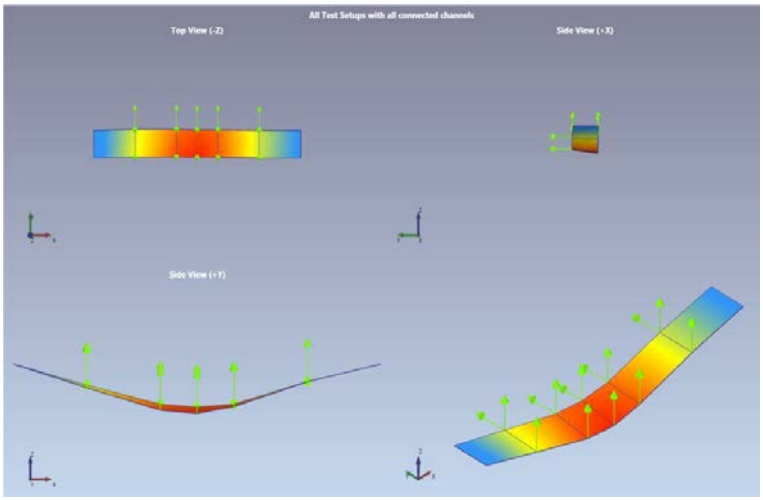

Figure 5.20 Mode 1, f = 3.714Hz

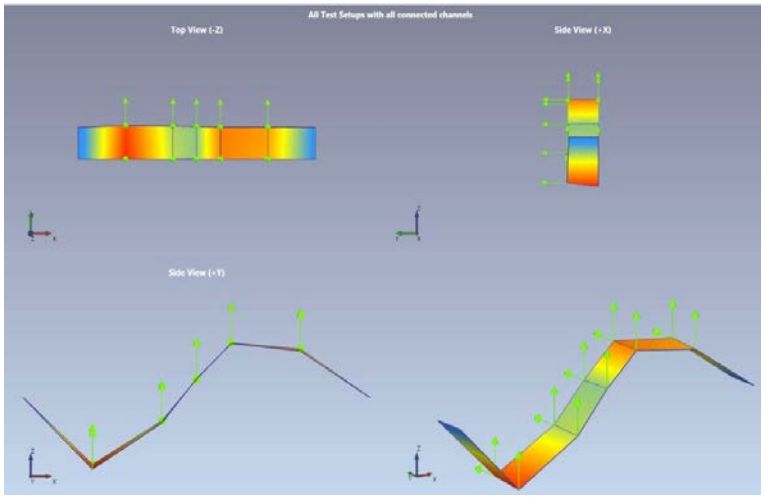

Figure 5.21 Mode 2, f = 5.8754Hz

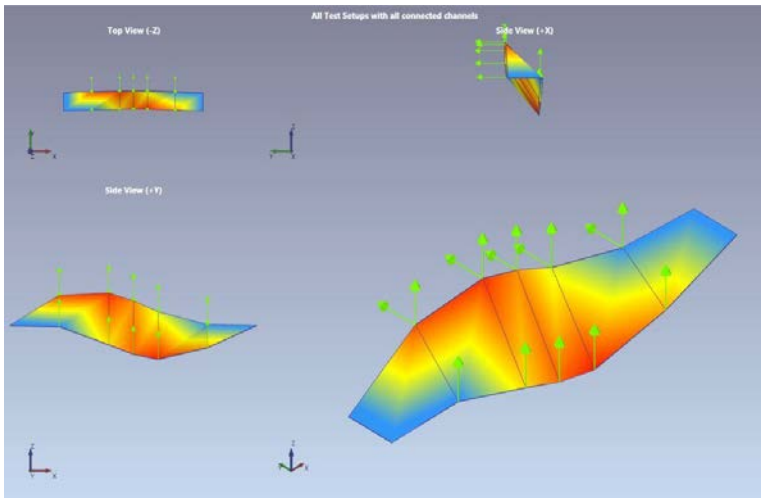

Figure 5.22 Mode 3, f = 5.9704Hz

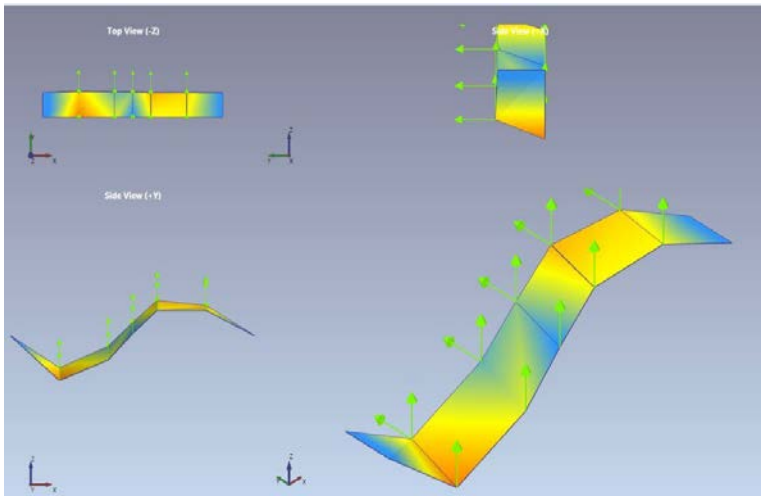

Figure 5.23 Mode 4, f = 8.369Hz

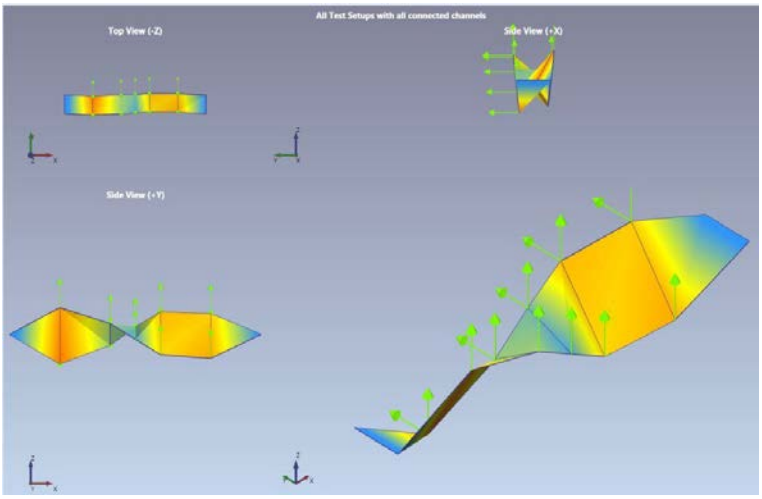

Figure 5.24 Mode 5, f = 10.4074Hz

Experimentally investigated natural frequencies and mode shapes for the bridge model case2 are listed in the table below (Table 5.6). The graphical representation of the mode shapes are illustrated in the Figure 5.25 to Figure 5.29.

Table 5.6 Cable tension and natural frequencies - case 2

	Tension Force (N)
Top Supporting Cable	1403
Pre-tensioned Reverse Profile Bottom Cable (Vertical)	485
Pre-tensioned Bi-concave Side Cables (Horizontal)	270
Mode Shape	Natural Frequency (Hz)
1st Bending - Symmetric	3.791
2nd Bending - Anti-symmetric	6.094
1st Torsion	6.077
3rd Bending - Symmetric	8.719
2nd Torsion	10.625

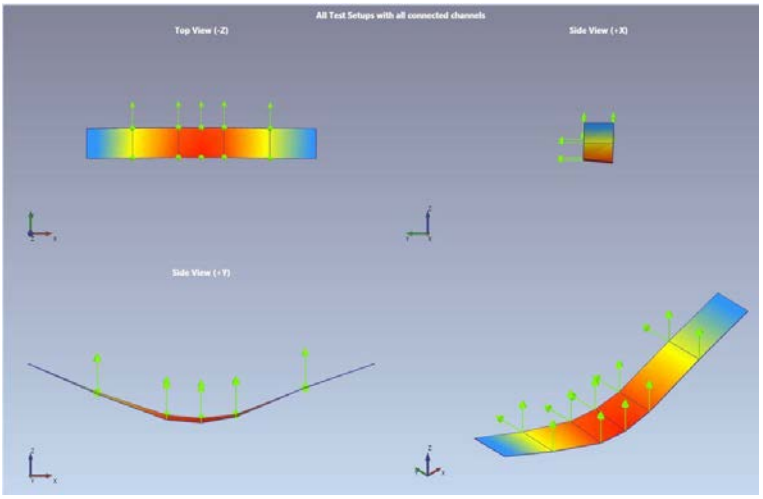

Figure 5.25 Mode 1, f = 3.7914Hz

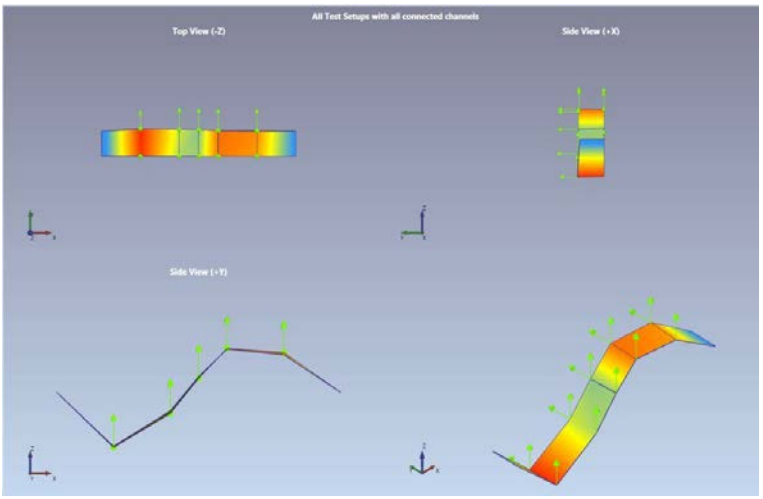

Figure 5.26 Mode 2, f = 6.094Hz

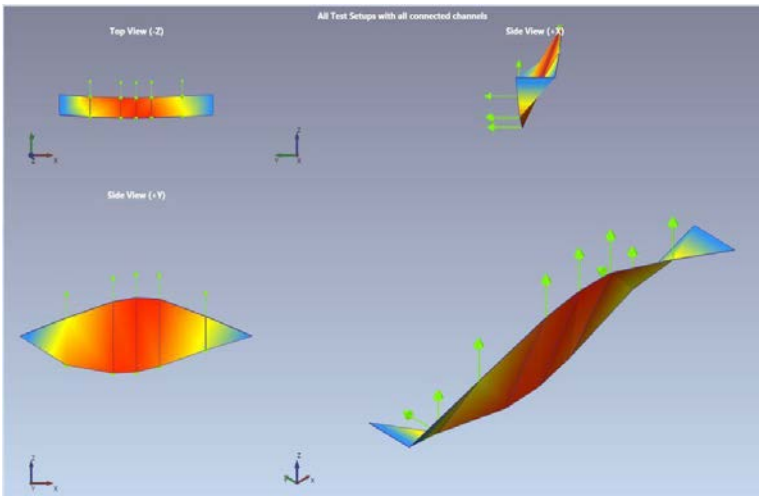

Figure 5.27 Mode 3, f = 6.077Hz

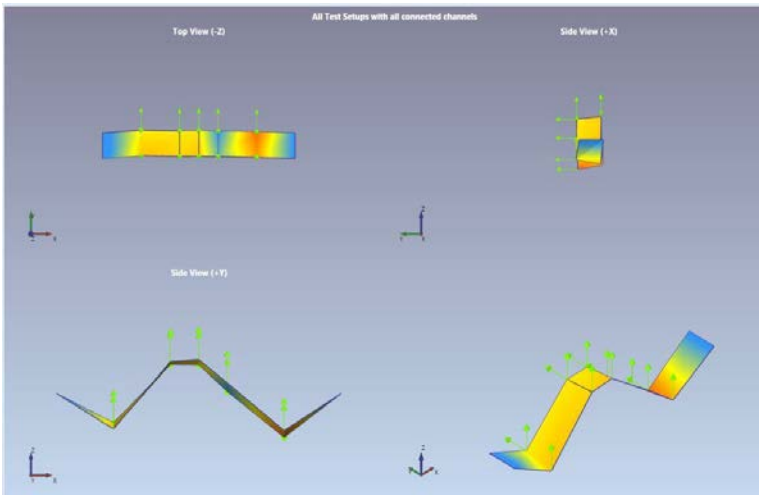

Figure 5.28 Mode 4, f = 8.719Hz

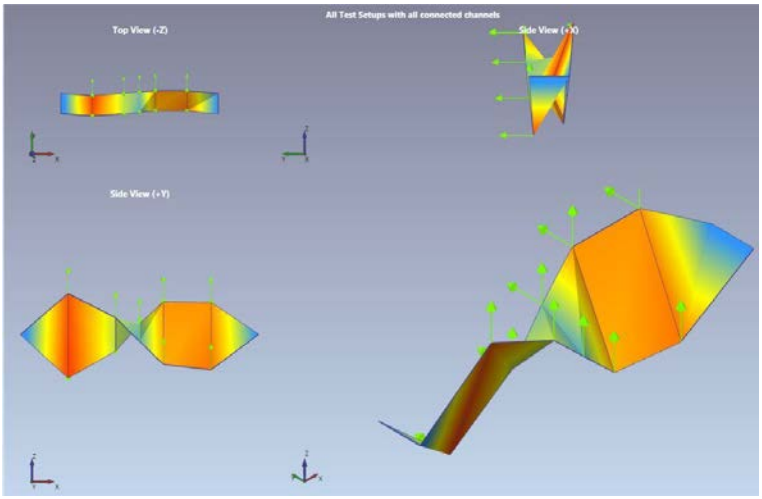

Figure 5.29 Mode 5, f = 10.625Hz

According to the results, natural frequencies increased with the increase of the tension force. No lateral vibration modes appeared in the experimental results due to tightening of the screws in the deck elements to the bridge frame. Some mode shapes not captured in the SSI-DATA (UPC) method were obtained by FDD method. All the experimental results were compared with the FE model in the next chapter for the model validation process.

5.7 SUMMARY

This chapter describes both static and dynamic testing of the laboratory cable bridge. Background information on the OMA techniques and SSI-DATA (UPC) method were described briefly. Description of the laboratory cable bridge and its reconstruction/renovation and calibration before testing were presented. Instrument

setup, testing method and test results were described along with graphical information on both static and dynamic tests.

Examining the static test results, it can be concluded that the bridge is symmetrical not only across the centre line of the bridge deck but also along the longitudinal direction of the bridge deck. Further, results obtained from the static test will be used to validate the geometry, boundary condition of the FE model of the bridge in the next chapter. The laboratory cable bridge has three sets of cables which are serving different structural purposes of the bridge. Dynamic test was conducted in two bridge model cases and SSI-DATA (UPC) in ARTeMIS modal analysis software was used to extract the modal parameters. Bridge model case 1, comprised of top supporting cables and pre-tensioned reverse profiled (bottom) cables in vertical plane while bridge model case 2, comprised of top supporting cables, pre-tensioned reverse profiled (bottom) cables in vertical plane and pre-tensioned bi-concave side cables in the horizontal plane. The main function of bi-concave side cables in the horizontal plane is to provide additional stiffness to the bridge; which resulted in stiffer bridge model in case2 than the case1. This was clearly verified by dynamic test results with higher natural frequencies in bridge model case2. Due to complex nature of the bridge model, attempt to create physical damage on the cable bridge was unsuccessful. In order to validate the FE model to use in damage detection studies, all the dynamic parameters (natural frequencies and mode shapes) extracted in the dynamic test will be compared with those obtained by FE model in the next chapter.

Chapter 6: Damage Detection in the Laboratory Cable Bridge Structure

6.1 INTRODUCTION

The main focus of this chapter is investigating the potential of the modal flexibility based DIs for detecting and locating damage in the various cables of the cable bridge model under different damage scenarios. Towards this end, a FE model of the cable bridge was developed in the ANSYS Workbench and validated using previously obtained experimental results (vertical deflections, cable tensions, natural frequencies). Next, three different damage scenarios namely; single damage scenarios, multiple damage scenarios and tension reduction in cables were simulated in the validated FE model with varied location and severity and modal parameters at both damaged and undamaged states were extracted. Using these modal parameters, damage detection capability of the DIs were examined and discussed. The impact of random measurement noise in the modal data on the damage detection capability of DIs was finally examined.

6.2 FE MODELLING OF LABORATORY CABLE BRIDGE STRUCTURE

FE modelling is extensively used in damage detection studies due to the difficulty of applying a physical damage to real structures and the time consuming nature of experimental testing. Validated FE models therefore, facilitates the simulation of various possible damage cases in a structure without consuming time and labour in experiments and avoiding inaccuracies in laboratory testing. In this research, a validated FE model using self-performed experiments of the laboratory cable bridge structure, will be used for simulating various damage scenarios and obtain vibration properties at both damaged and undamaged states to verify the proposed damage detection methodology.

6.2.1 Geometry of the Laboratory Cable Bridge Structure

The objective of the FE modelling of the laboratory cable bridge is to develop a numerical model that represents the actual laboratory structure as close as possible to

use in damage detection studies. Therefore, an attempt was made to accurately replicate all the geometric features of this complex structure precisely. To achieve this, the commercial FE analysis software package ANSYS Workbench which is facilitated with graphical user interface for developing complex models as multibody parts, is used.

The geometry of the laboratory cable bridge was modelled in the DesignModeler module of ANSYS Workbench. It was modelled as a 3D FE model with three parts namely; bridge (nine transverse bridge frames and cables), deck and end supports. These three parts were connected by joint feature in the Mechanical module of the ANSYS Workbench. The entire bridge system was mainly made from aluminium and stainless steel. All the elements of the nine bridge frames are aluminium except the thread rods which are stainless steel. 7x19 stainless steel wires with different diameters are used as the bridge cables. Bridge deck also made of aluminium with different material properties. Table 6.1 below illustrates the material characteristics used in developing the FE model. Member sizes used for the FE modelling of the laboratory cable bridge structure are tabulated in Table 6.2.

Table 6.1 Material characteristics

Material	Density (kg/m^3)	Young's Modulus E (N/m^2)	Poisson's Ratio ν
Aluminium	2745	6.700E+10	0.33
Stainless Steel	7850	2.000E+11	0.25
3.2mm - 7x19 Stainless steel wire	5679	4.725E+10	0.30
1.6mm - 7x19 Stainless steel wire	4765	4.688E+10	0.30
Aluminium-Deck	3026	6.900E+10	0.33

Table 6.2 Cross section dimension of the bridge elements

Member	Cross Section Dimension (mm)
End Cap	60 x 25 x 10
Side Member	300 x 25 x 10
Cross Member	400 x 25 x 30
Deck Unit	450 x 48 x 5
Thread road	5 mm diameter
Top supporting cables	3.2 mm 7 x 19 strand
Pre-tensioned reverse profiled (bottom) cables in vertical plane	1.6 mm 7 x 19 strand
Pre-tensioned bi-concave side cables in the horizontal plane	1.6 mm 7 x 19 strand

6.2.2 Analysis of the Laboratory Cable Bridge Structure

Geometry of the cable bridge was created in the DesignModeler module and transferred into the Mechanical module of the ANSYS Workbench for analysis. In Mechanical module, correct material characteristics were assigned to each element of the bridge and point masses of each 0.132kg (weight of accelerometers + weight of aluminium equal angle) were added to the bridge frames at where locations only accelerometers were attached. Since accelerometers were attached to the bridge while dynamic testing, those point masses were added to the FE model only in the dynamic analysis.

All the elements of the bridge were modelled as beam and link elements except the end supports. BEAM188 element and SHELL181 element types (as described in chapter 3) were used to simulate bridge frames and deck respectively. All cables associated in this laboratory cable bridge, including the top supporting cables, pre-tensioned reverse profiled (bottom) cables in vertical plane and pre-tensioned bi-concave side cables in the horizontal plane are very thin cables having very small bending stiffness. Therefore these cables were simulated by LINK180 element with tension only option.

Connectivity of bridge (bridge frames and cables), deck and end support were established by joint feature in the Mechanical module. In the FE model, connectivity of the cables and cable plugs in bridge frames were modelled as rigid connections as there was no allowance for the cables to rotate or displace at those locations in the cable bridge model. In order to connect the cables with the end support, body-body joint feature with fixed connectivity was established. Similarly, bridge frame and deck connectivity was also established by body-body joint feature allowing rotations perpendicular to the longitudinal axis of the deck. Member off set has been considered for the deck elements to represent the correct connectivity of the deck and cross members. In the nine transverse bridge frames, all the members were considered as rigidly connected together at the intersection locations.

Meshing of the structure was performed by an inbuilt algorithm in Mechanical module with following features. A FE model with a total of 5356 nodes and 2897 elements was created using basic meshing features in Mechanical module namely; Physical preference: mechanical; relevance: 100; relevance centre: fine and minimum edge length: 20mm. Initial tension forces were introduced to the cables using command features in Mechanical module as an initial stress load. Fixed support with no rotations and no translations were assigned to the end supports.

In the static load test, the loading system consisted of an aluminium plate supported by two aluminium bars on the bridge deck to transfer the vertical load to the deck units. The deck units at the two middle segments are hence subjected to uniform vertical line loads at their own half span lengths. Simulation of that loading in the FE model was done by applying a line load across the two middle segments of the bridge deck.

A Pre-stressed Modal Analysis was conducted to obtain the natural frequencies and mode shapes of the laboratory cable bridge FE model. Towards this end, first, a nonlinear static analysis with large deflection option was conducted to obtain the stress stiffening matrix caused by the internal forces due to the dead loads acting on the bridge. Second, vertical deflections were obtained at required locations of the bridge at the end of the static analysis. Finally, the modal analysis was performed on the basis of the deformed equilibrium configuration of the bridge to obtain the natural frequencies and mode shapes.

In the experiment, both static and dynamic tests were conducted for the pre-selected two bridge model cases. For the static test, two LVDT layouts were selected and for each layout, tests were conducted for two bridge model cases. FE models for each test case were developed and a comparison of results with those obtained experimentally is presented in the next section. FE model of the bridge is illustrated in the figure below.

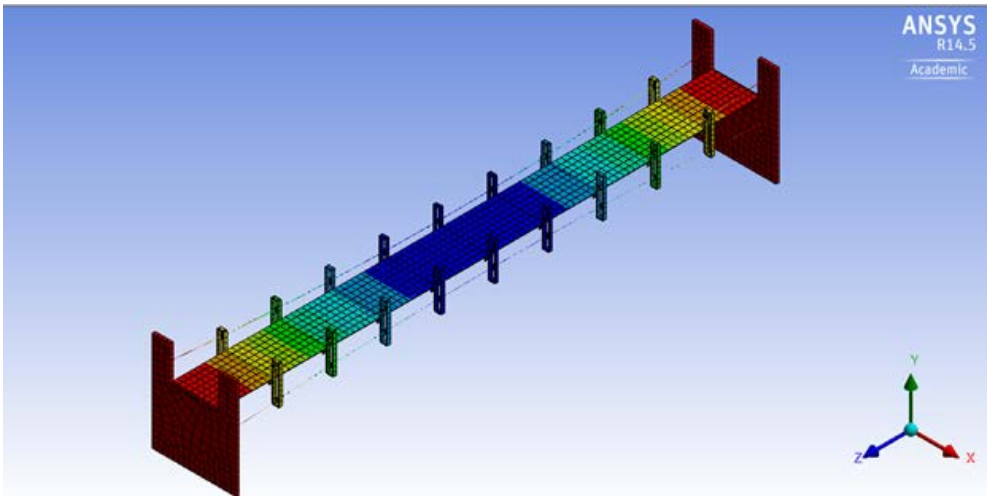

Figure 6.1 FE model of the laboratory cable bridge

6.3 VALIDATION OF FE MODEL OF THE LABORATORY CABLE BRIDGE STRUCTURE

To validate the FE model, a comparison of experimental and FE model results was made. Three parameters namely; vertical deflections, tension forces of cables and natural frequencies obtained in FE analysis were compared with those from the experiment in the static and dynamic tests respectively. Mode shapes were also compared for further verification of the dynamic analysis. In achieving the validation of the FE model of this study, model updating was done manually to tune in the structural parameters of the FE model such that deflections and natural frequencies obtained in the experiment and FE model are minimised. With the change of structural parameters such as cable tension, connectivity of structural elements, support conditions, member offsets and Young's Modulus, the initial FE model was updated to match the measured vertical deflections and natural frequencies as close as possible. Validation of the updated FE model results with measured parameters in the experiment will be presented in the next section.

6.3.1 Validation of Static Test Results

In order to investigate the symmericity and static behaviour of the laboratory cable bridge, two LVDT layouts were used to measure the vertical deflections under the pre-defined static load. In LVDT layout 1, bridge model case 1, top supporting cables and pre-tensioned reverse profiled (bottom) cables in vertical plane were setup to average tension values of 1446N and 326N respectively. In bridge model case 2, top supporting cables, pre-tensioned reverse profiled (bottom) cables in vertical plane and pre-tensioned bi-concave side cables in the horizontal plane were set up to average tension values of 1403N, 485N and 270N respectively.

In LVDT layout 2, bridge model case 1, top supporting cables and pre-tensioned reverse profiled (bottom) cables in vertical plane were setup to average tension values of 1469N and 332N respectively. In bridge model case 2, top supporting cables, pre-tensioned reverse profiled (bottom) cables in vertical plane and pre-tensioned bi-concave side cables in the horizontal plane were set up to average tension values of 1301N, 322N and 265N respectively.

The comparison of the Vertical deflections obtained from FE analysis and experiment was done by calculating the relative error, $\delta_{error} = \frac{(\delta_{exp} - \delta_{fem})}{\delta_{exp}} \times 100$. Where δ_{exp} is vertical deflection obtained by experiment and δ_{num} is vertical deflection obtained by FE analysis. Following tables and figures illustrate the comparison of the vertical deflections obtained from FE analysis and experiment in bridge model cases 1 and 2 of both LVDT layouts.

Table 6.3 Layout 1 – Vertical deflection case 1

Loading Sequence	Load	Total Load	Total Load	Vertical Deflection mm		δ_{error} (%)
	kg	kg	N	δ_{exp}	δ_{fem}	
Loading Frame	2.416	2.416	23.70	2.60	2.72	-4.5
Load 1	0.895	3.311	32.48	3.57	3.59	-0.7
Load 2	0.894	4.205	41.25	4.52	4.39	2.9
Load 3	0.900	5.105	50.08	5.54	5.16	6.8
Load 4	0.897	6.002	58.88	6.55	5.96	9.0
Load 5	0.886	6.888	67.57	7.50	6.71	10.5

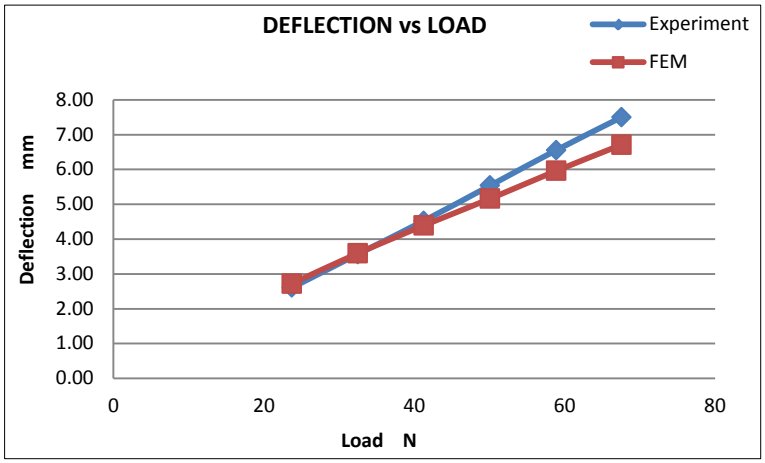

Figure 6.2 Vertical Deflection vs Load curve for Layout 1 – case 1

Table 6.4 Layout 1 – Vertical deflection case 2

Loading Sequence	Load kg	Total Load kg	Total Load N	Vertical Deflection mm		δ_{error} (%)
				δ_{exp}	δ_{fem}	
Loading Frame	2.416	2.416	23.70	2.18	1.98	9.2
Load 1	0.895	3.311	32.48	2.95	2.79	5.4
Load 2	0.894	4.205	41.25	3.99	3.64	8.7
Load 3	0.900	5.105	50.08	4.99	4.58	8.3
Load 4	0.897	6.002	58.88	6.05	5.49	9.3
Load 5	0.886	6.888	67.57	7.06	6.34	10.2

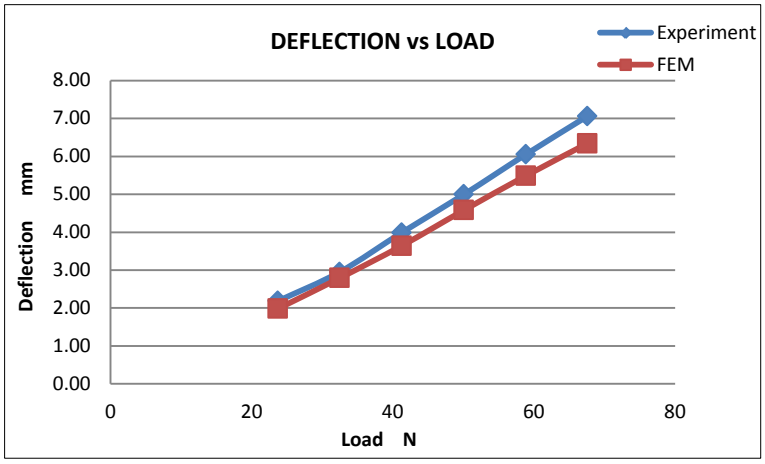

Figure 6.3 Vertical Deflection vs Load curve for Layout 1 – case 2

Table 6.5 Layout 2 – Vertical deflection case 1

Loading Sequence	Load kg	Total Load kg	Total Load N	Vertical Deflection mm		δ_{error} (%)
				δ_{exp}	δ_{fem}	
Loading Frame	2.416	2.42	23.70	2.56	2.65	-3.3
Load 1	0.894	3.31	32.47	3.56	3.45	3.2
Load 2	0.895	4.21	41.25	4.60	4.39	4.7
Load 3	0.886	5.09	49.95	5.72	5.35	6.5
Load 4	0.897	5.99	58.75	6.85	6.35	7.4
Load 5	0.900	6.89	67.57	7.91	7.42	6.2

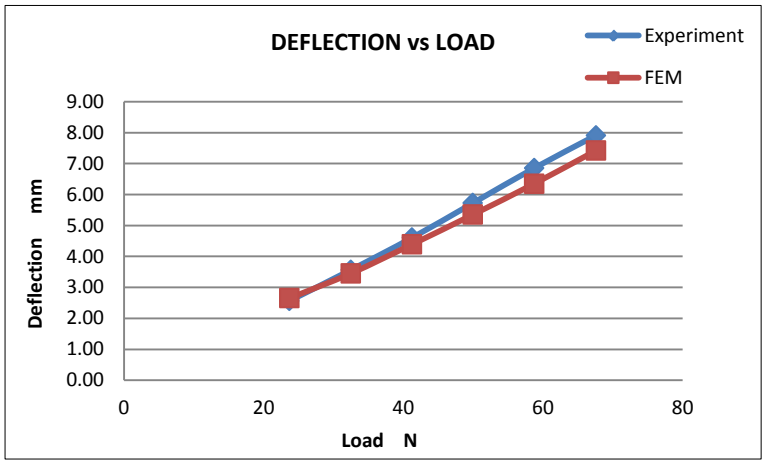

Figure 6.4 Vertical Deflection vs Load curve for Layout 2 – case 1

Table 6.6 Layout 2 – Vertical deflection case 2

Loading Sequence	Load kg	Total Load kg	Total Load N	Vertical Deflection mm		δ_{error} (%)
				δ_{exp}	δ_{fem}	
Loading Frame	2.416	2.42	23.70	2.85	2.69	5.5
Load 1	0.894	3.31	32.47	3.76	3.58	4.7
Load 2	0.895	4.21	41.25	4.76	4.48	5.9
Load 3	0.886	5.09	49.95	5.80	5.51	5.0
Load 4	0.897	5.99	58.75	6.77	6.55	3.2
Load 5	0.900	6.89	67.57	7.85	7.59	3.3

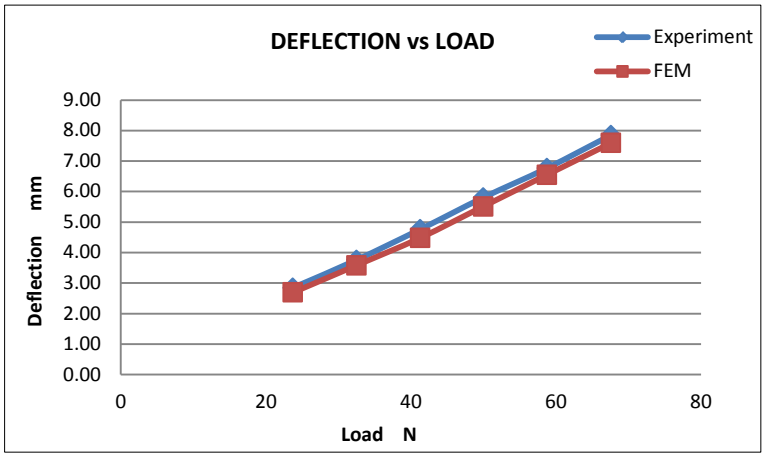

Figure 6.5 Vertical Deflection vs Load curve for Layout 2 – case 2

The above graphs show a very close correlation between experimental and FE results. Also, from the tables it is noted that the δ_{error} of the vertical deflections (experiment and FE analysis) is in general less than 10% except in one case. It can be observed that the vertical deflection vary when different pre-tensions have been introduced in the reverse profiled bottom and/or side cables. Overall it is concluded that the vertical deflection values agree well and FE model is able to represent the static behaviour of the laboratory cable bridge accurately.

6.3.2 Validation of Dynamic Test Results

In order to validate the FE model, a comparison between FE and experimental bridge tension forces and dynamic characteristics was conducted. As mentioned before, experiment was conducted for two bridge model cases. In bridge model case 1, top supporting cables and pre-tensioned reverse profiled (bottom) cables in vertical plane were setup to average tension values of 1446N and 326N respectively. In bridge model case 2, top supporting cables, pre-tensioned reverse profiled (bottom) cables in vertical plane and pre-tensioned bi-concave side cables in the horizontal plane were set up to average tension values of 1403N, 485N and 270N respectively. The comparison of the tension forces of the cables and natural frequencies of the bridge obtained from FE analysis and experiment was conducted by calculating relative error using the following equations;

$$T_{error} = \frac{(T_{exp} - T_{fem})}{T_{exp}} \times 100 \qquad 6.1$$

$$f_{error} = \frac{(f_{exp} - f_{fem})}{f_{exp}} \times 100 \qquad 6.2$$

Where $T_{\exp}$ and f_{exp} are tension forces and natural frequency obtained at experiment and T_{fem} and f_{fem} is natural frequency obtained by FE analysis. In addition, mode shapes were also compared. The following tables and figures illustrate the comparison of the natural frequencies and mode shapes obtained from FE analysis and experiment in bridge model cases1 and 2.

Table 6.7 Tension forces and frequencies of bridge model case 1

	Case 1		
Element	Tension Force (N)		T_{error} (%)
	T_{exp}	T_{fem}	
Top Cable N	1446	1442	0.28
Bottom Cable N	326	299	8.28
Bottom Horizontal cable N	-	-	-
Mode	Frequency (Hz)		f_{error} (%)
	f_{exp}	f_{fem}	
1st Bending - Symmetric	3.714	3.609	2.8
2nd Bending - Anti-symmetric	5.875	5.562	5.3
1st Torsion	5.970	5.703	4.5
3rd Bending - Symmetric	8.369	8.777	-4.9
2nd Torsion	10.407	10.731	-3.1

Table 6.8 Tension forces and frequencies of bridge model case 2

	Case 2		
Element	Tension Force (N)		T_{error} (%)
	T_{exp}	T_{fem}	
Top Cable N	1403	1450	-3.35
Bottom Cable N	485	476	1.86
Bottom Horizontal cable N	270	261	3.33
Mode	Frequency (Hz)		f_{error} (%)
	f_{exp}	f_{fem}	
1st Bending - Symmetric	3.791	3.736	1.5
2nd Bending - Anti-symmetric	6.094	5.793	4.9
1st Torsion	6.077	6.001	1.3
3rd Bending - Symmetric	8.719	9.423	-8.1
2nd Torsion	10.625	10.906	-2.6

Mode	FEM	Experiment
1st Mode	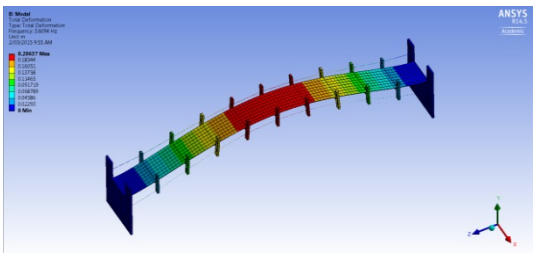	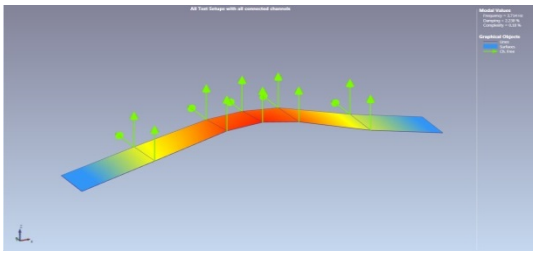
2nd Mode	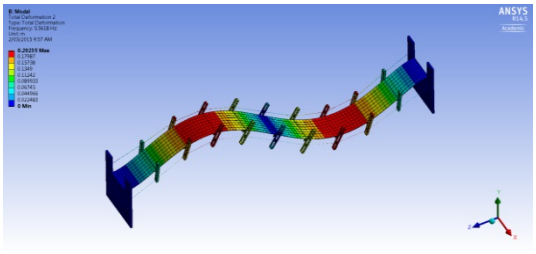	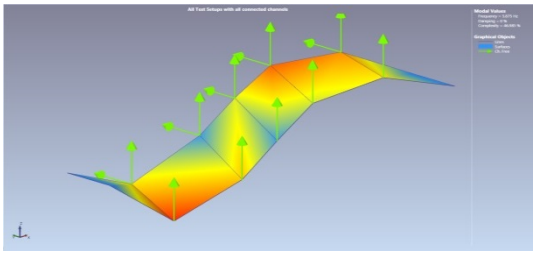
3rd Mode	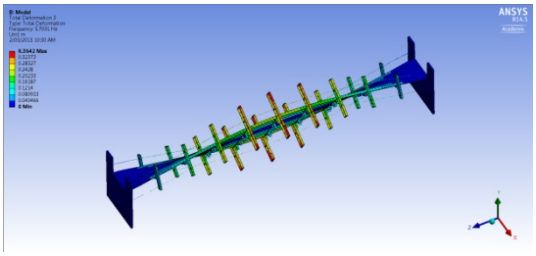	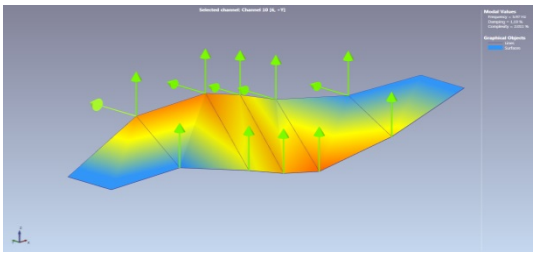
4th Mode	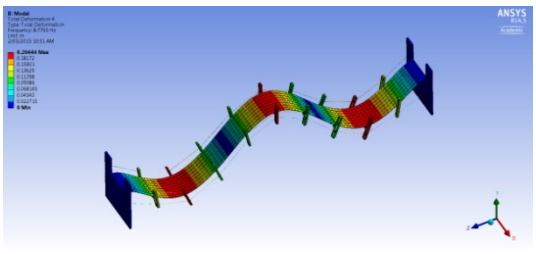	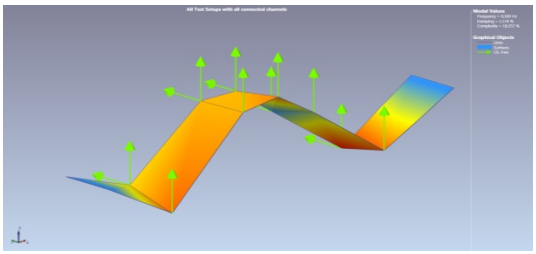
5th Mode	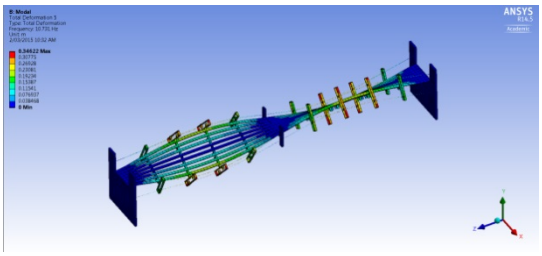	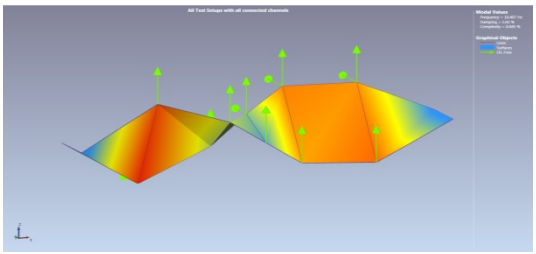

Figure 6.6 Comparison of mode shapes - bridge model case 1

Mode	FEM	Experiment
1st Mode	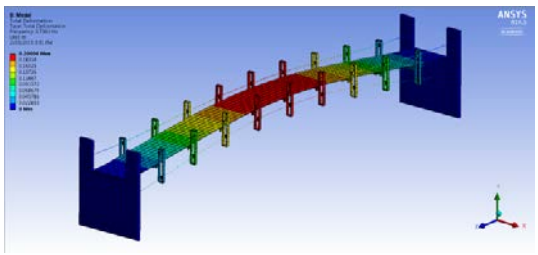	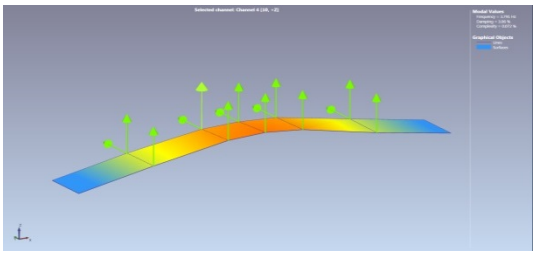
2nd Mode	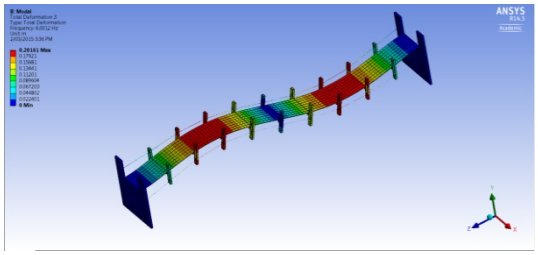	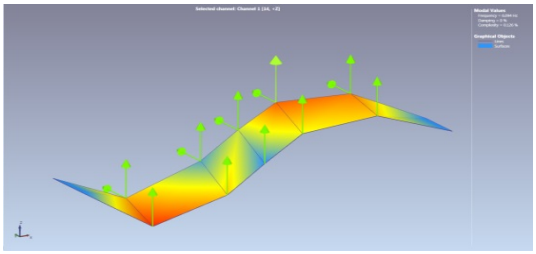
3rd Mode	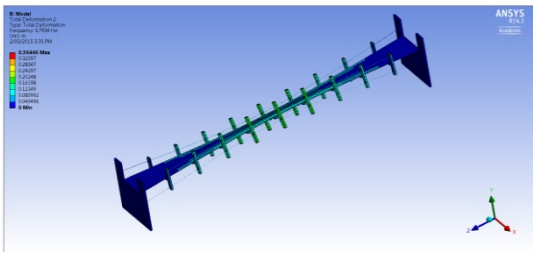	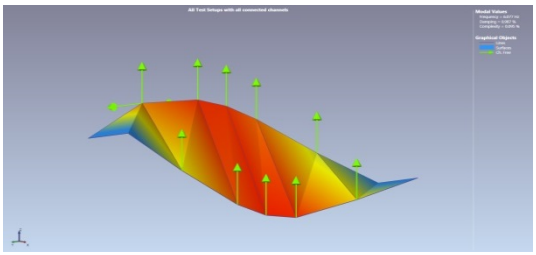
4th Mode	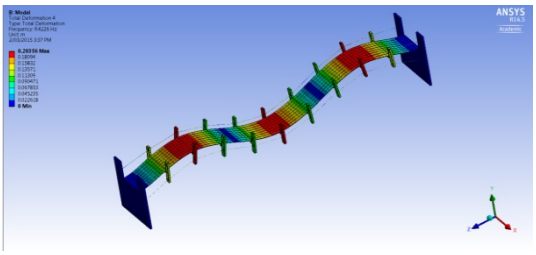	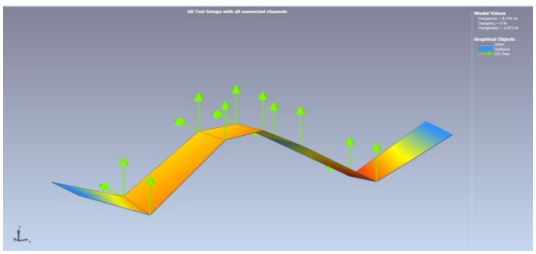
5th Mode	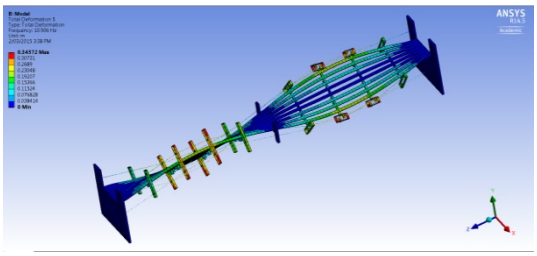	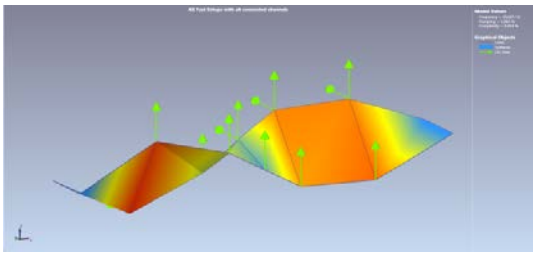

Figure 6.7 Comparison of mode shapes - bridge model case 2

Table 6.7 and Table 6.8 illustrate the tension forces and first five natural frequencies of the FE model and laboratory cable bridge structure. From the results, it can be observed that the errors in tension forces of cables and the frequencies of the FE analysis are smaller than 9%, which demonstrates a very good correlation of results. From the outcomes of the above comparison, it can be concluded that the FE model is a good representation of the laboratory cable bridge model and hence the FE modelling techniques were verified. The validated FE model then provides the base line model for vibration based damage detection applications which will be described in the next section.

6.4 DAMAGE DETECTION IN CABLES

In this study main objective is evaluating competency of damage detection of DIs in different types of cables which provides different structural purposes, therefore all the damage cases study here are only confined to the cables. The practical difficulties in damaging to the bridge cables and the difficulties in obtaining mass normalized mode shapes by the Output Only modal analysis were limited this study to the vibration data from the numerically simulated damage in the FE model.

The FE model validated in the previous section of this chapter is considered as the undamaged baseline model for vibration based damage detection application. Eighteen damage cases were introduced in the FE model to synthesize the various damage scenarios. It includes three different damage scenarios namely; single damage scenarios, multiple damage scenarios and tension reduction in cables. Since this bridge consists of three types of cables, three damage cases were examined on each cable type at the mid span, quarter span and near the support, with all together nine damage cases to represent single damage scenarios. Similarly, two damage cases for each cable type with a total of six damage cases were examined under the multiple damage scenarios. Further, three damage cases were examined to cater for the reduction of tension force in cables.

In the discussion of results, damage detection capability of component specific DIs compared with MF difference is presented. Two DIs namely: vertical damage index and lateral damage index (defined in chapter 3) were calculated by using the vertical and lateral components of the first five mode shapes respectively. Similarly, MF difference vertical and MF difference lateral were calculated using vertical and

lateral components of the first five mode shapes respectively. Following abbreviations are used in the presentation of the results.

DI_V Damage Index Vertical - calculated by using vertical components of mode shapes

DI_L Damage Index Lateral - calculated by using lateral components of mode shapes

MFD_V Modal Flexibility Difference Vertical - calculated by using vertical components of mode shapes

MFD_L Modal Flexibility Difference Lateral - calculated by lateral components of mode shapes

6.4.1 Damage Scenarios

Damage in FE models can be simulated by changing the Young's modulus or changing the cross section area or removing elements at damage location. This study simulated damage in the cables by reducing Young's modulus of the specified elements. Tables below represent the exact locations of the damage cases considered in this study. In order to calculate the modal flexibility based DIs defined previously, natural frequencies and both vertical and lateral components of the first five modes were extracted from the FE analysis in both damaged and undamaged states of the bridge.

In single damage scenarios, 20% stiffness reduction at the mid span, quarter span and near the support of the cable were considered, while 10% and 20% stiffness reduction in two different locations of the cable were considered to cater for multiple damage scenarios. In the discussion of results abbreviation used for top supporting cables, pre-tensioned reverse profiled (bottom) cables in vertical plane and pre-tensioned bi-concave side cables in the horizontal plane are TSC, RPC and BCSC respectively. Here X is measured along the span of the bridge starting from end support.

Table 6.9 Single damage scenarios

Damage Case	Location	Severity of Damage
Single Damage Scenario		
DC 1	Damage at middle of top supporting cable 1 (X=2.250m to X=2.475m)	20%
DC 2	Damage at quarter of top supporting cable 1 (X=1.125m to X=1.350m)	20%
DC3	Damage at corner of top supporting cable 2 (X=4.275m to X=4.500m)	20%
DC 4	Damage at middle of reverse profiled cable 1 (X=2.025m to X=2.475m)	20%
DC 5	Damage at quarter of reverse profiled cable 1 (X=0.900m to X=1.350m)	20%
DC 6	Damage at corner of reverse profiled cable 1 (X=4.275m to X=4.500m)	20%
DC 7	Damage at middle of bi-concave side cable 1 (X=2.025 to X=2.475)	20%
DC 8	Damage at quarter of bi-concave side cable 1 (X=0.900m to X=1.350m)	20%
DC 9	Damage at corner of bi-concave side cable 1 (X=4.275m to X=4.500m)	20%

Table 6.10 Multiple damage scenarios

Damage Case	Location	Severity of Damage
Multiple damage scenario		
DC 10	Damage at two locations of top supporting cable 1 (X=1.125m to X=1.350m) and (X=3.150m to X=3.375m)	20% 10%
DC 11	Damage at two locations of top supporting cable 1 (X=2.025m to X=2.250m) and (X=3.150m to X=3.375m)	20% 10%
DC 12	Damage at two locations of reverse profiled cable 1 (X=0.900m to X=1.350m) and (X=3.150m to X=3.600m)	20% 10%
DC 13	Damage at two locations of reverse profiled cable 1 (X=2.025m to X=2.475m) and (X=3.150m to X=3.600m)	20% 10%
DC 14	Damage at two locations of bi-concave cable 1 (X=0.900m to X=1.350m) and (X=3.150m to X=3.600m)	20% 10%
DC 15	Damage at two locations of bi-concave cable 1 (X=2.025m to X=2.475m) and (X=3.150m to X=3.600m)	20% 10%

Table 6.11 Tension reduction in cables

Damage Case	Location	Severity of Damage
Tension Reduction in Cables		
DC 16	Tension reduction in top supporting cable 1	2%
DC 17	Tension reduction in pre-tensioned reverse profiled cable 1	15%
DC 18	Tension reduction in pre-tensioned bi-concave side cable 1	20%

6.4.2 Damage Detection without Noise in Modal Data

Damage detection results for each damage case considered are illustrated below. Results include plots of damage indices (DI_V and DI_L) and plots of modal flexibility difference (MFD_V and MFD_L) in both damaged and undamaged cables. Damage location is indicated with red dotted lines.

- Single Damage Scenarios

  Nine damage cases were examined to study the damage locating capability of DIs and MF difference calculated using vertical and lateral components of mode shape.

1. Damage Case 1 (DC 1)

The first damage case studied is that in the middle of the top supporting cable 1 with a 20% stiffness reduction. Numerical results of the damage indices (a) DI_V (b) DI_L and modal flexibility difference (c) MFD_V and (d) MFD_L are shown in Figure 6.8 respectively. In Figure 6.8 (a), the DI_V for the damaged cable (TSC 1) reaches its maximum value at the nodes of the damaged location and no changes can be observed to the DI_V curve in undamaged cable (TSC 2). In Figure 6.8 (b), the DI_L curves reach their maximum values at damaged location in both damaged and undamaged cables, however unable to identify the damaged cable. Similar trends can be observed in the MF difference in Figure 6.8 (c) and (d). In this damage case, DI_V and MFD_V detect the damage successfully at the middle of the cable, and confirm the actual location of the damage considered.

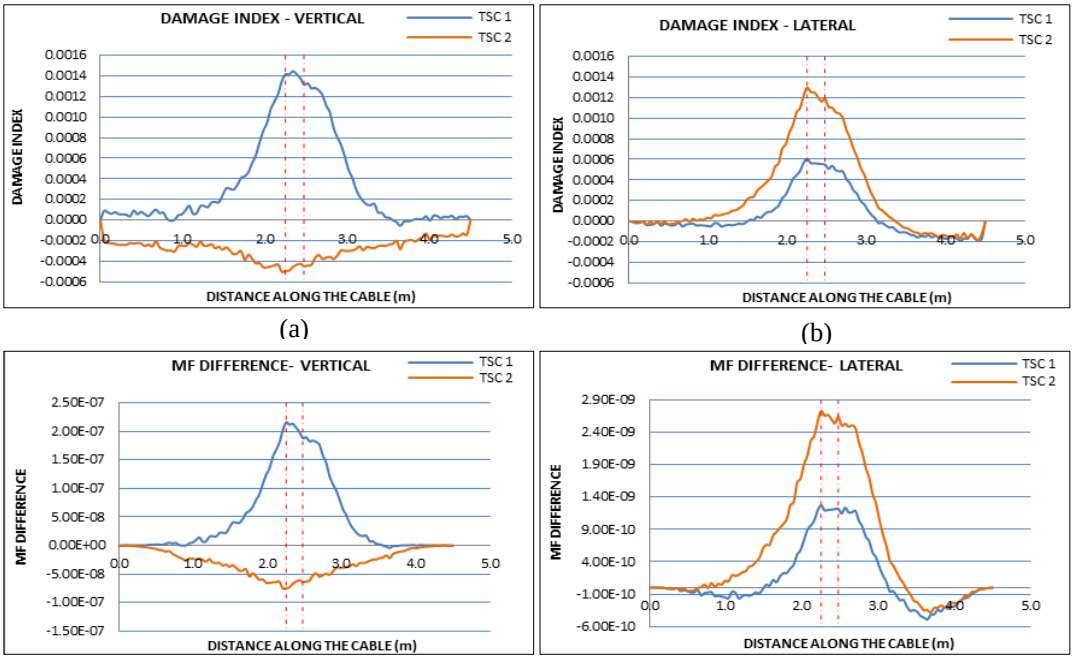

Figure 6.8 DC1 - Damage indices (a) DI_V (b) DI_L and MF difference (c) MFD_V (d) MFD_L

2. Damage Case 2 (DC 2)

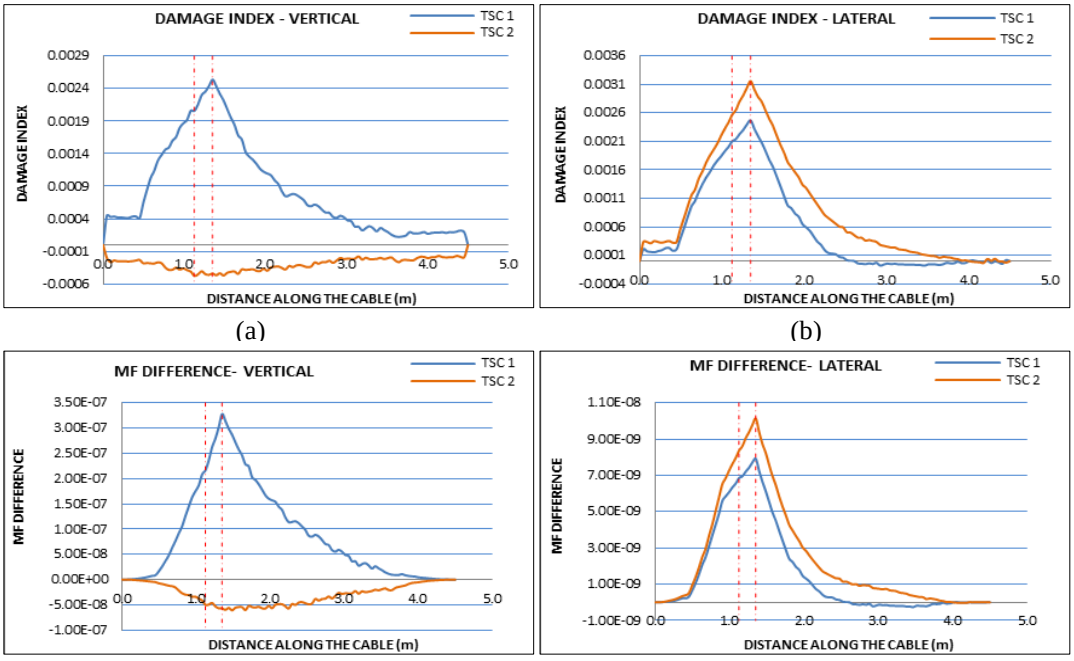

Figure 6.9 DC2 - Damage indices (a) DI_V (b) DI_L and MF difference (c) MFD_V (d) MFD_L

Figure 6.9 illustrates both the DIs and MF difference curves for the second damage case with a 20% stiffness reduction in quarter span of the top supporting cable 1. The curve (Figure 6.9 (a)) related to the DI_V peaks at the exact damage location being considered at the TSC 1 and no any changes to the DI_V in the TSC 2 is observed. However, DI_L peaks not only at the TSC 1 at damage location but also at

the corresponding location in TSC 2. MFD_V curve peaks at damage location in TSC 1 and successfully locates the damage. The MFD_L curves reach their maximum values at damaged location in both damaged and undamaged cables and unable to identify the damaged cable successfully. Based on the examination of the four graphs, it can be concluded that incorporating vertical component of mode shapes for detecting damage in a suspended cable of a structure is a successful approach. Therefore, competency of DI_V and MFD_V in damage detection of cables is further evaluated through Damage Case3 considered in this study.

3. Damage Case 3 (DC 3)

Two curves of the damage indices for damage case 3 are shown in Figure 6.10 (a) and (b). Damage Case 3 is simulated near the support in the top supporting cable 2 with 20% stiffness reduction. The DI_L shows peaks representing the damage location in both TSC 1 and TSC 2. However, a plot of the DI_V demonstrates one peak in the TSC 2, as in Figure 6.10 (a) for the exact damage location considered. However, both graphs related to the MFD_V and MFD_L demonstrate incorrect damage locating results. This verifies DI_V computed for a suspended cable structure have the ability to detect damage more accurately than DI_L.

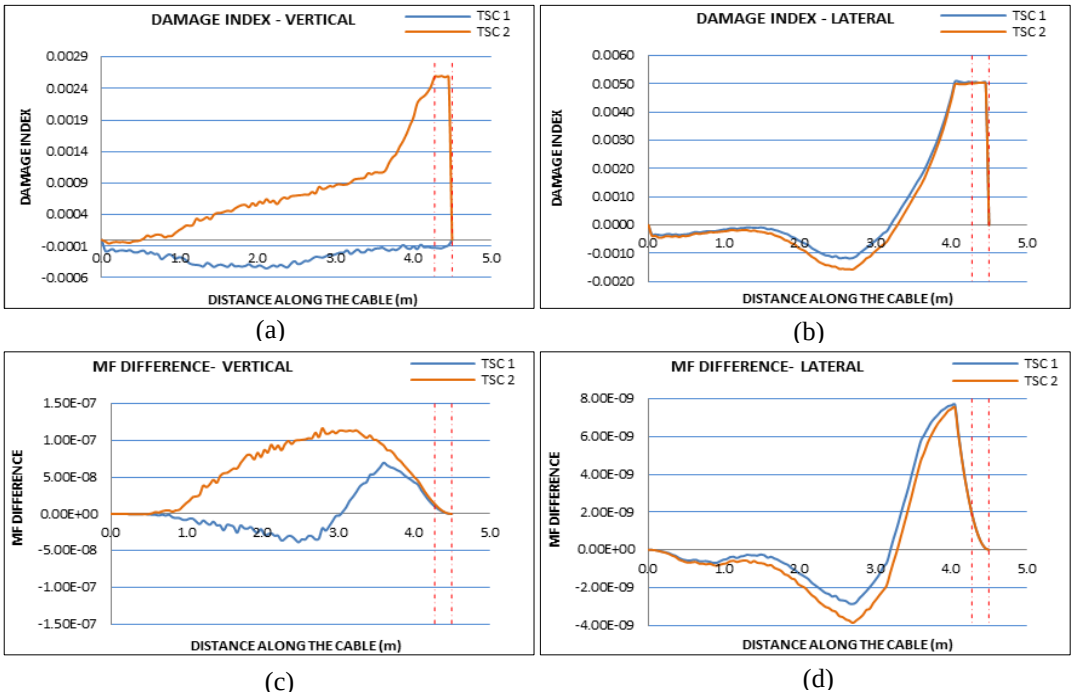

Figure 6.10 DC3 - Damage indices (a) DI_V (b) DI_L and MF difference (c) MFD_V (d) MFD_L

In other damage cases, similar trends were observed in both MFD_V and MFD_L curves. Hereafter, therefore, only DI_V and DI_L curves examined for the other damage cases are illustrated.

4. Damage Case 4 (DC 4)

The fourth damage case studied is that in the middle of the pre-tensioned reverse profiled (bottom) cable 1 in vertical plane with a 20% stiffness reduction. Numerical results of the damage indices (a) DI_V (b) DI_L and are shown in Figure 6.11 respectively. Figure 6.11 (a) shows the DI_V curve for the damaged cable (RPC 1), which reaches its maximum value at the nodes of the damaged location. However, no changes can be observed to the DI_V curve in undamaged cable (RPC 2). In Figure 6.11 (b), the DI_L curves reach their minimum values at damaged location in both damaged and undamaged cables demonstrating a stiffness increment in both cables instead of stiffness reduction. This again verifies DI_V calculated for a cable structure have ability to detect damage more accurately than DI_L.

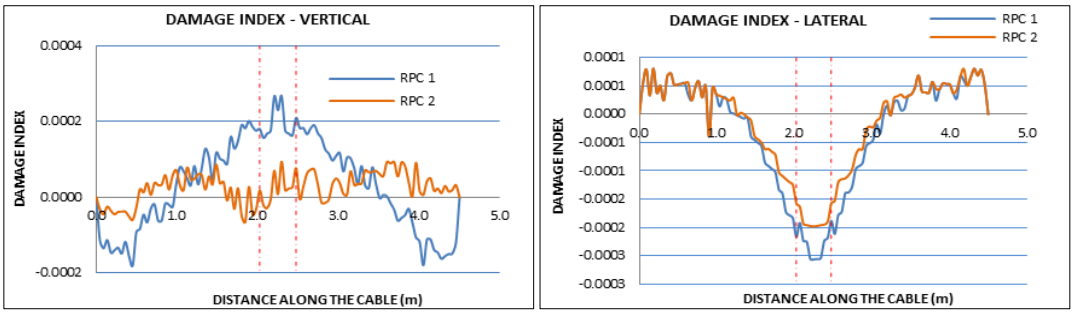

(a) (b)

Figure 6.11 DC4 - Damage indices (a) DI_V (b) DI_L and MF difference

5. Damage Case 5 (DC 5)

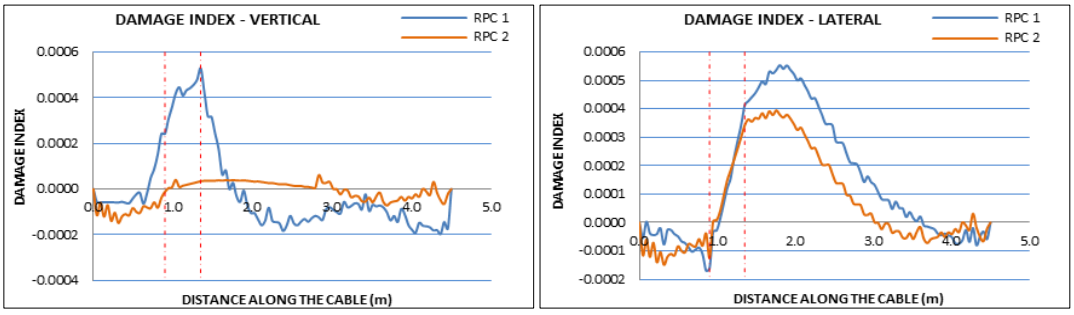

(a) (b)

Figure 6.12 DC5 - Damage indices (a) DI_V (b) DI_L and MF difference

In this damage case, 20% stiffness reduction is simulated at quarter span of the pre-tensioned reverse profiled (bottom) cable 1. Two curves of the DIs are shown in Figure 6.12 (a) and (b). The DI_L shows peaks near the damage location in both RPC

1 and RPC 2. However, a plot of the DI_V demonstrates one peak in the RPC 1, as in Figure 6.12 (a) for the exact damage location considered. Based on the examination of the two graphs, it can be concluded that incorporating vertical component of mode shapes for detecting damage in a suspended cable of a structure is a successful approach.

6. Damage Case 6 (DC 6)

Damage case six considered in this study is simulated with 20% stiffness reduction in the pre-tensioned reverse profiled (bottom) cable 1 near the support. Again, DI_V verifies its competency in damage detection of a cable in a structure. As mentioned earlier, DI_L locates the damage without identifying the damaged cable correctly.

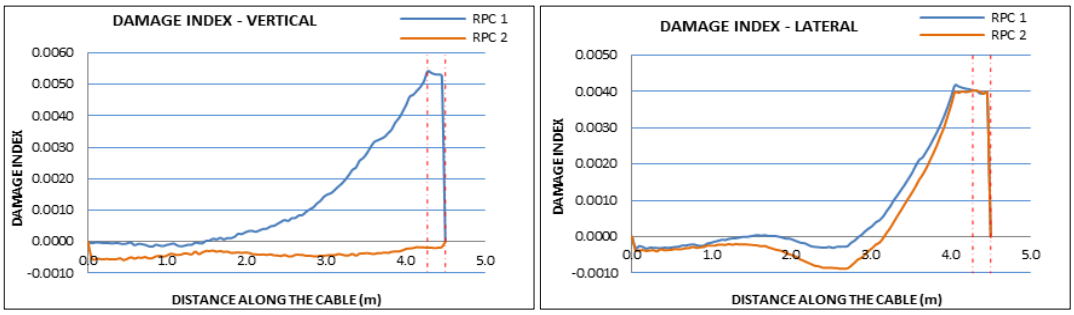

(a) (b)

Figure 6.13 DC6 - Damage indices (a) DI_V (b) DI_L and MF difference

7. Damage Case 7 (DC 7), Damage Case 8 (DC 7) and Damage Case 9 (DC 7)

The last damage cases studied under the single damage scenarios are with 20% stiffness reduction in the pre-tensioned bi-concave side cables in the horizontal plane at three locations namely; middle, quarter span and near the support. Those are described together due to the similar patterns in the damage detection results. Damage detection results of both DI_V and DI_L of each case considered are illustrated in Figure 6.14. The results verified that only the DI_V is competent enough to detect and locate damage in cables of a suspension bridge structure. Again, it is seen that DI_L can locate the damage in each cable but unable to identify the damaged cable.

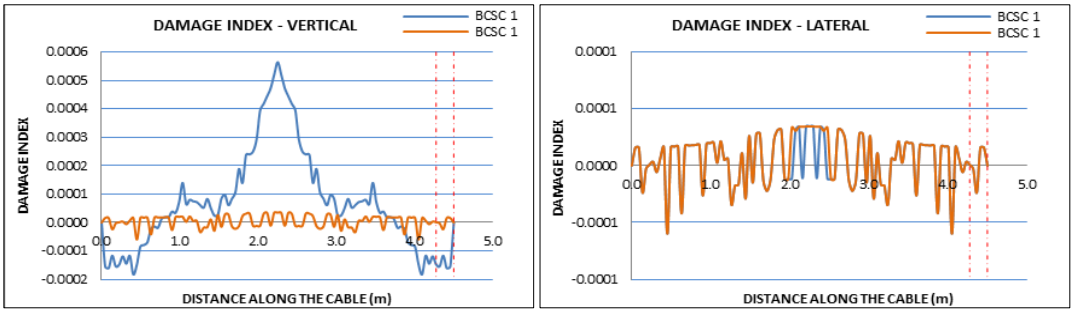

(a)

(b)

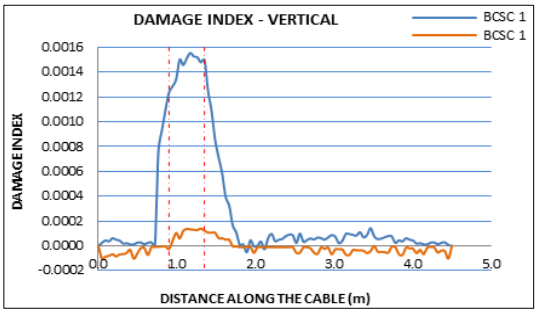

(c)

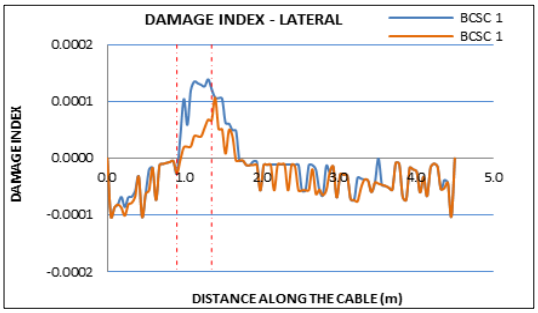

(d)

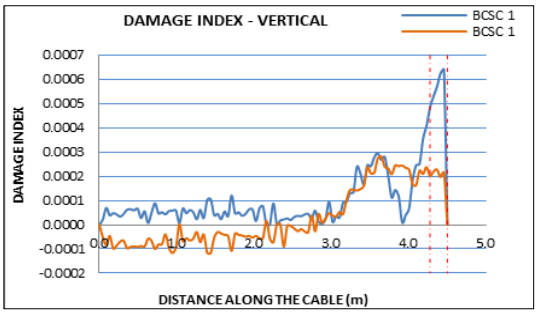

(e)

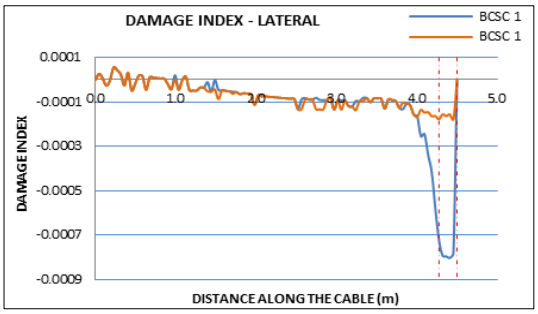

(f)

Figure 6.14 DC7 - Damage indices (a) DI_V (b) DI_L, DC8 - Damage indices (c) DI_V (d) DI_L and DC9 - Damage indices (e) DI_V (f) DI_L

- Multiple Damage Scenarios

  Six damage cases are examined to study the damage locating capability of DIs and MF difference calculated using vertical and lateral components of mode shapes.

8. Damage Case 10 (DC 10)

Damage case 10 is set up to study the capability of DIs and MF difference to locate damage in multiple damage cases. In this case, two locations are subjected to a 20% and 10% stiffness reduction in the top supporting cable in the FE model to simulate damage. The behaviour of the DI_V and DI_L are illustrated in Figure 6.15 (a) and (b), respectively. The DI_V index shows two maximum points (peaks) in TSC 1 at the damage location considered. The DI_L has two peaks not only at TSC 1 but also at TSC 2 which corresponds to the actual damage locations considered in the

simulations. Similar damage locating patterns are also observed in the plots of MF difference. An analysis of the four graphs identified that the DI_V and MFD_V have better damage detection capability than those calculated in lateral direction. DI_L and MFD_L locate the damage accurately, but unable to identify the damaged cable. In this case, therefore, DI_V and MFD_V detect the damage successfully

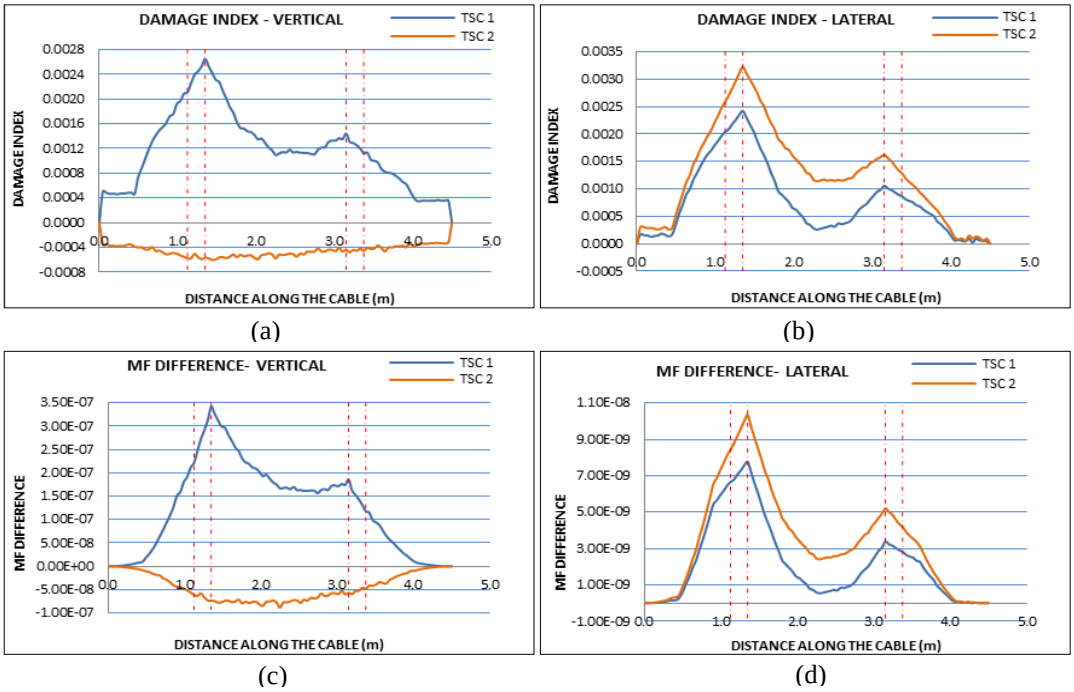

Figure 6.15 DC10 - Damage indices (a) DI_V (b) DI_L and MF difference (c) MFD_V (d) MFD_L

9. Damage Case 11 (DC 11)

Figure 6.16 illustrates both the DIs and MF difference curves for the next multiple damage case with 20% and 10% stiffness reduction in mid and quarter span of the top supporting cable 1. The curve (Figure 6.9 (a)) related to the DI_V peaks at the exact damage location being considered at the TSC 1 and no any significant changes to the DI_V in the TSC 2. However, the DI_L peaks not only at the TSC 1 at damage location but also in TSC 2. The MFD_V curve peaks at damage location in TSC 1 without any changes in TSC 2. However, MFD_L shows false damage detection in TSC 2. Based on the examination of the four graphs, it can be concluded that incorporating vertical component of mode shapes for detecting damage in a suspended cable of a structure is a successful approach. Therefore, competency of DI_V calculated in damage detection of cables is further evaluated through Damage Case 12 considered in this study.

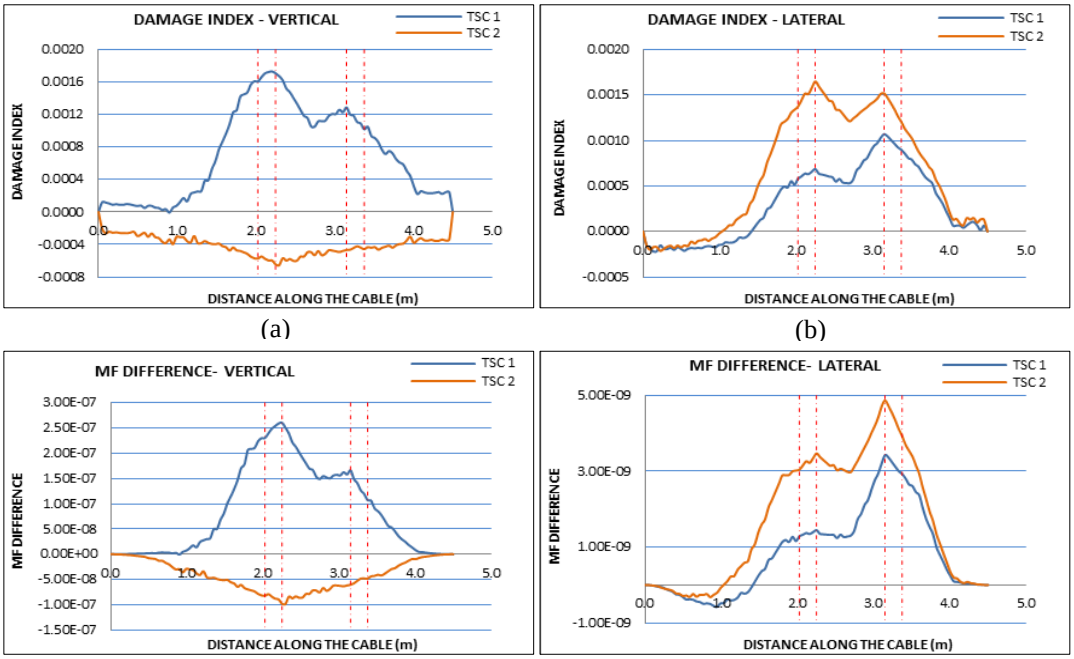

Figure 6.16 DC11 - Damage indices (a) DI_V (b) DI_L and MF difference (c) MFD_V (d) MFD_L

10. Damage Case 12 (DC 12)

Similar to the other multiple damage cases, 20% and 10% stiffness reduction in two locations of the pre-tensioned reverse profiled (bottom) cable 1 in vertical plane is simulated. Numerical results of the damage indices (a) DI_V and (b) DI_L are shown in Figure 6.17 respectively. Figure 6.17 (a), the DI_V curve shows two peaks in the RPC 1 at the nodes of the damaged location. However, very little change can be observed in the DI_V curve in the undamaged cable (RPC 2). Further, DI_L curve demonstrates false damage detection. This again verifies DI_V calculated for a cable structure have the ability to detect damage more accurately than lateral damage index.

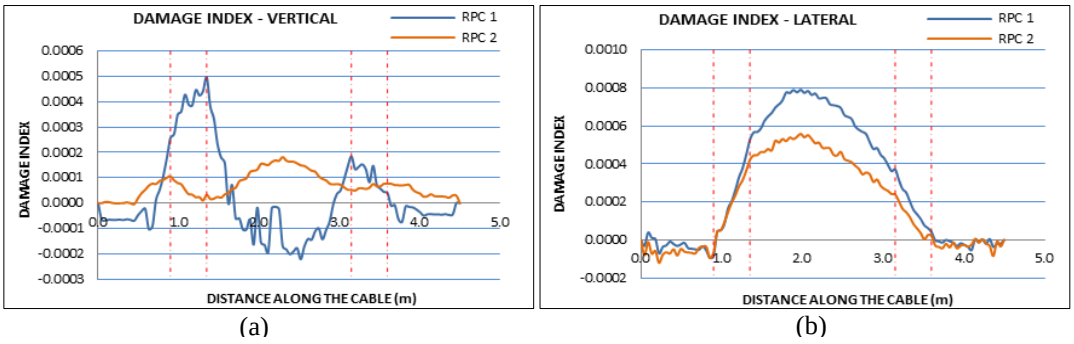

Figure 6.17 DC12 - Damage indices (a) DI_V (b) DI_L

11. Damage Case 13 (DC 13)

In this damage case, 20% and 10% stiffness reduction is simulated at mid and quarter span of the pre-tensioned reverse profiled (bottom) cable 1. Two curves of the DIs are shown in Figure 6.12 (a) and (b). The DI_L for RPC 1 and RPC 2 show a peak between the damage locations. However, a plot of the DI_V demonstrates two peaks in the RPC 1, as in Figure 6.18 (a) at the exact damage locations. Based on the examination of the two graphs, it can again be concluded that incorporating vertical component of mode shapes for detecting damage in a suspended cable of a structure is a successful approach.

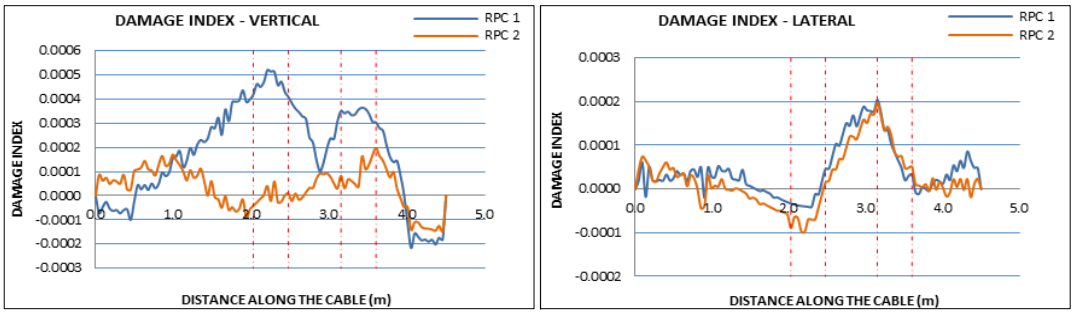

(a) (b)

Figure 6.18 DC13 - Damage indices (a) DIV (b) DIL

12. Damage Case 14 (DC 14) and Damage Case 15 (DC 15)

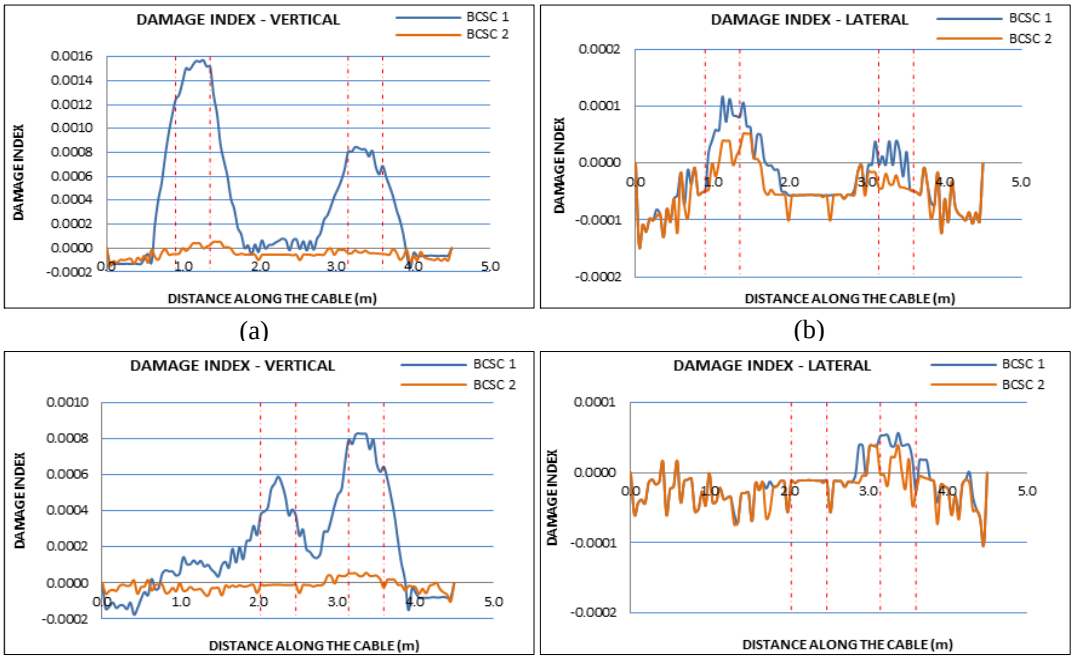

(a) (b)

(c) (d)

Figure 6.19 DC14 - Damage indices (a) DI_V (b) DI_L, DC15 - Damage indices (c) DI_V (d) DI_L

The last damage cases studied under the multiple damage scenarios are with 20% and 10% stiffness reduction in the pre-tensioned bi-concave side cables in the

horizontal plane at different locations and the results are shown in Figure 6.19. Since, these demonstrate a similar pattern in damage detection results, they are described together here. The results verified that the DI_V is competent to detect and locate damage in the pre-tensioned bi-concave side cables of a suspension bridge structure.

- Tension reduction in cables

  Three damage cases are setup to study the identification of tension reduction in cables by both DIs and MF difference calculated using vertical and lateral components of mode shape.

13. Damage Case 16 (DC 16)

The first tension reduction damage case simulated is with 2% reduction in tension values of the top supporting cable 1. Figure 6.20 (a) and (b) illustrates the DI_V and DI_L curves respectively. The DI_L shows the similar curves for both TSC1 and TSC2, which gives the incorrect estimation about the tension force reduction. However the DI_V captured the tension reduction correctly by indicating the flexibility increase in the TSC1. Also it is noted that there is an increment in flexibility of TSC 2. This is due to tension redistribution among the cables. However, there is no significant difference in the DI_L and MFD_L curves in the TSC1 and TSC2. According to the results it can be concluded that both DI_V and MFD_V is successfully identified the tension reduction in the top supporting cable1 of the bridge.

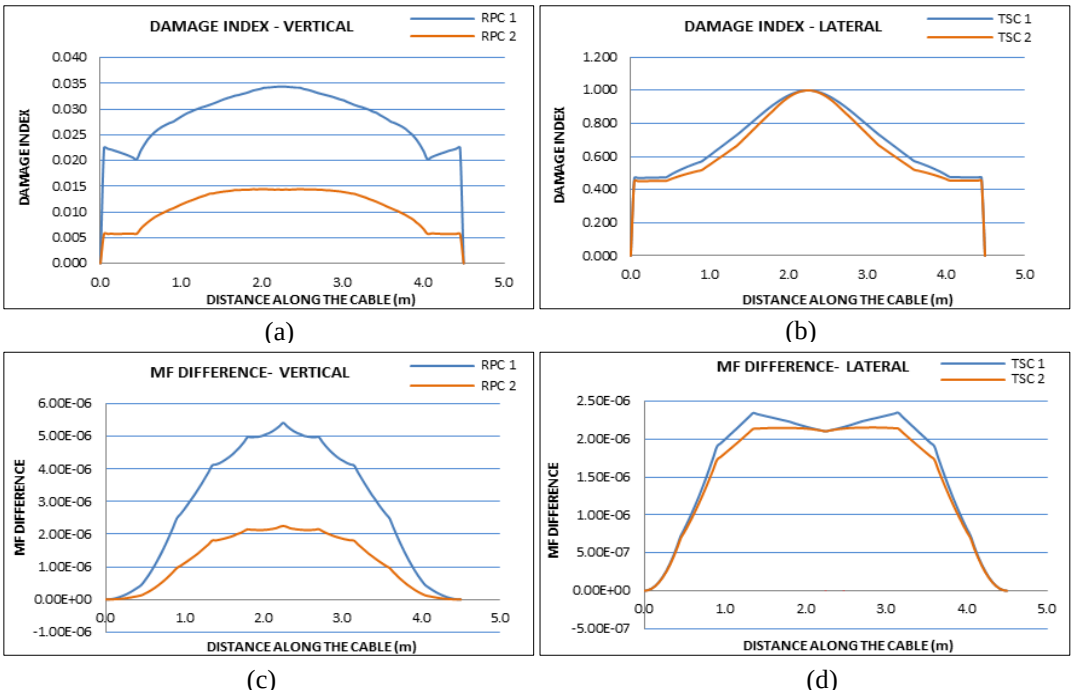

Figure 6.20 DC16 - Damage indices (a) DI_V (b) DI_L and MF difference (c) MFD_V (d) MFD_L

14. Damage Case 17 (DC 17)

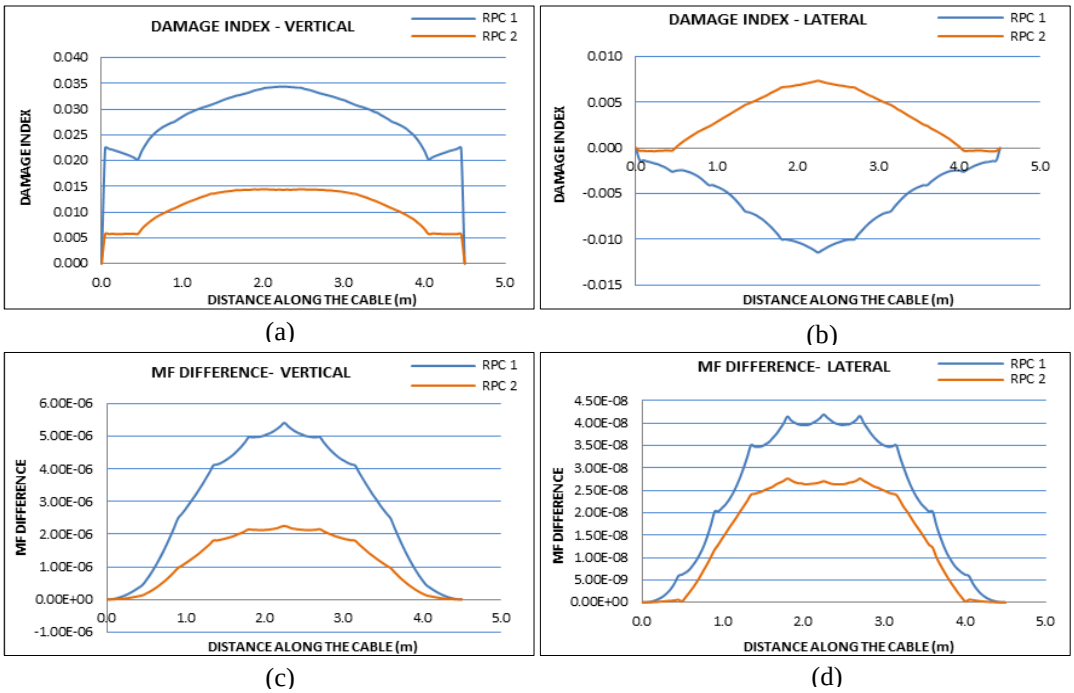

Figure 6.21 DC17 - Damage indices (a) DI_V (b) DI_L and MF difference (c) MFD_V (d) MFD_L

This damage case examined a 15% tension reduction in pre-tensioned reverse profiled (bottom) cable 1. Plots of DI_V and MFD_V capture tension reduction in RPC 1 as evident by increment in the values (or shift in) of the curves. The DI_L is unable to identify the tension reduction in RPC1; however this was successfully captured by the MFD_L.

15. Damage Case 18 (DC 18)

Final damage case examined a 20% tension reduction in the pre-tensioned bi-concave side cable1 in the horizontal plane and results are illustrated in Figure 6.22. Results indicate the DI_V, DI_L, MFD_V and MFD_L capture the tension reduction successfully.

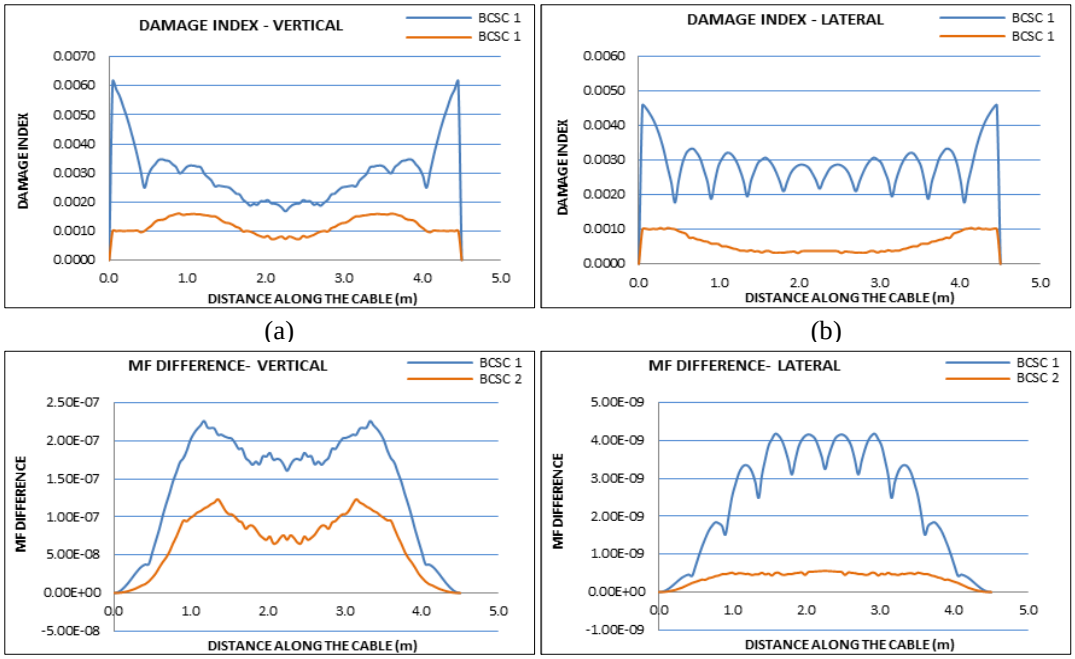

Figure 6.22 DC18 - Damage indices (a) DI_V (b) DI_L and MF difference (c) MFD_V (d) MFD_L

Analysing the above damage cases, it is evident that the damage index based on the vertical component of mode shapes (DI_V) is capable of detecting and locating damage under single and multiple damage scenarios successfully. This is due to more mass (modal mass) being distributed in vertical direction of the vibration modes of a suspension bridge structure. Both damage index (DI_V) and MF difference (MFD_V) calculated using the vertical component of mode shapes is also successful in identifying the tension reduction in cables. The next section examines the competency of the (DI_V) under the influence of measurement noise.

6.4.3 Damage Detection with Noise in Modal Data

A similar method as in chapter 4 is used in calculating the effect of noise in modal parameters which are generated from the FE model. Since, the measurement noise associated with frequency is very low; 5% random noise is introduced to mode shapes. Few selected damage cases were examined under the noisy modal data.

Figure 6.23 to Figure 6.28 below illustrate the results for locating damage using the DI_V with and without noise. The DI_V plots under noisy modal data, for the damage cases considered have similar features as observed earlier for noise free condition. It has very clear sharp peaks at the damage locations in both single and multiple damage cases and tension reduction case considered in the cables. Therefore it can be concluded that the damage indicator based on vertical component of

vibration modes (DI_V) performs well for locating damage even the presence of 5% noise in the mode shape data. This implies the vertical component of mode shapes is suitable in detecting damage in cable structures.

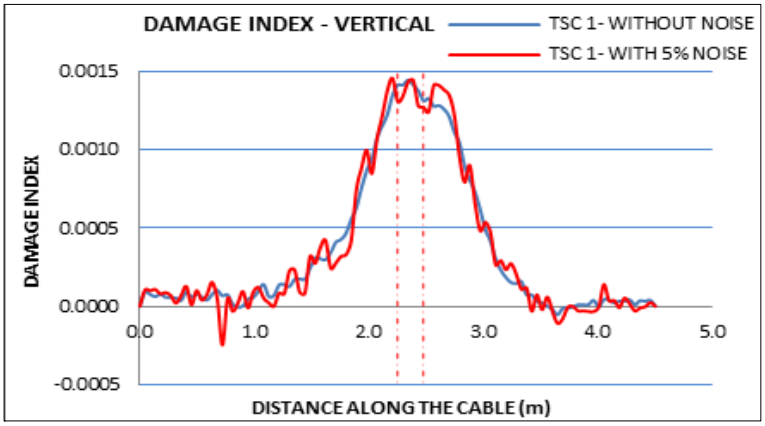

Figure 6.23 DC1 - DI_V

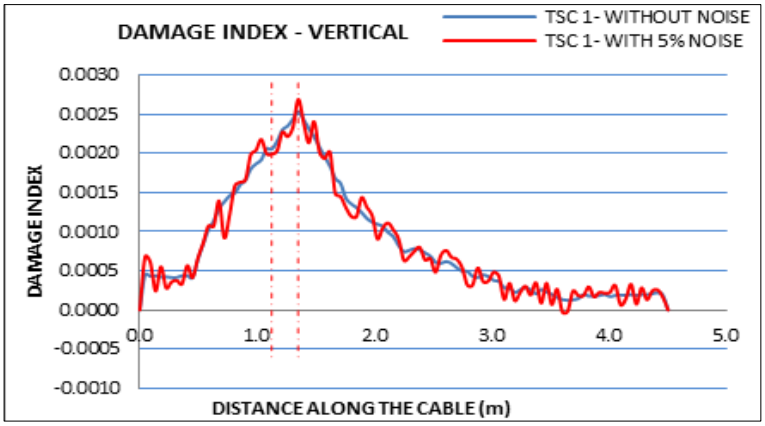

Figure 6.24 DC2 - DI_V

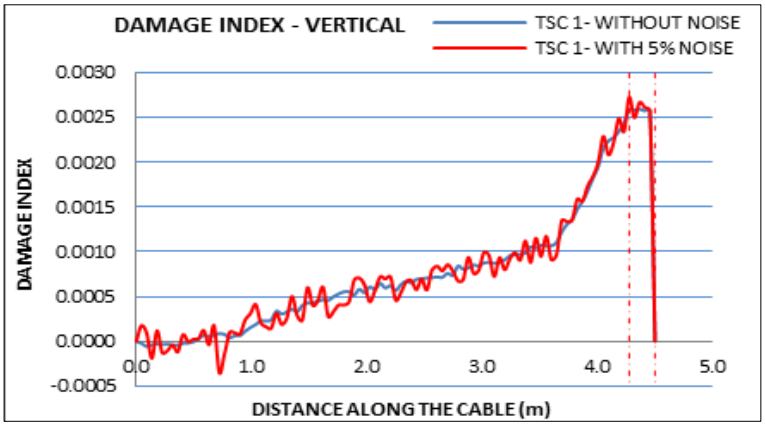

Figure 6.25 DC3 - DI_V

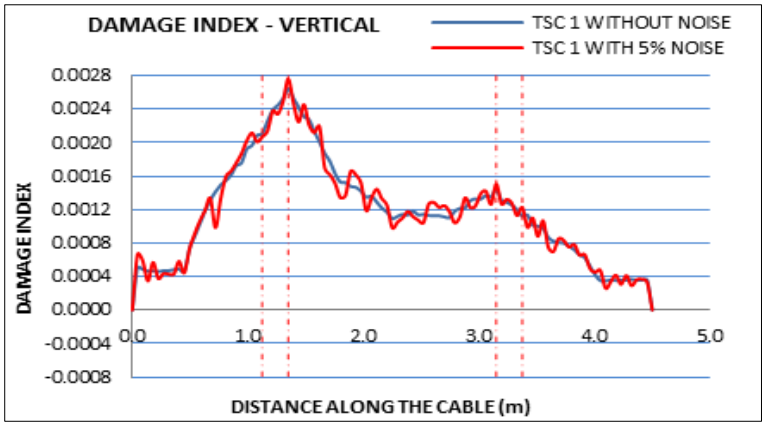

Figure 6.26 DC10 - DI_V

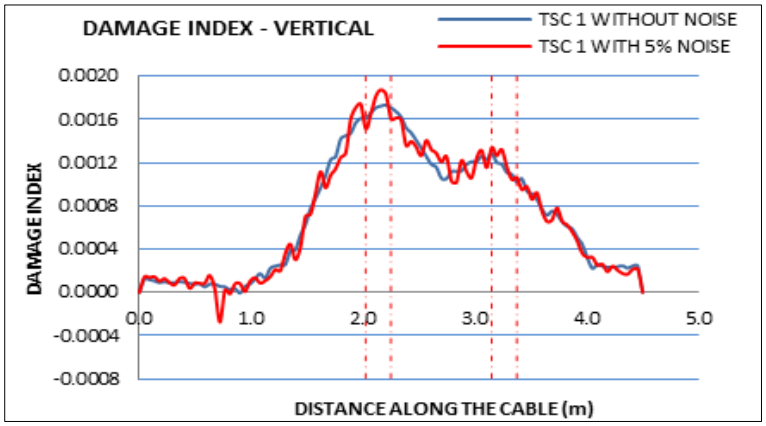

Figure 6.27 DC11 - DI_V

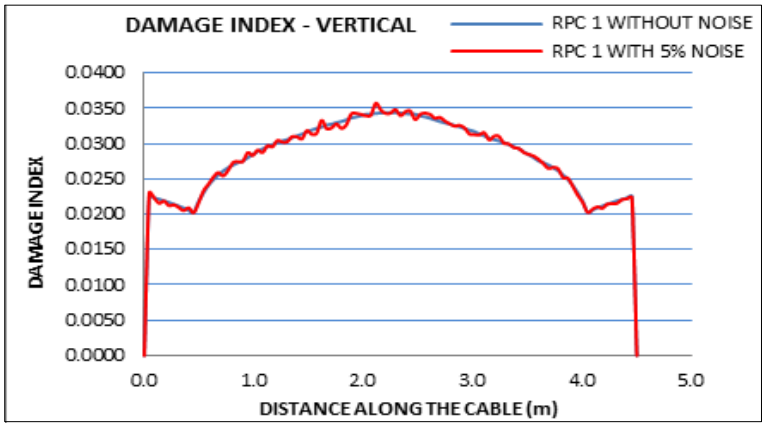

Figure 6.28 DS17 - DI_V

6.5 SUMMARY

This chapter described the FE modelling of the laboratory cable structure in ANSYS Workbench. A comparison was undertaken to validate the FE model in terms of vertical deflections, tension forces and natural frequencies with reference to experimental results. The initial FE model was updated manually by changing the

cable tension, connectivity of structural elements, support conditions, member offsets and Young's Modulus and obtained the validated FE model with error below 9% as the base line model for vibration based damage detection applications. In order to verify the competency of DIs proposed in this study, three types of damage scenarios namely; single damage scenarios, multiple damage scenarios and tension reduction in cables were evaluated. The laboratory bridge consists of three types of cables; three damage cases were examined on each cable; at the mid span, quarter span and near the support with all together nine damage cases to represent single damage scenarios. Similarly, two damage cases for each cable with a total of six damage cases were examined under the multiple damage scenarios. Further, three damage cases were examined to cater to the reduction of tension force in cables. In all damage scenarios except the tension reduction scenario, vertical damage indicator calculated using vertical components of mode shapes (DI_V) was able to detect damage successfully. Further, both DI_V and MFD_V are successful in identifying the tension reduction in cables. The damage detection capability of the vertical damage index was evaluated with and without noise in numerically generated modal data. The DI_V performs well in locating damage in the cables of the laboratory suspension bridge with single and multiple damage scenarios and tension reduction in cables even with the presence of 5% measurement noise in mode shapes. It can hence be concluded that the vertical damage index (DI_V) calculated using vertical component of mode shapes are more sensitive to damage and is competent in detecting and locating damage in cables of suspension bridges.

Chapter 7: Damage Detection in a 3D Suspension Bridge

7.1 INTRODUCTION

This chapter presents the application of modal flexibility based component specific DIs to detect and locate damage in the main cables and hangers of a real suspension bridge. The chapter begins by describing the development of a FE model of the Ölfusá Bridge using ANSYS Workbench. Secondly, validation of the FE model is carried out by comparing frequencies measured at the bridge site and those obtained numerically. Thirdly, different damage scenarios occurring in the main cables and hangers of the suspension bridge are simulated in the FE model. Next, damage detection capability of the DIs in both noise free and under 5% noise condition are presented and discussed. Further, behaviour of DIs are examined under some complex damage scenarios. Finally, the influence of higher order modes in damage detection using the DIs and application in the inverse problem is discussed.

7.2 BRIDGE DESCRIPTION

In this study, a validated FE model of the Ölfusá Bridge in Iceland is used to obtain vibration properties for the damage detection in the main cables and hangers. Details of the bridge are obtained from the MSc thesis of Guðni Páll Pálsson of the Department of Civil Engineering in the Technical University of Denmark (Pálsson, 2012). The Ölfusá Bridge was first constructed in 1891 over the river Ölfusá and the current bridge was built in 1945 after the failure that occurred in the upstream cable of the first bridge. It is a suspension bridge with a concrete deck supported and stiffened by a steel truss. Total length of the bridge is 132m of which the 84m main span is suspended by the cables which are anchored in concrete blocks on either river banks. The maximum cable sag and the tower height of the bridge are 10.5m and 10.2m respectively. Total width of the concrete deck is 8.7m and depth of the steel truss is 1.687m. A Schematic diagram of the bridge with some key dimensions is illustrated in Figure 7.1 below.

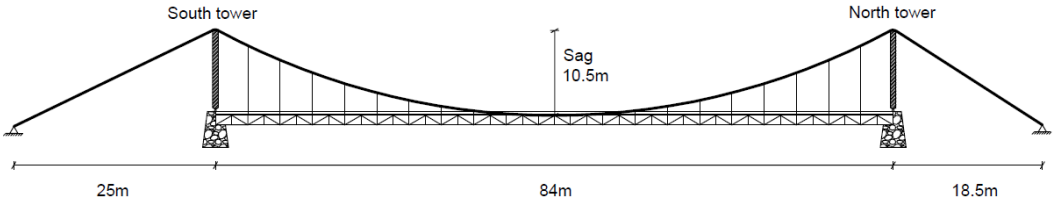

Figure 7.1 Schematic diagram of The Ölfusá Bridge (Pálsson, 2012)

The main cables consist of six individual 96 wires locked coil strands in each cable plane Figure 7.3 (a). The cable anchoring is not symmetric and the north back stay has an inclination of 34.8^0 from horizontal while the south one has 32.7^0. The concrete bridge deck is suspended from the main cables by 20 circular solid steel hangers on either side with 4m intervals. The bridge deck designed in 1945 was completely renovated in 1992 and has a total width of 8.7m with 6.2m wide road way and one walking lane of 1.8m wide. This deck arrangement leads to unsymmetrical loading resulting in higher tension force in the upstream cable of the empty bridge and higher tension in the downstream cable during heavy traffic.

Figure 7.2 Stiffening girder of the Ölfusá Bridge (Pálsson, 2012)

The next major structural member of the Ölfusá Bridge is the steel stiffening girder (Figure 7.2) which consists of trusses in longitudinal and transverse directions. This Stiffening girder includes three longitudinal trusses and 22 transverse trusses positioned 4m apart. Longitudinal truss consists of two primary longitudinal vertical trusses and a wind stiffening truss which connects the primary trusses at the bottom of the chords. Height between centroids of the chords of a vertical primary

longitudinal truss is 1.687m. The bridge consists of a total of 22 transverse trusses of which 20 are located across the span with 1.176m height and two others at each end with a height of 1.496m.

Pylons of the bridge have a height of 10.2m and are made from I beams riveted together by steel plates and filled with concrete. Base of the pylons are hinged as shown in Figure 7.3 Figure 7.3(b). These are free to rotate about transvers direction of the bridge. All the structural element sizes and properties are described in the next section.

(a) (b)

Figure 7.3 (a) Main Cables (b) Pylons (Óskarsson, 2012)

7.3 FE MODELLING OF SUSPENSION BRIDGE

A 3D FE model of the Ölfusá bridge is developed in the FE analysis software package ANSYS Workbench. Main objective of the FE modelling is to develop a numerical model which can be validated and then used to obtain vibration properties for use in damage detection studies. An effort was therefore made to accurately replicate all the geometric features of this structure as available in literature (Óskarsson, 2012; Pálsson, 2012).

7.3.1 Geometry of the Ölfusá Bridge

The geometry of the Ölfusá Bridge was modelled in the DesignModeler module of ANSYS Workbench. It was modelled as a 3D FE model with two parts namely; bridge (deck, stiffening girder, hangers and cables) and pylons. They were then, connected by joint feature in the Mechanical module of the ANSYS Workbench. All the material properties primarily used in simulation are in Table 7.1.

Table 7.1 Material properties

Material	Density (kg/m^3)	Young's Modulus E (GPa)	ν
Steel cables	8000	135	0.3
Steel hangers	8000	135	0.3
Pylon Steel	8000	210	0.3
Concrete fill in Pylon	2500	32	0.2
Bridge deck concrete	2500	32	0.2
Steel used in truss	9000	210	0.3

The main cables are 9.3m apart with cross sections of the cable and diameter of a hanger being 0.0131m^2 and 50.8mm respectively. As shown in Figure 7.4, pylons are constructed by concrete filled in between two I-girder sections (24" x 7 1/2" 95) and connected by steel plates (28" x 15/16"). This pylon section was considered as a composite section and equivalent section properties are calculated according to the following equations (Fan et al., 2013);

$$A_{eq} = (E_c A_c + E_s A_s)/E_s \quad 7.1$$

$$I_{xeq} = (E_c I_{xc} + E_s I_{xs})/E_s \quad 7.2$$

$$I_{yeq} = \left(E_c I_{yc} + E_s I_{ys}\right)/E_s \quad 7.3$$

where, A_{eq}, $I_{xeq,}$ I_{yeq} are the equivalent cross sectional area, equivalent moment of inertia about x-axis and the equivalent moment of inertia about y-axis respectively. A_c and A_s are the cross-sectional area of concrete and steel, respectively; I_{xc}, I_{yc}, I_{xs}, I_{ys} are the moment of inertia of concrete and steel, respectively; E_c and E_s are the elastic modulus of concrete and steel, respectively. The two parameters including cross-sectional area and moment of inertia calculated using above equations are used as input parameters to the pylon cross section in DesignModeler

module to ensure the axial rigidity and flexural rigidity are the same as the steel concrete composite member.

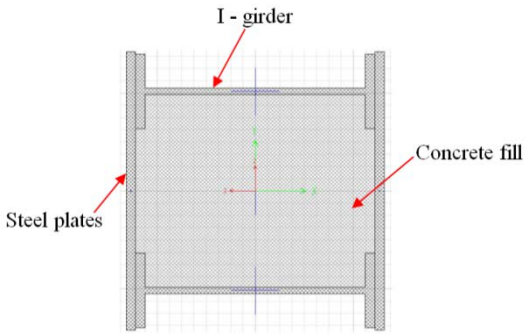

Figure 7.4 Pylon Section (Óskarsson, 2012)

Section properties of the four upper longitudinal I-beams that carry the bridge deck and the two 90^0 tilted lower I-beams are in Table 7.2. Structural members of the two longitudinal trusses are summarized in Table 7.3. The vertical double angles are adjacent to the transverse intermediate trusses while the vertical single angles are located in between.

Table 7.2 Longitudinal I-girder section properties

Section Type		Additional Plates (in)	Area (mm^2)	I_{xx} (mm^4)	I_{yy} (mm^4)
Inner top chord	15" x 6" x 45	-	8514	1.8E+08	8.7E+06
Outer top chord (end)	14" x 8" x 40	-	7996	1.6E+08	1.5E+07
Outer top chord (mid)	14" x 8" x 40	10 x 3/8 (web)	12743	1.9E+06	1.1E+07
Bottom chord (end)	14" x 8" x 70	-	13068	2.6E+08	2.5E+07
Outer top chord (mid)	14" x 8" x 70	8 x 3/8 (flanges)	16708	2.9E+08	2.6E+07

The transverse trusses at the end of piers, and transverse trusses in the span (4 m intervals), consists of angle sections. The horizontal bottom wind bracing, which is a single angle section connects to every other transverse truss. Section properties of the transverse trusses and wind bracing are given in

Table 7.4, Table 7.5 and Table 7.3 respectively. The wind bracing and the lower I-beams are positioned at the same elevation as the bottom of the end

transverse trusses. These are connected to the in-span transverse trusses by plated connections at joints.

Table 7.3 Longitudinal truss girder section properties

Section Type		Area (mm^2)	I_{xx} (mm^4)	I_{yy} (mm^4)
Diagonals (0-4 m)	2L:4" x 4" x 5/8"	5956	5.6E+06	1.4E+07
Diagonals (4-8 m)	2L:4" x 4" x 1/2"	4838	4.6E+06	1.1E+07
Diagonals (rest of span)	2L:4" x 4" x 3/8"	3680	3.6E+06	8.2E+06
Vertical angles (2, 6,10m….)	L:3" x 3" x 3/8"	1357	7.3E+05	7.3E+05
Vertical angles (4, 8,12m….)	2L:3 1/2" x 2 1/2" x 3/8"	2660	2.1E+06	2.2E+06
Wind bracing	L:4 1/2" x 4 1/2" x 3/8"	2060	2.6E+06	2.6E+06

Table 7.4 Section properties of transverse truss at span

Section Type		Additional Plates (in)	Area (mm^2)	I_{xx} (mm^4)	I_{yy} (mm^4)
Horizontal top angle	2L:4" x 4" x 7/16"	4" x 1/2"	4247	4.1E+06	9.4E+06
Horizontal bottom angle	2L:4" x 4" x 7/8"	4" x 1/2"	8247	7.3E+06	2.2E+07
Diagonals (inner)	2L:3 1/2" x 2 1/2" x 3/8"	-	2660	2.1E+06	2.2E+06
Cross bracing (middle)	L:3 1/2" x 2 1/2" x 3/8"	-	1345	1.1E+06	4.5E+05
Diagonals (Outer)	2L:3 1/2" x 3 1/2" x 3/8"	3 1/2 " x 1/2"	3170	2.4E+06	5.6E+06
Vertical Angles	2L:3 1/2" x 2 1/2" x 3/8"	-	2660	2.1E+06	2.2E+06

Table 7.5 Section properties of transverse truss at piers

Section Type		Additional Plates (in)	Area (mm^2)	I_{xx} (mm^4)	I_{yy} (mm^4)
Horizontal top angle	2L:3 1/2" x 3 1/2" x 3/8"	3 1/2 " x 1/2"	3170	2.4E+06	5.6E+06
Horizontal bottom angle	2L:3 1/2" x 3 1/2" x 3/8"	3 1/2 " x 1/2"	3170	2.4E+06	5.6E+06
Diagonals (inner)	2L:3 1/2" x 2 1/2" x 3/8"	-	2660	2.1E+06	2.2E+06
Cross bracing (middle)	L:3 1/2" x 2 1/2" x 3/8"	-	1345	1.1E+06	4.5E+05
Vertical Angles	2L:3 1/2" x 3 1/2" x 3/8"	-	3170	2.4E+06	5.6E+06

The weights due to the non-structural elements such as parapets, gondola beams and pipe lines under the bridge are provided in the table 7.6. These are included to the FE model as a form of applied loading in Mechanical module of the ANSYS Workbench.

Table 7.6 Loading of non-structural elements

Non-structural element	Load (kN)
Parapets	126
Gondola beams	25
Pipe lines	375

7.3.2 Analysis of the Ölfusá Bridge

Geometry of the Ölfusá Bridge was created in the DesignModeler module and transferred into the Mechanical module of the ANSYS Workbench for analysis. In Mechanical module, correct material characteristics mentioned in Table 7.1 were assigned to each element. All the elements of the bridge were modelled as beam elements except the deck. BEAM188 element and SHELL181 element types (as described in chapter 3) were used to simulate bridge frames and deck respectively.

In each cable plane, the main cables are composed of six individual locked coil strands which are modelled as single cable in the FE model. Since anchor blocks are not modelled, fixed supports with no rotation and no translations are assigned at the ends of main cables. Connectivity of cables and Pylons were established by joint feature in the Mechanical module. In the FE model cables are considered as fixed over pylon saddles by assigning fixed joint feature to join the pylons and main cables.

The stiffening girder is modelled with different cross sections as given in Table 7.2 - Table 7.5. While updating the FE model of the laboratory cable bridge structure, (described in chapter 6) it was found that the member offset is a very significant parameter in the model updating process. In this FE model, therefore member offset has been considered for the deck elements to represent the correct elevation of the deck and longitudinal I-beams. In order to model the correct configuration of the longitudinal I-beams placed on transverse truss, member offsets are introduced again to the longitudinal I-beams. Since the bottom angle sections of the intermediate transverse truss and bottom chords of the longitudinal truss are in two elevations, a 320mm high connecting plate was fastened by rivets to connect them. Rigid links were used to represent that connection while same is used to ensure the connection between the horizontal wind bracing and intermediate transverse trusses.

The transverse trusses at the either end of piers are hinged (Pálsson, 2012), theoretically therefore, rotation need to be allowed at both ends. However considering the age (approximately 70 years old) of the bridge, may be possible to prevent the rotations in some directions. Consequently, this analysis releases the rotations about the transverse and longitudinal directions. As previously mentioned bridge pylons are hinged at the base and it is free to rotate about the transverse direction of the bridge. Similar condition is simulated in the FE model by assigning no translation at the base of the pylons and releasing rotation about the transvers direction only.

Meshing of the structure was performed by an inbuilt algorithm in Mechanical module with following features. A FE model with total of 5732 nodes and 3652 elements was created using basic meshing features in Mechanical module namely; Physical preference: mechanical; relevance: 100; relevance centre: fine and

Minimum edge length: 0.250m. Initial tension forces were introduced to the cables using command features in Mechanical module as an initial strain.

In the analysis, a pre-stressed Modal Analysis was conducted to obtain vibration parameters. In pre-stressed modal analysis, initially, a nonlinear static analysis with large deflection on was conducted in order to obtain the stress stiffening matrix caused by the internal forces due to the dead loads acting on the bridge. Next, the modal analysis was performed on the basis of the deformed equilibrium configuration of the bridge to obtain the natural frequencies and mode shapes. FE model of the bridge is illustrated in Figure 7.5 below. Natural frequencies obtained from the FE model and those obtained from field measurements of the Ölfusá Bridge are compared in the next section.

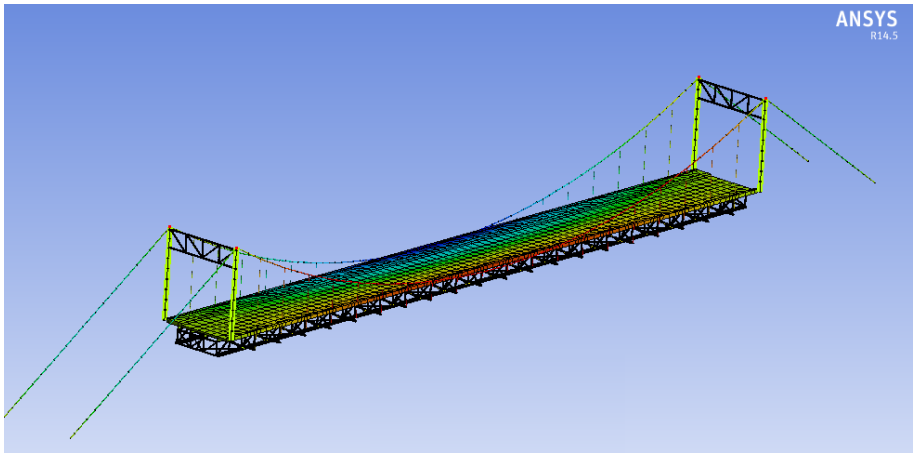

Figure 7.5 FE model of the Ölfusá Bridge

7.4 VALIDATION OF THE FE MODEL WITH MEASUREMENT DATA

The detailed description of the modal testing of the Ölfusá Bridge is in the literature (Pálsson, 2012). However description of the test and analysis procedure is summarized in this section briefly. The modal identification of the Ölfusá Bridge was conducted using a total of 7 accelerometers, of which four were uni-axial and three are tri-axial. Eight accelerometer layouts were planned to capture the vibration properties of the bridge and in each layout, two accelerometers were retained as reference (1 uni-axial and 1 tri-axial) and five were roved along the bridge. The data was collected for twenty minutes at a sampling rate of 2048Hz. In order to obtain the vibration properties, the acceleration time histories and simple bridge deck geometry had been input to the ARTeMIS software. Two different OMA methods namely; EFDD and ISS-PC were used to extract the vibration properties. Nine modes were

extracted by the above two methods and correlation study of two methods was conducted by calculating MAC values for nine mode shapes. All the mode shapes, except mode 2 (which had extraction difficulties) showed a good correlation of the two methods. Even though, linear interpolation had been used to obtain the missing values of mode 2, it was unable to identify clearly using EFDD. Therefore frequencies extracted from SSI-PC are selected to compare those obtained from FE model.

To achieve the validation of the FE model used in his study, model updating was carried out manually to alter the structural parameters of the FE model such that the differences between the natural frequencies obtained from the field testing and from the FE model were minimised. Changes to the FE model have been specially introduced in the cable cross section (due to the corrosion in the cable of the bridge), steel mass (estimation of the density of seel due to bulky connections of the bridge), support conditions and cross section of the wind bracings. A large reduction in the axial stiffness of the cross bracing under the bridge had to be introduced in the FE mode due to their detachment as seen in the Figure 7.6 (Pálsson, 2012).

Figure 7.6 Cross bracing detachment at the support (Pálsson, 2012)

Table 7.7 lists the natural frequencies obtained from the field measurements (f_{field}), and those obtained in updated FE model by current study (f_{fem}). To validate the FE model developed in the current study, f_{field} of the bridge from a series of OMA tests with the numerical f_{fem} results were compared by Equation 7.4.

$$f_{error} = \frac{(f_{field} - f_{fem})}{f_{field}} \times 100 \quad 7.4$$

From the results, it can be observed that the calculated (f_{error}) errors in each mode are less than 1.5% except the 1st torsional mode which is 12.5%. Error in similar magnitude (11.0%) can be observed in the 1st torsional mode of the FE model updated using automatic algorithm in the previous study (Pálsson, 2012).

Due to the extraction errors of closely spaced modes, this kind of higher error can be expected for some modes. In the field testing, only the deck vibration was measured and some of the modes dominated by cable modes in the FE model were not extracted and hence cable (dominated) modes in the FE model (mode 5 to mode 8) are disregarded in the FE model validation. With the availability of limited amount of the bridge data, it can be concluded that the FE model developed in this study demonstrates good correlation with the (field measured) Ölfusá Bridge. The validated FE model therefore provides the base line model for vibration based damage detection applications which will be carried out in the next section. Mode shapes of the first five modes of the FE model are shown in Figure 7.7 to Figure 7.11.

Table 7.7 Comparison of the natural frequencies of the Ölfusá Bridge

Mode Type	Field Measurement		FEM of This Study		
	Mode No	Frequency f_{field} Hz	Mode No	Frequency f_{fem} Hz	f_{error} (%)
1st Vertical Symmetric	1	1.078	1	1.071	0.6
Horizontal Symmetric	2	1.588	2	1.608	-1.2
1st Vertical anti-symmetric	3	1.705	3	1.713	-0.5
1st Torsion	4	2.090	4	2.352	-12.5
2nd Torsion	5	2.793	9	2.831	-1.3

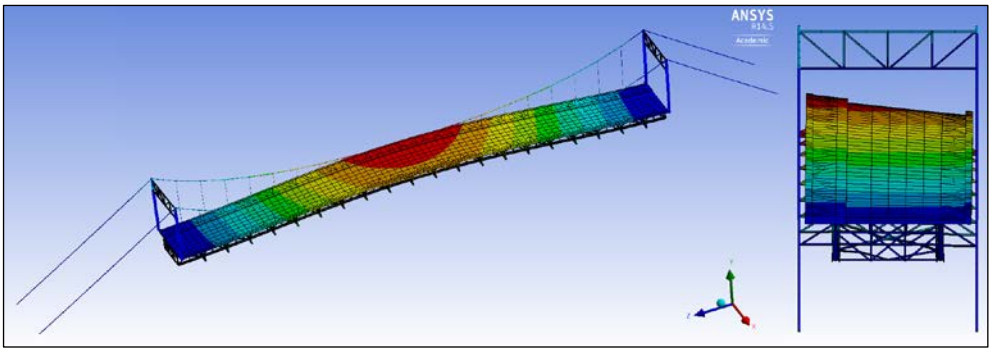

(a)

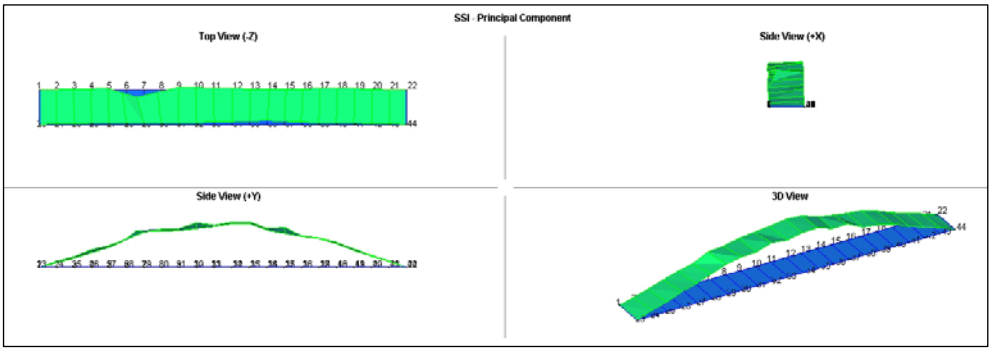

(b)

Figure 7.7 1st Vertical symmetric (mode 1) (a) FE Analysis 1.071Hz (b) Measured 1.078Hz (Pálsson, 2012)

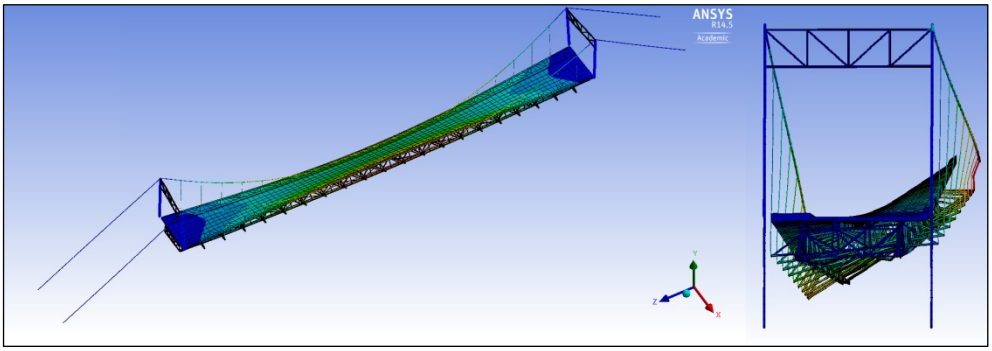

(a)

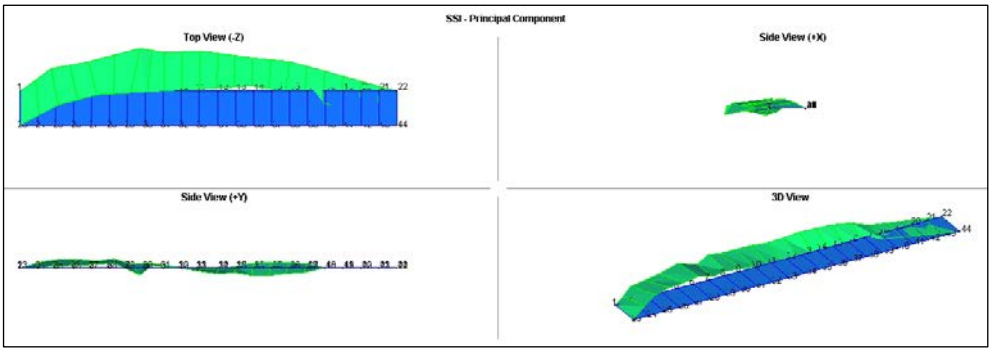

(b)

Figure 7.8 Horizontal symmetric (mode 2) (a) FE Analysis 1.608Hz (b) Measured 1.588Hz (Pálsson, 2012)

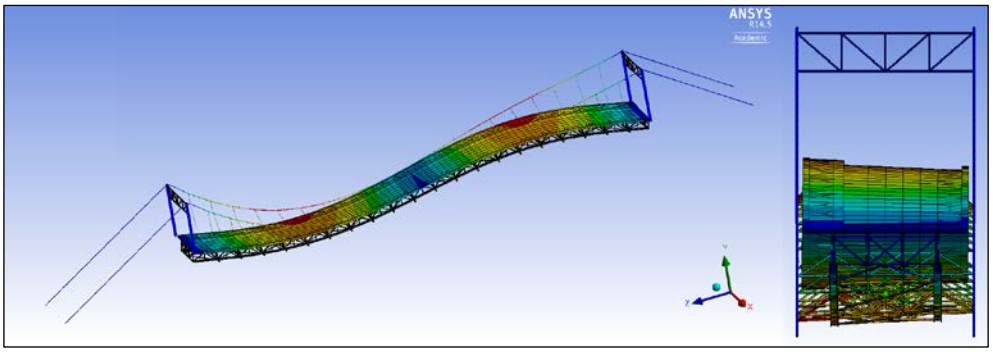

(a)

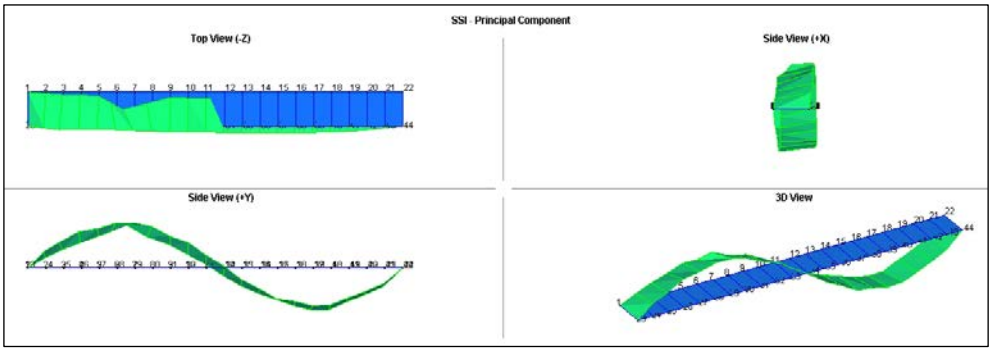

(b)

Figure 7.9 1st Vertical anti-symmetric (mode 3) (a) FE Analysis 1.713Hz (b) Measured 1.705Hz (Pálsson, 2012)

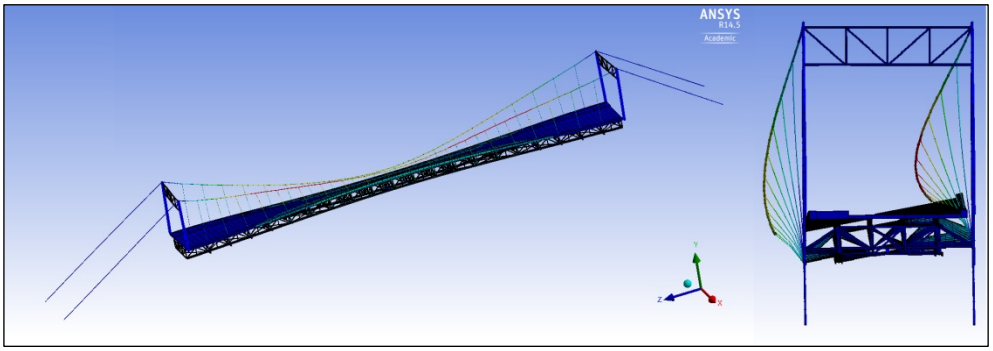

(a)

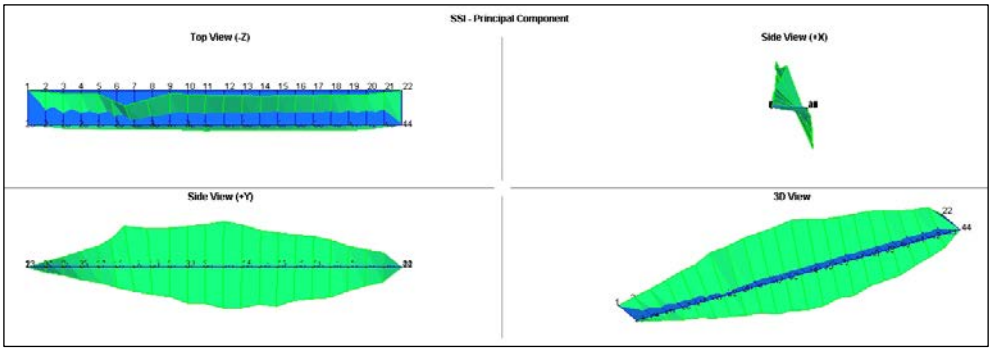

(b)

Figure 7.10 1st Torsion (mode 4) (a) FE Analysis 2.352Hz (b) Measured 2. 090Hz (Pálsson, 2012)

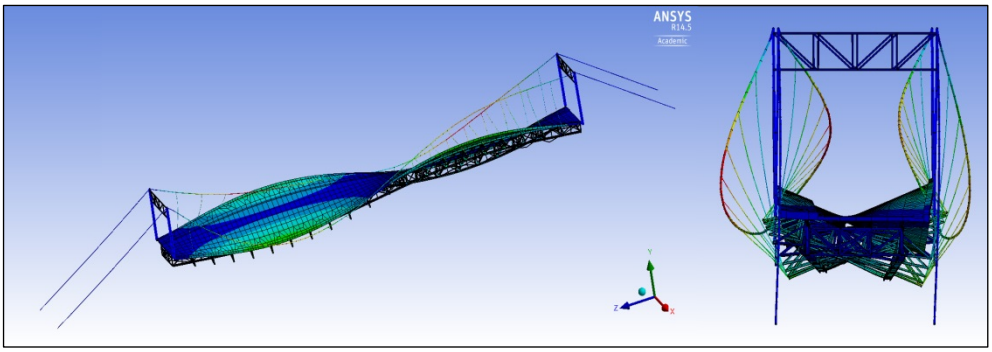

(a)

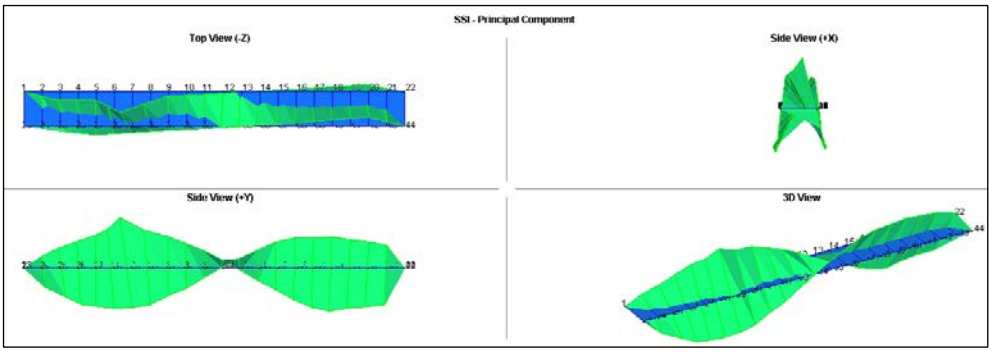

(b)

Figure 7.11 2nd Torsion (mode 9) (a) FE Analysis 2.831Hz (b) Measured 2.793Hz (Pálsson, 2012)

7.5 DAMAGE DETECTION IN CABLES

The FE model validated in the previous section of this chapter is considered as the undamaged baseline model for vibration based damage detection application. Seven damage cases were introduced in the FE model to simulate the various damage scenarios in the cables. It includes two different damage scenarios namely; single damage scenarios and multiple damage scenarios.

In the discussion of results, damage detection capability of the component specific DIs is compared with that of the MF difference (as also done previously in Chapters 4 and 6). The component specific DIs namely: vertical damage index (DI_V) and lateral damage index (DI_L) (defined in chapter 3) were calculated by using the vertical and lateral components of the first four mode shapes respectively. Similarly, MF difference vertical (MFD_V) and MF difference lateral (MFD_L) were calculated using the vertical and lateral components of the first four mode shapes respectively.

7.5.1 Damage Scenarios

This study simulated damage in the upstream cable by reducing the Young's modulus of the specific elements in the cable. In order to calculate the modal flexibility based DIs defined previously, natural frequencies and both vertical and lateral components of the first four mode shapes were extracted from the FE analysis in both damaged and undamaged state of the bridge. In single damage scenarios, 20% stiffness reduction at the mid span, quarter span and near the support of the cable were considered, while 15% and 30% stiffness reduction in two different locations at the cable were considered to cater for multiple damage scenarios. Table 7.8 and Table 7.9 below give the details of the locations of the damage cases considered in this study. Figure 7.12 illustrates the x direction measured along the span of the bridge and locations of damage considered. DIs are plotted along the cable and the damage locations are indicated with vertical red dotted lines.

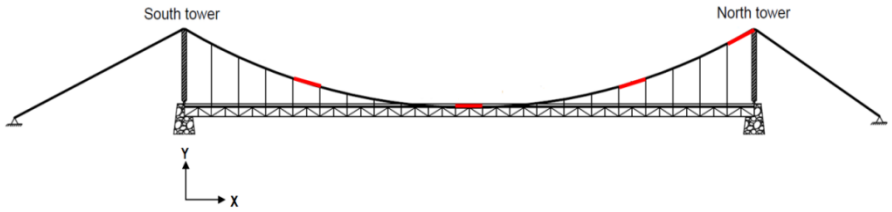

Figure 7.12 Direction notations

Table 7.8 Single damage scenarios

Damage Case	Location	Severity of Damage
Single damage scenario		
DC 1	Upstream cable (X=40m to X=44m)	20%
DC 2	Upstream cable (X=64m to X=68m)	20%
DC 3	Upstream cable (X=80m to X=84m)	20%
DC4	Upstream cable (X=40m to X=44m)	20% 40%

Table 7.9 Multiple damage scenarios

Damage Case	Location	Severity of Damage
Multiple damage scenario		
DC 5	Damage at two locations of upstream cable (X=40m to X=44m) and (X=64m to X=68m)	30% 15%
DC 6	Damage at two locations of upstream cable (X=16m to X=20m) and (X=64m to X=68m)	30% 15%
DC 7	Damage at two locations of upstream cable (X=16m to X=20m) and (X=80m to X=84m)	30% 15%

7.5.2 Damage Detection without Noise in Modal Data

Damage detection results for each damage case considered are illustrated below. Results include plots of damage indices (DI_V and DI_L) and plots of modal flexibility difference (MFD_V and MFD_L) in both damaged (upstream cable) and undamaged (downstream cable) cables.

- Single Damage Scenarios

  Four damage cases were examined to study the damage locating capability of DIs and MF difference calculated using vertical and lateral components of mode shapes.

1. Damage Case 1 (DC 1)

The first damage case studied is that in the middle of the upstream cable with 20% stiffness reduction. Numerical results of the damage indices (a) DI_V (b) DI_L and MF difference (c) MFD_V (d) MFD_L are shown in Figure 7.13. Figure 7.13 (a) shows

the DI_V curve of upstream cable increased its value at the nodes of the damaged location. However, no changes can be observed to the DI_V curve in undamaged cable (downstream cable). In Figure 7.13 (b), the DI_L index curve corresponding to upstream cable reached its minimum values at damaged location and change in the downstream cable is insignificant. The MFD_V curve in Figure 7.13 (c) shows the maximum in the upstream cable and minimum in the downstream cable at the location of damage considered. However, the MFD_L curve in Figure 7.13 (d) does not accurately indicate the damage location. In this case, the DI_V and MFD_V detect the damage successfully at the middle of the cable, and confirm the actual location of the damage considered. Since damage detection results for the other damage cases considered in this study follow the similar trends, only results for the two DIs are henceforth illustrated.

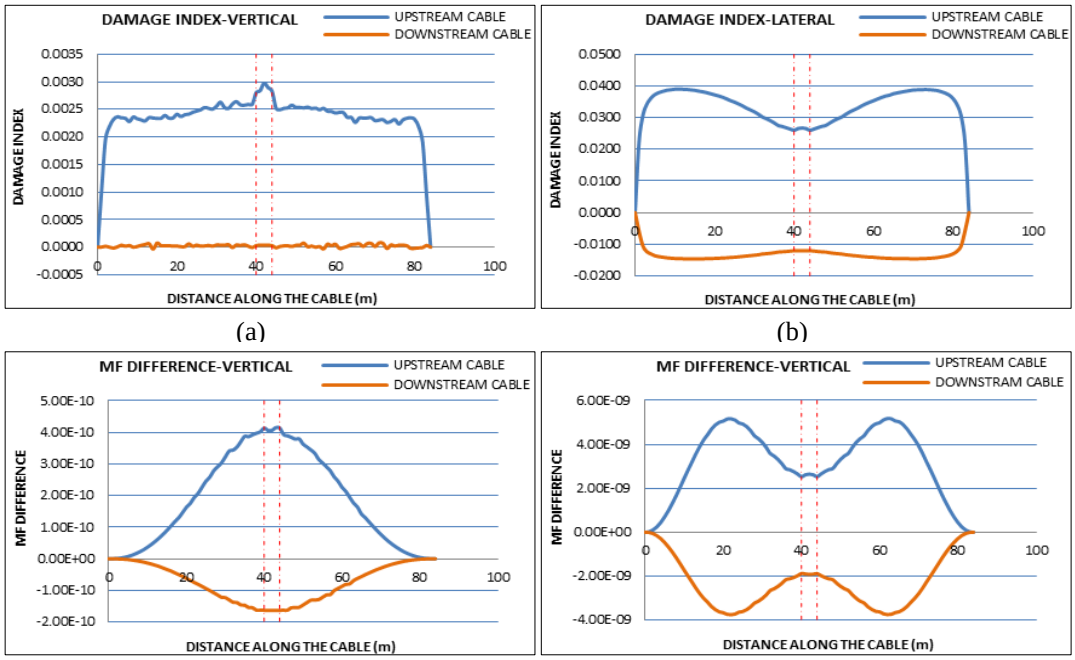

Figure 7.13 DC1 - Damage indices (a) DI_V (b) DI_L and MF difference (c) DI_V (d) DI_L

2. Damage Case 2 (DC 2)

Figure 7.14 illustrates the plots of both the damage indices for the second damage case with a 20% stiffness reduction at the quarter span of the upstream cable. The curves in Figure 7.14 (a) show that DI_V peaks at the exact damage location in the upstream cable while no significant change in DI_V is observed for the downstream cable. However, the DI_L curves in Figure 7.14 (b) show a very small change (negative) at the damage location for the upstream cable and no significant change

for the downstream cable. Based on the examination of the two graphs, it can be concluded that incorporating vertical components of mode shapes for detecting damage in a suspended cable of a structure is a successful approach. Therefore, competency of the DI_V (calculated by using the vertical components of the mode shapes) in damage detection of cables is further evaluated through Damage Case3 considered in this study.

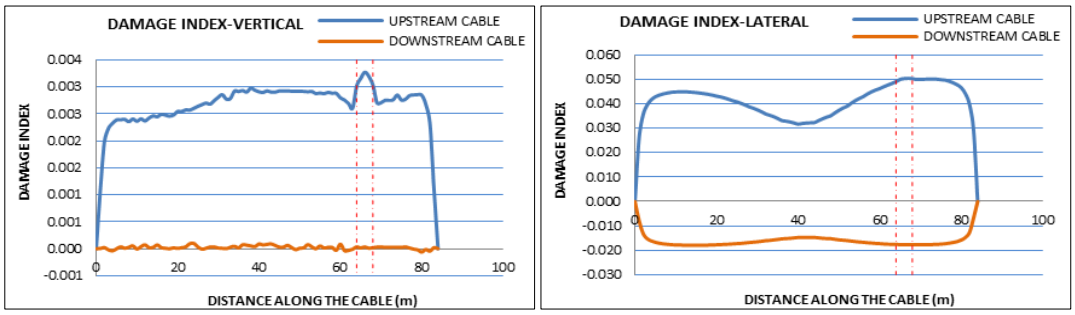

(a) (b)

Figure 7.14 DC2 - Damage indices (a) DI_V (b) DI_L

3. Damage Case 3 (DC 3)

Two curves of the DIs for damage case 3 are shown in Figure 7.15 (a) and (b). Damage case 3 is simulated near the support in the upstream cable with 20% stiffness reduction. Both damage indices show peaks representing the damage location in upstream cable without any significant changes in the downstream cable.

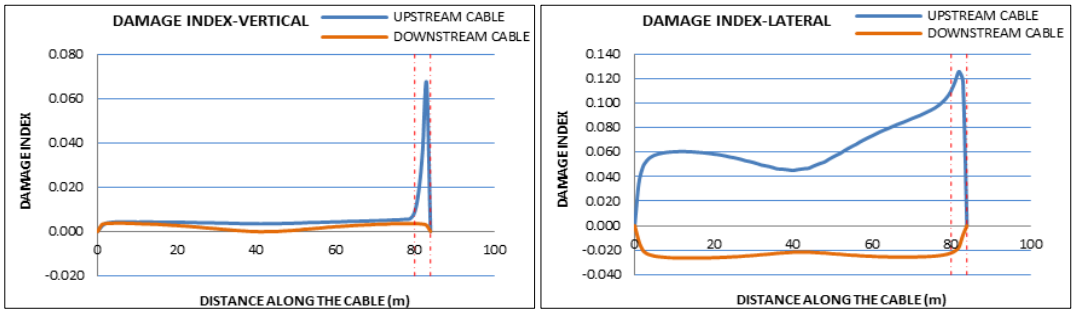

(a) (b)

Figure 7.15 DC3 - Damage indices (a) DI_V (b) DI_L

Considering all the damage cases that were examined, it can be confirmed that the DI_V calculated using the vertical components of the mode shapes of a suspension bridge structure have the ability to detect damage more accurately than DI_L (calculated using the lateral components of the mode shapes).

4. Damage Case 4 (DC 4)

In damage case 4 the DI_V was plotted for two different damage severities as illustrated in Figure 7.16. The magnitude of the DI changes according to the damage severity and it demonstrates that there is a potential for damage quantification using DI_V (a modal flexibility based damage index) in suspension bridges.

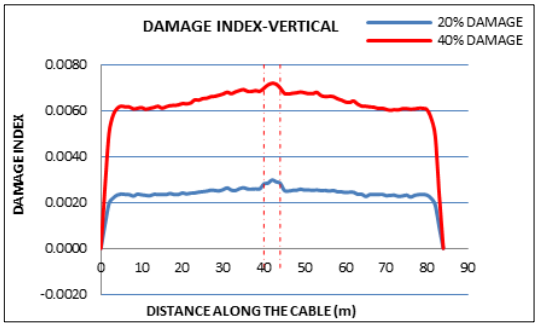

Figure 7.16 DC4 - DI_V

- Multiple Damage Scenarios

  Three damage cases were examined to study the damage locating capability of the DIs and MF difference calculated using vertical and lateral components of the of mode shapes.

5. Damage Case 5 (DC 5)

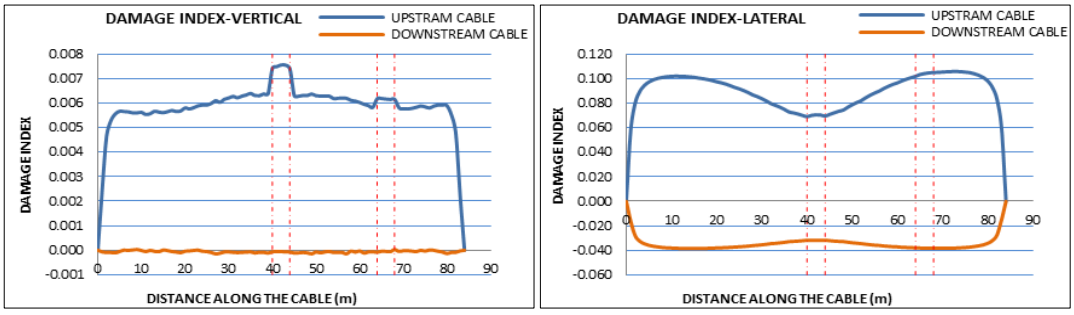

(a) (b)

Figure 7.17 DC5 - Damage indices (a) DI_V (b) DI_L

Damage case 5 is set up to study the damage locating capability of DIs in multiple damage locations. In this case, two locations are subjected to a 30% and 15% stiffness reduction in the upstream cable in the FE model to simulate damage. The behaviour of the DI_V and DI_L are illustrated in Figure 7.17 (a) and (b), respectively. The DI_V shows two peaks in the upstream cable at the damage locations considered. The DI_L curve of the upstream cable on the other hand has no significant indication of the damage locations considered. These results indicate that the DI_V has

the ability to detect damage in suspension bridge cables under multiple damage scenarios.

6. Damage Case 6 (DC 6)

Figure 7.18 illustrates curves corresponding to both the damage indices for the next multiple damage case with 30% and 15% stiffness reduction in two locations in the quarter span of the upstream cable. The curve (Figure 7.18 (a)) related to the DI_V peaks at the exact damage location being considered at the upstream cable and no any significant changes to the DI_V in the downstream cable. However, there is no any indication of damage location in the upstream cable can be observed in the plots of DI_L. Based on the examination of the two graphs, it can be concluded that incorporating vertical components of the mode shapes for detecting damage in the main cable of a suspension bridge is a successful approach. The competency of these damage indices DI_V and DI_L (calculated by using the vertical and lateral components of the mode shapes respectively) for damage detection in cables is further evaluated through Damage Case 7 in this study.

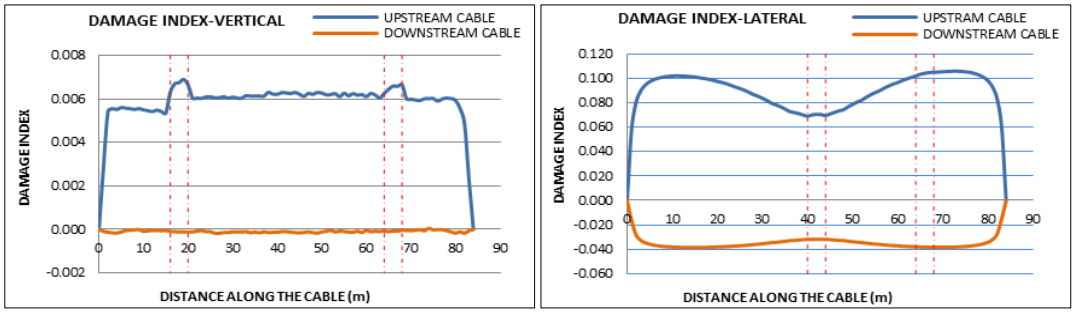

(a) (b)

Figure 7.18 DC6 - Damage indices (a) DI_V (b) DI_L

7. Damage Case 7 (DC 7)

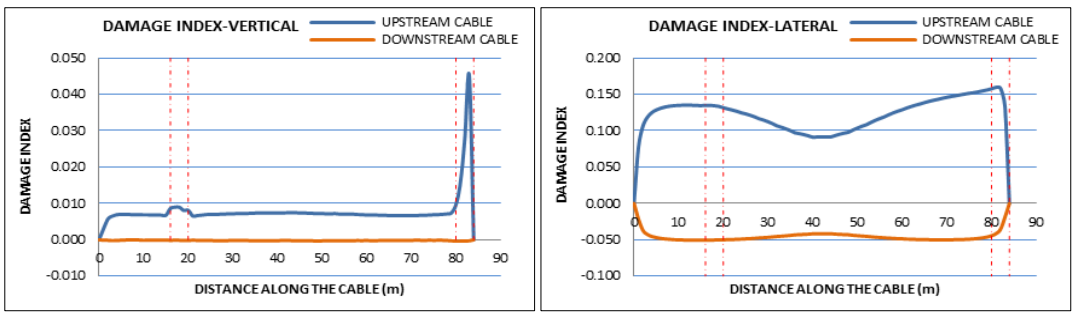

(a) (b)

Figure 7.19 DC7 - Damage indices (a) DI_V (b) DI_L

The results of last damage case studied under the multiple damage scenarios are with 30% and 15% stiffness reduction in quarter span and near the support at the upstream cable are as shown in Figure 7.19. The results verified that the DI_V is only competent enough to detect and locate damage in main cables of a suspension bridge structure. In a suspension bridge, modal mass is mainly distributed in the vertical direction. Therefore the DI_V shows the better damage detection capability compared to the DI_L.

7.5.3 Damage Detection with Noise in Modal Data

A method similar to that in chapter 4 is used to calculate the noise in modal parameters which are generated from the FE model. Since, the measurement noise associated with frequency is very low; 5% random noise is introduced to mode shapes. Few selected damage cases were examined under the noisy modal data.

Figure 7.20 to Figure 7.24 below illustrate the damage locating results of the DI_V with and without noise. For all the damage cases considered, the DI_V plots under noisy modal data have features similar to those observed earlier for noise free condition. There are clear indications of the damage locations for both single and multiple damage cases considered in the upstream cable. Therefore it can be concluded that the damage index calculated using the vertical component of the vibration modes performs well in locating damage even with the presence of 5% noise in the mode shape data. This implies that the vertical components of the mode shapes are more suitable for detecting damage in the main cables of suspension bridges.

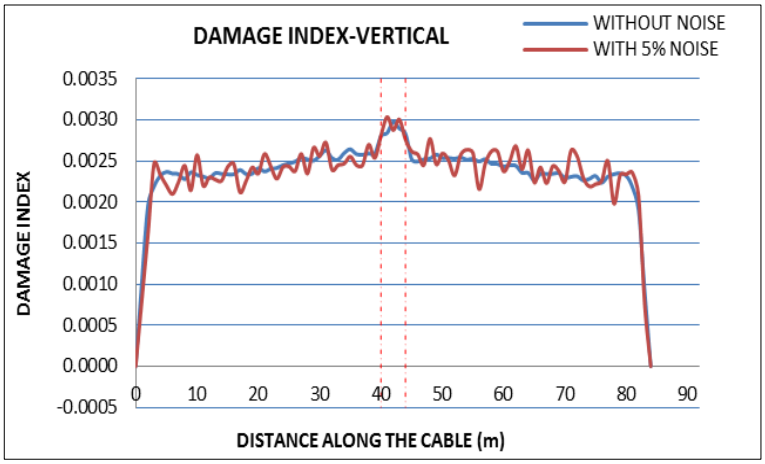

Figure 7.20 DC1 - DI_V

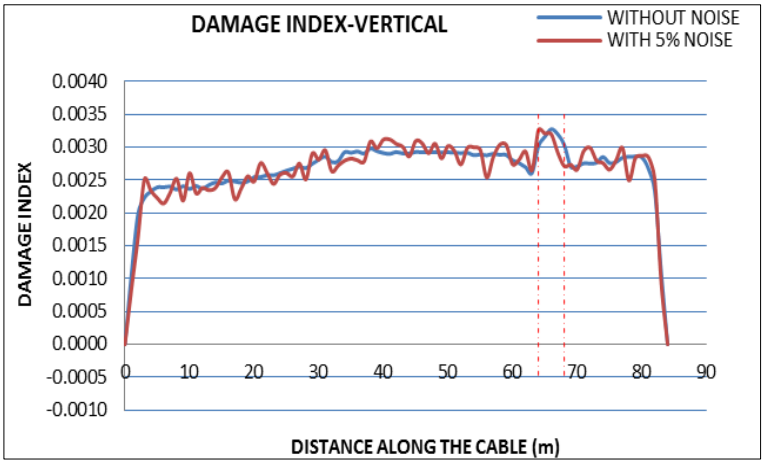

Figure 7.21 DC2 - DI_V

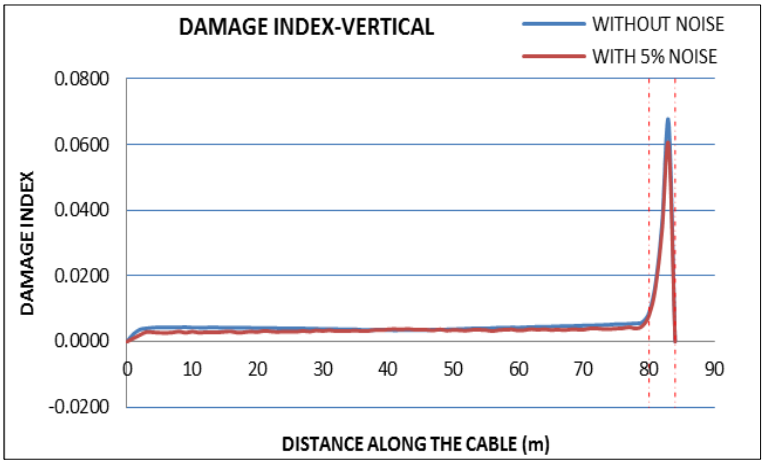

Figure 7.22 DC3 - DI_V

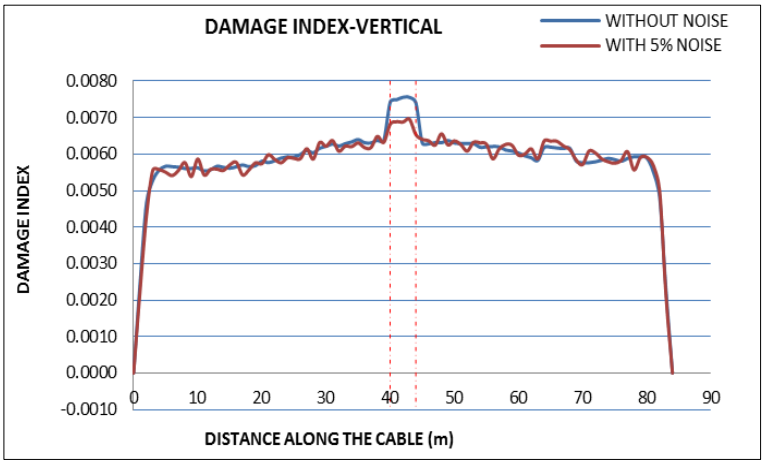

Figure 7.23 DC5 - DI_V

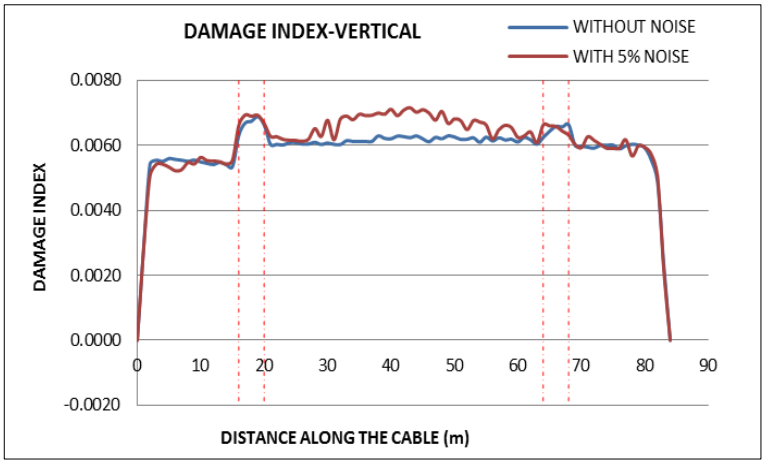

Figure 7.24 DC6 - DI_V

7.5.4 Influence of Higher Order Mode in Damage Detection of Cables

In this section, the influence of higher order mode on competency of the DI_V is examined. In order to do that, second torsional mode which appeared as mode nine in the analysis is incorporated to calculate the DI_V. Four cable dominant modes were appeared in between mode 4 and mode 9 was disregarded in the calculation due to unavailability of these modes in the field measurement data for FE model validation and their low mass participation ratio in vibration modes.

It can be seen that damage detection results for damage cases 3 (Figure 7.27) and 7 and (Figure 7.30) are not influenced by the higher order mode while damage cases 2 (Figure 7.26) and 6 (Figure 7.29) are slightly influenced by higher order modes. However, higher influence for the damage detection results using higher order modes can be observed in damage case 1(Figure 7.25) and 5 (Figure 7.28). Overall, it can be conclude that lower order modes are contributing to the better estimation of the damage location and hence confirm the applicability of the DI_V to detect and locate damage in main cables of suspension bridges.

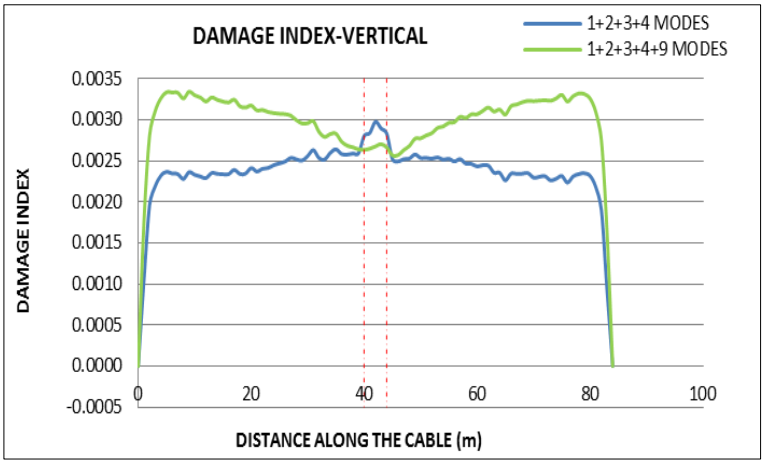

Figure 7.25 DC1 - DI_V

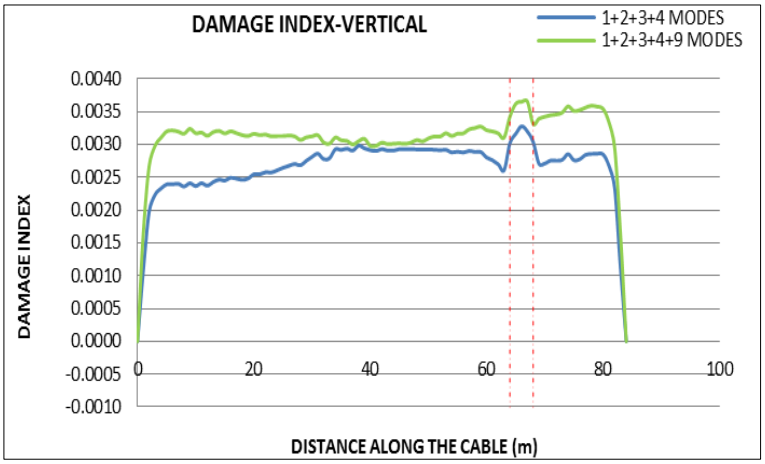

Figure 7.26 DC2 - DI_V

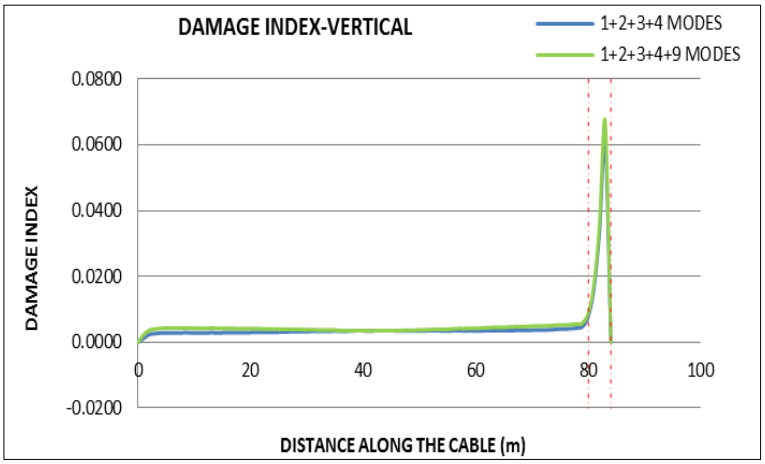

Figure 7.27 DC3 - DI_V

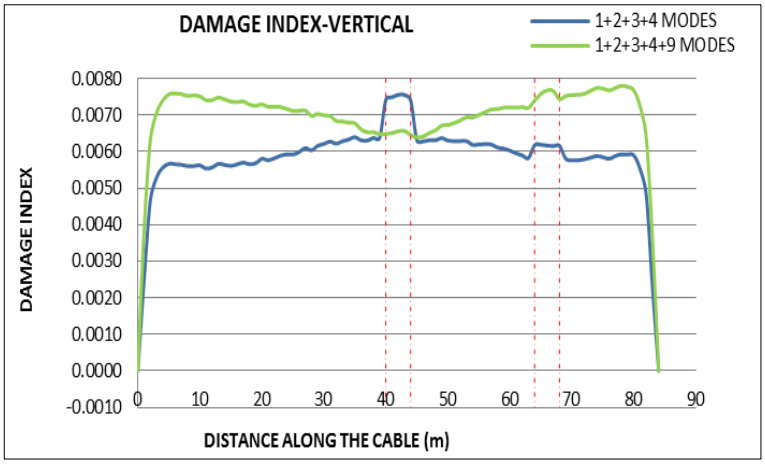

Figure 7.28 DC5 - DI_V

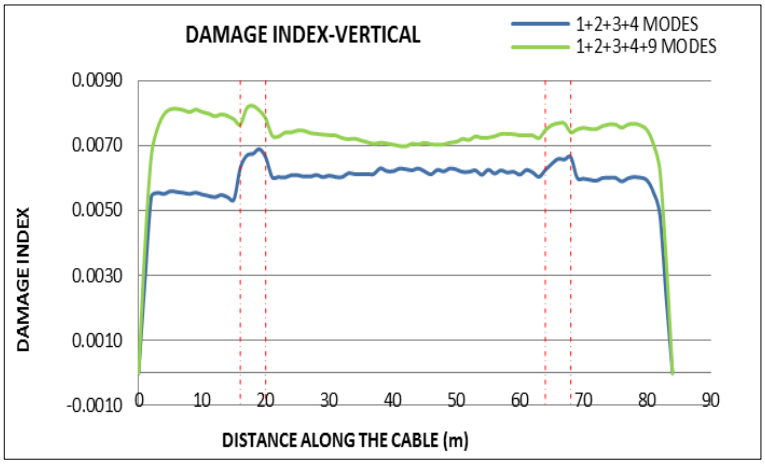

Figure 7.29 DC6 - DI_V

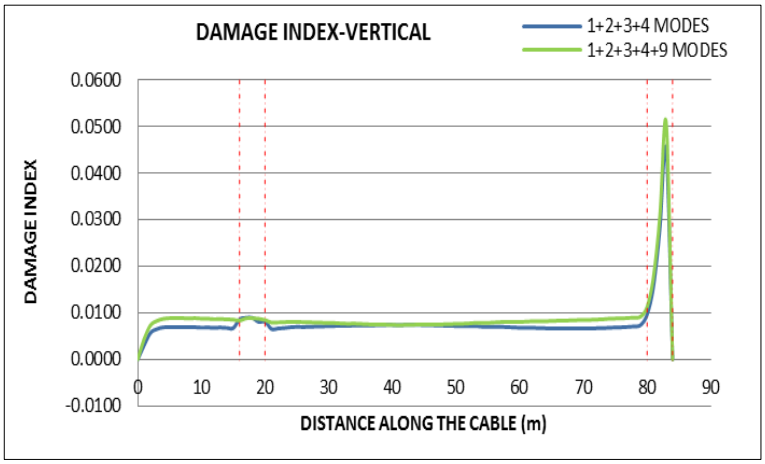

Figure 7.30 DC7 - DI_V

7.6 DAMAGE DETECTION IN HANGERS

The FE model developed and validated in the previous section of this chapter is considered as the undamaged baseline model for damage detection in the hangers. Six damage cases were introduced to the hangers at the upstream cable plane in the FE model to simulate the various damage scenarios. It includes two different damage scenarios namely; single damage scenarios and multiple damage scenarios. Three damage cases with 20% stiffness reduction at the hanger 10, hanger 5 and hanger 1 and one damage case with different damage severities in hanger 1 are included in the single damage scenarios. Two damage cases are defined with 20% and 10% stiffness reduction in two different hangers to cater for multiple damage scenarios.

In the previous section, it has been clearly shown that DI_V calculated by using the vertical components of the mode shapes had the ability to detect and locate damage in the main cables of the suspension bridge. The capabilities of both DI_V and DI_L and the two MF differences: MFD_V and MFD_L for detecting and locating damage in hangars are investigated herein. The component specific damage indices (defined in chapter 3) were calculated by using the vertical and lateral components of the first four mode shapes respectively. Similarly, the MF difference vertical and MF difference lateral were also calculated using the vertical and lateral components of the first four mode shapes respectively.

DI_V, DI_L, MFD_V and MFD_L are initially calculated for each node in every hanger. Next, the average values of these damage indices for each hanger are calculated and presented in bar graphs.

7.6.1 Damage Scenarios

Since, damage in FE models can be simulated by changing the Young's modulus or changing the cross section area or removing elements at damage location, this study simulated damage in the FE model of the Ölfusá Bridge by reducing Young's modulus of the specified hangers. Figure 7.31 and Table 7.10 represent the details of the damage cases considered in this study. Natural frequencies and mode shapes corresponding to first four vibration modes were extracted from the FE analysis of both damaged and undamaged state of the hanger.

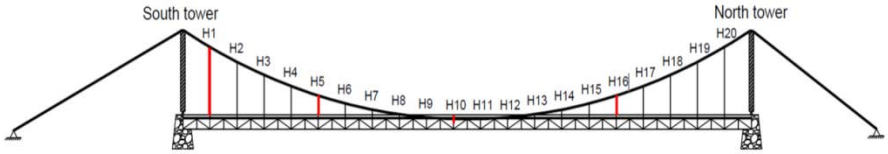

Figure 7.31 Locations of damaged considered in hangers at upstream cable plane

Table 7.10 Damage cases considered in hangers

Damage Case	Location	Severity of Damage
Single damage scenario		
DC 1	Hanger 10	20%
DC 2	Hanger 5	20%
DC 3	Hanger 1	20%
DC 4	Hanger 1	10% , 20%
Multiple damage scenario		
DC 5	Hanger 5 and Hanger 10	20% 10%
DC 6	Hanger 5 and Hanger 16	10% 20%

7.6.2 Damage Detection without Noise in Modal Data

Damage detection results for each damage case considered are illustrated below. Results include bar graphs of DI_V, DI_L, MFD_V and MFD_L corresponding to each hanger in both cable planes (upstream and downstream).

• Single Damage Scenarios

Four damage cases were examined to study the damage locating capability of component specific DIs and MF difference calculated using both vertical and lateral components of the mode shapes.

1. Damage Case 1 (DC 1)

The first damage case studied is that with a 20% stiffness reduction of the hanger 10. Figure 7.32 illustrates the bar graphs of DIs and MF difference corresponds to each hanger respectively. Both graphs for DI_V and MFD_V indicate the higher value at hanger 10 in upstream cable plane which confirms the damaged hanger. However DI_L and MFD_L did not highlight the damaged hanger. In this case, both DI and MF difference calculated using vertical components of the mode shapes are able to successfully detect and locate the damaged hanger.

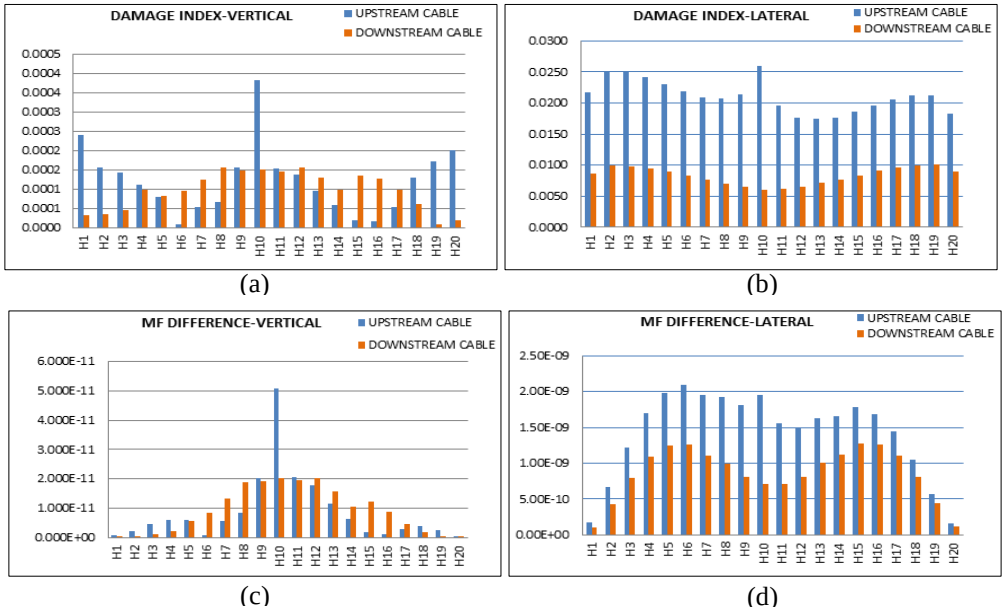

Figure 7.32 DC1 - Damage indices (a) DI_V (b) DI_L and MF difference (c) DI_V (d) DI_L

2. Damage Case 2 (DC 2)

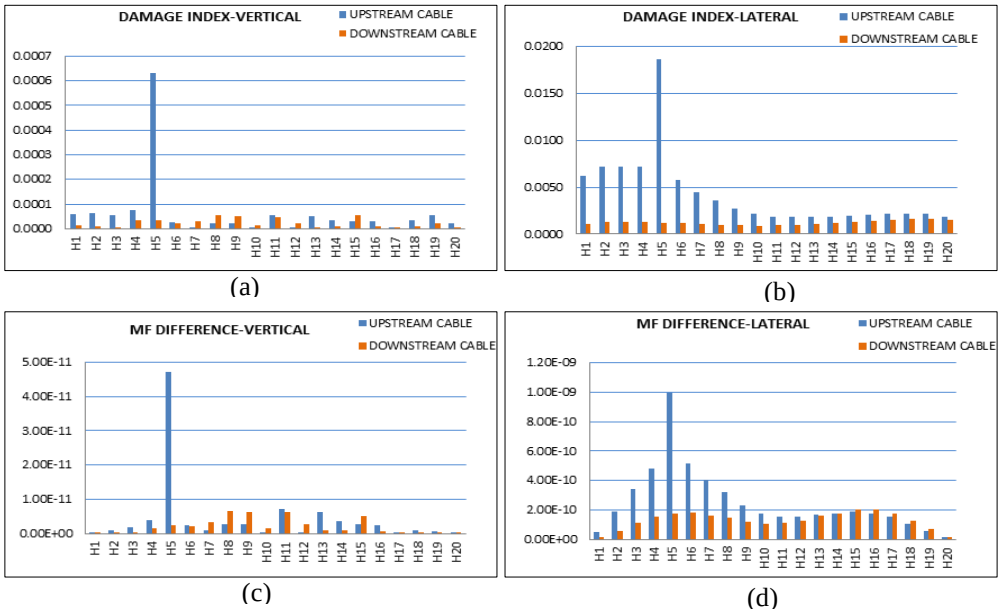

Figure 7.33 DC2 - Damage indices (a) DI_V (b) DI_L and MF difference (c) DI_V (d) DI_L

Figure 7.33 show the DIs and MF differences for the second damage case with a 20% stiffness reduction in hanger 5 at upstream cable plane. The bar graphs for DI_V and MFD_V clearly indicate the damaged hanger. Though DI_L and MFD_L calculated using the lateral components of mode shapes also indicate the damaged hanger, there are considerable numbers of false alarms in the results. Based on the examination of the four graphs, it can be concluded that incorporating vertical components of the mode shapes for detecting and locating damage in hangers is a successful approach using either DI_V or MFD_V. The competency of both these damage indices for detecting and locating damage in hangers is further evaluated through damage case 3 considered in this study.

3. Damage Case 3 (DC 3)

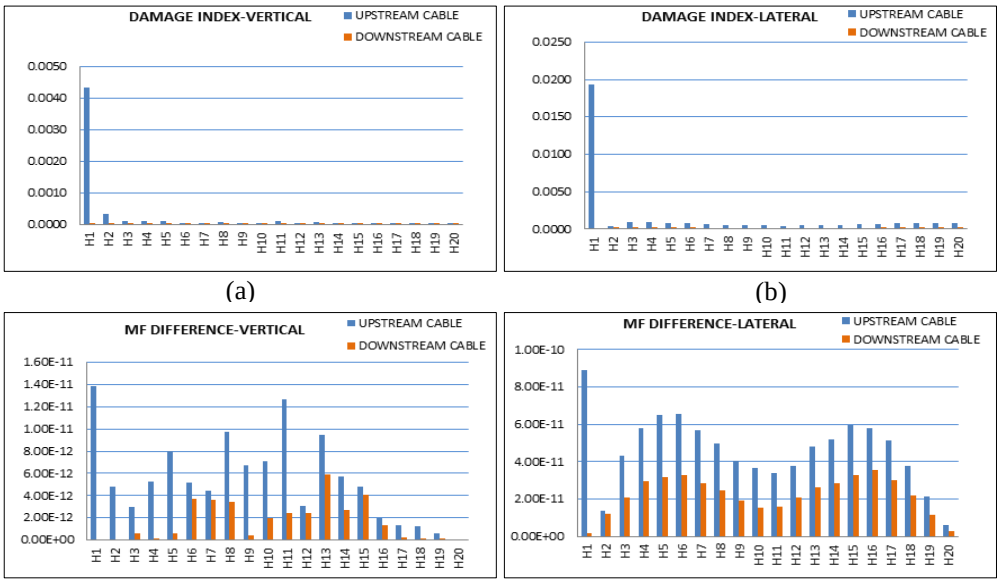

Figure 7.34 DC3 - Damage indices (a) DI_V (b) DI_L and MF difference (c) DI_V (d) DI_L

Four bar graphs related to the DIs and MF difference for damage case 3 is shown in Figure 7.34. Damage Case 3 is simulated in hanger 1 of the FE model with 20% stiffness reduction. The DI_V and DI_L indicate the damage location correctly. The plots of MFD_V and MFD_L do have peaks at the damaged hanger, but they also demonstrate the presence of false alarms as shown in Figure 7.34 (c) and (d). Again, it has been shown that the DIs have better ability to detect and locate damage more accurately than MFDs.

4. Damage Case 4 (DC 4)

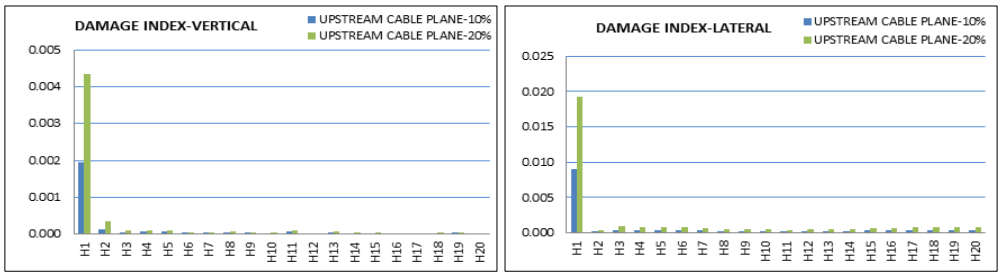

(a) (b)

Figure 7.35 DC4 - Damage indices (a) DI_V (b) DI_L

In damage case 4, DI_V and DI_L were plotted for two different damage intensities as illustrated in Figure 7.35. Both damage indices are able to locate the damage hanger successfully. Furthermore, that peaks of the DIs vary according to the damage intensity and these results demonstrate that there is a potential for damage quantification in suspension bridge cables and hangers using these modal flexibility based damage indices.

- Multiple Damage Scenarios

  Two damage cases were examined to study the damage locating capability of DIs and MF difference. These damage cases include damage in hangers at two different locations.

5. Damage Case 5 (DC 5)

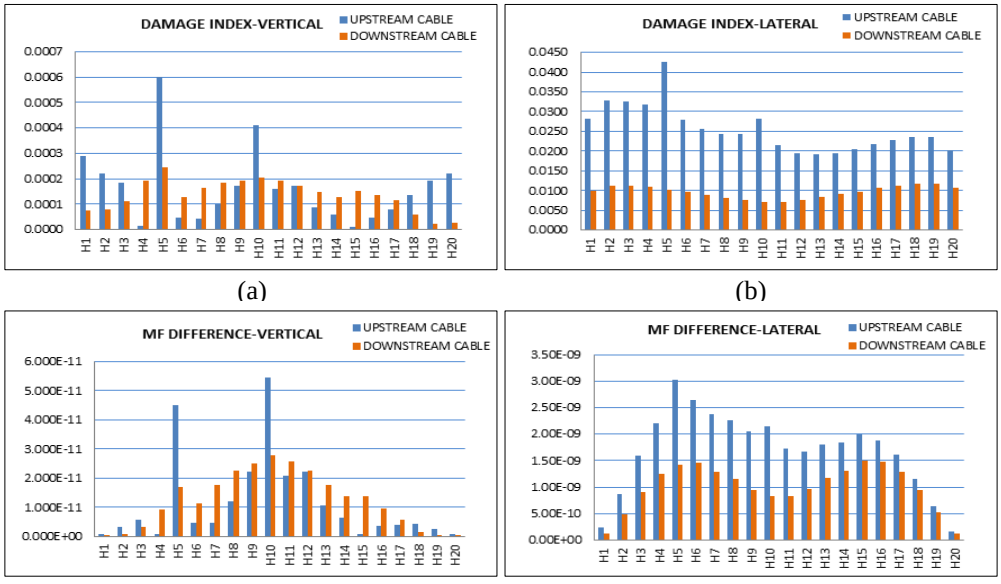

(a) (b)

(c) (d)

Figure 7.36 DC5 - Damage indices (a) DI_V (b) DI_L and MF difference (c) DI_V (d) DI_L

In damage case 5 hangers 5 and 10 are subjected to a 20% and 10% stiffness reduction in the FE model to simulate damage. The bar charts above show that both DI_V and MFD_V are able to locate the damage successfully. Further, changes in peak values of DI_V in Figure 7.36 (a) vary according to the damage intensity (hanger 5-20% and hanger 10-10%) and confirm its accuracy compared to that of MFD_V.

6. Damage Case 6 (DC 6)

The results of last damage case studied under the multiple damage scenarios are with 10% and 20% stiffness reduction in hanger 5 and 16 as shown in Figure 7.37. The results verify that DI_V and MFD_V are more competent in detecting and locating damage in hangers of a suspension bridge than their counterparts which are calculated by using the lateral components of the mode shapes.

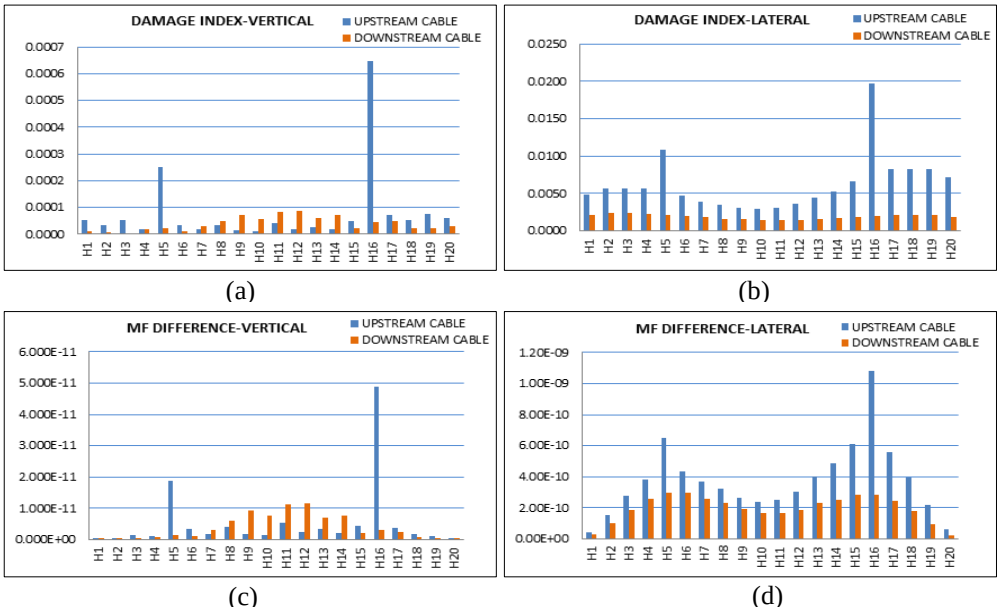

Figure 7.37 DC6 - Damage indices (a) DI_V (b) DI_L and MF difference (c) DI_V (d) DI_L

Based on the above damage detection results for the hangers, it is clearly evident that the damage index (DI_V) calculated by using the vertical components of the mode shapes is capable of detecting and locating damage under single and multiple damage scenarios. Further, the results indicate a possibility of damage quantification in hangers using this vertical damage index. The next section examines the competency of the DI_V under the influence of measurement noise.

7.6.3 Damage Detection with Noise in Modal Data

A method similar to that in chapter 4 is used to calculate the noise in modal parameters which are generated from the FE model. Few selected damage cases were

examined under the noisy modal data. Figure 7.38 - Figure 7.42 illustrate the damage locating results of the DI_V calculated using the vertical components of the mode shapes with and without noise in the modal data. Based on the analysis of the bar graphs, it is clearly evident that the DI_V index successfully locates the damage in every damage case considered. Therefore it can be concluded that the DI_V performs well in locating damage even in the presence of 5% noise in the mode shape data.

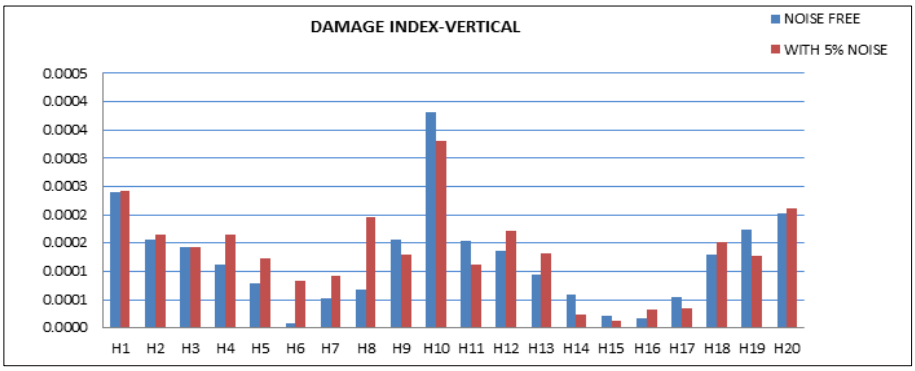

Figure 7.38 DC1 - DI_V

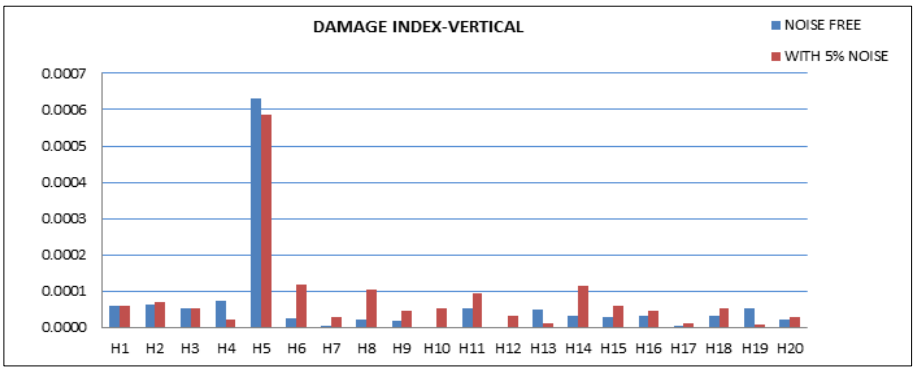

Figure 7.39 DC2 - DI_V

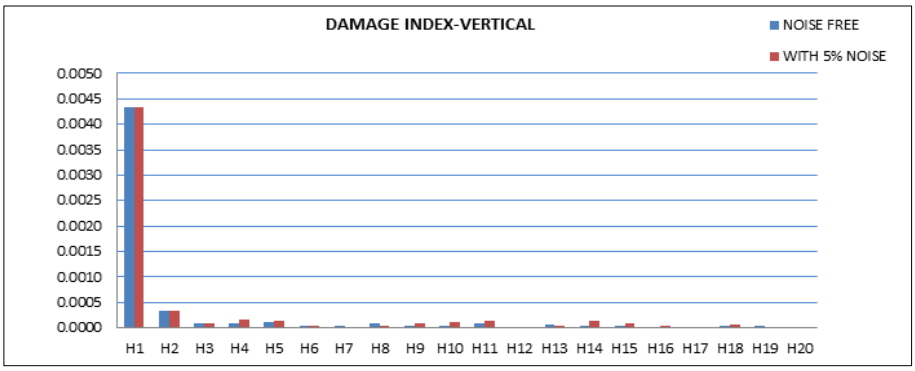

Figure 7.40 DC3 - DI_V

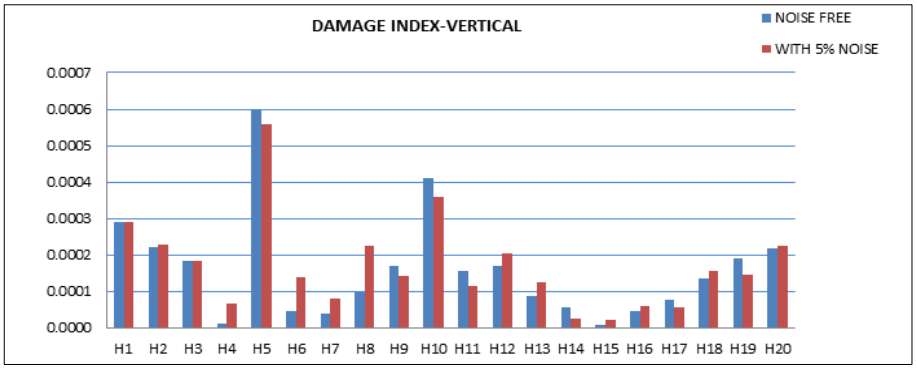

Figure 7.41 DC5 - DI_V

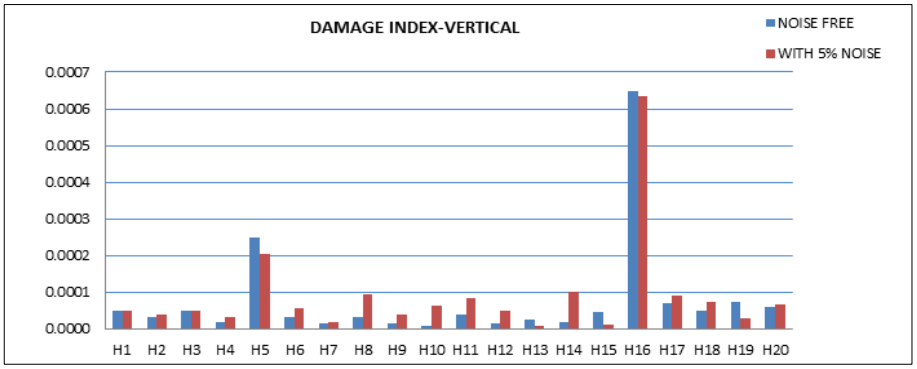

Figure 7.42 DC6 - DI_V

7.6.4 Influence of Higher Order Mode in Damage Detection of Hangers

In this section, the influence of higher order modes on the competency of the DI_V is examined. The second torsional mode which appeared as mode nine in the analysis is also used to calculate the DI_V. However cable modes that appeared in between are disregard. Damage detection results for damage cases 1 (Figure 7.43) and 3 (Figure 7.45) are little influenced by the higher order mode while the results of the other damage cases have been influenced by the inclusion of the higher mode, often with several false alarms. Overall, it can be concluded that the lower order modes contribute adequately towards the calculation of the DI_V to detect and locate damage in the hangers of suspension bridges.

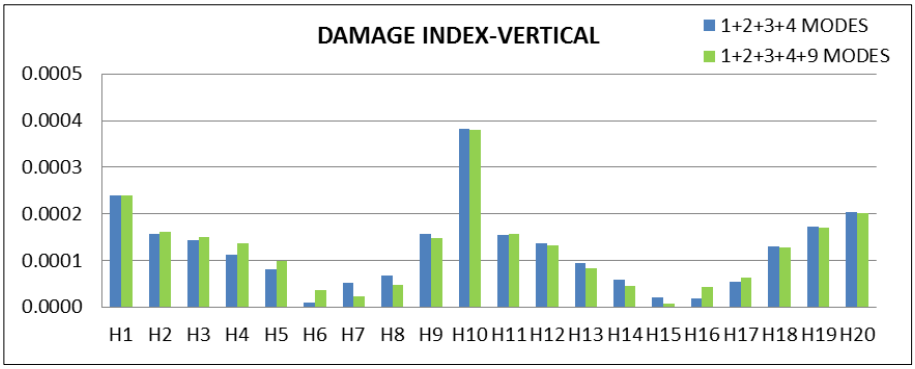

Figure 7.43 DC1 - DI_V

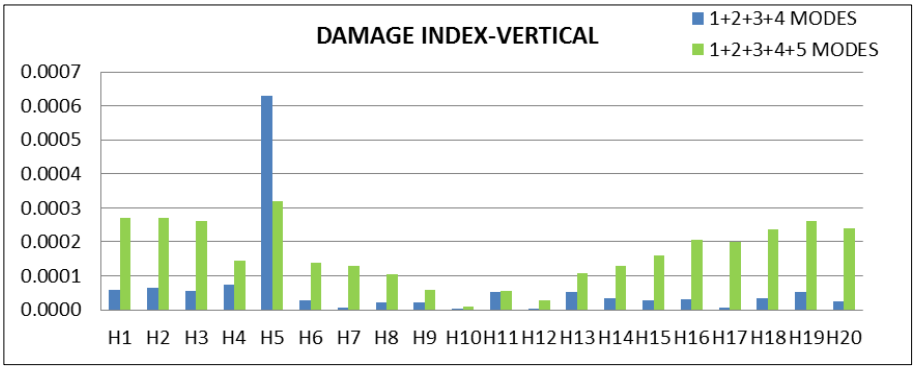

Figure 7.44 DC2 - DI_V

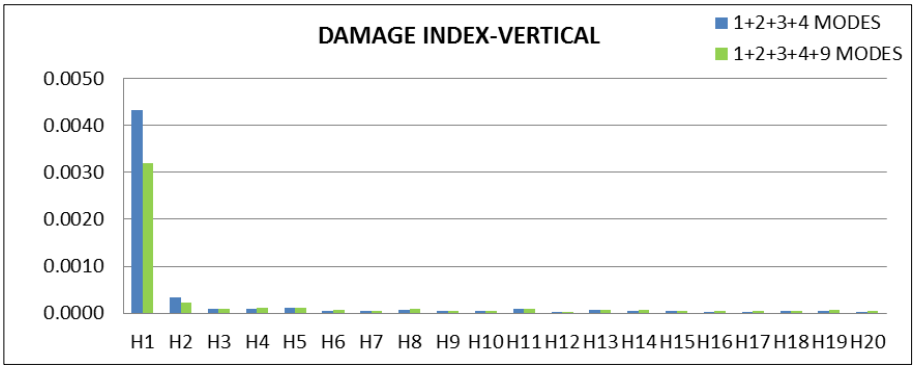

Figure 7.45 DC3 - DI_V

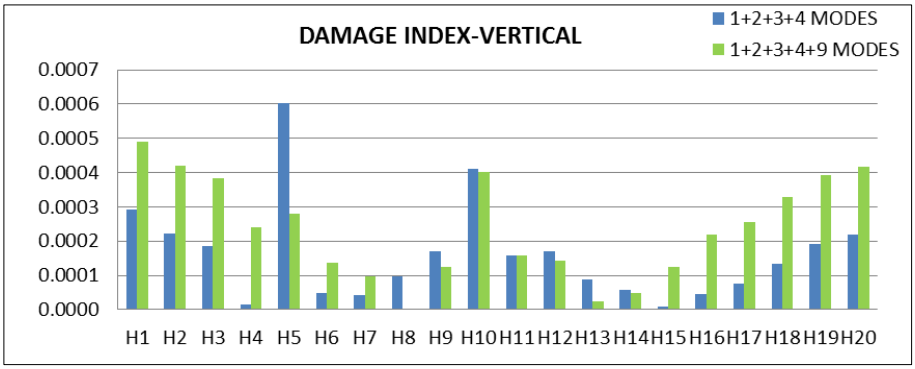

Figure 7.46 DC5 - DI_V

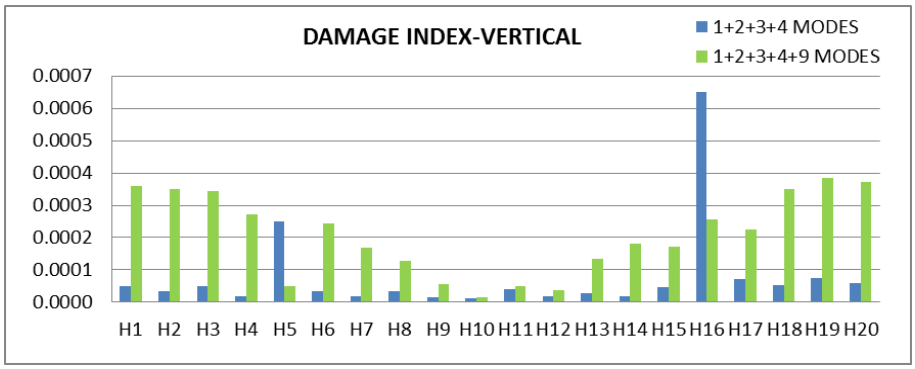

Figure 7.47 DC6 - DI_V

7.7 COMPLEX DAMAGE SCENARIOS

A variety of damage types that can occur in a suspension bridge main cable and hangers were studied separately in the previous sections. In some circumstances, damage in the main cables and hangers occur simultaneously and the damage detection problem becomes more complex. The objective of this section is to evaluate the competency of DI_V for its accuracy of damage detection in such complex damage scenarios. Five different damage cases were considered to cover the various combinations of complex damage as illustrated in Table 7.11. Four damage cases were selected to cater for simultaneous damage in cable and hanger. Further, one damage case was considered in the one of middle steel girder to examine whether the DI_V demonstrates a false alarm in the cables and hangers. In presenting damage detection results of hangers, the DI_V is initially calculated for each node in every hanger and the average value of the DI_V for each hanger is calculated and plotted in bar graphs. In the case of cables, the DI_V is plotted along the cable and the damage locations are indicated with vertical red dotted lines.

Table 7.11 Complex damage scenarios

Damage Case	Location	Severity of Damage
DC 1	Damage at middle of upstream cable (X=40m to X=44m) and Damage at Hanger 5 of upstream cable plane	20% 20%
DC 2	Damage at quarter of upstream cable (X=64m to X=68m) and Damage at Hanger 5 of upstream cable plane	20% 20%
DC 3	Damage at middle of upstream cable (X=40m to X=44m) and Damage at Hanger 5 of downstream cable plane	20% 20%
DC 4	Damage at corner of upstream cable (X=80m to X=84m) and Damage at Hanger 5 of downstream cable	20% 20%
DC 5	Damage at middle of the steel girder (X=40m to X=44m)	20%

1. Damage Case 1 (DC 1)

The first damage case studied is that in the middle of the upstream cable and at hanger 5 in the upstream cable with 20% stiffness reduction. In the Figure 7.48 (a), the DI_V curve along the cable illustrates a one down peak near location of the hanger 5 and a peak at the middle of the cable. At the same time, the bar graph of the DI_V detects the damaged hanger at the upstream cable plane. This verifies the DI_V is competent in detecting and locating damage in complex damage cases.

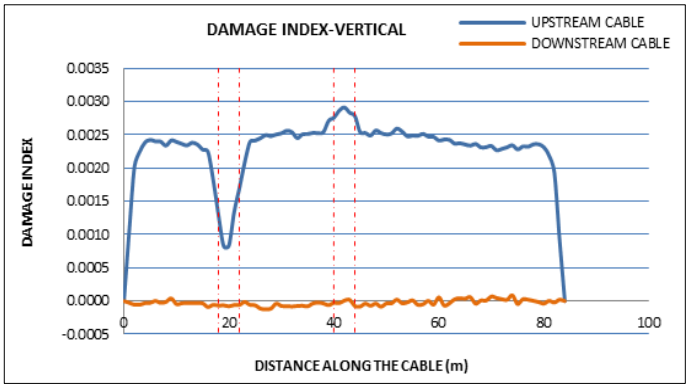

(a)

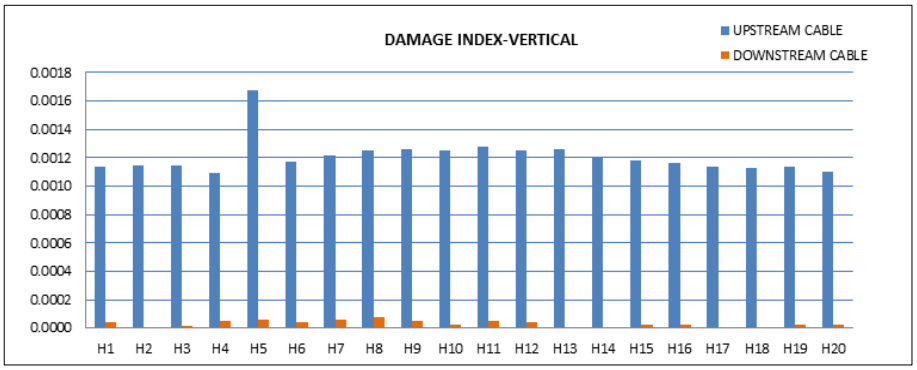

(b)

Figure 7.48 DC1 - Damage index DI_V (a) plotted along the cable (b) plotted in hangers

2. Damage Case 2 (DC 2)

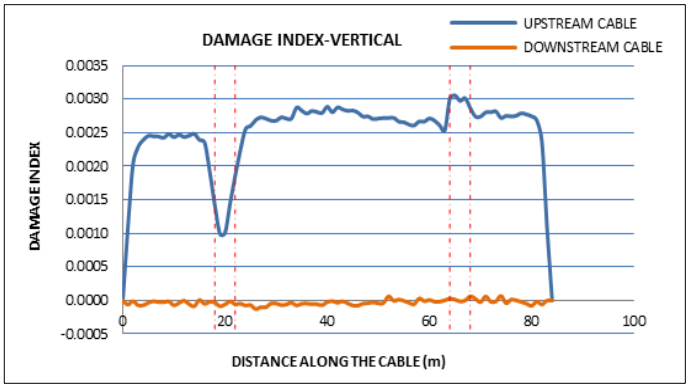

(a)

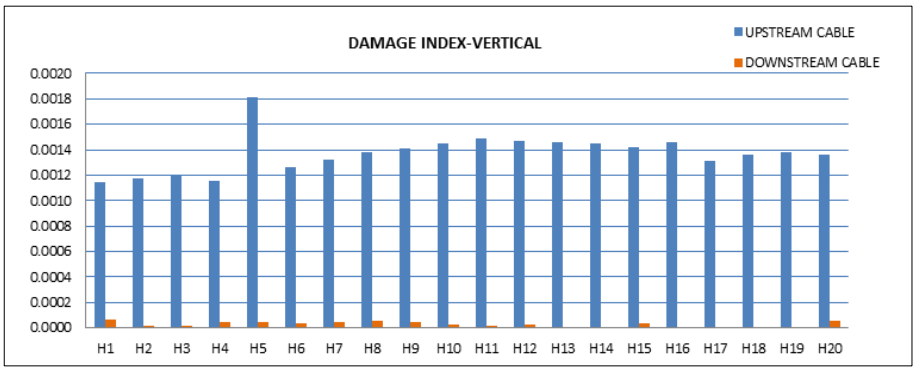

(b)

Figure 7.49 DC2 - Damage index DI_V (a) plotted along the cable (b) plotted in hangers

Figure 7.49 illustrates the plots of the DI_V for the second damage case studied under complex damage scenarios with 20% stiffness reduction at the quarter span of the upstream cable and hanger 5 in the upstream cable. The curves in the Figure 7.49(a) show a down peak and a peak at damage locations of the upstream cable while no significant change can be observed in the downstream cable. Based on the examination of the Figure 7.49 (b) graph, it is clearly evident that hanger 5 is damaged. Therefore, the DI_V plotted separately for cables and hangers can be used to distinguish the occurrence of simultaneous damage in those elements.

3. Damage Case 3 (DC 3)

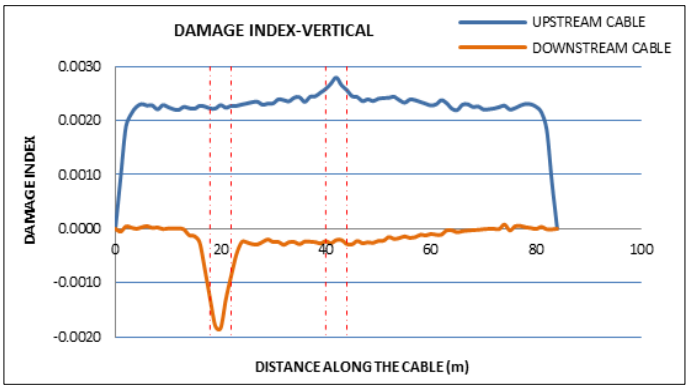

(a)

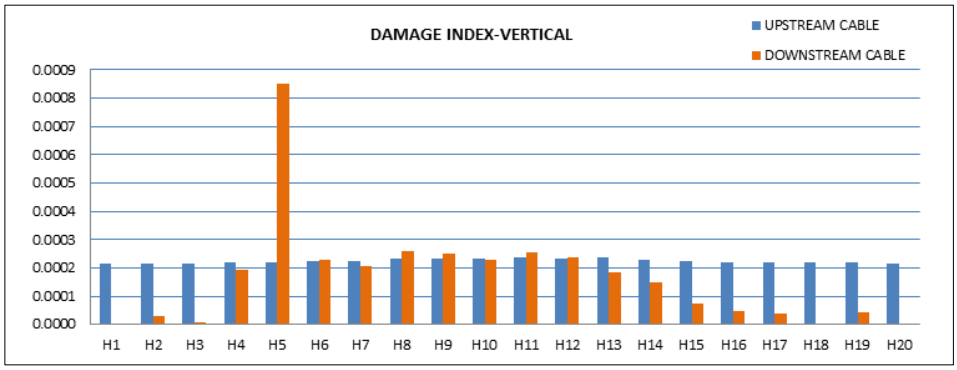

(b)

Figure 7.50 DC3 - Damage index DI_V (a) plotted along the cable (b) plotted in hangers

The damage case 3 is set up to study the damage locating capability of the DI_V when damage occurred at different cable planes. In this case, two damage locations are subjected to a 20% stiffness reduction in the middle of the upstream cable and hanger 5 of the downstream cable. In Figure 7.50 (a) the DI_V curve plotted related to the upstream cable correctly shows the damage location and that in the downstream cable indicates the damaged hanger location precisely and it is confirmed by the DI_V plots associated with hangers (Figure 7.50 (b)).

4. Damage Case 4 (DC 4)

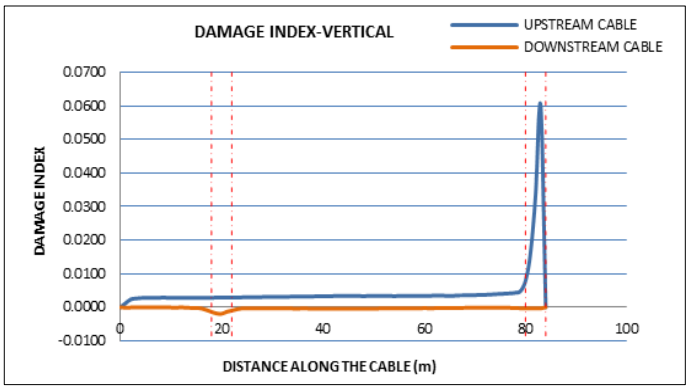

(a)

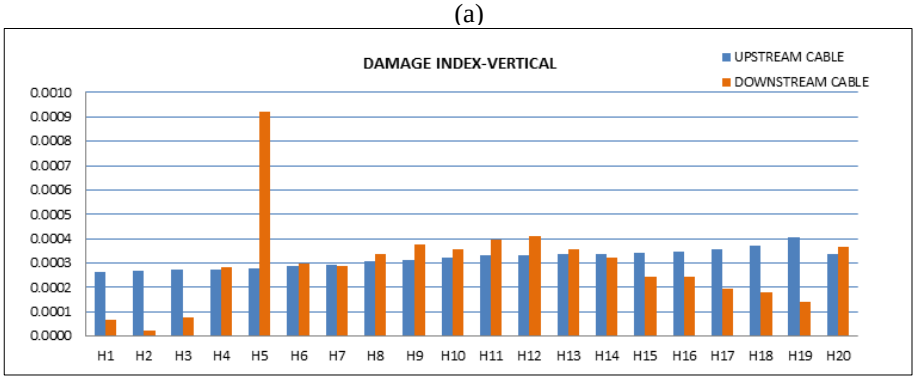

(b)

Figure 7.51 DC4 - Damage index DI_V (a) plotted along the cable (b) plotted in hangers

The two graphs of the DI_V for damage case 4 are shown in Figure 7.51(a) and (b). Damage case 4 is simulated near the support in the upstream cable and hanger 5 of the downstream cable with 20% stiffness reduction. Similar results can be observed in this case as other damage cases examined. The damage detection capability of the DI_V is further evaluated through the damage case 5.

5. Damage Case 5 (DC 5)

Damage with 20% stiffness reduction is simulated in one of the middle steel girder which supports the deck. This damage case was treated intentionally to examine whether DI_V when plotted for the cables and hangers eliminates the indication of damage in them (it does not show any false alarms), when the damage occurs elsewhere in the bridge. According to the Figure 7.52 (a) and (b), it is clearly evident that DI_V plots along the cable and at each hanger are not sensitive to the damage at the steel girder of the bridge. Results indicate that there is no false detection of damage when DI_V is used for the purpose of damage detection in cables and hangers.

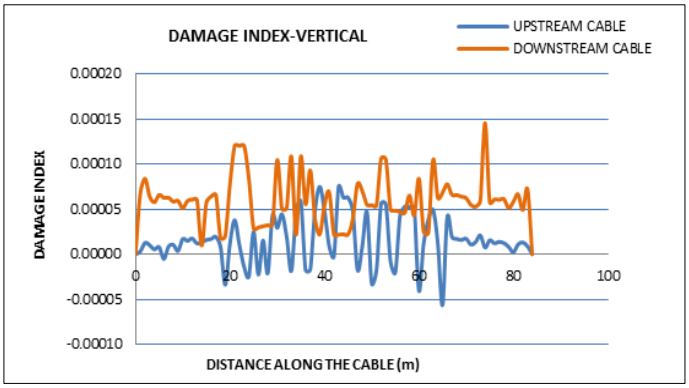

(a)

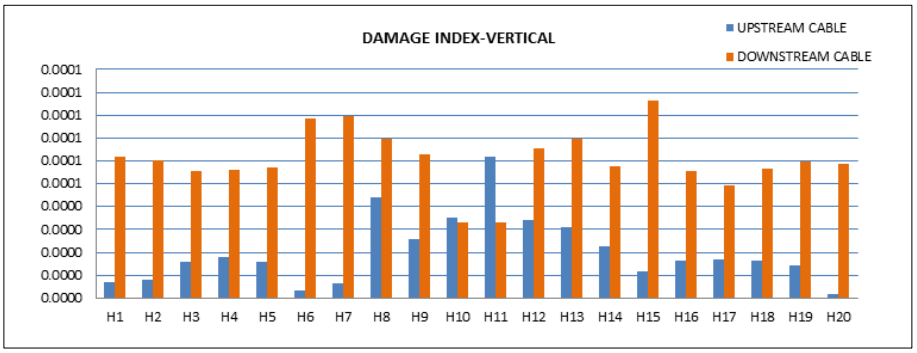

(b)

Figure 7.52 DC5 - Damage index DI_V (a) plotted along the cable (b) plotted in hangers

The damage detection results of the first four damage cases studied under the complex damage scenarios indicated a down peak in the corresponding location of the damaged hanger (in the plots of the DI_V for the cable). This is due to the stiffness increment of the cable near the damaged hanger location. Based on the above damage detection results for the cables and hangers, it is clearly evident that the damage index (DI_V) calculated by using the vertical components of the mode shapes is capable of distinguishing and locating damage in cables and hangers under complex damage scenarios.

7.8 APPLICATION OF DAMAGE INDICES IN REAL CABLE SUPPORTED STRUCTURES (INVERSE PROBLEM)

This thesis used dynamic computer simulations to investigate the suitability of modal flexibility based DIs to detect and locate damage in suspension bridge main cables and hangers. It has shown that the lateral damage index (DI_L) is efficient in detecting and locating damage in large diameter suspended cables which are used in cable structures. Further, the damage index (DI_V), calculated by suing the vertical components of the first 5 mode shapes, can be used to detect and locate damage in the cables of a complex 3D cable bridge model (which has 3 different structural

cables). In addition, this study also confirmed that damage in the main cables and hangers of suspension bridges can be detected and located by using the DI_V calculated using the vertical components of the mode shapes of the first four vibration modes. This study mainly focused on damage intensities varying from 5% to 30% stiffness reduction and severity levels varying between 2% to 10% (the percentage affecting total length of the cable). All these applications used the numerically simulated damage scenarios to check the competency of DIs in damage detection. The following steps are suggested in order to apply the selected DIs in the real application, where the occurrence and location of the damage are unknown. The flow chart is illustrated in Figure 7.53.

Step 1: Obtain acceleration measurements from the SHM system installed on the structure and assume the structure is intact.

Step 2: Conduct OMA and obtain frequencies and mode shapes of the structure.

Step3: Develop a FE model based on the design/as built information and update of the FE model of the structure using the frequencies and mode shapes obtained from OMA.

Step 4: Acquire frequencies and mode shapes from the two models .The first model is the undamaged model or the base line model and the second is the damaged model.

Step 5: Calculate the lateral damage index DI_L, if the structure is a cable only. (eg: Cable ways, long distance transmission lines)

Calculate the vertical damage index DI_V, if the cables are in a suspension bridge.

(In order to distinguish the damage is in the cable or hanger; it is required to plot the DI_V, for cables and hangers. The down peaks in the DI_V plot will indicate the damaged hanger location and it will be confirmed by the higher value of the DI_V plots for hangers.)

Step 6: Observe the peaks in the graph to confirm occurrence of damage and then observe the location of the peak to locate the damage. Closer

inspections can be conducted at these locations to further confirm damage.

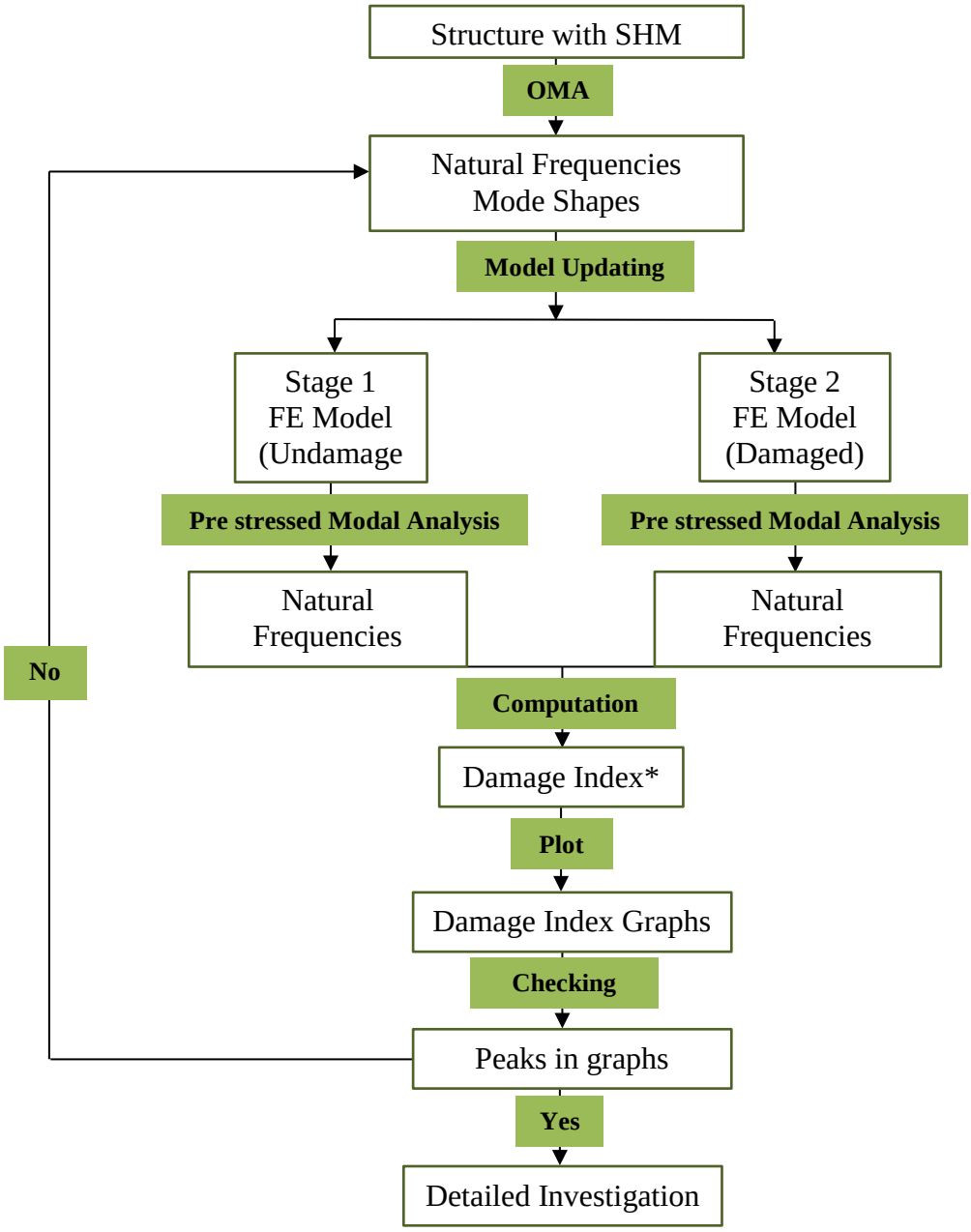

*Damage index

Vertical Damage Index (DI_V) - Suspension Bridges (Main cables and hangers)

Lateral Damage Index (DI_L) - Suspended cable structures (Eg. Cable cars, Transmission lines)

Figure 7.53 Flow chart for damage detection procedure

7.9 SUMMARY

This chapter described the application of modal flexibility based DIs to detect and locate damage in the cables and hangers of a 3D suspension bridge. The Ölfusá Suspension Bridge in Iceland was selected for the application as there was modal data for validating a FE model. The FE modelling of the Ölfusá Suspension Bridge was carried out in ANSYS Workbench. In order to validate the FE model, natural frequencies obtained from the FE model were compared with those obtained in the field testing of that bridge. The validated FE model was then used in damage detection studies of main cables and hangers of the Ölfusá Suspension Bridge using the first four vibration modes. This study first, proposed a special damage index calculated by using only the vertical components of the mode shapes and demonstrated its successful application in detecting and locating damage in the main cable and hangers of the suspension bridge. This study was carried out by examining different damage cases including single and multiple damage scenarios in these structural members with different damage severities. Secondly, the same damage cases were used to confirm the damage detecting and locating ability of the vertical damage index in the presence of 5% noise in the modal data. This was successful for both main cables and hangers. Thirdly, influence of a higher order mode, which was a torsional mode, in the damage detection of suspension bridge main cables and hangers using the vertical damage index was investigated. Results confirmed that the vertical damage index performs well in damage detection using the lower order modes, without the inclusion of higher modes. Further, study confirmed that damage occurred simultaneously at hanger and cable can be distinguished by the DI_V and also it is not showing false damage detection when the damage occurrence in other elements of the structure. This confirms the applicability of the vertical damage index DI_V to accurately detect damage in real suspension bridges using only the first few modes. Finally, this study proposes the use of this damage index in real applications.

Chapter 8: Conclusions

8.1 INTRODUCTION

Advances in structural engineering and material technology have resulted in increasing applications of cables as key structural components in cable supported structures. These include suspension and cable stayed bridges, overhead transmission lines, cable supported roofs, cable cars, and guyed towers. Among these structures, suspension bridges are given more attention in today's infrastructure systems due to their cost effective structural form, lightness and aesthetics. However their main cables and hangers can suffer from severe corrosion and fatigue damage. Damage detection, followed by timely retrofitting of these structural members is therefore necessary for the safe operation of the bridge and for optimal allocation of public resources for retrofitting and maintenance.

Use of local methods to detect damage in suspension bridges is limited and applying global methods based on vibration characteristics for this task has been promising. However only a very limited number of vibration based damage detection applications have been identified for suspension bridges and these applications draw their foci towards the damage detection of decks, bearings and towers. Further, few investigations attempted to detect damage in cables and hangers recently, but these were limited only to very high severity single damage cases. This research has proposed an improved vibration based damage detection method to detect and locate damage in the main cables and hangers of suspension bridges. It proposes component specific DIs for efficient damage detection in the main cables and hangers of suspension bridges and demonstrates their application under a range of operating conditions.

Numerical investigations using FE models were employed to study the potential of the proposed damage detection method in detecting and locating damage in the main cables and hangers of suspension bridges. Self-performed experiments and vibration data in the literature were used to validate these FE models. Investigations were conducted on four case studies namely; cable structure (Tsing Ma Suspension Bridge main cable), main span of a 2D suspension bridge (New

Carquienz Bridge main span), a complex cable bridge structure and a 3D suspension bridge (Ölfusá Bridge). Also this research studied the variation of damage severity from 10% to 30% with single and multiple damage scenarios. Further, this study was extended to investigate the influence of 5% noise in the modal data and cable parameters in the proposed damage detection method. In addition, the impact of higher order vibration modes and complex damage scenarios in damage detection using the proposed method was examined. Finally, a flowchart representing the application of the proposed damage detection methodology to the inverse problem was presented.

8.2 CONTRIBUTIONS TO KNOWLEDGE

As mentioned before, very few attempts have been made to apply vibration based damage detection methods to detect damage in the main cables and hanger of a suspension bridge. Due to the difficulties of extracting many vibration modes in large civil structures like suspension bridges, applicability of existing vibration based damage detection methods has been limited. Moreover, these bridges vibrate with lateral, vertical, torsional and coupled modes and their vibration patterns are complex making it very difficult to identify the damage sensitive modes. This research therefore focused on effective application of a vibration based damage detection method which incorporates only a few lower order modes to detect and locate damage in main cables and hangers of suspension bridges. In order to achieve this aim, mode shape component specific DIs based on modal flexibility were derived and applied. Four case studies were conducted to evaluate the competency of these damage indices and the main results are summarised below.

Results of damage detection of cable structures

In this case study, a cable model representing the Tsing Ma Suspension Bridge main cable was developed. The lower order vibration modes of the cable model are vertical and lateral. In this case study, therefore both DIs (DI_L and DI_V) were evaluated to identify their competencies in detecting and locating damage. Following results were obtained;

- Lateral damage index calculated using lateral components of the mode shapes (DI_L) successfully locate damage in both single and multiple damage scenarios.

- The comparison of results of DI_L with those of the modal flexibility difference (original modal flexibility method) demonstrates the improved damage detection capability of DI_L
- It is identified that DI_L is more robust in locating damage even in the presence of 5% noise in mode shape data.
- Influence of cable parameters namely; bending stiffness and sag-extensibility on the damage detection capability of the DI_L was investigated. It was observed that DI_L was competent in detecting and locating damage across a range of these cable parameters under all damage scenarios considered.
- Due to the higher modal mass distribution in the lateral direction of the cable structure, DI_L indicates superior performance in damage detection. Not only the increase in the modal mass distribution, but also the reduced lateral stiffness of the cable also contribute towards the performance of DI_L to accurately detect and locate damage in a suspended cable.

Results of damage detection of main span of 2D suspension bridge

Main span of 2D suspension bridge model was setup to vibrate only in the vertical direction and the first few vertical vibration modes were obtained. The performance of DIV in detecting damage in the hangers of this bridge was studied. Damage detection in cables was treated extensively in later case studies. The following results were obtained;

- The vertical damage index calculated using the vertical components of the mode shapes (DI_V) performs well in locating damage in hangers for both single and multiple damage scenarios.
- The comparison of results using DI_V with those using the modal flexibility difference (original modal flexibility method) demonstrates the improved damage detection results of DI_V.
- It is identified that DI_V performs well in locating damage even in the presence of 5% noise in mode shape data.

- Due to the higher modal mass distribution in the vertical direction of the 2D suspension bridge model, DI_V indicates higher performance in damage detection.

Results of damage detection in (model) cable bridge structure

The cable bridge consisted of three types of cables namely; top supporting cables, pre-tensioned reverse profiled (bottom) cables in vertical plane and pre-tensioned bi-concave side cables in the horizontal plane. These cables serve different structural actions in the bridge. Vertical and torsional vibration modes are present in the first few vibration modes. Therefore both DIs (DI_L and DI_V) were evaluated in this case study to determine their competence in detecting and locating damage. Following results were obtained;

- The vertical damage index calculated using vertical components of mode shapes (DI_V) can detect and locate damage successfully in all three types of cables with single, multiple and tension reduction damage scenarios.
- The comparison of DI_V with the modal flexibility difference (original modal flexibility method) demonstrated improved damage detection results with the component specific DI_V.
- It was identified that the DI_V successfully detects and locates damage even in the presence of 5% measurement noise in mode shape data for the all damage scenarios considered.
- Due to the higher modal mass distribution in the vertical direction of the cable bridge, the DI_V shows better performance in damage detection. The higher lateral stiffness of the cable bridge which caused the early modes to be vertical vibration modes, also contributed to the better performance of the DI_V in this case study.

Results of damage detection of a 3D suspension bridge

The Ölfusá suspension Bridge in Iceland was selected for the final case study to investigate the performance of component specific DIs. The first few vibration modes were mainly vertical and coupled (lateral and torsional). Hence performance of both DIs were evaluated. Following results were observed;

- The vertical damage index calculated using vertical components of mode shapes (DI_V) can detect and locate damage successfully in the main cables and hangers under single and multiple damage scenarios.
- The comparison of DI_V with the modal flexibility difference (original modal flexibility method) demonstrates the improved damage detection results of DI_V.
- The DI_V is more robust in detecting and locating damage in the main cables and hangers even with 5% noise in mode shape data.
- Due to the higher modal mass distribution in the vertical direction of the suspension bridge, DI_V shows better performance in damage detection. The lateral stiffness of the 3D suspension bridge in this case study is high and allows it to vibrate vertically in the lower order modes leading to the better performance of the DI_V in detecting and locating damage in suspended cables and hangers.
- The DI_V successfully detects and locates damage using few of the lower order modes of vibration.
- The DI_V successfully distinguishes damage occurring simultaneously in cables and hangers.
- The DI_V does not indicate false damage detection in cables and hangers, when damage occurred in any other element of the bridge.

Considering the research outcomes presented above, the main findings of this study can be summarises as follows:

- This research developed and applied special damage indices which are component specific to detect and locate damage in cable structures and in the main cable and hangers of suspension bridges.
- In pure cable structures DI_L based on the lateral components of the vibration modes can successfully detect and locate damage
- In suspension bridges, DI_V based on the vertical components of the mode shapes is able to detect and locate damage in the main cables and hangers.

- These damage indices show better results compared to those from the traditional modal flexibility method when used for this purpose
- The component specific damage indices are able to perform well even in the presence of 5% noise in the mode shape data
- These component specific DIs can be calculated by using a few of the early modes of vibration of the structure and depend on the direction of mass distribution in the early modes.
- The DI_V is able to perform well even damage occurred simultaneously in cables and hangers.
- The DI_V is not indicating false damage detection in cables and hangers, when damage occurred in any other elements of the bridge

8.3 RECOMMENDATIONS FOR FURTHER RESEARCH

The scope of this research work was limited to level 2 of damage detection (detecting and locating damage) in suspension bridge main cables and hangers using numerical simulations. Therefore following future studies are recommended.

1. Extension of this research for damage quantification of suspension bridges.

   This study has achieved greater success in detecting and locating damage in suspension bridge main cables and hangers using component specific damage indices. Even though these DIs showed the potential for damage quantification, further research is needed to address the damage quantification problems in suspension bridges using vibration based methods.

2. Application of damage indices to the field measured ambient vibration responses.

   This study used validated FE models and dynamic computer simulations to obtain vibration characteristics of suspension bridges at both damaged and undamaged states. This is due to limitation of obtaining mass normalized mode shapes using ambient vibration responses. Some researchers have developed various methods to calculate the mass normalized mode shapes by ambient vibration measurements only for buildings and no attempt has been made for large scale structures such as suspension bridges. Therefore

it is necessary to develop methods to obtain mass normalized mode shapes using ambient vibration responses for suspension bridges.

3. Development of FE Model Updating Method

   There are many successful model updating methods in the literature to develop accurate FE models to represent real structures. Substructure based methods in particular, have achieved greater success in this regard. Further, model updating methods applicable to long span suspension bridges are still in the development stage. Moreover, a precise numerical model is required to apply the DIs proposed by this study and make this research feasible for practical applications. Therefore, it is desirable to develop improved FE model updating methods to obtain precise numerical models.

4. Simulation of different damage

   In this study cable and hanger damage were simulated by reducing their stiffness values in the damaged location. The corrosion of high strength steel wires is a very complex phenomenon and it includes several different mechanisms. Studying how these realistic damage cases can be associated in the numerical models to simulate the resultant stiffness loss will be an interesting topic linked with damage detection.

Bibliography

Abdel Wahab, M., & De Roeck, G. (1999). Damage detection in bridges using modal curvatures: application to a real damage scenario. *Journal of Sound and Vibration, 226*(2), 217-235.

Allemang, R. J. (2003). The modal assurance criterion–twenty years of use and abuse. *Sound and vibration, 37*(8), 14-23.

Alvandi, A., & Cremona, C. (2006). Assessment of vibration-based damage identification techniques. *Journal of Sound and Vibration, 292*(1), 179-202.

Andersen D, B. J. A. (2004, June 16-19, 2004). *The Waldo Hancock Bridge Inspection, Monitoring and Strengthening of the Main Cables.* Paper presented at the The 4th International Cable Supported Bridge Operators' Conference, The Society of Danish Engineers' Conference Centre.

ANSYS Inc.(Canonsburg, P., 2012). Version 14.5 *Workbench, ANSYS*.

Bai, R., Ostachowicz, W., Cao, M., & Su, Z. (2014). Crack detection in beams in noisy conditions using scale fractal dimension analysis of mode shapes. *Smart Materials and Structures, 23*(6), 065014.

Betti, R., & Yanev, B. (1998). *Conditions of suspension bridge cables.* Paper presented at the Proc., The New York City Cable Study, Workshop on Safety Appraisal of Suspension Bridge Main Cables.

Betti, R., & Yanev, B. (1999). Conditions of suspension bridge cables: New York City case study. *Transportation Research Record: Journal of the Transportation Research Board, 1654*(1), 105-112.

Bouaanani, N. (2006). Numerical investigation of the modal sensitivity of suspended cables with localized damage. *Journal of Sound and Vibration, 292*(3), 1015-1030.

Brincker, R., & Andersen, P. (2006). Understanding stochastic subspace identification. *Proceedings of the 24th IMAC, St. Louis, 126*.

Brincker, R., Andersen, P., & Cantieni, R. (2001). Identification and level I damage detection of the Z24 highway bridge. *Experimental techniques, 25*(6), 51-57.

Brincker, R., Ventura, C., & Andersen, P. (2001). *Damping estimation by frequency domain decomposition.* Paper presented at the 19th International Modal Analysis Conference.

Cantieni, R. (2005). *Experimental methods used in system identification of civil engineering structures.* Paper presented at the Proceedings of the International Operational Modal Analysis Conference (IOMAC).

Cao, M., Radzieński, M., Xu, W., & Ostachowicz, W. (2014). Identification of multiple damage in beams based on robust curvature mode shapes. *Mechanical Systems and Signal Processing, 46*(2), 468-480.

Carden, E. P., & Fanning, P. (2004). Vibration based condition monitoring: a review. *Structural Health Monitoring, 3*(4), 355.

Catbas, F. N., Susoy, M., & Frangopol, D. M. (2008). Structural health monitoring and reliability estimation: Long span truss bridge application with environmental monitoring data. *Engineering Structures, 30*(9), 2347-2359. doi: 10.1016/j.engstruct.2008.01.013

Cawley, P., & Adams, R. (1979). The location of defects in structures from measurements of natural frequencies. *The Journal of Strain Analysis for Engineering Design, 14*(2), 49.

Chan, T. H. T., Guo, L., & Li, Z. (2003). Finite element modelling for fatigue stress analysis of large suspension bridges. *Journal of Sound and Vibration, 261*(3), 443-464.

Chan, T. H. T., Wong, K. Y., A Li, Z. X., & Ni, Y.-Q. (2011). Structural health monitoring for long span bridges : Hong Kong experience & continuing onto Australia *Structural Health Monitoring in Australia* (pp. 1-32): Nova Publishers.

Chang, P. C., Flatau, A., & Liu, S. (2003). Review paper: health monitoring of civil infrastructure. *Structural Health Monitoring, 2*(3), 257-267.

Chang, S., & Kim, S. (1996). *On-line structural monitoring of a cable-stayed bridge.* Paper presented at the 1996 Symposium on Smart Structures and Materials.

Choi, F., Li, J., Samali, B., & Crews, K. (2008). Application of the modified damage index method to timber beams. *Engineering Structures, 30*(4), 1124-1145.

Choi, F. C., Li, J., Samali, B., & Crews, K. (2007). An experimental study on damage detection of structures using a timber beam. *Journal of mechanical science and technology, 21*(6), 903-907.

Conte, J. P., He, X., Moaveni, B., Masri, S. F., Caffrey, J. P., Wahbeh, M., . . . Elgamal, A. (2008). Dynamic testing of Alfred Zampa memorial bridge. *Journal of Structural Engineering, 134*(6), 1006-1015.

Contursi, T., Messina, A., & Williams, E. (1998). A multiple-damage location assurance criterion based on natural frequency changes. *Journal of Vibration and Control, 4*(5), 619-633.

Cornwell, P., Doebling, S. W., & Farrar, C. R. (1999). Application of the strain energy damage detection method to plate-like structures. *Journal of Sound and Vibration, 224*(2), 359-374.

Cunha, A., Caetano, E., & Magalhães, F. (2007). Output-only dynamic testing of bridges and special structures. *Structural Concrete, 8*(2), 67-85.

Curadelli, R., Riera, J., Ambrosini, D., & Amani, M. (2008). Damage detection by means of structural damping identification. *Engineering Structures, 30*(12), 3497-3504.

Dawari, V., & Vesmawala, G. (2013). Modal Curvature and Modal Flexibility Methods for Honeycomb Damage Identification in Reinforced Concrete Beams. *Procedia Engineering, 51*, 119-124.

Deeble Sloane, M. J., Betti, R., Marconi, G., Hong, A. L., & Khazem, D. (2012). Experimental analysis of a nondestructive corrosion monitoring system for main cables of suspension bridges. *Journal of Bridge Engineering, 18*(7), 653-662.

Doebling, S. W., & Farrar, C. R. (1996). *Computation of structural flexibility for bridge health monitoring using ambient modal data.* Paper presented at the Proceedings of the 11th ASCE Engineering Mechanics Conference.

Doebling, S. W., Farrar, C. R., & Prime, M. B. (1998). A summary review of vibration-based damage identification methods. *Shock and Vibration Digest, 30*(2), 91-105.

Doebling, S. W., Farrar, C. R., Prime, M. B., & Shevitz, D. W. (1996). Damage identification and health monitoring of structural and mechanical systems from changes in their vibration characteristics: a literature review: Los Alamos National Lab., NM (United States).

Enrique Luco, J., & Turmo, J. (2010). Linear vertical vibrations of suspension bridges: a review of continuum models and some new results. *Soil Dynamics and Earthquake Engineering, 30*(9), 769-781.

Fan, F., Wang, H., Zhi, X., Huang, G., Zhu, E., & Wang, H. (2013). Investigation of construction vertical deformation and pre-deformation control for three super high-rise buildings. *Advances in Structural Engineering, 16*(11), 1885-1898.

Fan, W., & Qiao, P. (2011). Vibration-based damage identification methods: a review and comparative study. *Structural Health Monitoring, 10*(1), 83-111.

Farrar, C. R., & Jauregui, D. A. (1998). Comparative study of damage identification algorithms applied to a bridge: I. Experiment. *Smart Materials and Structures, 7*(5), 704.

Farrar, C. R., & Worden, K. (2007). An introduction to structural health monitoring. *Philosophical Transactions of the Royal Society A: Mathematical, Physical and Engineering Sciences, 365*(1851), 303-315.

Farrar, C. R., & Worden, K. (2012). *Structural health monitoring: a machine learning perspective*: John Wiley & Sons.

Furuya, K., Kitagawa, M., Nakamura, S.-i., & Suzumura, K. (2000). Corrosion mechanism and protection methods for suspension bridge cables. *Structural engineering international, 10*(3), 189-193.

Gao, Y., & Spencer, B. (2002). Damage localization under ambient vibration using changes in flexibility. *Earthquake Engineering and Engineering Vibration, 1*(1), 136-144.

Hamey, C. S., Lestari, W., Qiao, P., & Song, G. (2004). Experimental damage identification of carbon/epoxy composite beams using curvature mode shapes. *Structural Health Monitoring, 3*(4), 333-353.

Hejll, A. (2004). Structural health of bridges: monitor, assess and retrofit.

Higgins, M. S. (2004). Health Monitoring Combined With Visual Inspections-Obtaining a Comprehensive Assessment of Cables.

Hong, A. L., Ubertini, F., & Betti, R. (2010). Wind analysis of a suspension bridge: identification and finite-element model simulation. *Journal of Structural Engineering, 137*(1), 133-142.

Hopwood, I., & Havens, J. H. (1984). Inspection, prevention, and remedy of suspension bridge cable corrosion problems.

Huang, M. H. (2006). *Dynamic characteristics of slender suspension footbridges.* (PhD).

Huang, M. H., Thambiratnam, D. P., & Perera, N. J. (2005). Vibration characteristics of shallow suspension bridge with pre-tensioned cables. *Engineering Structures, 27*(8), 1220-1233.

Huang, Q., Gardoni, P., & Hurlebaus, S. (2012). A probabilistic damage detection approach using vibration-based nondestructive testing. *Structural Safety, 38*, 11-21.

Jianchun, L., Bijan, S., Choon, C. F., & Ulrike, D. (2005). Damage Identification of Timber Bridge Using Vibration Based Methods.

Kim, J.-T., & Stubbs, N. (2002). Improved damage identification method based on modal information. *Journal of Sound and Vibration, 252*(2), 223-238.

Kim, J. T., Park, J. H., & Lee, B. J. (2007). Vibration-based damage monitoring in model plate-girder bridges under uncertain temperature conditions. *Engineering Structures, 29*(7), 1354-1365.

Kim, J. T., & Stubbs, N. (2003). Crack detection in beam-type structures using frequency data. *Journal of Sound and Vibration, 259*(1), 145-160.

Lepidi, M., Gattulli, V., & Vestroni, F. (2009). Damage identification in elastic suspended cables through frequency measurement. *Journal of Vibration and Control, 15*(6), 867-896.

Li, H., Deng, X., & Dai, H. (2007). Structural damage detection using the combination method of EMD and wavelet analysis. *Mechanical Systems and Signal Processing, 21*(1), 298-306.

Li, H., Yang, H., & Hu, S.-L. J. (2006). Modal strain energy decomposition method for damage localization in 3D frame structures. *Journal of engineering mechanics, 132*(9), 941-951.

Li, H. N., Li, D. S., & Song, G. B. (2004). Recent applications of fiber optic sensors to health monitoring in civil engineering. *Engineering Structures, 26*(11), 1647-1657.

Lieven, N., & Ewins, D. (1988). *Spatial correlation of mode shapes, the coordinate modal assurance criterion (COMAC).*

Liu, Y., Li, Y., Wang, D., & Zhang, S. (2014). Model Updating of Complex Structures Using the Combination of Component Mode Synthesis and Kriging Predictor. *The Scientific World Journal, 2014*.

Magalhães, F., Cunha, A., & Caetano, E. (2012). Vibration based structural health monitoring of an arch bridge: from automated OMA to damage detection. *Mechanical Systems and Signal Processing, 28*, 212-228.

Materazzi, A. L., & Ubertini, F. (2011). Eigenproperties of suspension bridges with damage. *Journal of Sound and Vibration*.

Mayrbaurl, R. M. (2000). *Corrosion in suspension bridge cables*. Paper presented at the IABSE Congress Report.

Mehrjoo, M., Khaji, N., Moharrami, H., & Bahreininejad, A. (2008). Damage detection of truss bridge joints using Artificial Neural Networks. *Expert Systems with Applications, 35*(3), 1122-1131.

Messina, A., Williams, E., & Contursi, T. (1998). Structural damage detection by a sensitivity and statistical-based method. *Journal of Sound and Vibration, 216*(5), 791-808.

Montazer, M., & Seyedpoor, S. (2014). A New Flexibility Based Damage Index for Damage Detection of Truss Structures. *Shock and Vibration, 2014*.

Moragaspitiya, P. H. N., Thambiratnam, D. P., Perera, N. J., & Chan, T. H. T. (2013). Development of a vibration based method to update axial shortening of vertical load bearing elements in reinforced concrete buildings. *Engineering Structures, 46*, 49-61.

Myrvoll, F., Dibiagio, E., & Hansvold, C. (1996). Instrumentation for monitoring the Skarnsundet cable-stayed bridge. *Publikasjon-Norges Geotekniske Institutt, 196*.

Nguyen, T., Chan, T. H., & Thambiratnam, D. P. (2014). Effects of wireless sensor network uncertainties on output-only modal analysis employing merged data of multiple tests. *Advances in Structural Engineering, 17*(3), 319-330.

Ni, Y.-Q., Wang, J., & Chan, T. H. (2015). Structural damage alarming and localization of cable-supported bridges using multi-novelty indices: A feasibility study. *Structural Engineering and Mechanics, 54*(2).

Ni, Y., Jiang, S., & Ko, J. (2001). Application of adaptive probabilistic neural network to damage detection of Tsing Ma suspension bridge (Vol. 4337, pp. 347-356): SPIE.

Ni, Y., Zhou, H., Chan, K., & Ko, J. (2008). Modal Flexibility Analysis of Cable-Stayed Ting Kau Bridge for Damage Identification. *Computer-Aided Civil and Infrastructure Engineering, 23*(3), 223-236.

Ni, Y. Q., Ko, J. M., & Zheng, G. (2002). Dynamic analysis of large-diameter sagged cables taking into account flexural rigidity. *Journal of Sound and Vibration, 257*(2), 301-319.

Óskarsson, K. U. (2012). *Structural health modeling of the Ölfusá Suspension Bridge.* (MSc), University of Iceland.

Pakzad, S. N., & Fenves, G. L. (2009). Statistical analysis of vibration modes of a suspension bridge using spatially dense wireless sensor network. *Journal of Structural Engineering, 135*(7), 863-872.

Palacz, M., & Krawczuk, M. (2002). Vibration Parameters for Damage Detection in Structures. *Journal of Sound and Vibration, 249*(5), 999-999. doi: 10.1006/jsvi.2001.3761

Pálsson, G. P. (2012). *Finite Element Modelling and Updating of Medium Span Road Bridges.* (M.Sc.), Technical University of Denmark.

Pandey, A., & Biswas, M. (1995). Experimental verification of flexibility difference method for locating damage in structures. *Journal of Sound and Vibration, 184*(2), 311-328.

Pandey, A., Biswas, M., & Samman, M. (1991). Damage detection from changes in curvature mode shapes. *Journal of Sound and Vibration, 145*(2), 321-332.

Pandey, A. K., & Biswas, M. (1994). Damage detection in structures using changes in flexibility. *Journal of Sound and Vibration, 169*(1), 3-17.

Parloo, E., Cauberghe, B., Benedettini, F., Alaggio, R., & Guillaume, P. (2005). Sensitivity-based operational mode shape normalisation: application to a bridge. *Mechanical Systems and Signal Processing, 19*(1), 43-55.

Patjawit, A., & Kanok-Nukulchai, W. (2005). Health monitoring of highway bridges based on a Global Flexibility Index. *Engineering Structures, 27*(9), 1385-1391.

Petrini, F., & Bontempi, F. (2011). Estimation of fatigue life for long span suspension bridge hangers under wind action and train transit. *Structure and Infrastructure Engineering, 7*(7-8), 491-507.

Qiu, W., Jiang, M., & Huang, C. (2014). Parametric study on responses of a self-anchored suspension bridge to sudden breakage of a hanger. *The Scientific World Journal, 2014*.

Quan, Q., & Weiguo, Z. (1998). *Damage detection of suspension bridges.* Paper presented at the Proc. the 16th International Modal Analysis Conference. Santa Barbara, California, USA.

Rainieri, C., & Fabbrocino, G. (2014). *Operational Modal Analysis of Civil Engineering Structures: An Introduction and Guide for Applications*: Springer.

Razak, H. A., & Choi, F. (2001). The effect of corrosion on the natural frequency and modal damping of reinforced concrete beams. *Engineering Structures, 23*(9), 1126-1133.

Ren, W.-X., & Peng, X.-L. (2005). Baseline finite element modeling of a large span cable-stayed bridge through field ambient vibration tests. *Computers & Structures, 83*(8), 536-550.

Reynders, E. (2012). System identification methods for (operational) modal analysis: review and comparison. *Archives of Computational Methods in Engineering, 19*(1), 51-124.

Rytter, A. (1993). *Vibrational based inspection of civil engineering structures.* Department of Building Technology and Structural Engineering, University of Aalborg.

Salawu, O. (1997). Detection of structural damage through changes in frequency: a review. *Engineering Structures, 19*(9), 718-723.

Salawu, O. S., & Williams, C. (1995). Bridge assessment using forced-vibration testing. *Journal of Structural Engineering, 121*(2), 161-173.

Salehi, M., Rad, S. Z., Ghayour, M., & Vaziry, M. (2011). A non model-based damage detection technique using dynamically measured flexibility matrix. *IJST, 35*(M1), 1-13.

Schneidewind, N., Montrose, M., Feinberg, A., Ghazarian, A., McLinn, J., Hansen, C., . . . Linger, R. (2010). IEEE Reliability Society Technical Operations Annual Technical Report for 2010. *Reliability, IEEE Transactions on, 59*(3), 449-482.

Shi, Z., Law, S., & Zhang, L. (1998). Structural damage localization from modal strain energy change. *Journal of Sound and Vibration, 218*(5), 825-844.

Shi, Z., Law, S., & Zhang, L. (2002). Improved damage quantification from elemental modal strain energy change. *Journal of engineering mechanics, 128*(5), 521-529.

Shi, Z. Y., Law, S. S., & Zhang, L. M. (2000a). Damage localization by directly using incomplete mode shapes. *Journal of engineering mechanics, 126*(6), 656-660.

Shi, Z. Y., Law, S. S., & Zhang, L. M. (2000b). Structural damage detection from modal strain energy change. *Journal of engineering mechanics, 126*, 1216.

Shih, H. W., Thambiratnam, D., & Chan, T. H. T. (2009). Vibration based structural damage detection in flexural members using multi-criteria approach. *Journal of Sound and Vibration, 323*(3), 645-661.

Shih, H. W., Thambiratnam, D., & Chan, T. H. T. (2011a). Damage detection in truss bridges using vibration based multi-criteria approach. *Structural Engineering and Mechanics, 39*(2), 187-206.

Shih, H. W., Thambiratnam, D., & Chan, T. H. T. (2011b). Damage localisation in beams and plates using vibration characteristics *Structural Health Monitoring in Australia* (pp. 33-53): Nova Publishers.

Shih, H. W., Thambiratnam, D , & Chan, T H T. (2009). *Damage assessment in structures using vibration characteristics.* (PhD), Queensland University of Technology. Retrieved from http://eprints.qut.edu.au/30319/

Siringoringo, D. M., & Fujino, Y. (2008). System identification of suspension bridge from ambient vibration response. *Engineering Structures, 30*(2), 462-477.

Sloane, M. J. D., Betti, R., Marconi, G., Hong, A. L., & Khazem, D. (2012). An Experimental Analysis of a Non-Destructive Corrosion Monitoring System for Main Cables of Suspension Bridges. *Journal of Bridge Engineering*.

Stubbs, N., & Kim, J.-T. (1996). Damage localization in structures without baseline modal parameters. *Aiaa Journal, 34*(8), 1644-1649.

Stubbs, N., Kim, J.-T., & Farrar, C. (1995). *Field verification of a nondestructive damage localization and severity estimation algorithm.* Paper presented at the Proceedings-SPIE the international society for optical engineering.

Stubbs, N., Kim, J., & Topole, K. (1992). *An efficient and robust algorithm for damage localization in offshore platforms.* Paper presented at the Proc. ASCE Tenth Structures Congress.

Sung, S., Koo, K., & Jung, H. (2014). Modal flexibility-based damage detection of cantilever beam-type structures using baseline modification. *Journal of Sound and Vibration*.

Suzumura, K., & Nakamura, S.-i. (2004). Environmental factors affecting corrosion of galvanized steel wires. *Journal of materials in civil engineering, 16*(1), 1-7.

Talebinejad, I., Sedarat, H., Emami-Naeini, A., Krimotat, A., & Lynch, J. (2014). *Implementation of damage detection algorithms for the Alfred Zampa memorial suspension bridge.* Paper presented at the SPIE Smart Structures and Materials+ Nondestructive Evaluation and Health Monitoring.

Toksoy, T., & Aktan, A. (1994). Bridge-condition assessment by modal flexibility. *Experimental Mechanics, 34*(3), 271-278.

Ubertini, F. (2008). *Wind Effects on Bridges:Response, Stability and Control.* (PhD), University of Pavia, University of Pavia.

Ubertini, F. (2014). Effects of cables damage on vertical and torsional eigenproperties of suspension bridges. *Journal of Sound and Vibration, 333*(11), 2404-2421.

Wahalathantri, B. L., Thambiratnam, D. P., Chan, T. H., & Fawzia, S. (2015). Vibration based baseline updating method to localize crack formation and propagation in reinforced concrete members. *Journal of Sound and Vibration, 344*, 258-276.

Wahalthantri, B., Thambiratnam, D., Chan, T. H., & Fawzia, S. (2012). An improved method to detect damage using modal strain energy based damage index. *Advances in Structural Engineering, 15*(5), 727-742.

Wang, B. S., Liang, X. B., & Ni, Y. (2000). *Comparative study of damage indices in application to a long-span suspension bridge*.

Wang, F. L., Chan, T. H., Thambiratnam, D. P., Tan, A. C., & Cowled, C. J. (2012). Correlation-based damage detection for complicated truss bridges using multi-layer genetic algorithm. *Advances in Structural Engineering, 15*(5), 693-706.

Wang, H., Li, A.-q., & Li, J. (2010). Progressive finite element model calibration of a long-span suspension bridge based on ambient vibration and static measurements. *Engineering Structures, 32*(9), 2546-2556.

Wang, J. Y., Ko, J. M., & Ni, Y. Q. (2000). *Modal sensitivity analysis of Tsing Ma Bridge for structural damage detection.* Paper presented at the SPIE's 5th Annual International Symposium on Nondestructive Evaluation and Health Monitoring of Aging Infrastructure.

Wang, L., Chan, T. H., Thambiratnam, D. P., & Tan, A. C. (2010). *Improved correlation-based modal strain energy method for global damage detection of truss bridge structures.* Paper presented at the Proceedings of the International Symposium on Life-Cycle Performance of Bridge and Structures.

Weng, S., Xia, Y., Xu, Y.-L., & Zhu, H.-P. (2011). Substructure based approach to finite element model updating. *Computers & Structures, 89*(9), 772-782.

Weng, S., Xia, Y., Zhou, X.-Q., Xu, Y.-L., & Zhu, H.-P. (2012). Inverse substructure method for model updating of structures. *Journal of Sound and Vibration, 331*(25), 5449-5468.

West, W. M. (1986). *Illustration of the use of modal assurance criterion to detect structural changes in an orbiter test specimen*.

Wit, M. D., & Hovhanessian, G. (2013). *Assessment and monitoring of cable supported structures-theory and practice.* Paper presented at the The 6th International Conference on Structural Health Monitoring of Intelligent Infrastructure, Hong Kong.

Wolff, T., & Richardson, M. (1989). *Fault detection in structures from changes in their modal parameters.* Paper presented at the Proceedings of the 7th international modal analysis conference.

Worden, K., & Dulieu-Barton, J. (2004). An overview of intelligent fault detection in systems and structures. *Structural Health Monitoring, 3*(1), 85-98.

Xu, Y. L., Ko, J. M., & Yu, Z. (1997). Modal analysis of tower-cable system of Tsing Ma long suspension bridge. *Engineering Structures, 19*(10), 857-867.

Xu, Y. L., & Xia, Y. (2011). *Structural health monitoring of long-span suspension bridges*: CRC Press.

Yan, A., & Golinval, J.-C. (2005). Structural damage localization by combining flexibility and stiffness methods. *Engineering Structures, 27*(12), 1752-1761.

Yan, Y., Cheng, L., Wu, Z., & Yam, L. (2007). Development in vibration-based structural damage detection technique. *Mechanical Systems and Signal Processing, 21*(5), 2198-2211.

Yanaka, Y., & Kitagawa, M. (2002). Maintenance of steel bridges on Honshu-Shikoku crossing. *Journal of Constructional Steel Research, 58*(1), 131-150.

Yang, Y., Li, Y., & Chang, K. (2014). Constructing the mode shapes of a bridge from a passing vehicle: a theoretical study. *Smart Structures and Systems, 13*(5), 797-819.

Yeung, W., & Smith, J. (2005). Damage detection in bridges using neural networks for pattern recognition of vibration signatures. *Engineering Structures, 27*(5), 685-698.

Zapico, J. L., & González, M. P. (2006). Numerical simulation of a method for seismic damage identification in buildings. *Engineering Structures, 28*(2), 255-263.

Zhang, L., Brincker, R., & Andersen, P. (2009). An overview of operational modal analysis: major development and issues. *Mechanical Systems and Signal Processing*.

Zhang, Y., Wang, L., Lie, S. T., & Xiang, Z. (2013). Damage detection in plates structures based on frequency shift surface curvature. *Journal of Sound and Vibration, 332*(25), 6665-6684.

Zhong, S., Oyadiji, S. O., & Ding, K. (2008). Response-only method for damage detection of beam-like structures using high accuracy frequencies with auxiliary mass spatial probing. *Journal of Sound and Vibration, 311*(3), 1075-1099.

Appendices

Appendix A: Load cell calibration curves

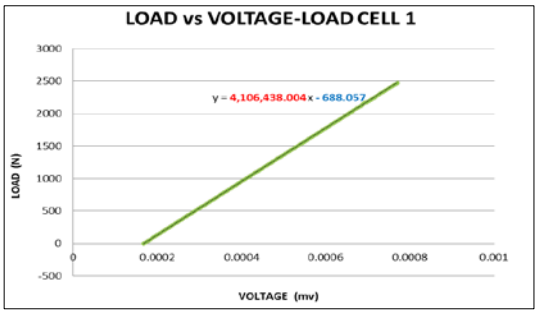

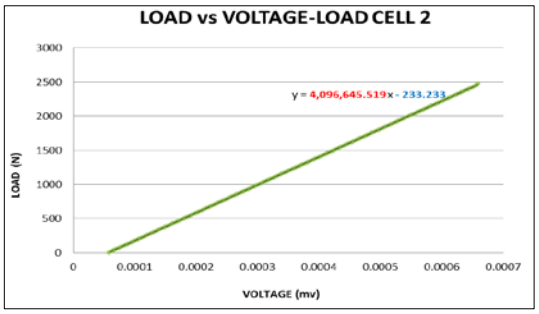

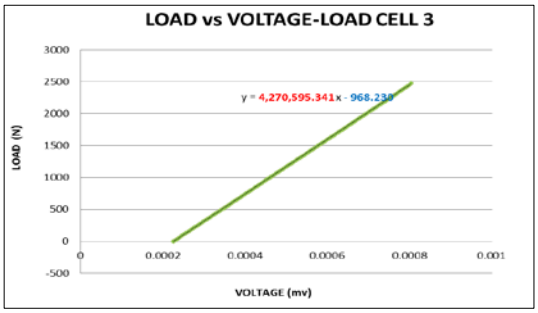

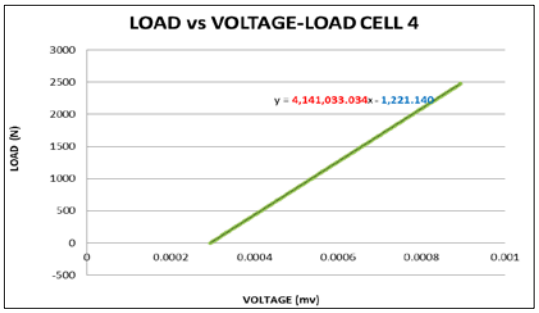

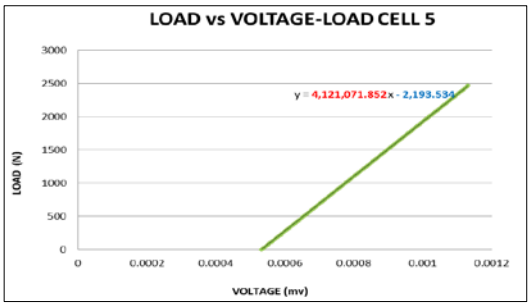

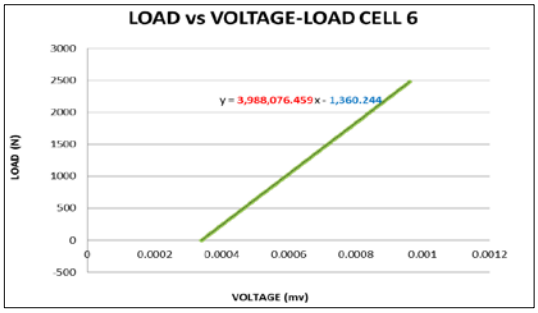

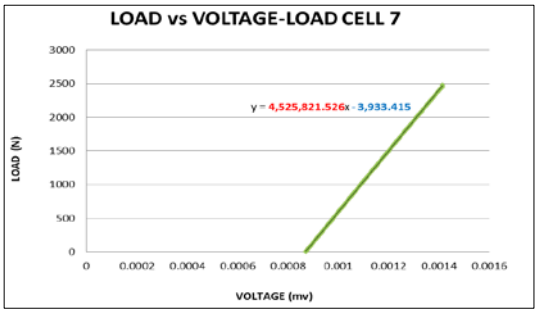

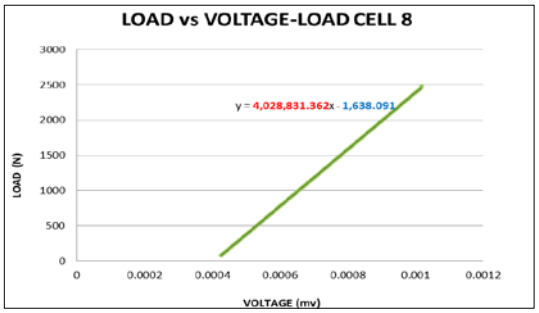

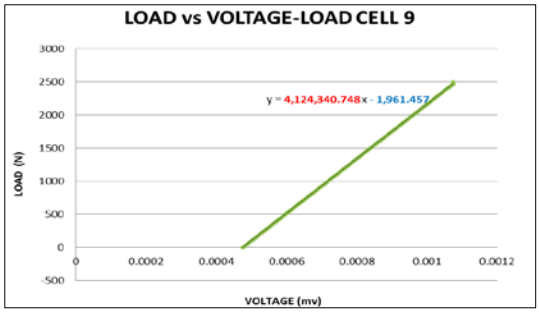
LOAD vs VOLTAGE-LOAD CELL 9
y = 4,124,340.748x - 1,961.457
LOAD (N)
VOLTAGE (mv)

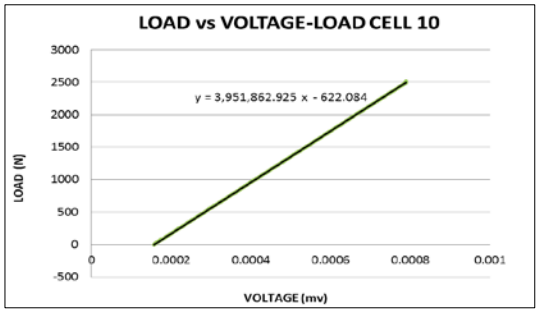
LOAD vs VOLTAGE-LOAD CELL 10
y = 3,951,862.925 x - 622.084
LOAD (N)
VOLTAGE (mv)

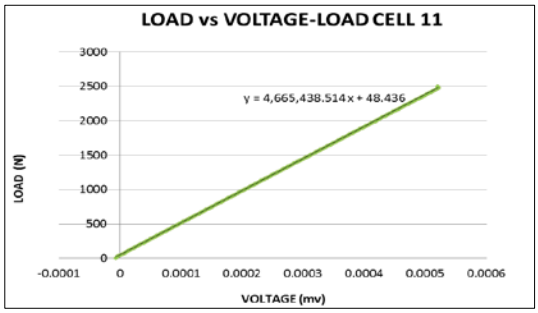
LOAD vs VOLTAGE-LOAD CELL 11
y = 4,665,438.514x + 48.436
LOAD (N)
VOLTAGE (mv)

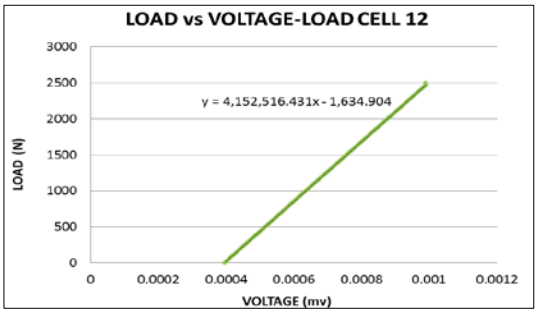
LOAD vs VOLTAGE-LOAD CELL 12
y = 4,152,516.431x - 1,634.904
LOAD (N)
VOLTAGE (mv)